UNIVERSITI TEKNOLOGI MARA

DEVELOPMENT OF MgO-Al_2O_3 SUPPORTED ON SINGLE AND BIMETALLIC OXIDE CATALYSTS FOR NH_3 DECOMPOSITION TO H_2 PRODUCTION

AISHA HAMID

PhD

August 2026

UNIVERSITI TEKNOLOGI MARA

DEVELOPMENT OF MgO-Al_2O_3 SUPPORTED ON SINGLE AND BIMETALLIC OXIDE CATALYSTS FOR NH_3 DECOMPOSITION TO H_2 PRODUCTION

AISHA HAMID

Thesis submitted in fulfilment
of the requirements for the degree of
Doctor of Philosophy
(Science)

Faculty of Applied Sciences

August 2026

CONFIRMATION BY PANEL OF EXAMINERS

I certify that a Panel of Examiners has met on 20th April 2026 to conduct the final examination of Aisha Hamid on her Doctor of Philosophy thesis entitled "Development of MgO-Al_2O_3 Supported on Single and Bimetallic Oxide Catalysts for NH_3 Decomposition to H_2 Production" in accordance with Universiti Teknologi MARA Act 1976 (Akta 173). The Panel of Examiners recommends that the student be awarded the relevant degree. The Panel of Examiners was as follows:

Norizan Ahmat @ Abdul Hamid, PhD
Professor
Faculty of Applied Sciences
Universiti Teknologi MARA
(Chairman)

Hamizah Mohd Zaki, PhD
Senior Lecturer
Faculty of Applied Sciences
Universiti Teknologi MARA
(Internal Examiner)

Juan Joon Ching, PhD
Professor
Nanotechnology and Catalysis
Research Centre
Universiti Malaya
(External Examiner)

PROFESSOR DR HJH ZURAEDA BINTI IBRAHIM
Dean
Institute of Postgraduate Studies
Universiti Teknologi MARA

Date: 14 August 2026

AUTHOR'S DECLARATION

I declare that the work in this thesis was carried out in accordance with the regulations of Universiti Teknologi MARA. It is original and is the results of my own work, unless otherwise indicated or acknowledged as referenced work. This thesis has not been submitted to any other academic institution or non-academic institution for any degree or qualification.

I, hereby, acknowledge that I have been supplied with the Academic Rules and Regulations for Post Graduate, Universiti Teknologi MARA, regulating the conduct of my study and research.

Name of Student	:	Aisha Hamid
Student ID. No.	:	2023264226
Programme	:	Doctor of Philosophy (Science) – AS950
Faculty	:	Faculty of Applied Sciences
Thesis Title	:	Development of $MgO\text{-}Al_2O_3$ Supported on Single and Bimetallic Oxide Catalysts for NH_3 Decomposition to H_2 Production

Signature of Student	:	……..
Date	:	August 2026

ABSTRACT

Ammonia (NH_3) decomposition is a promising route for carbon-free hydrogen (H_2) production; yet its industrial viability remains limited by the scarcity of low-cost, high-activity catalysts with long-term thermal stability. This study aimed to develop and optimize non-noble single-metal (CoO, FeO, ZnO) and bimetallic (CoFeO, CoZnO) oxide catalysts supported on $MgO\text{-}Al_2O_3$ for efficient NH_3 decomposition. The novelty of this work lies in the development of low-cost, non-noble metal catalysts that achieve high ammonia conversion efficiency and good thermal stability for NH_3 decomposition. The catalysts were synthesized through hydrothermal carbonization and comprehensively characterized using X-ray diffraction (XRD), field-emission scanning electron microscopy with energy-dispersive X-ray analysis (FESEM-EDX), Brunauer-Emmett-Teller (BET) surface area measurements, thermogravimetric analysis (TGA), H_2 temperature-programmed reduction (H_2-TPR) and X-ray Photoelectron Spectroscopy (XPS). Among the single-metal catalysts, $CoO/MgO\text{-}Al_2O_3$ exhibited the highest NH_3 conversion (77.7% at 650 °C), prompting the design of cobalt-based bimetallic systems. While the $CoFeO/MgO\text{-}Al_2O_3$ catalyst achieved superior conversion (87.2% at 650 °C), attributed to synergistic Co-Fe electronic interactions that enhanced N-H bond cleavage kinetics. Kinetic studies revealed a high hydrogen yield of 92.4% at optimal conditions, further solidifying the catalyst's potential. Structural and textural analyses confirmed the formation of mixed-oxide nanodomains, uniform metal dispersion, and mesoporosity retention favorable for active-site exposure. Using Response Surface Methodology (Box-Behnken design), process variables were statistically optimized, yielding a robust predictive model for maximum conversion. The recyclability studies further revealed sustained catalytic activity and stability over 9 cycles. Overall, $CoFeO/MgO\text{-}Al_2O_3$ emerges as a cost-effective, thermally durable, and high-performance non-noble catalyst for ammonia decomposition and hydrogen production advancing ammonia-to-hydrogen technology toward scalable green-energy applications.

ACKNOWLEDGEMENT

Firstly, I wish to thank God for giving me the opportunity to embark on my PhD and for completing this long and challenging journey successfully. My gratitude and thanks go to my supervisor Associate Professor. Dr. Mohd Lokman Ibrahim for his inspiring guidance, constant encouragement, stimulating discussions and valuable suggestions during my research work and preparation of this thesis. I am deeply indebted to him for the help he extended to me in this academic endeavour.

I wish to record my thankfulness to my co-supervisors Associate Professor Dr. Raja Razuan Raja Deris, and Prof Datuk Dr. Taufiq Yap Yun Hin for their continuous inspiration during my research work. I do want to thank the School of Environment and Chemistry and the Graduate School at UiTM Shah Alam for offering me this opportunity to pursue my studies at UiTM. My sincere thanks also go to the laboratory staff for their help in all official and technical issues.

My appreciation goes to the captain and crewmembers of the MMC who provided the facilities and assistance during sampling. Special thanks to my colleagues and friends for helping me with this project.

Finally, I am especially grateful to my parents and Husband, who supported me emotionally and financially. I always knew that you believed in me and wanted the best for me. Thank you for teaching me that my job in life was to learn, to be happy, and to know and understand myself; only then could I know and understand others. This piece of victory is dedicated to both of you. Alhamdulilah.

Last but not least, I would like to express my gratitude to my siblings and friends for their invaluable assistance, and I am deeply grateful to everyone who has contributed to the successful completion of this journey.

TABLE OF CONTENTS

		Page
CONFIRMATION BY PANEL OF EXAMINERS		**ii**
AUTHOR'S DECLARATION		**iii**
ABSTRACT		**iv**
ACKNOWLEDGEMENT		**v**
TABLE OF CONTENTS		**vi**
LIST OF TABLES		**x**
LIST OF FIGURES		**xi**
LIST OF ABBREVIATIONS		**xv**
LIST OF NOMENCLATURES		**xvi**
CHAPTER 1: INTRODUCTION		**1**
1.1	Research Background	1
1.2	Problem Statement	3
1.3	Objectives of Study	4
1.4	Significance of Study	5
1.5	Scope of Research	6
CHAPTER 2: LITERATURE REVIEW		**8**
2.1	Hydrogen as an Energy Source	8
2.2	Storage of Hydrogen	11
2.3	Hydrogen Production	13
	2.3.1 Hydrogen Production from Ammonia	16
2.4	Ammonia Decomposition	17
	2.4.1 Reaction Mechanism of NH_3 Decomposition	23
	2.4.2 Reaction Kinetics of Ammonia Decomposition	25
	2.4.3 Operating Variables of Ammonia Decomposition	29
2.5	Types of Catalyst for NH_3 Decomposition	34
	2.5.1 Noble Metals for NH_3 Decomposition	37

2.5.2 Non-Noble Metals Catalysts for NH_3 Decomposition 39
2.5.3 Bimetallic Catalyst for NH_3 Decomposition 42
2.6 Role of Supports for NH_3 Decomposition 44
2.6.1 Aluminium Oxide (Al_2O_3) 46
2.6.2 Magnesium Oxide (MgO) 47
2.6.3 Synergistic Effect of Mixed Oxide Supports (MgO-Al_2O_3) 49
2.6.4 Role of Promoters 50
2.7 Catalyst Preparation Methods 51
2.7.1 Hydrothermal Method 54
2.7.2 Electrodeposition Method 55
2.7.3 Comparison with Other Synthesis Techniques 58
2.8 Response Surface Methodology (RSM) 59
2.9 Reactor for The Ammonia Decomposition 60
2.9.1 Fixed-Bed Reactors 61
2.9.2 Catalytic Membrane Reactors 61
2.9.3 Microreactors 61
2.9.4 Micro-Post Reactors 62
2.10 Catalytic Membrane Reactor for Ammonia Decomposition 63
2.11 Fixed Bed Reactor for NH_3 Decomposition 65

CHAPTER 3: RESEARCH METHODOLOGY 67
3.1 Introduction 67
3.2 Materials and Methods 69
3.2.1 Chemicals 69
3.2.2 Equipment and Apparatus 70
3.3 Development of Catalyst 70
3.3.1 Preparation of MgO-Al_2O_3 Support (Step 1) 70
3.3.2 Preparation of Single-Metal Catalysts of CoO, FeO, ZnO Supported on MgO-Al_2O_3 (Step 2) 70
3.3.3 Preparation of Bimetallic Catalysts (CoFeO and CoZnO Supported on MgO-Al_2O_3) (Step 3) 71
3.4 Catalyst Characterization 72
3.4.1 Catalyst Phase and Crystallinity 72

3.4.2 Catalyst Morphological and Elemental Analyses 72
3.4.3 Surface Characteristics by Brunauer-Emmett-Teller Surface Area and Porosity Analyser 72
3.4.4 Catalyst Thermal Stability 73
3.4.5 Catalyst Reduction Potential 73
3.4.6 X-Ray Photoelectron Spectroscopy 73
3.5 Catalytic Performance Evaluations 73
3.6 Experimental Design Using Box-Behken Design (BBD) 75
3.7 Kinetic Study of Catalyst 76
3.8 The Recyclability of Catalyst 77

CHAPTER 4: RESULTS AND DISCUSSION 78
4.1 Introduction 78
4.2 Catalyst Characterization of Single Metal 79
4.2.1 Catalyst Phase and Crystallinity of Single Metal 79
4.2.2 Catalyst Morphological and Elemental Analyses of Single Metal 80
4.2.3 Brunauer-Emmett-Teller (BET) Surface Area Analysis of Single Metal 83
4.2.4 Thermal Stability Analysis (TGA) of Single Metal 85
4.2.5 Temperature-Programmed Reduction (H_2-TPR) Analysis of Single Metal 87
4.2.6 XPS Analysis of CoO/MgO-Al_2O_3 Catalyst 89
4.3 Catalytic Activity of Single Metal Oxide Catalysts for NH_3 Decomposition 91
4.4 Catalyst Characterization of Bimetallic 93
4.4.1 Catalyst Phase and Crystallinity of Bimetallic 93
4.4.2 Catalyst Morphological and Elemental Analyses of Bimetallic 95
4.4.3 Brunauer-Emmett-Teller (BET) Surface Area Analysis of Bimetallic 97
4.4.4 Thermal Stability Analysis (TGA) of Bimetallic 99
4.4.5 Temperature-Programmed Reduction (H_2-TPR) Analysis of Bimetallic 100
4.4.6 XPS Analysis of CoFeO/MgO-Al_2O_3 Catalyst 101

4.5 Catalytic Activity of Bimetallic Oxide Catalysts for NH_3 Decomposition 104
4.6 Response Surface Methodology of CoFeO/MgO-Al2O3 106
4.6.1 Box-Behnken Design 106
4.6.2 Analysis of Variance 107
4.6.3 Effect of Input Variables 109
4.6.4 Three-Dimensional Response Surface 110
4.6.5 Validation Study 111
4.7 Kinetic Analysis of CoFeO/MgO-Al_2O_3 Catalyst 112
4.8 The recyclability of CoFeO/MgO-Al_2O_3 Catalyst 114
4.9 Summary 115

CHAPTER 5: CONCLUSION AND RECOMMENDATIONS 117
5.1 Conclusion 117
5.2 Recommendations 118
5.3 Future Work 118
REFERENCES 120
APPENDICES 158
AUTHOR'S PROFILE 164

LIST OF TABLES

Tables	Title	Page
Table 2.1	Comparison Method for NH_3 Decomposition Process	18
Table 2.2	Comparison of Selected Ammonia Decomposition Catalysts Highlighting Temperature, Conversion, Stability/Reusability, and Research Gaps Addressed by This Study	23
Table 2.3	Reaction and Activation Energies on the Catalyst Surfaces During the NH_3 Decomposition Process	24
Table 2.4	Catalysts Used for the Kinetics of Ammonia Decomposition, Elucidating the RateLimiting Step in the Reaction Mechanism	28
Table 2.5	Effect of Operating Variables on the NH_3 Decomposition and H_2 Production.	30
Table 2.6	Different Catalysts for Hydrogen Production from Ammonia Decomposition	33
Table 2.7	Preparation Method and Kinetic Analysis of Bimetallic Catalysts	43
Table 3.1	Codes and Actual Variables and Their Levels in BBD	75
Table 3.2	The BBD Three-Variable Matrix for NH_3 Conversion Using $CoFeO/MgO-Al_2O_3$	76
Table 4.1	Surface Characteristics Analysis of $MgO-Al_2O_3$, $CoO/ MgO-Al_2O_3$, $FeO/ MgO-Al_2O_3$ and $ZnO/ MgO-Al_2O_3$ Catalysts	85
Table 4.2	Surface Characteristics Analysis of $CoFeO/MgO- Al_2O_3$, and $ZnO/MgO- Al_2O_3$ Catalysts	99
Table 4.3	The BBD Three-Variable Matrixfor NH_3 Conversion Using $CoFeO/MgO- Al_2O_3$	107
Table 4.4	Analysis of Variance (ANOVA) for $CoFeO/MgO- Al_2O_3$ Catalytic Activity for NH_3 Conversion	109
Table 4.5	PFO and PSO Kinetic Parameters for NH_3 Conversion by $CoFeO/MgO- Al_2O_3$	114

LIST OF FIGURES

Figures	Title	Page
Figure 2.1	Hydrogen as an Energy Source (Hamid et al., 2025) (Adapted with Permission from Elsevier)	11
Figure 2.2	Hydrogen Manufacturing Process (Nailwal et al., 2024b) (Adapted with Permission from Elsevier).	13
Figure 2.3	Hydrogen Production Process (Hamid et al., 2025) (Adapted with Permission from Elsevier)	15
Figure 2.4	Important Role of NH_3 as an Energy Carrier in Current and Future Energy Systems (Chen et al., 2023)	17
Figure 2.5	Catalytic NH_3 Decomposition into N_2 and H_2 (Faheem et al., 2021)	22
Figure 2.6	Apparent Activation Energy Values for the Decomposition of Ammonia Recorded on Different Metal-Based Catalysts (Adapted from Kassi & Hattab, 2024)	32
Figure 2.7	Strategies for the Rational Design of Ru-Based Catalysts (B) Schematic Representation of NH_3 Decomposition Reaction over Ru Catalysts (Li et al., 2024) (Adapted with Permission from Elsevier)	38
Figure 2.8	Reaction Pathway for Ammonia Decomposition over Ni/Canh Catalysts Through an NH_2- Vacancy-Mediated Mars-Van Krevelen Mechanism (Muhammed Et Al., 2023) (Adapted with Permission from Elsevier)	41
Figure 2.9	Schematic of Hydrogen Permeation and Ammonia Decomposition Test: (a) Flow Diagram of the Testing Rig, (b) Membrane Reactor Module, and (c) Schematic of the Membrane Reactor (Ghannadi & Dincer, 2024)	62
Figure 2.10	Schematic Diagram of (a) Membrane Reactor for NH_3 Decomposition and (b) NH_3 Cracker Integrated with Membrane Separator (Alharthi et al., 2023) (Adapted with Permission from Elsevier)	64

Figure 3.1	Flowchart of the Research Methodology Showing Catalyst Screening, Bimetallic Synthesis and Optimization, Characterization, Performance Testing, RSM Optimization, and Kinetic/Recyclability Analysis	69
Figure 3.2	Schematic Illustration of the Three-Step Hydrothermal and Calcination Process Used for Synthesizing MgO-Al_2O_3 Support (Step 1), Single Metal/MgO-Al_2O_3 Catalyst (Step 2), and Bimetallic/MgO-Al_2O_3 Catalyst (Step 3)	71
Figure 3.3	(a) Photographs of the Experimental Reactor System Used for Catalytic Performance Evaluation and (b) Schematic Diagram of the Thermocatalytic Reactor Setup for NH_3 Decomposition	74
Figure 4.1	XRD Patterns of (a) MgO, Al_2O_3, and MgO-Al_2O_3 Supports (b) CoO/MgO-Al_2O_3 (c) FeO/MgO-Al_2O_3 and (d) ZnO/MgO-Al_2O_3 Catalysts	80
Figure 4.2	FESEM and EDX Analysis of the Synthesized Single-Metal Catalysts. Morphological Comparison of MgO, Al_2O_3, MgO-Al_2O_3, CoO, CoO/MgO-Al_2O_3, FeO, FeO/MgO-Al_2O_3, ZnO and ZnO/MgO-Al_2O_3 Catalysts	82
Figure 4.3	FESEM and EDX Analysis of the Synthesized Single-Metal Catalysts. Elemental Mapping and EDX Spectra of CoO/MgO-Al_2O_3, FeO/MgO-Al_2O_3 and ZnO/ MgO-Al_2O_3	83
Figure 4.4	BET Isotherms Plot of (a) MgO-Al_2O_3,(b) CoO/ MgO-Al_2O_3, (c) FeO/ MgO-Al_2O_3 and (d) ZnO/ MgO-Al_2O_3 Catalysts	85
Figure 4.5	Comparison of TGA Profiles for Al_2O_3, MgO-Al_2O_3, CoO/MgO-Al_2O_3, FeO/MgO-Al_2O_3, and ZnO/MgO-Al_2O_3 Catalysts, Indicating Differences in Thermal Stability	87
Figure 4.6	H_2-TPR Profiles of MgO-Al_2O_3 and Metal-Supported Catalysts (CoO, FeO, ZnO). The Introduction of Transition Metals Generates Additional Reduction Peaks at Lower Temperatures, Indicating Enhanced Hydrogen Activation and Stronger Metal-Support Interactions	89
Figure 4.7	XPS Spectra of the CoO/MgO-Al_2O_3 Catalyst Showing the Deconvoluted (a) Co 2p, (b) O 1s, (c) Mg 2p, (d) Al 2p, and (e) C 1s Regions.	91

Figure 4.8	NH_3 Conversion of $MgO\text{-}Al_2O_3$ and Metal-Supported Catalysts (CoO, FeO, ZnO) at 450-650 °C, Showing the Superior Catalytic Activity of $CoO/MgO\text{-}Al_2O_3$	93
Figure 4.9	XRD Patterns of (a) $MgO\text{-}Al_2O_3$ Support, (b) $CoFeO/MgO\text{-}Al_2O_3$, and (c) $CoZnO/MgO\text{-}Al_2O_3$ Catalysts	95
Figure 4.10	FESEM and EDX Analysis of the Synthesized Bimetallic Catalysts. Morphological Comparison of MgO, Al_2O_3, $MgO\text{-}Al_2O_3$, CoO, FeO, ZnO, $CoFeO/MgO\text{-}Al_2O_3$, and $CoZnO/MgO\text{-}Al_2O_3$ Catalysts	96
Figure 4.11	FESEM and EDX Analysis of the Synthesized Bimetallic Catalysts. Elemental Mapping and EDX Spectra of $CoFeO/MgO\text{-}Al_2O_3$, $CoFeO/MgO\text{-}Al_2O_3$	97
Figure 4.12	BET Isotherms Plot of $CoFeO/MgO\text{-}Al_2O_3$ (a) and $CoZnO/MgO\text{-}Al_2O_3$ (b) Catalysts	98
Figure 4.13	Comparison of TGA Profiles for $MgO\text{-}Al_2O_3$, $CoFeO/MgO\text{-}Al_2O_3$, and $CoZnO/MgO\text{-}Al_2O_3$ Catalysts, Indicating Differences in Thermal Stability	100
Figure 4.14	H2-TPR Profiles of $MgO\text{-}Al_2O_3$, $CoFeO/MgO\text{-}Al_2O_3$ and $CoZnO/MgO\text{-}Al_2O_3$ Catalysts. The Introduction of Transition Metals Generates Additional Reduction Peaks at Lower Temperatures, Indicating Enhanced Hydrogen Activation and Stronger Metal Support Interaction	101
Figure 4.15	XPS Spectra of the $CoFeO/MgO\text{-}Al_2O_3$ Catalyst Showing the Deconvoluted (a) Co 2p, (b)Fe 2p, (c) Mg 2p, (d) Al 2p, (e) C 1s Regions and (f) O 1s	104
Figure 4.16	NH_3 Conversion of $MgO\text{-}Al_2O_3$ and Metal-Supported Catalysts (CoO, FeO, ZnO, CoFeO and CoZnO) at 450-650 °C, Showing the Superior Catalytic Activity of $CoFeO/MgO\text{-}Al_2O_3$	106
Figure 4.17	(a) Predicted vs. Cctual Values of NH_3 Conversion Using $CoFeO/MgO\text{-}Al_2O_3$ Catalyst, Demonstrating Model Accuracy (b) Normal Probability Plot of Residuals for $CoFeO/MgO\text{-}Al_2O_3$ Catalyst (c) Perturbation Plot for $CoFeO/MgO\text{-}Al_2O_3$ Catalyst	110

Figure 4.18 The Illustration of (a) Three-Dimensional (3D) Response Surface Plot Illustrates the Interaction Between CoFeO/MgO-Al_2O_3 Concentration and Temperature on NH_3 Conversion Efficiency (%) and (b) Two-Dimensional (2D) Contour Plot Representing the Same Data 111

Figure 4.19 Optimization and Validation of NH_3 Conversion: (a) Predicted NH_3 Conversion from the BBD Model Based on Response Surface Methodology (RSM); (b) Experimental Results Validating the Predicted Conversion Rate 112

Figure 4.20 Kinetic Modelling of NH_3 Decomposition at Different Temperatures (450-650°C) Using (a) Pseudo-First Order (PFO) and (b) Pseudo-Second Order (PSO) Models 113

Figure 4.21 The Recyclability Performance of the Synthesized Catalyst Over Multiple Reaction Cycles 115

LIST OF ABBREVIATIONS

Abbreviations

$FeCl_2 \cdot 6H_2O$	Iron Chloride Hexahydrate
$CoCl_2 \cdot 6H_2O$	Cobalt Chloride Hexahydrate
$ZnCl_2 \cdot 6H_2O$	Zinc Chloride Hexahydrate
$MgCl_2 \cdot 6H_2O$	Magnesium Chloride Hexahydrate
Al_2O_3	Activated Alumina Beads
HCl	Hydrochloric Acid
C_2H_5OH, 99.9%	Absolute Ethanol
RSM	Response Surface Methodology
BBD	Box-Behnken Design
FE-SEM-EDX	Field Emission-Scanning Electron Microscope with Energy Dispersive X-Ray
XRD	X-Ray Diffractometer
BET	Brunauer-Emmett-Teller Method
TGA	Thermogravimetric Analysis
TPR	Temperature-Programmed Reduction
XPS	X-Ray Photoelectron Spectroscopy

LIST OF NOMENCLATURES

Nomenclatures

g	Gram
m	Millie
min	Minute
%	Percentage
mol	Mole
λ	Lambda
mL	Millilitre
M	Molarity
cm	Centimetre
m^2	Square Metre
cm^3	Cubic Centimetre
cm^2	Square Centimetre

CHAPTER 1
INTRODUCTION

1.1 Research Background

The growing global energy demand, driven by population expansion, rapid industrialization, and urbanization, has intensified dependence on fossil fuels. This dependence has resulted in critical challenges such as resource depletion, greenhouse gas emissions, and environmental degradation. The urgent need to mitigate these issues has shifted research focus toward clean and sustainable energy alternatives (Nailwal et al., 2024). Among these alternatives, hydrogen (H_2) has attracted substantial attention as a versatile and carbon-free energy carrier. The H_2 possesses a high gravimetric energy density (120 MJ kg^{-1}), produces only water as a byproduct upon combustion or electrochemical conversion, and can be utilized in various sectors including transportation, power generation, and chemical synthesis (Oliveira et al., 2025).

Despite its advantages, the widespread application of hydrogen remains constrained by storage, transportation, and distribution limitations, which hinder its large-scale deployment. To overcome these obstacles, indirect hydrogen storage through chemical carriers has been proposed. Several hydrogen carriers such as methanol, formic acid, and ammonia (NH_3) have been investigated. Among them, ammonia is considered one of the most promising due to its high hydrogen content (17.6 wt.%), carbon-free composition, well established industrial production and distribution infrastructure, and ease of liquefaction at moderate pressure (8 bar) or low temperature (-33 °C)(Hamid et al., 2025).

Ammonia can be decomposed thermostatically according to the endothermic reaction (Eq 1.1)

$$2\,NH_3 \rightarrow 3\,H_2 + N_2, \Delta H° = 92.4 kJmol^{-1} \quad (1.1)$$

The decomposition of ammonia into hydrogen and nitrogen ($2NH_3 \rightarrow 3H_2 + N_2$) provides a direct, carbon free route to produce high purity hydrogen suitable for fuel cell applications. However, the ammonia decomposition reaction is endothermic ($\Delta H°$ = 92.4 kJ mol^{-1}) and requires elevated temperatures (700 °C) to achieve significant

conversion(Weinand et al., 2021). Hence, the design of an efficient and thermally stable catalyst is critical for practical implementation. Although noble metal catalysts, particularly Ru-based systems, exhibit superior catalytic activity at relatively low temperatures, their high cost, limited supply, and susceptibility to poisoning impede commercialization. Consequently, extensive research has shifted toward non-noble metal catalysts notably Co, Fe, Ni, Cu and Zn based systems due to their abundance, low cost, and reasonable intrinsic activity (Li et al., 2024c).

Nevertheless, these base metal catalysts often suffer from low surface dispersion, weak metal support interactions, and structural instability at high temperature, leading to rapid deactivation and inconsistent performance. To overcome these challenges, mixed metal oxides and bimetallic systems have been explored to exploit synergistic effects between metal species. The formation of heterometallic interfaces can promote N-H bond activation, enhance reducibility, and improve resistance to sintering and nitridation. For instance, Co-Fe and Co-Zn oxide catalysts have demonstrated improved activity and durability compared with their single metal analogues(Wang et al., 2025). The support material plays a pivotal role in catalyst performance by influencing dispersion, reducibility, and acid base balance(Faheem et al., 2021a). In this context, MgO-Al_2O_3 mixed oxide has emerged as an effective support due to its high surface area, strong basicity, excellent thermal stability, and capacity to anchor metal nanoparticles uniformly. These properties collectively enhance active site accessibility and minimize particle agglomeration during prolonged reaction cycles(Weinand et al., 2021).

In the present research, mixed-metal oxide catalysts comprising single-metal (CoO, FeO, ZnO) and bimetallic (CoFeO and CoZnO) oxides supported on MgO-Al_2O_3 were synthesized via the hydrothermal carbonization (HTC) method. This synthesis route enables uniform distribution of metal precursors within the support matrix, leading to improved structural integrity and metal support interaction. The catalysts were systematically characterized using XRD, FESEM/EDX, BET, TGA, TPR, and XPS to elucidate their physicochemical and surface properties. The catalytic activity was evaluated in a fixed-bed reactor for ammonia decomposition under various operating conditions, with emphasis on optimizing temperature and gas hourly space velocity (GHSV). Subsequently, Response Surface Methodology (RSM) employing the Box-Behnken Design (BBD) was utilized to statistically model the process variables,

identify interactive effects, and determine the optimum catalyst composition and operating conditions.

In addition, kinetic modelling analysis were performed to understand the reaction mechanism and energetic feasibility. The motivation behind this study lies in addressing the urgent need for cost-effective and sustainable catalysts that can efficiently convert ammonia into hydrogen while maintaining long-term stability under demanding reaction conditions. By combining mixed-metal oxides with an optimized $MgO\text{-}Al_2O_3$ support, the research aims to enhance both the intrinsic catalytic activity and the durability of non-noble metal systems. The integration of experimental design (RSM) with comprehensive physicochemical characterization ensures a data-driven understanding of the synthesis structure performance relationship. On a broader scale, the findings of this study contribute to the ongoing global efforts toward a hydrogen-based energy economy and align with Malaysia's and the international community's commitment to achieving net-zero carbon emissions. Developing efficient ammonia decomposition catalysts not only supports future hydrogen refuelling and storage technologies but also provides an environmentally friendly pathway for sustainable energy conversion.

1.2 Problem Statement

Ammonia (NH_3) decomposition is a promising route for on-demand, carbon-free hydrogen production, yet its large-scale implementation remains constrained by the absence of efficient, durable, and economically viable catalysts. Noble metal catalysts, particularly ruthenium (Ru) and platinum (Pt), exhibit exceptional catalytic activity and stability at moderate temperatures. However, their high cost, limited availability, and susceptibility to sintering or poisoning severely restrict their large-scale application in hydrogen production systems (Fang et al., 2022).

To reduce costs and improve sustainability, non-noble metal catalysts such as cobalt (Co), iron (Fe), and zinc (Zn) have been explored as potential alternatives. However, these catalysts suffer from insufficient activity at low temperatures (below 400°C) and poor long-term stability, limiting their practical hydrogen production efficiency. The introduction of bimetallic catalysts (e.g., Co-Fe and Co-Zn) offers a potential solution to these limitations, providing enhanced catalytic activity and improved stability due to synergistic interactions between metal species.

Despite these advancements, many non-noble metal catalysts still suffer from low conversion efficiency, particularly at lower temperatures (below 400°C), and inconsistent performance across different reaction conditions, such as gas hourly space velocity (GHSV) and reaction temperature.

The performance of non-noble metal catalysts is significantly influenced by the choice of support material, which governs metal dispersion, active site stability, and acid base properties. Conventional supports such as alumina (Al_2O_3) or magnesia (MgO) alone often fail to provide the optimal balance between basicity, surface area, and thermal stability required for sustained catalytic activity. Hence, mixed oxide supports, particularly MgO-Al_2O_3, have gained attention due to their ability to stabilize metal nanoparticles and promote synergistic metal support interactions.

In addition, most previous studies on ammonia decomposition have relied on trial-and-error experimental approaches, lacking systematic optimization frameworks. The absence of integrated optimization tools, such as Response Surface Methodology (RSM), has resulted in poorly understood interactions among synthesis parameters and reaction conditions, further limiting the optimal composition and operational conditions for non-noble mixed-metal catalysts.

Given these challenges, there is a critical need to design and optimize cost-effective mixed-metal oxide catalysts, specifically focusing on the development of CoO, FeO, and ZnO-based mixed-metal catalysts supported on MgO-Al_2O_3. This study aims to address these gaps by systematically optimizing the catalyst design using RSM to improve catalytic performance and stability at lower temperatures, contributing to the feasibility of sustainable hydrogen production through ammonia decomposition.

1.3 Objectives of Study

The aim of this research is to develop cost effective, thermally stable, and highly active mixed-metal oxide catalysts for the catalytic decomposition of ammonia (NH_3) into hydrogen (H_2). Furthermore, this study aims to achieve the following objectives.

i) To synthesize single metal (CoO, FeO, ZnO) and bimetallic (CoFeO, CoZnO) oxide catalysts supported on MgO-Al_2O_3 using the hydrothermal carbonization (HTC) method.
ii) To characterize the physicochemical properties of the synthesized catalysts using XRD, FESEM, EDX, BET, TGA, TPR, and XPS.

iii) To evaluate the catalytic performance of the synthesized catalysts for NH_3 decomposition in a fixed-bed reactor under varying reaction conditions, including temperature and gas space velocity.

iv) To optimize NH_3 decomposition performance using Response Surface Methodology (RSM) by evaluating key thermocatalytic reactor parameters such as reaction temperature, NH_3 flow rate, and feed concentration, and to perform kinetic modelling to determine the most active catalyst and its optimal operating conditions.

1.4 Significance of Study

The decomposition of ammonia (NH_3) into hydrogen (H_2) offers a carbon free and sustainable pathway for clean energy generation. However, achieving high catalytic efficiency using non-noble metal systems remains a major challenge due to limitations in activity, stability, and reducibility. This research holds significant scientific and practical importance by addressing these limitations through the rational design of mixed-metal oxide catalysts and the integration of statistical optimization techniques.

The study explores the synergistic interactions between single metal (CoO, FeO, ZnO) and bimetallic (CoFeO, CoZnO) supported on MgO-Al_2O_3, which are expected to improve active site distribution, electron transfer, and structural stability. These interactions can generate a greater number of active sites, enhance N-H bond activation, and promote sustained catalytic performance at elevated temperatures. Furthermore, the mesoporous and thermally stable nature of the MgO-Al_2O_3 support contributes to superior metal dispersion, improved basicity, and resistance to sintering factors that collectively enhance the overall hydrogen yield and catalyst durability(Solanki et al., 2025).

The application of (RSM) represents another key contribution of this study. By employing the Box-Behnken Design (BBD), the research systematically investigates and quantifies the combined effects of key operational parameters, including reaction temperature, gas hourly space velocity (GHSV), and metal composition, on NH_3 decomposition efficiency. This approach replaces traditional one-factor-at-a-time experimentation with a statistically robust and data-efficient optimization framework, enabling accurate identification of optimal conditions and variable interactions. Additionally, the implementation of a fixed-bed reactor system allows catalyst

evaluation under conditions that closely mimic practical applications. The setup ensures precise control of temperature, GHSV, and catalyst loading, thereby providing realistic performance data for kinetic modelling validation. Such an integrated experimental approach strengthens the understanding of structure activity relationships and enhances reproducibility and scalability in catalytic research. From a broader perspective, this study contributes to the advancement of sustainable hydrogen production technologies by developing low cost, high performance non-noble metal catalysts for ammonia decomposition. The outcomes are expected to generate valuable insights for designing durable catalytic materials, guide future process optimization strategies, and support Malaysia's and global efforts toward a hydrogen based, carbon neutral energy future.

1.5 Scope of Research

This research focuses on the development of cost effective and efficient mixed-metal oxide catalysts for the decomposition of ammonia (NH_3) into hydrogen (H_2). The work emphasizes the potential of NH_3 as a carbon-free hydrogen carrier, owing to its high hydrogen content, ease of storage and transportation, and well-established global production and distribution infrastructure. The experimental scope encompasses the synthesis, characterization, catalytic evaluation, and optimization of both single-metal (CoO, FeO, ZnO) and mixed-metal (CoFeO, CoZnO) oxide catalysts supported on $MgO\text{-}Al_2O_3$, prepared via the hydrothermal carbonization (HTC) method. The synthesis phase involves controlling key parameters such as precursor concentration, synthesis temperature, and reaction time, which directly influence the physicochemical structure and catalytic properties of the resulting materials. Comprehensive characterization techniques are employed to determine the structural, morphological, and surface properties of the synthesized catalysts.

These include X-ray Diffraction (XRD) for phase identification, Field Emission Scanning Electron Microscopy (FESEM) and Energy Dispersive X-ray Spectroscopy (EDX) for surface morphology and elemental mapping, Brunauer-Emmett-Teller (BET) analysis for surface area and porosity, Thermogravimetric Analysis (TGA) for thermal stability, Temperature-Programmed Reduction (TPR) for reducibility behaviour, and X-ray Photoelectron Spectroscopy (XPS) for surface chemical states and oxidation profiles.

Catalytic performance is evaluated in a fixed-bed reactor system to ensure accurate and reproducible testing under controlled conditions. The evaluation focuses on the effects of reaction temperature, gas hourly space velocity (GHSV), and catalyst composition on ammonia conversion and hydrogen yield. The data obtained are further analyzed and optimized using RSM based on the Box-Behnken Design (BBD). This statistical modelling approach allows the identification of significant factors and interactions influencing catalytic performance. Moreover, kinetic modelling analysis are performed to gain deeper insights into the reaction mechanism and energetic feasibility of the optimized systems. The research scope is therefore confined to CoO, FeO, and ZnO supported on MgO-Al_2O_3 catalysts synthesized via the hydrothermal method. This research provides a structured and data-driven approach to developing and optimizing non-noble metal catalysts for efficient ammonia decomposition, thereby contributing to the advancement of sustainable hydrogen production technologies.

CHAPTER 2
LITERATURE REVIEW

2.1 Hydrogen as an Energy Source

In the review of the second chapter, over the past century, clean and sustainable energy technologies have been created and brought to market to help lessen the effects of global warming. As a sustainable response to the harm that the widespread use of fossil fuels has caused to the environment, renewable energy has drawn a lot of attention (Oliveira et al., 2025). However, due to the remote locations of energy production and consumption sites, the production of electricity using renewable resources is erratic, unpredictable, and geographically unbalanced, making it challenging to meet the world's energy demand. It is essential to design a new supply and demand system to address these temporal and spatial disparities. Hydrogen-based energy carriers can realistically replace carbon-based fuels due to high energy storage density which is shown in Figure 2.1. There are new, highly efficient technologies available for producing H_2 from a variety of hydrogen-based resources.

At a global scale, hydrogen is increasingly positioned not only as a chemical feedstock, but as the strategic backbone for next-generation energy systems. International Energy Agency (IEA) roadmaps indicate that low-carbon hydrogen consumption will expand from ~95 Mt/year currently to more than 500 Mt/year by 2050 if nations follow Net-Zero trajectories. Several regional industrial clusters in Europe, Japan, China and the Gulf region have already established national hydrogen strategies and created policy instruments such as “Hydrogen Valleys”, carbon pricing, feed-in premium mechanisms, and green hydrogen procurement contracts. The logic is not merely technical; it is also geopolitical. Renewable electrical energy generation is no longer the limiting factor, variability and storage have become the true bottlenecks. Hydrogen offers a unique benefit in that it can interconnect multiple sectors (“sector coupling”) power industry transport chemicals which allows electrons to be stored in molecular form and dispatched to hard-to-abate sectors (steel, shipping, aviation) where direct electrification is not feasible.

Furthermore, global market projections show that hydrogen-based fuels can become a globally traded commodity similar to LNG (Li et al., 2024c). In fact, multiple

techno-economic studies comparing Levelized Cost of Hydrogen (LCOH) vs LCOE from renewables conclude that hydrogen provides a more stable long-term storage vector because its marginal cost of storage decreases relative to battery energy storage at durations > 24 hours. Therefore, hydrogen is not merely an energy “option”; it is becoming a structural requirement for deep decarbonization. This explains the accelerating global investment in hydrogen-ready gas turbines, hydrogen pipeline retrofits, and international shipping routes for hydrogen carriers such as ammonia.The biggest obstacles to the commercialization of H_2 as a fuel without carbon emissions are still storage and transportation (Wang et al., 2025) H_2 has a very low liquefaction temperature (approximately -250 °C) and requires a large volume per unit mass compared to other gases because it is the lightest gas. To get around these problems, H_2 can be changed into a different substance (referred to as an energy vector) for secure transportation and storage, and it can then be recycled using endothermic reforming or thermal breakdown of NH_3 (Jawad et al., 2025).Because of its high volumetric energy density, relative affordability, and ease of liquefaction, storage, and transportation, ammonia NH_3 stands out among all the potential candidates as a particularly promising hydrogen carrier. Ammonia must first be broken down into H_2 and N_2, and then the H_2 must be separated and purified to produce hydrogen fuel. On the other hand, ammonia decomposition technologies and procedures are less advanced (Yuan et al., 2025).

Although hydrogen is the most abundant element in the universe, it is rarely found in its pure form on Earth and is instead bound within various compounds. Therefore, hydrogen production requires processes that separate it from other molecular structures (Solanki et al., 2025). Hydrogen can be sourced from a range of feedstocks from fossil-based materials such as coal, natural gas, and crude oil to renewable sources including biomass and water (Lee et al., 2024a). Currently, fossil fuels provide the most cost-effective route for hydrogen generation. However, concerns over their finite availability and negative environmental impacts have accelerated research into alternative production methods. For instance, in certain processes, carbon monoxide can be introduced into the water-gas shift reaction to increase hydrogen yield after gas separation steps. Pyrolysis, while considered a renewable method for hydrogen production, generates not only hydrogen but also carbon emissions, SO_x, and NO_x, along with various organic pollutants, posing environmental risks. In contrast, water splitting which utilizes renewable energy and emits no carbon represents a promising pathway for generating high-purity hydrogen in a sustainable manner (Fu et al., 2021a).

Electrolysis represents the most widely used approach for water splitting, although thermal and photocatalytic methods have also been investigated for hydrogen production. At room temperature, the electrochemical splitting of water requires a minimum thermodynamic voltage of 1.23 V to proceed. Since its development in the 18th century, water electrolysis technology has undergone steady improvements and is now employed in various industrial applications (AlAmoudi et al., 2024). The evolution of this technology can be broadly described in terms of five generational trends. A key advantage of electrochemical water splitting is its portability and ability to utilize widely available resources, such as tap water, to generate hydrogen for potential uses including vehicle power. Additionally, electrolysis systems are scalable and can be designed to operate across a wide capacity range, from a few kilowatts to multiple megawatts. Despite these benefits, the economic feasibility of electrolysis remains constrained by the relatively high cost of the required electricity compared to the value of the hydrogen produced. As a result, only about 3.9% of global hydrogen is currently derived from electrochemical water splitting (Shokry et al., 2014).

In parallel, hydrogen's role is increasingly evaluated within the future circular carbon economy. Rather than relying solely on direct combustion elimination, advanced energy systems envision hydrogen as the central reducing agent to simultaneously drive high-temperature industrial transformations and serve as indirect carbon mitigation enabler. For example, green hydrogen coupled to captured CO_2 can form synthetic fuels (e-methanol, e-kerosene) which allow existing supply chains to become progressively decarbonized without immediate infrastructure replacement. Moreover, techno-economic projections clearly show that 60-70 % of total abatement potential in shipping and aviation is unrealizable without a molecular energy carrier such as hydrogen or ammonia. Therefore, hydrogen is no longer positioned merely as a storage medium, but as a cornerstone molecule in deep industrial decarbonization pathways. These considerations justify the present research direction of replacing noble metals with non-noble transition metal catalysts for NH_3 cracking, since cost and durability are the eventual constraints for hydrogen carrier deployment at scale (Gonzalez et al., 2024).

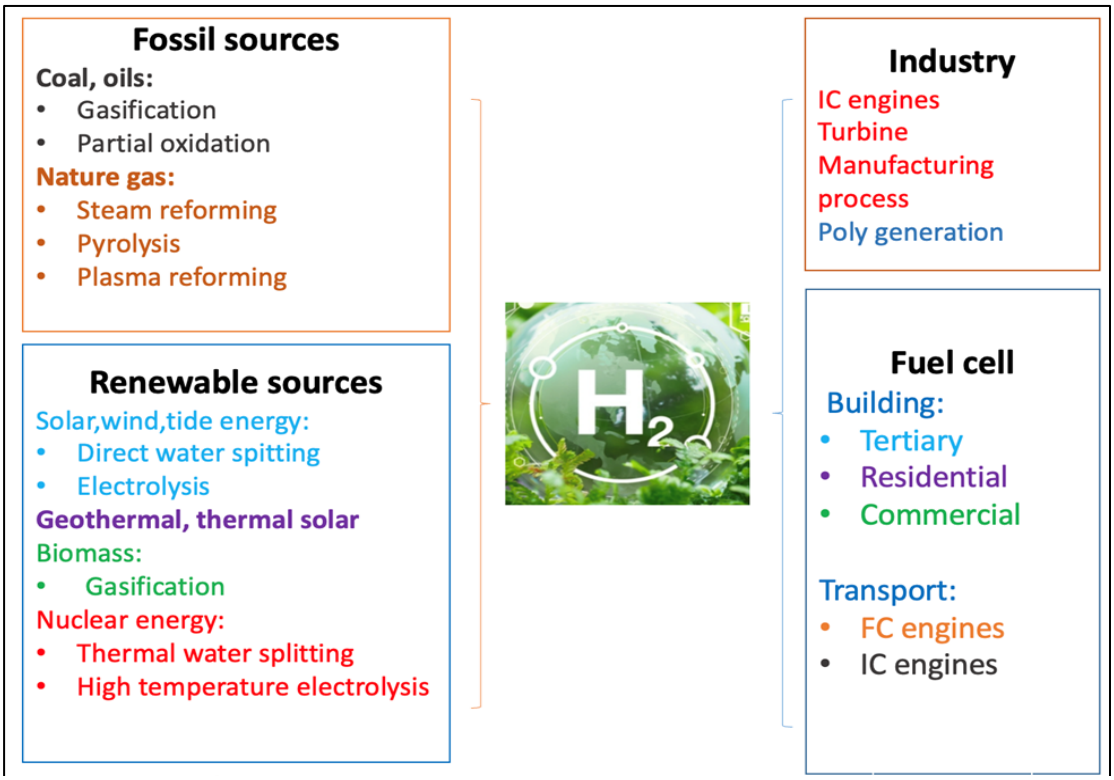


Figure 2.1 Hydrogen as an Energy Source (Hamid et al., 2025) (Adapted with Permission from Elsevier)

2.2 Storage of Hydrogen

A critical challenge in establishing a sustainable hydrogen economy is the development of efficient and reliable hydrogen storage systems (Charisiou et al., 2020). When evaluating storage methods and materials, multiple factors must be considered, such as high-pressure tank design, gravimetric and volumetric hydrogen densities, energy efficiency, refueling duration, system durability, cost, regulatory standards, technological maturity, and life cycle assessments (Jiang et al., 2024). Particularly for transportation applications, hydrogen must achieve a higher energy density to be viable. To meet this need, several storage approaches have been proposed, including liquefaction, compression, metal hydride formation, liquid organic hydrogen carriers (LOHCs), and conversion into energy-dense vectors like methanol and ammonia (Alharthi et al., 2024). Hydrogen interaction with storage materials involves various physical and chemical mechanisms such as molecular adsorption, diffusion, chemical bonding, van der Waals forces, and dissociation that enable its capture and release. Controlling parameters such as pressure, temperature, or electrochemical potential can influence surface structure and bonding strength, thereby facilitating hydrogen storage

in either molecular or ionic form. An overview of the hydrogen manufacturing process is illustrated in Figure 2.2.

Recent advancements in hydrogen storage systems have focused on optimizing both gravimetric and volumetric energy densities while improving the technical feasibility of large-scale deployment. Cryogenic liquefaction, although industrially mature, requires extremely low temperatures (-253 °C) and high energy input during liquefaction which significantly increases operational costs and limits practicality in decentralized hydrogen distribution networks (Meng et al., 2021). Furthermore, compressed H_2 gas storage at 350-700 bar demands thick-walled carbon-fiber tanks and contributes to higher capital investment in vehicle integration. In contrast, solid-state storage materials such as metal hydrides (e.g., MgH_2, $LaNi_5H_6$) demonstrate superior volumetric density compared to compressed gas; however, these materials often suffer from slow kinetics, high desorption temperatures, and poor cycle durability (Khosroshahi et al., 2024). Therefore, alternative storage methods based on physical or chemical carriers such as formic acid, methanol, sodium borohydride, and ammonia have received increasing attention. Ammonia has emerged as a strategically superior hydrogen vector because it is easily liquefied at mild conditions (-33 °C at 1 bar), it has high hydrogen content (17.6 wt%), and a globally established infrastructure already exists for its storage, transportation, and handling (Liu et al., 2022). Unlike compressed hydrogen, NH_3 can be transported using conventional pressurized tanks like LPG systems, which dramatically reduces the need for new capital infrastructure. Importantly, hydrogen can be regenerated through catalytic ammonia decomposition, releasing N_2 and H_2 without CO_2 emissions, making ammonia the most technically attractive hydrogen carrier for future decarbonized energy transitions (Tao et al., 2025). In addition, emerging research on materials such as nanoporous metal-organic frameworks (MOFs), carbon nanotubes (CNTs), and doped graphene-based sorbents has shown promising adsorption capacities due to enhanced surface area, tunable pore structures, and engineered active sites that promote reversible H_2 uptake (Lee et al., 2024). Nonetheless, scalability, desorption kinetics, and cost barriers remain critical barriers for industrial adoption. Thus, storage technologies are evolving toward hybrid concepts that combine chemical carriers, advanced nanostructured sorbents, and catalytic integration, enabling safe, compact, and energy-efficient hydrogen storage and release. Within this technological landscape, ammonia-based storage presents the strongest future potential because it simultaneously addresses production,

transportation, and end-use conversion barriers in a practical and economically viable manner. As a result, most industrial roadmaps for future hydrogen supply chains now position ammonia conversion and cracking processes at the center of next-generation hydrogen logistics frameworks.

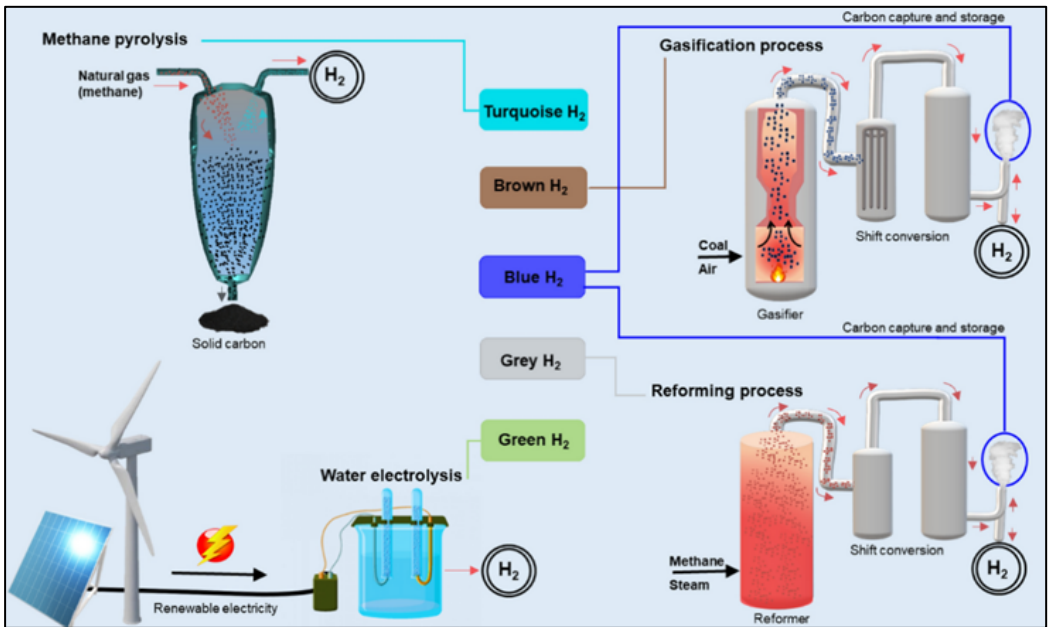


Figure 2.2 Hydrogen Manufacturing Process (Nailwal et al., 2024b) (Adapted with Permission from Elsevier).

2.3 Hydrogen Production

To mitigate the consequences of global warming, clean and sustainable energy solutions have been developed and introduced to the market throughout the past century. Renewable energy has gained significant attention as a sustainable answer to the environmental harm caused by the widespread use of fossil fuels (Nailwal et al., 2024). However, renewable power generation is inconsistent and geographically uneven, making it difficult to meet the world's energy demand (Shi et al., 2023). Hydrogen-based energy carriers offer a promising solution by having high energy storage density and efficient production methods available from a range of hydrogen-based resources (Fu et al., 2021). As we have established, storage and transportation remain significant barriers to commercializing H_2 as a carbon-free fuel (Gao et al., 2025). Being the lightest gas, hydrogen requires a larger volume per unit mass than other gases and has a low liquefaction temperature (about -250 °C) (Al Amoudiet al., 2024b; Ronduda et al., 2024). To overcome these issues, H2 can be converted into new materials (energy vectors) for safe transit and storage, such as ammonia (NH_3). This is particularly viable due to its high volumetric energy density, affordability, and simplicity of liquefaction,

storage, and transportation (Li et al., 2025). Ammonia decomposition methods need further development to support hydrogen fuel production (Duan et al., 2012). While hydrogen is a prevalent element in the cosmos, it is largely combined with other elements on Earth. This necessitates isolating it by breaking chemical bonds to obtain its pure form from other molecules (Koo et al., 2024).

Power-to-Hydrogen (P2H) pathways directly couple variable renewable electricity with electrolysis to generate H_2 that can be stored, transported, or reconverted to electricity ("power-to-power," P2P) via fuel cells, as depicted in Figure 2.3 In practice, wind and photovoltaic sources feed rectifiers to deliver stable DC to the electrolyzer stack, minimizing ripple that accelerates electrode degradation (Alekseev & Nilsson, 2024a) Among commercial electrolyzers, alkaline (AEL) systems are mature and low-cost but operate at modest current densities; PEM units tolerate fast load-following, reach higher differential pressures, and are favored in hybrid wind/solar plants; solid-oxide (SOEC) devices run at 600-850 °C and can achieve the highest electrical efficiency by internally utilizing heat, albeit with stricter materials constraints (Zhao et al., 2024a). Typical lower-heating-value electrical efficiencies are ~58-65% for AEL, ~60-70% for PEM, and >70% (electric-only) for SOEC when thermal integration is effective (Saeidi et al., 2023a). The co-product O_2, shown routed to storage in (Figure 2.3), can be valorized (medical/industrial oxygen or oxycombustion), improving system economics (Emam et al., 2024).

Because renewable output is intermittent, H_2 serves as a long-duration storage medium with near-lossless standing storage compared with batteries, which self-discharge over weeks. Pressurized tanks (short-term buffering), underground caverns (seasonal storage), or conversion to energy vectors (NH_3, LOHCs) extend reach to mobility and industry (Shah et al., 2024). In the P2P branch, proton-exchange-membrane fuel cells reconvert H_2 to electricity and water at point-of-use; round-trip (electrolyzer storage fuel cell) electrical efficiency is typically 30-45%, but system-level exergy is improved when by-products (O_2, heat) are recovered (Jung & Chung, 2024). Alternatively, power-to-ammonia (P2A) synthesizes NH_3 that can be shipped globally and cracked where high-purity H_2 is needed; this thesis focuses on improving the decomposition (cracking) step via non-noble catalysts to unlock that pathway. Overall, emphasizes three design levers that dominate the techno-economics of renewable H_2: (i) electrolyzer dynamics and efficiency under variable load, (ii) buffering/storage choice that matches temporal mismatch between generation and demand, and (iii)

conversion back-ends (fuel cell or NH_3 cracking) that minimize kinetic and transport penalties. By targeting faster N-H bond activation with robust mixed-oxide catalysts, the present work addresses lever (iii), enabling ammonia to function as a practical, carbon-free hydrogen carrier tightly integrated with renewable electricity systems (Lee et al., 2024c). H_2 can be generated from various sources, including renewable resources such as biomass and water and fossil fuels like coal, natural gas, and crude oil (Abdullah et al., 2020). Once gaseous products are separated, CO can be added to enhance the H_2 yield through the water gas shift reaction, which increases the efficiency of hydrogen production (Cerrillo et al., 2022a). Among the techniques for high purity hydrogen production, water splitting is particularly promising, utilizing renewable resources and producing no carbon dioxide emissions (Kim et al., 2022) Electrolysis remains the most prevalent method, supplemented by thermal and photocatalytic processes. This method requires a cell voltage of 1.23 V at ambient temperature and has been advanced and implemented industrially since the 18th century (Cechetto et al., 2021). Electrolysis is versatile and scalable from a few kilowatts to several megawatts. However, it accounts for only 3.9% of hydrogen production as the cost of the required electricity often outweighs the value of the hydrogen produced (Jolaoso et al., 2018).

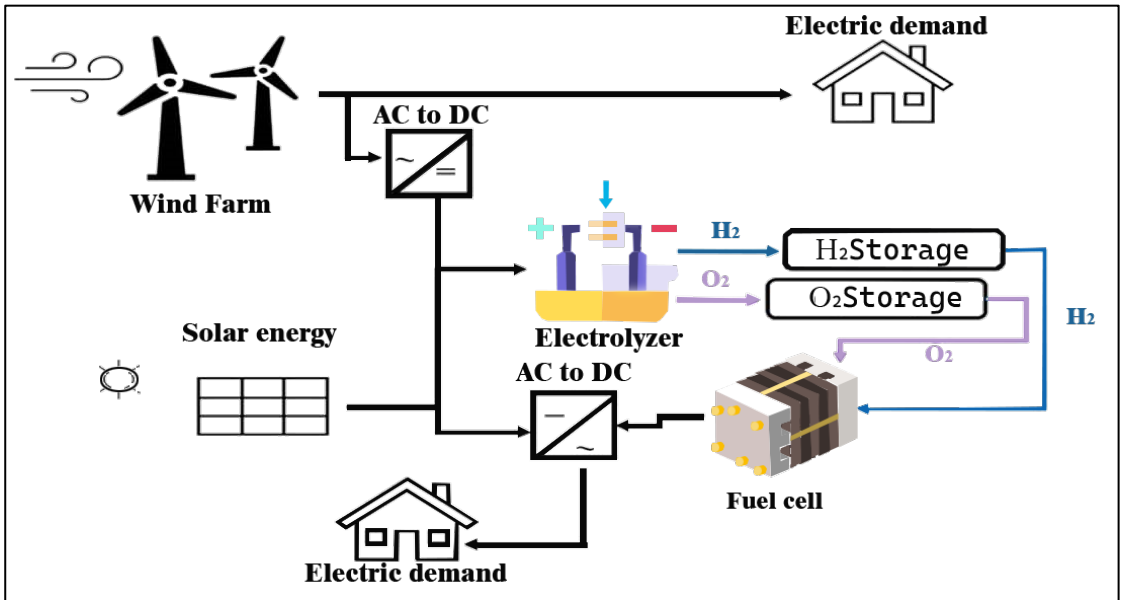


Figure 2.3 Hydrogen Production Process (Hamid et al., 2025) (Adapted with Permission from Elsevier)

To mitigate the consequences of global warming, clean and sustainable energy solutions have been developed over the past century. Renewable energy has gained significant attention as a sustainable answer to the environmental harm caused by fossil

fuels (Nailwal et al., 2024). However, renewable power generation is often inconsistent and geographically uneven, making it difficult to meet global energy demand (Shi et al., 2023). Hydrogen-based energy carriers offer a promising solution due to their high energy storage density and diverse production pathways (Fu et al., 2021). Nevertheless, storage and transportation remain barriers to commercializing hydrogen as a carbon-free fuel because it is the lightest gas, requiring large volumes and very low liquefaction temperatures (Al Amoudi et al., 2024b; Ronduda et al., 2024). One solution is to convert hydrogen into energy vectors, such as ammonia (NH_3), which has high volumetric energy density, is affordable, and is relatively simple to liquefy, store, and transport (Li et al., 2025). Developing efficient ammonia decomposition methods is crucial to unlock hydrogen fuel production from these energy vectors (Duan et al., 2012).

In contrast, catalytic ammonia decomposition converts NH_3 into H_2 and N_2 at 500–900 °C with high volumetric energy density and safe storage. This method was selected for this study because it allows monodirectional hydrogen production, high efficiency, scalability, and integration with renewable electricity systems. Existing catalysts often show low activity at lower temperatures, rapid deactivation, and limited reusability. This study focuses on Co-Fe-Zn mixed-metal catalysts supported on MgO-Al_2O_3, optimized via RSM and reactor considerations to enhance activity, stability, and hydrogen yield. Bimetallic interactions improve N-H bond cleavage and metal dispersion, while mixed oxide supports enhance thermal stability and active site availability (Marcoberardino et al., 2017).

2.3.1 Hydrogen Production from Ammonia

Its component elements are H_2 gas, and N_2 (Liu et al., 2024). Endothermic in nature, this reaction needs the input of energy, and it takes place at high temperatures, usually between 500 and 900 °C. Usually, a catalyst is used in this procedure to quicken the pace of the response. The equation can be used to express the process's chemical reaction. Clean H_2 can be easily produced by NH_3's breakdown. All that is required is a suitable catalyst that is robust, scalable, and extremely active. A well-thought-out catalyst design is essential for using ammonia as a clean future of energy (Ouabi et al., 2024). NH_3 will be used as an energy vector in both present and future technologies to create a green hydrogen economy.

The conventional (Haber-Bosch) process depends on H_2 generated through the thermal or catalytic cracking of fossil fuels over metal-based catalysts at temperatures

between 400 and 500 °C and pressures between 15 and 30 MPa. The (Haber-Bosch) process's overall energy usage makes up about 2% of the world's energy production. Furthermore, methane steam reforming is the primary method used in the (Haber-Bosch) process to produce H_2, which has a significant impact on greenhouse gas emissions (Aker & Ayas, 2023). Figure 2.4 shows the function of ammonia as an energy vector in present and future technologies, contributing to the establishment of a green hydrogen economy. Technological advances in large-scale water electrolysis have shown encouraging outcomes to produce green hydrogen on a commercial scale. Carbon-free solar and wind energy can be used to generate electricity, which can then be used to establish a sustainable water electrolysis process.

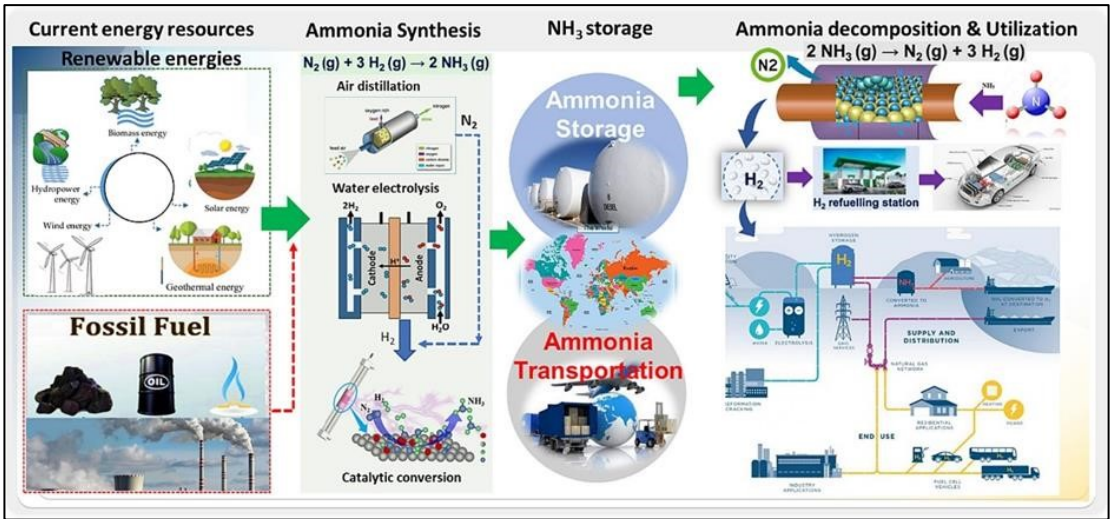


Figure 2.4 Important Role of NH_3 as an Energy Carrier in Current and Future Energy Systems (Chen et al., 2023)

2.4 Ammonia Decomposition

Ammonia decomposition is a well-established reaction that proceeds at elevated temperatures, either in the presence or absence of a catalyst. A comparative summary of ammonia decomposition methods is provided in Table 2.1. Research has demonstrated that catalytic decomposition can dissociate ammonia into hydrogen and nitrogen in an environmentally benign manner. Due to its scalability, this catalytic approach is suitable for integration into ammonia-cracking reactors for hydrogen generation. In another study, (Amiri et al., 2020) outlined the historical development and various techniques for NH_3 decomposition, particularly in the context of industrial hydrogen production.

Studies in this field commonly investigate the influence of reaction parameters such as temperature, pressure, and catalyst composition on decomposition efficiency.

Beyond conventional thermal catalysis, alternative activation methods have been proposed, including the use of electric currents, electron beams, ionic bombardment, microwaves, plasma, and solar energy to supply the required activation energy. Integrated systems that combine ammonia decomposition with complementary chemical processes have also been explored. Many of these methods, which can operate with or without catalysts, are specifically designed to minimize carbon emissions.

Table 2.1
Comparison Method for NH_3 Decomposition Process

Decomposition Methods	Description of decomposition	NH_3 Decomposition Temperature	Surface Material	Ref.
Catalytic Decomposition	Environmentally friendly method to utilize catalysts to break down NH_3 into hydrogen and nitrogen	700 to 1000 °C	Metals or metal alloys	(Zhou, et al., 2024)
Electrolysis Decomposition	Utilizes electrochemical processes for breaking down ammonia and involves an electrolytic cell where ammonia is split into hydrogen and nitrogen	200 to 500°C	Electrochemical cells and catalyst	(Su et al., 2024)
Solar Energy Decomposition	Suggested as a potential source of activation energy particularly in solar technologies	Starts at 700 K (approx. 427°C)	Catalyst	(Do et al., 2023)
Decomposition with plasma technologies	Proposed as a source of activation energy	Temperature varies between 400 °C and 700 K (approx. 427°C)	-	(Arsad et al., 2024)
Thermal Decomposition	Ammonia can decompose at high temperatures, either with or without catalysts.	Starts at 700 K, highly reactive	Quartz, SUS304 (Stainless Steel)	(Horri & Ozcan, 2024)

A study by Yadav et al., (2024) demonstrated that surface reactions are critical to the thermal decomposition of ammonia, noting that such reactions can proceed even

on materials conventionally considered inert, such as quartz. The research further revealed that stainless steel actively facilitates ammonia decomposition, primarily through the formation of iron nitride on its surface. These findings have important implications for the optimization of reaction kinetics in systems where ammonia is utilized as a hydrogen carrier and clean fuel. A schematic representation of catalytic ammonia decomposition into nitrogen and hydrogen is provided in Figure 2.5 found that the surface reactions of ammonia play an important role in its thermal decomposition, and these reactions can occur even on supposedly inert surfaces such as quartz. The study also highlights the reactivity of stainless steel in facilitating ammonia decomposition, specifically through the formation of iron nitride. These results carry important implications for understanding and optimizing the kinetics of ammonia as a hydrogen carrier and clean fuel and Figure 2.5 shows the catalytic NH_3 decomposition into N_2 and H.

In recent years, special attention has been directed toward understanding the mechanistic pathway of NH_3 decomposition at the atomic scale because the reaction does not simply depend on temperature,but strongly depends on the type of active metal site, metal oxidation state, coordination environment, and N-H bond activation pathway (Yadav et al., 2023). The overall reaction mechanism generally proceeds through stepwise dehydrogenation of adsorbed NH_3 molecules: $NH_3 \rightarrow NH_2 \rightarrow NH \rightarrow N^*$, followed by combinative desorption of N* to N_2 gas (Ahmad & Yadav, 2024). For the first hydrogen abstraction step ($NH_3 \rightarrow NH_2$), the activation barrier is typically the highest, and thus metals that can easily donate electrons to the antibonding orbital of N-H bond (e.g., Co, Fe, Ru) accelerate the rate-determining step (Cheng et al., 2023)**.** Multiple DFT investigations have shown that non-noble metals, especially cobalt, can approach the activation capability of Ru under specific electronic tuning, such as alloy formation, oxygen vacancy engineering, or strong metal support interactions (Ouabi et al., 2024)**.** Moreover, mixed oxide supports can modulate basicity, surface electron density, and metal electron back donation, which can suppress poison formation (e.g. metal nitrides) and enhance turn-over frequency (Afzali & Keshavarzi, 2024)**.**

Hydrogen is also produced industrially via steam reforming of hydrocarbons, which remains the most established method. Methane and water react over Ni-based catalysts at high temperatures (700–1100 °C) to produce H_2 and CO, followed by the water-gas shift reaction to generate additional hydrogen. While industrially mature, this method relies on fossil fuels and emits CO_2, necessitating carbon capture and storage

(CCS) to reduce emissions (Yadav et al., 2024). Improvements focus on catalyst innovations, operating at reduced temperatures, and integrating CCS to lower energy inputs and emissions (Jeje et al., 2024; Zainal et al., 2024). Process intensification in reformers and water-gas shift sections, along with downstream purification (pressure-swing adsorption), ensures fuel-cell-grade hydrogen with ≥99.9% purity (Cerrillo et al., 2022). Catalyst deactivation arises from carbon deposition, sulfur poisoning, and Ni sintering, mitigated by surface promoters and robust supports (Liu et al., 2020; Felice et al., 2023). These constraints motivate parallel development of green routes, such as ammonia decomposition.

Biomass gasification thermochemically converts agricultural residues, municipal waste, and coal into syngas (H_2, CO, CO_2, CH_4) at 800–1200 °C. The water-gas shift reaction can further enhance hydrogen yield (Kuttin et al., 2024). Flexibility in feedstock selection, integration with CCS, and catalyst engineering improve sustainability and efficiency (Fu et al., 2019; Lucentini et al., 2021). Challenges include tar formation, alkali contamination, and catalyst poisoning, addressed via pre-treatment, torrefaction, pelletization, leaching, and catalytic reforming with Ni, Co, Fe, or mixed oxides (Meng et al., 2024). Advanced membranes and PSA units ensure high-purity hydrogen streams, making biomass gasification a robust pathway when integrated into modular H_2 platforms.Autothermal reactors (ATR) combine partial oxidation and steam reforming in a single reactor, achieving self-sustaining thermal balance and improved energy efficiency (Amin, 2024). ATRs typically operate at 800–1000 °C, using Ni-based catalysts; however, these suffer from coke formation, sintering, and sulfur poisoning. Bimetallic catalysts (Ni-Co, Ni-Ru, Ni-Fe, Ni-Mo) on mixed-oxide supports (CeO_2-ZrO_2, MgO-Al_2O_3, La_2O_3-Al_2O_3) improve stability and oxygen mobility, enhancing hydrogen yield (Zhang et al., 2023). Computational modeling guides ATR design, optimizing heat transfer and active sites, while techno-economic assessments show ATR plus CCS lowers levelized hydrogen costs compared to standalone steam reforming or electrolysis (Molinari et al., 2014).

Photochemical water splitting uses solar energy to dissociate water into H_2 and O_2 using semiconductor photocatalysts such as TiO_2 and CdS, often enhanced with co-catalysts (Ahmed & Mohamed, 2024; Pattana yak et al., 2022). It is sustainable and carbon-free but faces low solar-to-hydrogen efficiency, limited stability, and scale-up challenges. Ongoing research targets nanostructured photocatalysts and hybrid integration with renewable energy systems. Water electrolysis splits water using

electrical energy, producing H_2 and O_2. When coupled with renewable electricity, it achieves near-zero carbon emissions and grid-balancing capabilities (Arsad et al., 2024; Emam et al., 2024). PEM and SOE electrolyzers improve efficiency and durability, though energy costs remain high (Jolaoso et al., 2018; Cechetto et al., 2021).

In addition, NH_3 decomposition at industrial scale is highly sensitive to heat transfer, gas hourly space velocity (GHSV), and catalyst bed architecture. Fixed-bed reactors historically dominated NH_3 cracking research, but in last 4 years, microreactor systems, membrane reactors, and catalytic membrane reformers have been reported to achieve higher hydrogen purity with simultaneous in situ N_2 separation (Ouardi et al., 2024). Furthermore, energy integration studies indicate that coupling NH_3 cracker modules with green electricity, solar thermal reactors, or high temperature PEM electrolyzer waste heat can reduce overall energy penalty of cracking by up to 27% compared with stand-alone reactor operation (Zhou et al., 2020). Advanced process modelling using Aspen HYSYS and CFD simulation tools now allows predictive design for millisecond-contact time reactors, which are being explored for on-board ammonia crackers for maritime applications, aviation refuelling, and stationary micro-grid hydrogen supply (Jia et al., 2022). Catalyst deactivation is another critical issue. Most non-noble catalysts suffer from surface nitride formation, sintering at >700 °C, or metal particle agglomeration which reduce metal dispersion and block active sites. Current research strategies to overcome deactivation include (i) bimetallic alloying, (ii) tuning oxygen vacancies, (iii) anchoring metals into spinel lattices, and (iv) using structured supports such as foams and lattices.These recent developments clearly demonstrate that ammonia decomposition is evolving from fundamental laboratory studies to integrated system engineering, with increasing emphasis on catalyst stability, reactor miniaturization, and hybrid renewable energy coupling. Therefore, understanding the interplay of metal electronic structure, support chemistry, and reactor engineering is essential to accelerate commercial adoption of NH_3 as a carbon-free hydrogen carrier (Chen & Kyprianidis, 2024).

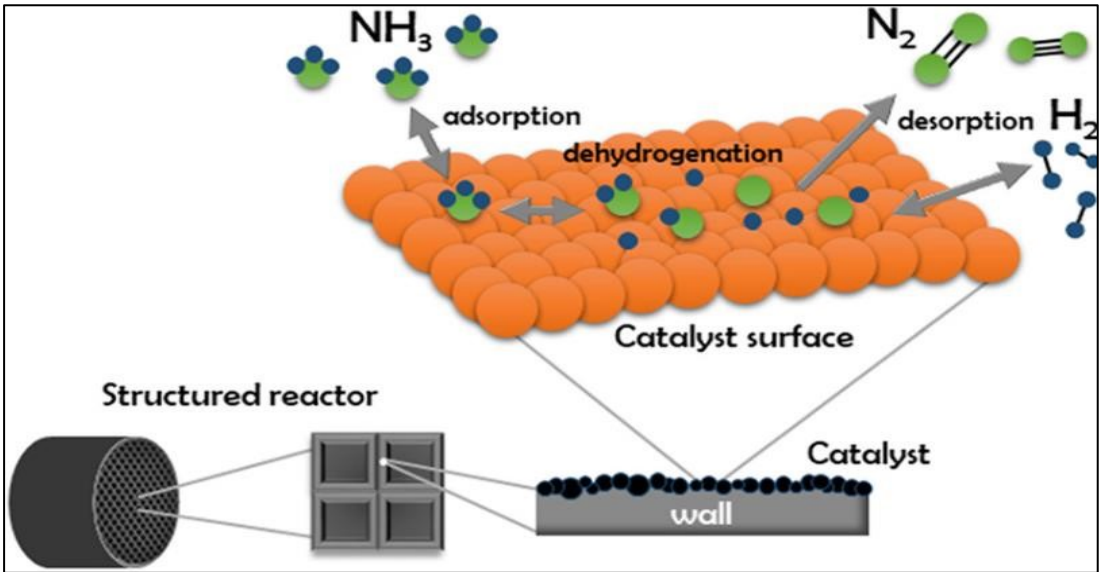


Figure 2.5 Catalytic NH_3 Decomposition into N_2 and H_2 (Faheem et al., 2021)

Introduced a low-cost catalyst based on cobalt and copper (Co-Cu) for solar-thermal ammonia decomposition, (Nemitallah et al., 2024) reporting both high efficiency and a significant reduction in energy consumption. This catalyst substantially increases the rate of hydrogen generation, presenting a promising advancement for solar-powered hydrogen fuel cells. In a separate investigation, (Falascino et al., 2024) examined ammonia decomposition via air plasma, a process that enables nitrogen recycling through conversion to ammonium nitrate (NH_4NO_3). Their study highlighted the importance of temperature variation in the catalytic breakdown of ammonia into hydrogen, a reaction facilitated by a ruthenium (Ru) catalyst supported on silica (SiO_2). Together, these works offer valuable insights into efficient ammonia decomposition and nitrogen recovery for sustainable hydrogen production.

Despite extensive research on ammonia decomposition, most current catalysts face significant challenges. Non-noble metal catalysts often show low activity at moderate temperatures, limiting hydrogen production efficiency. They also suffer from rapid deactivation during repeated cycles, poor dispersion, and insufficient interaction with support materials, resulting in reduced stability and reusability. Noble metal catalysts, although highly active, are expensive and scarce, making them impractical for large-scale applications. To address these limitations, this study develops Co-Fe-Zn mixed-metal catalysts supported on $MgO\text{-}Al_2O_3$, designed to achieve high NH_3 conversion, improved thermal stability, and repeated-cycle durability. Table 2.2 summarizes the key catalysts reported in recent studies, their operating conditions,

limitations, and the research gaps addressed by this study, highlighting how the proposed catalysts overcome deficiencies in activity and stability.

Table 2.2
Comparison of Selected Ammonia Decomposition Catalysts Highlighting Temperature, Conversion, Stability/Reusability, and Research Gaps Addressed by This Study

Catalyst Type	NH_3 Decomposition Temp (°C)	Conversion (%)	Stability Reusability	Research Gap	Reference
Ni-based	700–1000	75–80	Poor	Stability improvement	Zhou et al., 2024
Ru-based	500–900	85–95	Moderate	Cost-effective alternative	Su et al., 2024
Co-based	600–850	70–78	Low	Reusability & activity improvement	Do et al., 2023

2.4.1 Reaction Mechanism of NH_3 Decomposition

The activation energy for the ammonia (NH_3) decomposition reaction is determined by the stepwise removal of the three hydrogen atoms bonded to nitrogen, as represented in Eq. 2.2 to Eq. 2.4. A detailed summary of the corresponding reaction energies and activation barriers on various catalyst surfaces is provided in (Table 2.3).

$$NH_3 \rightarrow NH_2 + H\bullet \quad (2.2)$$

$$NH_2 \rightarrow NH + H\bullet \quad (2.3)$$

$$NH \rightarrow N + H\bullet \quad (2.4)$$

According to (Falascino et al., 2024) investigated the catalytic decomposition of ammonia, with a focus on energy requirements, thermodynamic behavior, and the

underlying reaction mechanism on catalyst surfaces. The initial step of the process, represented in Eq. 2.1, involves the adsorption of NH_3 onto the catalyst. Upon removal of the first hydrogen atom, the final state consists of adsorbed NH_2 and H species. Reported distances for the detached hydrogen and nitrogen atoms from the surface are 2.37 Å and 2.60 Å, respectively. The NH_2 and H fragments were observed to preferentially bind near metal sites on the surface. The corresponding activation energies for this step are 1.52 eV and 1.22 eV, respectively. According to (Okolie et al., 2021), this step is endothermic, with reaction energies of 1.43 eV and 0.49 eV on the catalyst surface. The study further identified the most stable adsorption geometry for NH_2 on the catalyst. Removal of a second hydrogen atom as the final state, as shown in Eq. 2.8. During this step, the hydrogen atom traverses a distance greater than the activation energy barrier. The reported distances of nitrogen atoms from the surface are 2.62 Å and 2.15 Å, with activation energies of 0.72 eV and 2.05 eV, respectively. This reaction step was also determined to be endothermic, with reaction energies of 0.42 eV and 1.54 eV on the catalyst surfaces.

A summary of the reaction and activation energies for all steps during catalytic ammonia decomposition is presented in Table 2.3.

Table 2.3
Reaction and Activation Energies on the Catalyst Surfaces During the NH_3 Decomposition Process

Reaction Step	Reaction Energy (eV)	Activation Energy Ea/eV	Ref.
$NH_3 \rightarrow NH_2 + H$	1.52 (Cu)	1.43 (Cu)	
$NH_2 \rightarrow NH + H$	0.72 (Cu)	0.42 (Cu)	(Karka & Kamesh, 2024)
$NH \rightarrow N + H$	0.64 (Cu)	0.14 (Cu)	
$NH_3 \rightarrow NH_2 + H$	1.22 (Pt)	0.49 (Pt)	
$NH_2 \rightarrow NH + H$	1.22 (Pt)	1.54 (Pt)	(Hussain et al., 2023)
$NH \rightarrow N + H$	2.78 (Pt)	2.33 (Pt)	
$NH_3 \rightarrow NH_2 + H$	–0.97 (Mo)	–1.18 (Mo)	

$NH_2 \rightarrow NH + H$	–3.11 (Mo)	–3.67 (Mo)	(Joshi et al., 2024)
$NH \rightarrow N + H$	–5.11 (Mo)	–5.96 (Mo)	

In the final decomposition step ($NH \rightarrow N + H$), a hydrogen atom dissociates from the nitrogen atom adsorbed on the metal catalyst surface, as shown in Eq. 2.3. The reported distances between the nitrogen and hydrogen atoms relative to the catalyst surface are 2.56 Å and 2.52 Å, respectively. For this step, (Mekaoui et al., 2024) determined the activation energy to be 2.78 eV and the reaction energy to be 0.64 eV. Positive reaction energy values (+0.14 eV and +2.33 eV) confirm the endothermic nature of the process on the studied catalyst surfaces. These energy values reflect the thermodynamic favorability of the reaction on different catalysts. Lower activation and reaction energies generally indicate a more favorable reaction environment, whereas higher energies suggest greater energetic barriers and reduced likelihood of the reaction proceeding. Such differences often arise from distinct catalyst properties, such as surface structure, electronic effects, and metal-support interactions (Sikiru et al., 2024).

2.4.2 Reaction Kinetics of Ammonia Decomposition

A significant body of research has examined the kinetics of ammonia decomposition, employing various catalysts to derive rate expressions and elucidate the underlying reaction mechanisms. Early kinetic models often described the decomposition using first-order kinetics, an approach that remains applicable in certain contexts. However, more recent studies indicate a more complex picture, with some researchers proposing mixed zero- and first-order kinetics, especially when accounting for the inhibitory effect of hydrogen on the reaction. The accumulation of adsorbed hydrogen on the catalyst surface, as observed through multiple experimental techniques, supports this view (Godfrey et al., 2024). Among the established kinetic frameworks, the Temkin–Pyzhev model identifies the desorption of adsorbed nitrogen as the rate-limiting step and describes the reaction rate using a power-law expression when the reverse reaction is negligible. Alternatively, the Tamaru model emphasizes that the choice of kinetic model should depend on the specific temperature and pressure conditions of the system (Nemitallah et al., 2024).

Hernández et al., (2024) validated one such expression on a particular catalyst and demonstrated its applicability to other catalytic systems. Parameter estimation is typically carried out by evaluating different kinetic expressions derived from a quasi-equilibrium approach, where each elementary step is successively treated as rate-limiting while the others are assumed to be at equilibrium. The widely referenced mechanism proposed by Temkin begins with ammonia adsorption onto the catalyst surface, proceeds through sequential dehydrogenation steps, and concludes with the desorption of nitrogen and hydrogen atoms, ultimately forming N_2 and H_2 (Eqs. 2.5-2.10). In the equations below, 's' denotes an empty site on the catalyst surface, and the subscript '(a)' indicates an adsorbed species.

$$NH_3\ (g) \leftrightarrows NH_3\ (a) \tag{2.5}$$

$$NH_3\ (a) \leftrightarrows NH_2\ (a) + H\ (a) \tag{2.6}$$

$$NH_2\ (a) \leftrightarrows\ \ NH\ (a) + H\ (a) \tag{2.7}$$

$$NH\ (a) \leftrightarrows N\ (a) + H\ (a) \tag{2.8}$$

$$2N\ (a) \leftrightarrows N_2\ (g) + 2s \tag{2.9}$$

$$2H\ (a) \leftrightarrows\ \ H_2\ (g) + 2s \tag{2.10}$$

Initially, the rate-limiting step in ammonia decomposition was thought to be N–N bond cleavage in the nitrogen molecule. However, subsequent studies have identified the associative desorption of N_2 from the catalyst surface as the primary limiting step in many systems. Research examining reaction rates across various catalysts including Ni, Co, Rh, Pt, Ru, and Fe has shown that nitrogen desorption generally governs the overall rate, regardless of the metal used. However, the specific characteristics of each catalyst can shift the rate-determining step. For noble metals such as Ru, Rh, Ir, Pt, Pd, and Cu, cleavage of the N–H bond is often proposed as the limiting step, whereas for transition metals like Fe, Co, Ni, and Cr, nitrogen desorption tends to be limiting.

Experimental results for Ni and Ru illustrate this distinction (Hernández et al., 2024) demonstrated that for Ni, complete ammonia dehydrogenation acts as the rate-limiting step, whereas for Ru, nitrogen desorption is limiting due to its higher energy requirement. This difference underscores the significant influence of the catalyst support and metal–support interactions on the reaction mechanism. For Ni, especially in strongly interacting supports with low Ni–N bond energies, nitrogen desorption controls the rate via ammonia dehydrogenation pathways. Analysis of metal–nitrogen (M–N) binding energies reveal further trends. For surfaces with M–N binding energies below approximately 125 $kJ \cdot mol^{-1}$, removal of the second hydrogen atom Eq. 2.6 is rate-determining. For surfaces with higher M–N binding energies, the removal of the first and second hydrogen atoms Eqs. 2.5–2.6 as well as nitrogen desorption Eq. 2.8 become kinetically significant. This relationship has been used to predict catalytic activity in bimetallic systems, though nitrogen binding energy alone is insufficient to fully explain activity trends. For example, bimetallic Ni–Pt and Ni–Ru pairs exhibit different catalytic activities despite similar nitrogen binding energies. Studies comparing monometallic Ni and Pt with bimetallic Pt–Ni–Pt show a reduction in activation energy for the bimetallic form, and while molybdenum nitride binds nitrogen more strongly than molybdenum carbide, the latter exhibits higher activity due to a greater number of active sites.

Further kinetic investigations indicate that the reaction rate is influenced by both hydrogen and ammonia partial pressures, with nitrogen desorption remaining the rate-limiting step across a wide temperature range Eq. 2.9. (Sharifishourabi et al., 2024) observed that for some catalysts, the rate-determining step can shift from nitrogen desorption to final dehydrogenation Eqs. 2.6–2.7 depending on temperature. For metals such as Pt, Ni, and Rh, apparent activation energies can vary significantly with temperature. For example, Fe catalysts show an apparent activation energy of about 188 $kJ \cdot mol^{-1}$ up to ~370 °C, increasing to 210 $kJ \cdot mol^{-1}$ above 440 °C, with the rate plateauing near 580 °C, indicating a temperature-independent regime. Similar trends are observed for Ni, Mo, and Fe, where apparent activation energies shift for instance, from 83 $kJ \cdot mol^{-1}$ below 475 °C to 77 $kJ \cdot mol^{-1}$ at higher temperatures, comparable to trends seen with Ru/Al_2O_3. Variations in the reaction orders with respect to NH_3 and H_2 across temperature ranges further suggest complex kinetics, including temperature-dependent hydrogen inhibition.

At low temperatures, N–H bond cleavage typically governs the rate when the reaction follows an associative mechanism. At high temperatures, the rate becomes proportional to ammonia adsorption, and nitrogen desorption re-emerges as the limiting step. (Maleki et al., 2024) compared Pt and Fe catalysts, finding that Fe exhibits strong hydrogen inhibition, whereas Pt shows inhibition only at high pressures and low temperatures. For Ru, decomposition follows approximately first-order kinetics in ammonia with negligible hydrogen inhibition below 320 °C. These behaviors along with those of Fe, Co, and Fe–Co bimetallic catalysts highlight intrinsic differences among metals. For Fe, ammonia adsorption is limiting; for Co, both N–H cleavage and N_2 desorption are slow; and for Fe–Co bimetallic catalysts, nitrogen desorption is rate-limiting. Notably, bimetallic systems often demonstrate enhanced ammonia degradation potential compared to their monometallic counterparts. A summary of catalysts used in kinetic studies of ammonia decomposition and their associated rate-limiting steps is provided in Table 2.4.

Table 2.4
Catalysts Used for the Kinetics of Ammonia Decomposition, Elucidating the RateLimiting Step in the Reaction Mechanism

Catalyst	Rate-Limiting Step	Activation Energy (kJ mol^{-1})	NH_3 Conversion (%)	Reaction temp. (◦C)	Ref.
Ni	N_2 Desorption	21	-	440	(Evro et al., 2024)
Co	N_2 Desorption	70.8	96	450	(Gallenberger et al., 2023)
Fe	N_2 Desorption and for Fe, NH_3 adsorption is a limiting step.	8	100	450	(Karthik et al., 2024)
Mo	N_2 Desorption	77	-	-	(Karthik et al., 2024)
Ru	N_2 Desorption	83	99	475	(Kerschbaumer et al., 2023)
Rh	N_2 Desorption	-	-	370	(Dolganov et al., 2024)

Cu	N-H Bond Cleavage	317	-	450	(Liu et al., 2022)
Bimetallic Catalysts Fe−Co, Ni-Ru, NiFe, Mo-Co	Rate-limiting step varies with the composition and Bimetallic composition affects kinetics.	62-76	99.9	450-600	(Liu et al., 2022)
Noble Metals (Ru, Rh, Ir, Pt, Pd)	N-H Bond Cleavage and they have different rate-limiting steps.	37-68	-	-	(Wang & Tang, 2024)

The catalysts used to study the kinetics, apparent activation energies, and rate-limiting steps of ammonia decomposition are summarized in Table 2.3. For many catalysts, a single rate-determining step is difficult to identify, indicating that catalyst composition is just one of several factors influencing the reaction mechanism; other variables include synthesis method, metal loading, and operational conditions such as temperature and pressure. In general, bimetallic catalysts exhibit lower apparent activation energies than their monometallic counterparts. For example, Ni–Pt and Ni–Pd systems show some of the lowest apparent activation energies, whereas less active catalysts such as Fe and Cu yield significantly higher values. This trend aligns with the enhanced catalytic performance often observed in bimetallic systems for ammonia decomposition.

2.4.3 Operating Variables of Ammonia Decomposition

This section examines key operating variables including temperature, reaction pressure, and ammonia flow rate and their impact on the decomposition process. Drawing on experimental data from the literature, the analysis explains how variations in these parameters influence NH_3 conversion and H_2 yield (Bo et al., 2022). The effects of operating conditions on ammonia decomposition and hydrogen production are summarized in Table 2.5.

Table 2.5
Effect of Operating Variables on the NH_3 Decomposition and H_2 Production.

Type of catalyst	NH_3 flow rate (mL/min)	Reaction temp. (°C)	Reaction pressure (bar)	NH_3 decomposition (%)	H_2 production (%)	Ref.
Ru/Al_2O_3	500	450 °C	1	99.7%	90.5%	(Hoseinpour et al., 2024)
u/MgO	50	450 °C	7	99.8%	-	(Hoseinpour et al., 2024)
Ni/Al_2O_3	126	500 °C	5	99%	80%	(Sahu et al., 2024)
Ru	500	425 °C	4	99%	93%	(Makwana et al., 2023)
CoMo		500 °C	-	99%	90%	(Zainal et al., 2024)
Ba-CoCe	200	485 °C	5	>99%	92%	(Jeje et al., 2024)
Cs/Ru	-	450 °C	5	99%	-	(Samia et al., 2024)

2.4.3.1 Effect of temperature

According to (Pattanayak et al., 2022) investigated the influence of temperature on ammonia decomposition, noting that higher operating temperatures generally promote increased hydrogen production. This trend can be explained by the following principles:

i. Ammonia decomposition is endothermic; therefore, elevated temperatures thermodynamically favor the conversion of NH_3 to N_2 and H_2.
ii. Higher conversion raises the partial pressure of hydrogen in the reactor, which enhances the driving force for hydrogen removal and thereby increases overall H_2 yield.
iii. Greater conversion also reduces the concentration of ammonia in the retentate stream. This lowers the driving force for ammonia permeation across a selective membrane, resulting in a permeate stream with higher hydrogen purity.
iv. Nevertheless, from a practical standpoint, operating at lower temperatures is

desirable to maximize performance gains relative to conventional reactors, reduce operating costs, and improve overall energy efficiency.

2.4.3.2 Effect of reaction pressure

The influence of reaction pressure on ammonia decomposition performance has been examined in the literature (Arsad et al., 2024). In membrane-based reactors, an optimum pressure must be maintained to ensure adequate hydrogen recovery and to provide the driving force required for separation. Elevated retentate pressure can enhance reaction kinetics, shift thermodynamic equilibrium, and improve hydrogen extraction from the reaction zone. These effects can offset the thermodynamic decline in ammonia conversion that would otherwise occur at higher pressures, potentially leading to improved overall conversion. However, higher reaction pressures may also reduce hydrogen purity by increasing the driving force for the permeation of impurities such as N_2 and NH_3 into the permeate stream. Consequently, selecting an operating pressure involves a trade-off between maximizing hydrogen recovery and maintaining the desired hydrogen purity.

2.4.3.3 Effect of NH_3 feed flow rate

The influence of ammonia feed flow rate on decomposition performance was investigated by (Ma et al., 2023). Increasing the flow rate reduces the reactant residence time in the reactor, which lowers both NH_3 conversion and hydrogen recovery. However, the purity of the hydrogen produced tends to increase under these conditions. These results suggest that higher ammonia flow rates may be advantageous when high hydrogen purity at the reactor outlet is prioritized. In such cases, the overall plant design should account for the recycling of unreacted ammonia and residual hydrogen from the retentate stream, as well as their potential use as heat sources to sustain the endothermic reaction within the system's energy balance.

2.4.3.4 Catalytic decomposition of NH_3

Catalyst design plays a crucial role in ammonia decomposition for hydrogen production. Commonly used catalysts for this reaction are listed in Table 2.5. An effective catalyst must have a sufficiently strong binding energy to adsorb NH_3 at its active sites. Subsequently, dehydrogenation breaks the N–H bonds in adsorbed

ammonia, releasing H and N atoms. Finally, the catalyst must bind these atoms weakly enough to allow desorption and recombination into gaseous H_2 and N_2. Therefore, the optimal catalyst exhibits an intermediate binding energy for nitrogen on the metal surface. Apparent activation energies for ammonia decomposition over various metal-based catalysts are illustrated in Figure 2.6 (Abouemara et al., 2024b).

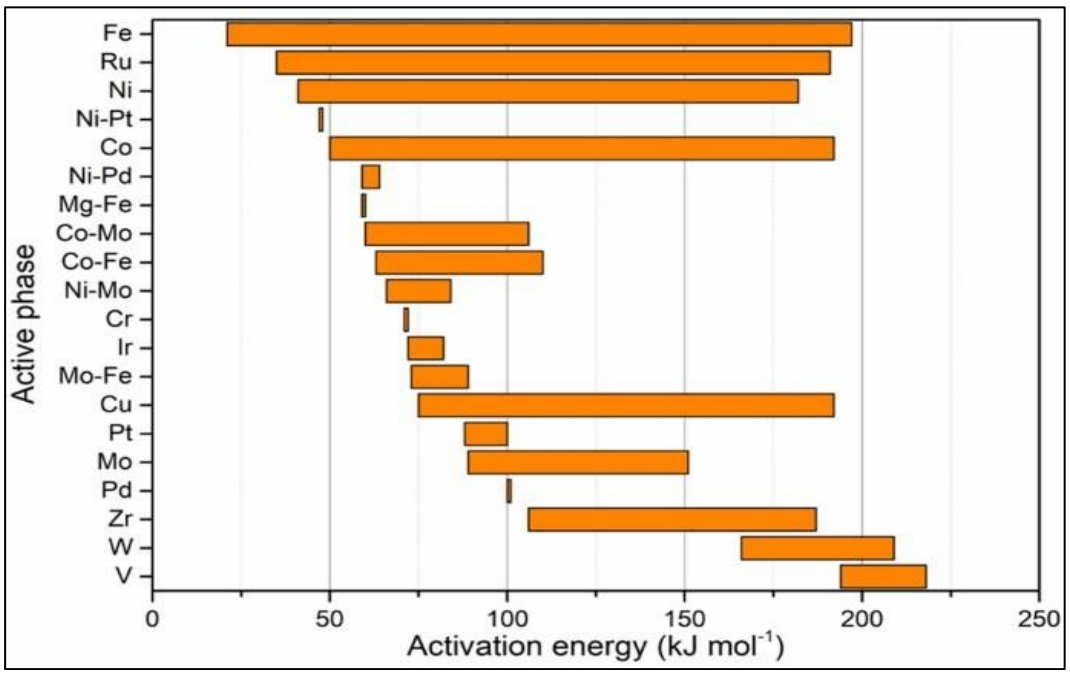


Figure 2.6 Apparent Activation Energy Values for the Decomposition of Ammonia Recorded on Different Metal-Based Catalysts (Adapted from Kassi & Hattab, 2024)

The acidity of active sites on a catalyst influence both the adsorption of NH_3 and the desorption of H_2 and N_2. Studies have shown that increased catalyst acidity enhances NH_3 adsorption, thereby promoting ammonia decomposition. For instance, one investigation reported that adding silicon (Si) increases the area fraction of chemically adsorbed NH_3 by generating additional acid sites, thus improving decomposition activity. Similarly, (Kuttin et al., 2024) observed that their most active catalyst possessed both highly active sites and a strongly acidic surface, which facilitates abundant NH_3 adsorption and enhances decomposition performance. However, excessively strong NH_3 adsorption can also negatively impact catalytic activity. If hydrogen binds too strongly to active sites, it can hinder nitrogen adsorption and lower overall activity, as noted by (Emam et al., 2024).

Likewise, overly strong binding between N_2 and the catalyst may disrupt chemical inertness. An effective catalyst should remain chemically inert toward atomic

H and N to avoid side reactions or catalyst deactivation. Catalyst regeneration is a desirable property for extending operational lifetime and maintaining efficiency. For example, one study demonstrated stable performance over 100 h with minimal sintering of Co and Ni particles and consistent metal content, indicating excellent stability. In contrast, other catalysts have deactivated within 20 h due to thermal aging processes such as sintering, diffusion, and volatilization. Therefore, thermal stability is critical for maintaining structural integrity and performance under the high temperatures typical of ammonia decomposition. A summary of different catalysts used for hydrogen production from ammonia decomposition is provided in Table 2.6.

Table 2.6
Different Catalysts for Hydrogen Production from Ammonia Decomposition

Catalyst	Reaction temperature	NH_3 decomposition	H_2 production	Ref.
Co-Ni/CeO_2	570 °C	95%	62%	(Kalinichenko et al., 2024)
Co-doped graphdiyne	600 °C	100%	42%	(Yadav et al., 2024)
Ni/ Ce0.25Zr0.75O2	500 °C	60%	19.6%	(Krishnan et al., 2023)
Ru-based metallic monolith	600 °C	>90.0 %	54.21%	(Amin, 2024)
Pd composite membrane	745 K	99.6%	87%	(Achomo et al., 2024)
Ru/C-rGO	400 °C	-	96%	(Kim et al., 2021)
Co0.5Ce0.1Al0.4O	550 °C	98%	53%	(Li et al., 2024)
Ni_5Co_5/SiO_2	550 °C	78.1%	-	(Ahmed & Mohamed, 2024)
Ni/La_2O_3	550 °C	78.9%	-	(Sahu et al., 2024)
α-Fe_2O_3 NPs	650–670 °C	100%	-	(Xie et al., 2023)

$Cu/ZnO/Al_2O_3$	550 °C	93%	-	(Xu et al., 2019)
Co/NC	500 °C	80%	-	(Theofanidis et al., 2018)
FeCe	550 °C	83%	-	(Ochoa et al., 2018)
$Ru/La_2O_2CO_3$-Al_2O_3	500 °C	80.1%	-	(Sun et al., 2023)
$Ru/Cs_2O/Pr_6O_{11}$	350 °C	-	79%	(Yao et al., 2020)
Cs–Ru	400 °C	90%	-	(Zheng et al., 2023)
Ru/La_2O_3	525 °C	90.7%	-	(Qi et al., 2023)

2.5 Types of Catalyst for NH_3 Decomposition

Catalysts are the central determinant of the efficiency, stability, cost-effectiveness, and industrial feasibility of ammonia (NH_3) decomposition, and their selection dictates whether NH_3 can practically function as a carbon-free hydrogen carrier. Unlike other hydrogen production routes where feedstock purity and reactor architecture dominate process performance, in NH_3 decomposition the intrinsic electronic structure, surface redox flexibility, and metal support interactions of the catalyst define both N-H bond scission energetics and N_2 recombination kinetics the latter being the rate-limiting step in nearly all mechanistic studies of NH_3 cracking. Globally, catalysts for NH_3 decomposition can be classified into multiple technological families' noble metals, non-noble transition metals, supported mixed oxides, promoted systems, metal nitrides/carbides, and emerging nanoengineered hybrids. These classes are not merely different "metal choices"; each class embodies a different strategy of controlling (i) adsorption energy of NH_3, (ii) activation of adsorbed NHx intermediates, (iii) recombinative desorption of N_2, and (iv) hydrogen spillover and desorption rates (Wei et al., 2024). In addition, each catalyst class comes with unique techno-economic constraints, which strongly affect upscaling decisions.

Noble metal catalysts (e.g. Ru, Pt, Rh) remain the benchmark due to near-zero activation barriers for N-H bond cleavage and exceptional stability under harsh temperature conditions, particularly Ru supported on carbon or alumina which routinely delivers >95% conversion at <600 °C in laboratory conditions (Sun et al., 2020). However, the cost and supply chain of noble metals eliminates them from any realistic gigawatt scale hydrogen economy. This triggered global re-direction toward non-noble metals.

Non-noble transition metal catalysts (e.g. Co, Fe, Ni, Mn, Zn) therefore represent the most active frontier for realistic hydrogen cost projections. They are far cheaper, more abundant, can form adjustable oxide or nitride phases and allow bimetallic synergies to be engineered. Co-based catalytic systems consistently appear the strongest within this group because Co exhibits higher intrinsic reducibility into active metallic Co^0 and forms strong interactions with oxygen-defective supports which enhance spillover (Zhang et al., 2023). Fe and Ni are widely studied but show lower turnover frequencies unless promoted or alloyed. Zn is typically inactive but highly tunable when used as a promoter to electronically modify Co/Ni active sites (Hu et al., 2020).

In parallel, the support is now recognized as not a "passive carrier" but an active thermochemical partner which controls metal dispersion, particle size, lattice strain, metal oxygen charge transfer and surface acid/base character. Traditional supports such as γ-Al_2O_3 and MgO have been replaced increasingly with mixed oxides such as MgO-Al_2O_3, ceria zirconia spinels, perovskites, and defect-rich oxides that can strongly anchor nanoscale metal species and stabilize sub-nanometric clusters under high temperature cracking (Brito et al., 2023).Spinel supports such as $MgAl_2O_4$ have gained momentum because they provide high thermal stability, basicity and lattice oxygen exchange pathways which facilitate N-H activation (Woo et al., 2023). Another class are promoted systems small quantities (0.5-5 wt%) of Cs, K, Ba, or Ca can drastically improve NH_3 cracking rates by increasing surface basicity, weakening N-H adsorption binding energy, and facilitating N_2 desorption (Xu et al., 2022). Promotion is now considered mandatory when designing non-noble industrial catalysts. Bimetallic systems (Co-Fe, Co-Ni, Ni-Fe, Co-Zn etc.) are a rapidly expanding category. In these systems, the second metal modifies the d-band center of the primary metal, adjusts electron density, alters reducibility, and stabilizes smaller crystallites against sintering. Bimetallics are also the most strategic pathway to close the "performance gap" between

Ru and non-noble metals without introducing excessive cost (Dudek et al., 2019). The catalyst developed in this thesis $CoFeO/MgO\text{-}Al_2O_3$ belongs to this frontier.

In recent literature, metal nitrides (Fe_3N, Co_2N, VN, Mo_2N), metal carbides (Mo_2C), perovskites and core shell nanostructures have also demonstrated promising performance, though their synthesis routes are often complex and their long-term stability under air/moisture remains uncertain (Cai et al., 2021). Therefore, selecting an optimal catalyst for NH_3 decomposition is not simply a question of "highest activity" it is a multi-dimensional optimization problem balancing catalytic turnover, supply chain cost, sintering resistance, sulfur poisoning tolerance, thermal cycling stability, promoter requirement, and compatibility with scalable supports. This explains why ammonia cracking remains an active research domain despite >100 years of published literature. Globally, catalyst research for ammonia decomposition is undergoing a strategic shift toward rational catalyst design, where catalytic performance is no longer viewed as the function of only metal identity, but instead as a function of cooperative structure activity relationships across compositional, morphological, electronic, and support-level variables (Gan et al., 2024).

Modern studies have demonstrated that the decomposition of NH_3 follows a sequence of fundamental elementary steps NH_3 adsorption, stepwise dehydrogenation to NH_2, NH, and N, recombinative desorption of N_2, and finally H_2 desorption. Among these steps, N-N recombination remains the rate controlling barrier, therefore catalysts with high density of coordinatively unsaturated metal sites, high electron density, and high reducibility can facilitate N-N coupling more efficiently (Zheng et al., 2022). Catalysts must therefore not only provide active sites, but must also stabilize reactive intermediates, suppress surface poisoning, and maintain structural integrity under elevated temperatures >600 °C. In this regard, current catalyst development strategies increasingly focus on (i) tuning metal oxidation states, (ii) manipulating metal-support synergistic anchoring, (iii) engineering oxygen vacancy concentration, and (iv) adopting dual metal combinations where electronic cross-interactions intentionally modify d-band filling to lower the activation barrier for N-H scission (Shi et al., 2022).

Another paradigm change is the recognition that supports act as "co-catalysts", not merely carriers. High-basicity supports (MgO, $MgAl_2O_4$) promote NH_3 adsorption, while reducible supports (CeO_2, TiO_2) can donate lattice oxygen electrons to improve H-spillover. Moreover, high-surface-area mesoporous supports (SBA-15, MCM-41, meso-Al_2O_3) improve dispersion, suppress sintering, and maintain metal nanodomains

under thermal cycling. In this way, the catalyst field is moving away from simple loading of active metal powders, toward engineered hybrid systems where every parameter metal identity, metal ratio, support lattice, and bond environment is tuned to collectively manipulate the energy landscape of NH_3 decomposition. Hence, the evaluation of catalysts for NH_3 decomposition must always be framed not only around maximum conversion but around understanding why conversion changes: which chemical bonds are weakened, which metallic species are generated under reaction temperature, which support sites stabilize reactive intermediates, and which structural configurations maintain performance over time. This conceptual framework guides the discussion of noble metal and non-noble metal catalysts in the following subsections (Chen et al., 2023).

2.5.1 Noble Metals for NH_3 Decomposition

Ammonia decomposition is a critical process in industrial hydrogen production and related refining operations (Fu et al., 2019). Effective catalysts for this reaction must exhibit both high activity and long-term stability under operating conditions. Among the most widely studied catalysts are noble metals, which often demonstrate superior performance. Commonly used noble-metal catalysts for ammonia decomposition include:

(a) Ruthenium (Ru)- Ruthenium-based catalysts are highly active and stable at elevated temperatures, making them a leading choice for promoting ammonia dissociation into nitrogen and hydrogen (Dang et al., 2021).

(b) Rhodium (Rh)- Rhodium catalysts are particularly effective at high temperatures and efficiently facilitate ammonia dissociation.

(c) Platinum (Pt)- Platinum-based systems also show high catalytic activity and stability under typical decomposition conditions. These noble metals are frequently supported on materials such as alumina, silica, or other refractory oxides to improve dispersion, enhance catalytic performance, and increase stability (Zheng et al., 2022). Catalyst selection depends on specific reaction conditions, desired rates, and stability requirements. For instance, (Zheng et al., 2023) examined the effect of ruthenium loading (wt%) on carbon supports. They found that increasing Ru loading initially improves reaction efficiency, but excessive loading leads to aggregation and sintering, which reduce activity. Similarly, (Li et al., 2022)observed that raising Ru loading boosts

the reaction rate up to about 5 wt%, beyond which agglomeration occurs, causing catalyst deactivation.

These results indicate that an optimal, moderate loading of noble metals on a support is essential for maximizing ammonia decomposition performance. Despite extensive research spanning more than a decade, challenges such as metal agglomeration and sintering remain unresolved for noble-metal catalysts, highlighting the need for continued development of stabilized catalyst architectures.

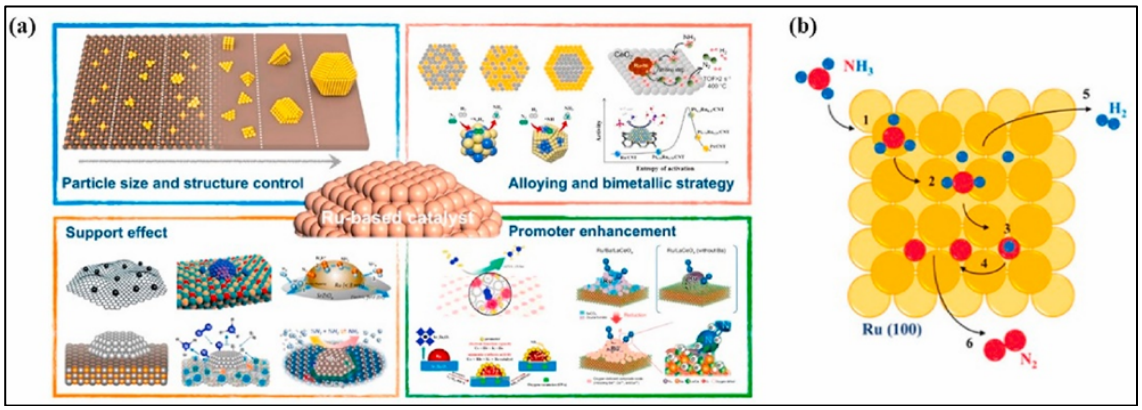


Figure 2.7 Strategies for the Rational Design of Ru-Based Catalysts (B) Schematic Representation of NH_3 Decomposition Reaction over Ru Catalysts (Li et al., 2024) (Adapted with Permission from Elsevier)

2.5.1.1 Kinetic Analysis of Noble Metal Catalysts for Ammonia Decomposition

Noble metal catalysts, especially ruthenium (Ru), play a central role in the kinetic analysis of ammonia decomposition a key reaction for hydrogen production in various industrial applications (Hassan et al., 2023). The reaction mechanism on noble metal surfaces typically begins with ammonia adsorption onto active metal sites, followed by sequential N–H bond cleavage. The released hydrogen atoms recombine and desorb as H_2, while nitrogen atoms combine and desorb as N_2. Studies comparing different crystal planes of Ru show significant variations in activity. For example, N_2 production is markedly higher on the stepped Ru(100) surface than on the flat Ru(100) surface Figure 2.7, highlighting how catalyst morphology influence's reaction kinetics and N–H bond cleavage efficiency (Zhou et al., 2022). Promoters are frequently used to modify the electronic properties of Ru, enhancing nitrogen recombination and desorption. This modification lowers the apparent activation energy and optimizes catalytic activity for industrial use. While the Temkin–Pyzhev model has been widely applied to describe these dynamics, some researchers caution that over-reliance on this model may oversimplify the complex reaction pathways involved (Andersen et al.,

2022). Recent advances combine Density Functional Theory (DFT) and microkinetic modeling to analyze elementary reaction steps in greater detail. For instance, adding potassium (K) to Ru-based catalysts can shift the rate-determining step from NH dissociation to NH_3 dissociation while facilitating N_2 desorption. Such studies demonstrate how integrated DFT-microkinetic approaches can improve predictions of catalyst behavior under varying conditions (Nailwal et al., 2024c). Additionally, the Transient Analysis of Products (TAP) method has enabled precise determination of kinetic constants, further clarifying the rate-determining steps for ammonia decomposition on Ru catalysts. This technique underscores the complexity of catalytic reactions, where both the electronic environment and the physical structure of active sites critically determine performance (Wu et al., 2024). In summary, kinetic analysis of noble-metal catalysts for ammonia decomposition reveals a complex interplay of chemical steps influenced by catalyst composition, surface structure, and operational conditions.

2.5.2 Non-Noble Metals Catalysts for NH_3 Decomposition

In response to the high cost of noble metals, research has shifted toward non-noble alternatives such as nickel, cobalt, iron, and copper. These metals are more abundant, less expensive, and can exhibit significant catalytic activity, making them attractive for large-scale industrial applications including chemical synthesis, fuel production, and catalytic decomposition processes (Chen et al., 2024). Efforts to optimize non-noble metal catalysts focus on improving their activity, selectivity, and stability to match or approach the performance of noble-metal systems while maintaining cost advantages. Many non-noble metals can be tailored through modifications to their structure, composition, and surface properties to enhance their catalytic function for specific reactions, such as hydrogenation or dehydrogenation (Pourali et al., 2022). Among non-noble metals, Fe, Co, and Ni have shown particular promise for ammonia decomposition due to their low cost, availability, and favorable catalytic properties. The addition of metals such as Co, Fe, or Ru often increases catalytic activity, especially when tuned to optimize the desorption energy of nitrogen. Other metals like Mn, Cu, and Zn which share similar electronic structures and reside in the same period also demonstrate potential for enhancing catalytic performance.

A key mechanism behind improved activity in non-noble systems is the reduction of activation energies (E_a). For example, bimetallic M/Ni-foam catalysts exhibit E_a values between 80 and 90 $kJ \cdot mol^{-1}$, significantly lower than those of isolated Ni (≈180 $kJ \cdot mol^{-1}$ for Ni film and 209 $kJ \cdot mol^{-1}$ for Ni wire). This lowering of the activation barrier enhances overall reaction rates and efficiency (Cechetto et al., 2021). Bimetallic catalysts often display synergistic effects that improve performance through mechanisms such as modified crystallite size, increased surface area, accelerated electron transfer, and a higher density of active sites. For instance, (Sitar et al., 2022) reported a synergistic effect in Ni–Co bimetallic catalysts, which improved ammonia decomposition compared to single-metal systems. While the Ni:Co ratio did not strongly influence the decomposition rate, it significantly affected the catalytic combustion temperature; a 1:1 ratio achieved combustion at only 130 °C due to enhanced electron transfer and more active sites. Similarly, (Cechetto et al., 2022) developed a Co–Ni bimetallic catalyst with a large surface area, mesoporous structure, and high metal dispersion. The addition of a second metal modifies the electronic structure by donating electrons, creating a synergistic interaction that improves ammonia binding, catalyst stability, and overall decomposition activity. In summary, non-noble metal catalysts particularly bimetallic systems offer a cost-effective and tunable alternative for ammonia decomposition, with synergistic effects often leading to lower activation energies and enhanced performance compared to their monometallic counterparts.

2.5.2.1 Kinetic Analysis of Non-Noble Metal Catalysts for Ammonia Decomposition

In the domain of ammonia decomposition, non-noble metal catalysts such as iron (Fe), cobalt (Co), and nickel (Ni) offer cost-effective alternatives to noble metals, characterized by their distinct kinetic behaviors and mechanisms. The primary mechanism for ammonia decomposition over these catalysts involves the sequential dehydrogenation of NH_3, leading to the desorption of nitrogen (N) in a complex manner (Nailwal et al., 2024). This differs fundamentally from the N-H bond dissociation seen in noble metal catalysts. Recent advancements in DFT have provided insights into how variations in metal particle size affect the kinetics of these reactions. For instance, smaller nickel nanoparticles have been shown to facilitate lower binding energies,

enhancing the desorption process. Such detailed analyses highlight the importance of physical properties in the catalytic performance of non-noble metals. The role of the metal-support interaction was emphasized in studies such as those by (Adamou et al., 2023). where the presence of Ni nanoparticles contributed to the formation of NH_2 vacancies on carrier surfaces. This structural feature significantly enhances the absorption efficiency of NH_3, facilitating its breakdown at lower temperatures. These interactions outline the complexity of catalyst design, where the choice of support material and metal can profoundly affect catalytic activity and stability. The incorporation of carbon atoms into the catalyst structure, particularly on or beneath the surface, has proven to be a strategic approach to modifying the electronic environment around the active metal sites.

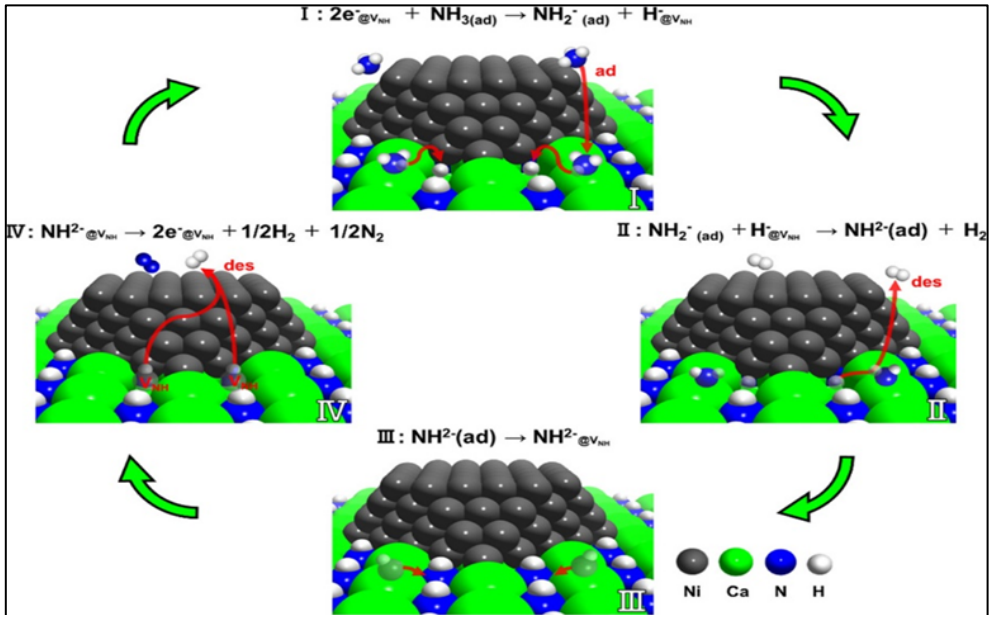


Figure 2.8 Reaction Pathway for Ammonia Decomposition over Ni/Canh Catalysts Through an NH_2- Vacancy-Mediated Mars-Van Krevelen Mechanism (Muhammed Et Al., 2023) (Adapted with Permission from Elsevier)

This modification aids in reducing the activation energy required for N composite desorption, which is crucial for effective ammonia breakdown (Peters et al., 2023). Such insights were bolstered by DFT calculations, which showed that Fe surfaces could undergo significant morphological changes that favorably impact the reaction kinetics. Ammonia decomposition over non-noble metal catalysts proceeds through several stages, beginning with the adsorption of NH_3 at the metal surface, followed by successive breakdowns into NH_2 and NH, and culminating in the

desorption of nitrogen and hydrogen (Bai et al., 2023) Figure 2.8. The reaction's rate-determining steps can vary significantly based on the metal used and its interaction with the support material. For example, while Fe catalysts exhibit high energy barriers for nitrogen desorption, Ni and Co catalysts demonstrate more favorable kinetics due to their lower barriers, reflecting their higher catalytic activity. Furthermore, the economic and practical viability of using non-noble metals like Ni, Co, and Fe in industrial applications also hinges on their ability to perform under high-temperature conditions without deactivation, a common challenge for noble metal. This attribute not only enhances their utility in ammonia decomposition but also opens avenues for broader applications across various industrial processes (Le et al., 2023).

2.5.3 Bimetallic Catalyst for NH_3 Decomposition

Bimetallic catalysts often exhibit synergistic effects that enhance catalytic performance beyond what is achievable with monometallic systems. These improvements arise from factors such as modified crystallite size, increased surface area, accelerated electron transfer, and a higher density of active sites. For example, (Sun et al., 2022) demonstrated that Ni–Co bimetallic catalysts show higher activity for ammonia decomposition compared to single-metal equivalents. While the Ni:Co ratio did not significantly affect the decomposition rate, it strongly influenced the catalytic combustion temperature; a 1:1 ratio enabled combustion at only 130 °C due to enhanced electron transfer and increased active site availability.

Similarly, (Lundin et al., 2016) developed a Co–Ni bimetallic catalyst with favorable characteristics, including a large surface area, mesoporous structure, and high metal dispersion. The improved activity was attributed to stronger binding energy between the catalyst and NH_3, as well as electronic modification from the second metal, which supplies electrons and creates a synergistic interaction. This synergy also enhances catalyst stability, extending operational lifetime while maintaining high activity. The development of cost-effective and efficient catalysts for ammonia decomposition has led to the exploration of various mono- and bimetallic combinations. Studies have investigated catalysts based on Co, Fe, Cu, Ni, and Mo, as well as bimetallic pairs such as Fe–Co, Fe–Ni, Mo–Ni, Mo–Co, Co–Ni, and Cu–Ni. These are often supported on modified Ni foam, chosen for its low cost and excellent catalytic activity (Asif et al., 2023). This approach aims to balance performance, stability, and economic viability for large-scale hydrogen production via ammonia decomposition.

2.5.3.1 Kinetic Analysis of Bimetallic Catalysts

Bimetallic catalysts, integrating multiple active metals, offer distinct advantages over monometallic ones by altering the kinetic and thermodynamic landscapes of catalytic reactions Table 2.6 is showing Preparation method and kinetic analysis of bimetallic catalysts. These catalysts facilitate the tuning of reaction pathways and rate-limiting steps through synergistic effects, which are often characterized by DFT and microkinetic modeling. Such models are invaluable for identifying optimal bimetallic combinations that lower activation energies and enhance catalytic efficiency (Lee et al., 2021). For instance, research highlights that in Ni-Ru bimetallic catalysts supported on CeO_2, the dehydrogenation of NH_3 is the primary rate-determining step, akin to the N-H bond dissociation seen in noble metal catalysts.

Comparative DFT studies of $CoNi/Al_2O_3$ and Ni/Al_2O_3 catalysts reveal that N desorption poses a significant energy barrier, which is effectively reduced in the $CoNi/Al_2O_3$ due to enhanced dispersion of Co, thereby improving the catalyst's overall activity. Further DFT analysis on CoNi (110) catalysts compared to Ni (110) shows that the addition of Co not only reduces the energy barriers for N desorption but also mitigates H_2 poisoning at active sites, thus promoting ammonia breakdown more effectively. The presence of Co enhances the electronic environment of the Ni sites, leading to improved catalytic performance (Struijk, et al., 2023). The synergy in bimetallic catalysts is not just a function of altered electronic properties but also results from physical properties such as increased surface area and optimized metal interaction, which prevent agglomeration and maintain high dispersion. These factors are crucial for maintaining high activity levels and achieving significant improvements in NH_3 decomposition (Zhang et al., 2024). The following table summarizes various bimetallic catalysts, their preparation methods, and kinetic analyses, outlining the diverse approaches and their effectiveness in enhancing ammonia decomposition:

Table 2.7
Preparation Method and Kinetic Analysis of Bimetallic Catalysts

Catalysts	Preparation Method	Kinetic analysis methods	Temperature (K)	NH_3 conversion (%)	Ref.
$6Fe4Ni/f\text{-}SiO_2$	Impregnation method		734	61	(Li et al., 2024)
$2.5Ni0.5Ru/CeO_2$	Impregnation method	LHHW method	724	＞99	(Lucentini et al., 2021)

$5Co_5Ni/SiO_2$	Impregnation method	Arrhenius equation	824	76.8	(Feng et al., 2023)
$Ni7.5Co2.5/CeO_2$	Co-precipitation method	Density Functional Theory	824	96.96	(Łuczak & Lieder, 2023)
$20Co–10Ni/Y_2O$	Co-precipitation method	Arrhenius equation	824	85.02	(González et al., 2023)
Fe0.75Cr0.25	Urea two-step hydrolysis method	Arrhenius equation	875	88.4	(Li et al., 2024)

This comprehensive examination of bimetallic catalysts demonstrates their potential to revolutionize ammonia decomposition processes, offering a promising route for the scalable production of hydrogen with enhanced environmental and economic viability.

2.6 Role of Supports for NH_3 Decomposition

In the field of heterogeneous catalysis, the choice of catalyst support plays a pivotal role in determining the physicochemical properties and overall performance of the catalyst system. Catalyst supports are not merely inert carriers; instead, they influence the dispersion, stability, reducibility, and reactivity of the active metal species (Wang et al., 2022). For catalytic ammonia (NH_3) decomposition, particularly under high-temperature conditions, the thermal stability, surface chemistry, and textural properties of the support are critical determinants of catalyst efficiency and longevity. Two of the most employed oxide supports in NH_3 decomposition systems are magnesium oxide (MgO) and aluminium oxide (Al_2O_3). Both materials have distinct and complementary properties that make them suitable for supporting transition metal-based catalysts in high-temperature reactions (Kanaan et al., 2023).

The support also dictates the acid base character of the catalytic surface, which strongly influences the adsorption strength and activation mode of NH_3 prior to N-H bond cleavage. Basic supports such as MgO possess high electron donor capacity, which enhances NH_3 chemisorption and facilitates the formation of adsorbed NHx intermediates. In contrast, Al_2O_3 exhibits amphoteric sites and relatively stronger metal anchoring strength, which stabilizes smaller metal nanoparticles but may weaken NH_3 adsorption if used alone. Therefore, hybrid supports such as $MgO\text{-}Al_2O_3$ have gained increasing interest because they combine the two functionalities: MgO provides strong basic sites for NH_3 activation, while Al_2O_3 delivers structural robustness, high melt

point and excellent metal dispersion capability(Lee et al., 2023). Mixing MgO with Al_2O_3 leads to formation of $MgAl_2O_4$ spinel domains during calcination, which thermally stabilise the catalyst at temperatures above 700 °C and prevent sintering of transition metals during long-term ammonia cracking (Oni et al., 2023). This synergistic effect is particularly relevant in NH_3 decomposition, which is strongly endothermic and requires extended operation above 550 °C.

Furthermore, the morphology and porosity of the support determine the accessibility of hydrogen desorption sites. Mesoporous supports enable enhanced molecular transport and hydrogen spill-over between adjacent metal clusters. MgO-Al_2O_3 composites frequently exhibit hierarchical pore networks that combine micro meso domains, enabling both high surface area and fast diffusion, which is essential in eliminating mass transfer limitations at industrial gas hourly space velocities (GHSV) (Oni et al., 2023) Supports with insufficient porosity typically result in metal blocking and reduced turnover frequencies (TOF).

Therefore, the design of support must simultaneously optimise (i) basicity, (ii) thermal resistance, (iii) porosity, and (iv) metal support binding energy. From a mechanistic perspective, the support also participates in electron exchange with the metal active sites. For example, Mg^{2+} and Al^{3+} cations can withdraw or donate electron density through oxygen bridges, modifying the d-band centre of metal species such as Co^{2+}, Fe^{2+} or Zn^{2+}. This electronic tuning affects the transition state barrier for NH_3 dissociation and N recombination, which is the rate controlling step in NH_3 decomposition (Zhong et al., 2023). Stronger metal oxygen support binding has been correlated with lower apparent activation energies in mixed oxide systems, which explains why metals deposited on MgO-Al_2O_3 often outperform those on single oxides. This is fully consistent with the principle that NH_3 decomposition is structure-sensitive, and thus highly dependent on surface electronic configuration.

Finally, supports also influence long-term durability. During extended operation, many transition metals form surface nitrides (e.g., FeN, CoN) that can deactivate the catalyst. Basic MgO-Al_2O_3 supports help suppress irreversible nitride formation by promoting reversible nitrogen desorption and preventing metal particle encapsulation. This is particularly advantageous for non-noble catalysts, which are more prone to structural changes than Ru-based systems. The combined mechanical stability, electron mediating ability, and enhanced NH_3 adsorption capacity makes MgO-Al_2O_3 one of the most rational and widely accepted supports for high-temperature

ammonia decomposition in next-generation green hydrogen processes (Daturi et al., 2023).

2.6.1 Aluminium Oxide (Al_2O_3)

Al_2O_3, particularly in its γ-phase form, is widely used in catalytic systems due to its high surface area, porosity, thermal stability, and mechanical robustness. Its surface characteristics enable effective dispersion of metal nanoparticles, which is essential for maximizing the number of accessible active sites during catalysis (Shamjitha & Vargeese, 2023). Additionally, Al_2O_3 provides strong anchoring sites for metal species, thereby minimizing sintering and particle agglomeration at elevated temperatures commonly encountered during NH_3 decomposition. However, Al_2O_3 also possesses certain limitations. It exhibits mild acidity, which may lead to undesirable metal-support interactions, especially with transition metals such as nickel, cobalt, or iron. In some cases, these interactions can result in the formation of inactive spinel-type phases (e.g., $CoAl_2O_4$ or $NiAl_2O_4$), which are catalytically less active or even inert. This can reduce the number of reducible metal species available during the reaction and, consequently, lower the overall NH_3 conversion efficiency. Therefore, the use of Al_2O_3 often requires careful optimization of preparation conditions to avoid such interactions and preserve catalytic activity(Khan et al., 2023).

Beyond its structural robustness, the catalytic performance of γ-Al_2O_3 is intricately governed by its surface hydroxyl groups and the distribution of Lewis and Brønsted acid sites (Wu et al., 2020). These acid sites can influence the initial adsorption and dissociation of NH_3 molecules, determining the availability of active intermediates such as NH_2*, NH*, and N*. While moderate acidity enhances NH_3 activation, excessive acidity can lead to strong chemisorption, limiting hydrogen desorption and thus hindering overall turnover frequency (TOF) (Tawalbeh et al., 2023). Therefore, controlling the surface acidity through modification or co-doping has become a critical strategy in tailoring Al_2O_3-based catalysts. Moreover, Al_2O_3's high surface area (typically 100-300 $m^2\ g^{-1}$) promotes homogeneous metal dispersion, yet its oxygen vacancies play a dual role. These vacancies can anchor metal species through M-O-Al linkages, improving dispersion, but they can also induce partial oxidation of metals such as Co, Fe, or Ni during calcination. This may lead to the formation of spinel structures (e.g., $CoAl_2O_4$, $NiAl_2O_4$), which exhibit poor reducibility below 800 °C (Hebish et al., 2024). Such phases trap the active metal ions within the alumina lattice, decreasing the

population of metallic sites responsible for N-H bond scission. To overcome this, researchers have explored pre-treatments such as mild reduction or the incorporation of secondary oxides (e.g., MgO or CeO_2) to moderate the metal–support interaction and facilitate easier reducibility (Miao et al., 2022). From a thermal standpoint, γ-Al_2O_3 transforms to δ- or α-Al_2O_3 at temperatures above 900 °C, causing a loss in surface area and pore collapse. This transformation can significantly impair catalytic performance during prolonged high-temperature NH_3 decomposition cycles. Consequently, stabilizing the alumina structure through spinel formation ($MgAl_2O_4$ or $CoAl_2O_4$) is often considered advantageous when the goal is to maintain mechanical integrity and inhibit sintering. However, this stabilization must be balanced to avoid excessive encapsulation of the active metal species (He et al., 2023).

In summary, γ-Al_2O_3 remains a cornerstone in catalyst design due to its excellent mechanical and thermal stability, high dispersion capability, and tunable surface chemistry. Nevertheless, its tendency to form strongly bound spinel phases and excessive acid sites can limit the availability of active metallic sites. This understanding has motivated the development of composite supports, such as MgO-Al_2O_3, that integrate the basic properties of MgO with the structural stability of Al_2O_3 to achieve enhanced reducibility, optimized metal support interaction, and superior catalytic activity for NH_3 decomposition (Meng et al., 2024).

2.6.2 Magnesium Oxide (MgO)

MgO is a basic support material with a relatively high melting point and excellent thermal stability. Its basicity plays a crucial role in NH_3 decomposition, as it enhances the adsorption and activation of ammonia molecules on the catalyst surface (Li et al., 2022). The presence of electron-rich oxygen species on MgO can facilitate electron transfer to the adsorbed NH_3, thereby weakening the N-H bonds and promoting their cleavage in the rate-determining step of the reaction. This property makes MgO a particularly attractive support for catalysts in reactions involving nitrogen-containing molecules. Additionally, MgO supports often contribute to improved metal dispersion and can enhance the reducibility of metal oxides, which is crucial for generating active metallic species under reaction conditions. Unlike acidic supports, MgO does not strongly interact with most transition metals, reducing the risk of forming stable but inactive mixed oxides. However, its relatively low surface area compared to Al_2O_3 can

limit the density of dispersed metal particles unless modified through structural engineering or support mixing strategies (Alekseev & Nilsson, 2024).

In addition, MgO exhibits a unique defect-rich electronic structure, where surface $O2^-$, O^- and oxygen vacancies act as basic sites with tunable electron donating ability. These surface defects are critical in NH_3 decomposition because they can stabilize reaction intermediates such as NH_2*, NH*, and N* while simultaneously facilitating the desorption of H_2 through facile proton electron recombination pathways (Zou et al., 2024). Compared to acidic supports which sometimes trap intermediates excessively, MgO accelerates their transformation into final products and thus improves turnover frequency (TOF). Moreover, MgO demonstrates exceptional stability under repeated high temperature cycles and does not undergo detrimental phase transformations in the 600-950 °C range used for NH_3 decomposition. This makes MgO superior to alumina when long-term thermal durability is a priority. However, pure MgO suffers from limited structural flexibility. A common strategy to overcome this limitation is to integrate MgO with Al_2O_3 to generate $MgAl_2O_4$ spinel phases (Shafie & Kambara, 2024).The resulting composite bridges the advantages of both materials: the basicity of MgO improves electron donation to adsorbed NH_3, while the spinel backbone derived from alumina prevents collapse of pore networks during calcination. This combination produces highly stable supports with enhanced mesoporosity, increased surface acidity/basicity balance, and improved mechanical rigidity at elevated temperatures. Such synergistic support engineering has been shown to significantly enhance metal dispersion and resist sintering, especially for Co- and Fe-based catalytic systems. Furthermore, controlled incorporation of MgO can tune the metal support interaction strength. For example, Co supported on pure Al_2O_3 frequently forms $CoAl_2O_4$, an unreducible spinel, but the addition of MgO weakens the anchoring energy and keeps cobalt in a reducible form (CoO/Co^0), enabling easier formation of active metallic sites during NH_3 decomposition (Chen et al., 2023). This is why MgO-containing supports are consistently preferred for systems targeting rapid N-H dissociation kinetics.

In summary, MgO's strong basicity, defect-rich surface sites, and thermal robustness make it an excellent support for non-noble metal catalysts. Its use in mixed-oxide frameworks such as $MgO-Al_2O_3$ delivers an optimised balance between stability, surface area, and reducibility properties essential for sustained high-temperature NH_3 decomposition for H_2 production (Brzhezinskaya et al., 2022).

2.6.3 Synergistic Effect of Mixed Oxide Supports (MgO-Al_2O_3)

To exploit the strengths and overcome the individual limitations of MgO and Al_2O_3, recent research has focused on mixed oxide supports, particularly MgO-Al_2O_3. These mixed supports combine the thermal stability, mechanical strength, and high surface area of Al_2O_3 with the basicity and favourable electronic properties of MgO (Luo et al., 2019). The result is a support system with tunable acid-base properties, enhanced metal dispersion, and improved resistance to deactivation through sintering or phase transformation. The synergy between MgO and Al_2O_3 in mixed oxide supports leads to the development of a heterogeneous surface environment that can better stabilize active metal nanoparticles, facilitate ammonia adsorption, and promote the formation of active sites necessary for N-H bond cleavage. Additionally, such mixed supports often exhibit intermediate reducibility profiles, allowing for easier activation of metal oxides during pre-treatment or in-situ reduction processes. The structural properties of MgO-Al_2O_3 can be further tailored using preparation techniques such as hydrothermal carbonization (HTC), which enhances pore structure and surface area. This is particularly beneficial for increasing the contact area between the support and active metal phases, ultimately leading to higher catalytic activity and improved stability under repeated use (Yu et al., 2024).

Moreover, MgO-Al_2O_3 mixed oxide supports have been reported to exhibit textural, structural and electronic tuning advantages that neither single oxide can achieve independently. Several studies have shown that during thermal treatment, partial solid-state reaction between MgO and γ-Al_2O_3 can generate $MgAl_2O_4$ spinel domains, which provide a thermodynamically stable backbone that resists collapse even above 800 °C (Jung & Chung, 2024). This spinel framework offers high oxygen vacancy density and modifies the electronic density around metal anchoring sites, creating a surface with balanced basic acidic characteristics that is highly beneficial for NH_3 activation. Such defect-rich surfaces improve the polarization of N-H bonds during initial activation steps and facilitate the recombination of adsorbed N-atoms, which is typically the rate controlling step during NH_3 decomposition (Zou et al., 2024). Furthermore, MgO-Al_2O_3 mixed oxides also demonstrate superior metal dispersion capability, because the interfacial heterogeneity between MgO and Al_2O_3 domains disrupts long-range diffusion of metal species during calcination. This prevents

sintering and results in nanometallic domains with high accessibility. The tuneable surface basicity also improves NH_3 uptake and suppresses undesirable side reactions such as formation of stable nitrides that deactivate active metal centres. In addition, the improved reducibility of metal oxide clusters supported on mixed $MgO\text{-}Al_2O_3$ has been linked to the enhanced hydrogen spillover phenomena over the interfacial boundaries between the two oxide phases (Muhammed et al., 2023). Hydrogen spillover accelerates in-situ generation of metallic active sites, which is crucial for productive catalytic turnover.

Finally, mixed oxide supports are compatible with multiple synthesis routes such as sol gel, co-precipitation, combustion, hydrothermal and HTC, allowing tailored pore architectures and targeted metal support interactions at different scales (Aslam et al., 2023). These synthesis flexibilities make $MgO\text{-}Al_2O_3$ systems highly attractive in future industrial ammonia cracking applications, where stability-to-cost ratio, scalability, and regeneration capability are decisive criteria. Overall, by simultaneously providing thermal robustness, adjustable acid base balance, high dispersion of transition metals and improved reducibility, $MgO\text{-}Al_2O_3$ mixed oxides represent one of the most rational support families for next-generation transition-metal catalysts designed for NH_3 decomposition and on-site hydrogen generation (Qin et al., 2024).

2.6.4 Role of Promoters

While the focus of this study is on support optimization, it is worth briefly noting that promoters when used can significantly modify the catalyst's electronic environment, reducibility, and dispersion behaviour. Promoters such as alkali metals (e.g., K, Cs) or rare earth elements are often added to enhance hydrogen desorption, reduce activation energy, or stabilize the active phase. They may also prevent the formation of undesirable surface species that hinder catalytic performance (Triviño et al., 2023). However, to isolate the specific effects of support properties in this research, no external promoters are applied. This approach enables a clearer understanding of how $MgO\text{-}Al_2O_3$ supports influence the activity, selectivity, and stability of single and bimetallic catalysts in NH_3 decomposition.

In the broader NH_3 decomposition literature, promoters have repeatedly been shown to play roles far beyond simple “additive effects”. For example, alkali promoters (K, Cs, Na) are known to donate electron density to transition metal surfaces, thereby increasing the electron population on metal d-orbitals and weakening the N-H bond

through back-donation mechanisms (Ali Shah et al., 2024). This electron donation accelerates the first dissociative adsorption step of NH_3 and dramatically improves turnover frequency. Furthermore, some promoters act as structural modifiers. Alkali metals tend to occupy terrace and step sites, suppressing sintering and improving dispersion of nanosized catalytic clusters (Emam et al., 2024). Several studies also report that promoter atoms can block strongly acidic sites on Al_2O_3 that otherwise form stable metal aluminates (e.g., $CoAl_2O_4$ spinel), which deactivate the catalyst by "locking" transition metal ions in unreducible oxidic structures (Tonelli et al., 2023). In addition, rare-earth promoters such as La, Ce, Sm, and Y have been used to enhance oxygen storage capacity and facilitate reversible redox cycling, improving the regeneration of metallic active sites under dynamic reaction environments (Grubert, 2023).Another important function of promoters is suppression of nitride formation. On Fe-based and Co-based NH_3 decomposition systems, bulk nitriding at high temperature is a well-known deactivation pathway. Alkali and alkaline earth promoters weaken metal nitrogen binding strength, preventing deep nitride formation and preserving metallic catalytic phases (Balgehshiri & Zohuri, 2023). Therefore, although this current study deliberately avoids the use of promoters to isolate the pure contribution of the MgO-Al_2O_3 support system, the literature makes it clear that promoters can serve as a powerful strategic lever to engineer electronic structure, improve reducibility, enhance dispersion, and prolong catalyst lifetime. In future work, once the fundamental support effects are fully established, systematic promoter incorporation can be used to further elevate the performance boundaries of the most promising system especially for Co-based catalysts, where synergistic electronic co-modification could potentially unlock near-complete NH_3 conversion at lower temperatures (Zhu et al., 2024).

2.7 Catalyst Preparation Methods

The preparation method of catalysts plays a pivotal role in determining their physicochemical properties, such as crystallite size, surface area, porosity, and metal dispersion, which in turn govern catalytic activity and stability. Catalyst preparation methods profoundly determine the eventual physicochemical properties, active site density, and operational stability of heterogeneous catalysts, especially for reactions involving bond dissociation steps such as NH_3 decomposition (Ganguli & Bhatt, 2023). In heterogeneous catalysis, the active phase does not operate independently; it is the

synthesis route that governs how the metal precursor interacts with the support surface, the formation of metal oxygen bonds, the development of particle size distribution, and ultimately the stability of redox couple(s) during reaction cycles. Thus, the preparation method cannot be regarded as a simple synthetic step, but is in fact a kinetic pathway toward creating specific surface coordination environments that determine catalytic performance (Ishaq & Crawford, 2023).

Over the past decade, a wide spectrum of preparation strategies has been developed commercially and academically, each attempting to maximize metal dispersion, optimize metal support interaction, control porosity, enhance reducibility, suppress sintering, and stabilise active sites under harsh conditions involved in dehydrogenation reactions (Nemitallah et al., 2024). Conventionally, aqueous phase approaches such as impregnation, co-precipitation, sol gel processing and ion-exchange have dominated the field due to their simplicity, scalability, and cost-effectiveness. Impregnation, for example, allows precursor salts to infiltrate porous supports through capillary action, followed by drying and calcination to anchor the metal species (Florez et al., 2024). This technique is widely adopted in industrial refineries and is the backbone of commercial NH_3-to-H_2 catalyst preparations based on Ni/Al_2O_3. Meanwhile, co-precipitation ensures homogenous metal support interaction at the molecular scale by simultaneously precipitating metal cations and hydroxide species in alkaline medium, forming mixed hydroxycarbonates that convert into mixed oxides upon calcination.

The sol-gel process, in contrast, uses hydrolysis and polycondensation to develop a 3-D inorganic network capable of embedding metal ions in a colloidal matrix, yielding exceptional control of surface area, pore size, and nanostructure. Ion-exchange strategies have further enabled tailoring of catalytic sites by exchanging surface acidic/basic sites with metal precursors especially for zeolites and basic oxide supports providing remarkable atomic scale anchoring that minimises sintering during high temperature operation (Hossein Ali & Shin, 2022).

In parallel, gas-phase synthetic strategies such as chemical vapour deposition (CVD), atomic layer deposition (ALD), combustion synthesis and spray pyrolysis have emerged as powerful tools for engineering ultrathin conformal coatings, uniformly dispersed metal clusters, and metastable phases difficult to achieve via liquid routes (Rolo et al., 2024). CVD has demonstrated capability to deposit nanoscale catalytically active metallic films with well-controlled thickness and compositional uniformity,

while ALD is now recognised as one of the most precise tools for conformal atomic layer growth, enabling periodic deposition of metal and oxide sub-layers to engineer bifunctional surfaces that synergise electronic and geometric effects. Combustion synthesis and spray pyrolysis, meanwhile, deliver extremely small crystallites due to ultra-fast nucleation rates triggered by exothermic combustion reactions, producing metastable phases and high-defect density nanosurfaces with remarkable reactivity in hydrogenation and dehydrogenation pathways (El-Shafie, 2023).

Recent research trends have shifted further toward hybrid and green synthesis routes to improve sustainability, avoid hazardous solvents, and produce superior nanostructures using low-temperature energy efficient conditions. Hydrothermal and solvothermal techniques have become especially attractive within NH_3 decomposition catalyst research because their superheated confined water phase enables controlled nucleation, crystal growth, and carbonate formation under autogenous pressure(Zhang et al., 2023). This provides high dispersion and homogeneous incorporation of metal ions within mixed oxide supports, such as MgO-Al_2O_3, while also enabling defect engineering in the oxygen sub-lattice. Mechanochemical synthesis (ball milling) has also gained momentum as a solvent-free approach capable of inducing intimate mixing, defect generation, and direct formation of metal oxide phases without requiring bulk solvents. In addition, electrodeposition and electrochemical routes provide direct electronic control over nucleation and the oxidation state of the deposited metal species, enabling fabrication of nanostructured films, core–shell architectures and uniform coatings with high surface coverage at ambient temperatures. These techniques are now widely applied for designing high-performance non-noble catalysts (Spatolisano et al., 2023).

The selection of a preparation method is not arbitrary; it is governed by the targeted mechanistic pathway. NH_3 decomposition is a structure-sensitive reaction, where the rate-determining step is N-H bond scission and the rate controlling descriptor is the ability of metal centres to undergo reversible redox transitions without structural collapse. Therefore, catalysts must not only provide large surface area; they must stabilise active metallic states in a manner that promotes electron transfer into the anti-bonding orbitals of adsorbed NH_3. Preparation routes that generate ultra-small metal clusters, tune basicity to enhance N-H activation, and promote oxygen vacancy formation are critically relevant (Zainal et al., 2024).

Mixed oxide systems, especially $MgO\text{-}Al_2O_3$ based supports, are now increasingly engineered using multi-step preparation strategies to combine thermal stability (from Al_2O_3), strong basicity (from MgO), and metal anchoring sites (from spinel interfaces). Synthesis techniques such as hydrothermal carbonization and controlled electrodeposition provide a pathway to achieve these requirements by copying the defect chemistry and thermodynamic stabilisation trends reported in recent literature. Thus, catalyst preparation methodology is not a passive section of experimental procedure; it is the foundational design parameter that dictates active phase formation, metal-support chemistry, defect generation, oxygen vacancy concentration, reducibility, and finally catalytic turnover performance in NH_3 decomposition (Yu et al., 2024).

2.7.1 Hydrothermal Method

The hydrothermal method is a solution-based bottom-up synthesis strategy that operates in a sealed pressurised autoclave at temperatures above the boiling point of water, generating autogenous pressure that drives controlled nucleation, crystallisation, and phase transformation of metal precursors (Saeidi et al., 2023). Unlike classical wet impregnation, where precipitation often occurs abruptly on the external surface of the support, hydrothermal treatment allows precursor ions to slowly diffuse, reorganize, nucleate and grow into oxide phases within confined aqueous domains. This environment facilitates the generation of metastable intermediates (such as mixed hydroxy-carbonates and hydroxo-complexes) which upon calcination convert into highly dispersed metal oxide nanodomains intimately anchored to the support. As a result, hydrothermal synthesis provides exceptional control over crystallinity, particle size distribution, morphology, and metal support interfacial chemistry (Badreldin et al., 2023). One of the major advantages of the hydrothermal route is that crystallisation occurs under equilibrium-like slow kinetics rather than violent supersaturation events. This suppresses uncontrolled agglomeration, minimises sintering during nucleation, and promotes uniform dispersion of metal precursors across complex mixed oxide surfaces. Furthermore, elevated temperature pressure conditions enhance solubility and ionic mobility of precursors, enabling metal ions to penetrate deeply into support pores. For mixed oxide supports such as $MgO\text{-}Al_2O_3$, this is particularly important, because the hydrothermal environment promotes the formation of M-O-support anchoring bridges, oxygen vacancy formation, and local lattice distortions that strengthen metal support

coupling. Strong anchoring sites later translate into higher reducibility and stability of metal species under NH_3 decomposition conditions (Zhang et al., 2023).

Hydrothermal synthesis is also highly tunable. Reaction parameters such as pH, mineralizer type, precursor concentrations, solvent polarity, reaction temperature, and mineralising agents can be varied to control nucleation density, growth rate and defect chemistry (Kabatas, 2023). For example, alkaline conditions favour formation of metal hydroxide intermediates, whereas acidic conditions can promote formation of complex ions which later yield different oxide phases. Additionally, hydrothermal synthesis can generate unique microstructures such as hollow spheres, nanorods, flower-like architectures or layered nanosheets (Zhao et al., 2024). Such morphologies offer high surface areas and enhanced mass transport pathways which are beneficial for adsorption-controlled catalytic reactions such as NH_3 decomposition.

In the present research, the hydrothermal method was employed to synthesise both single metal oxides (CoO, FeO, ZnO) and bimetallic oxides (CoFeO, CoZnO) supported on $MgO\text{-}Al_2O_3$. This method ensured homogeneous incorporation of Co, Fe and Zn species into the mixed support architecture, stabilising them as finely dispersed nanoscale domains (Ogbonnaya et al., 2019). The hydrothermal route therefore provided a structural foundation that directly impacted catalytic performance: enhanced dispersion preserved active sites, strong interfacial anchoring prevented metal sintering at 650 °C reaction conditions, and the defect-rich local environment facilitated electron transfer to weaken N-H bonds. Thus, hydrothermal synthesis was not merely a preparation choice; it was a strategic design decision to generate catalysts that possess structural, electronic and morphological features compatible with efficient NH_3 decomposition (Wang & Azam, 2024).

2.7.2 Electrodeposition Method

Electrodeposition is a surface-selective technique that involves the electrochemical reduction of metal ions onto a conductive substrate under applied potential. This method offers precise control over film thickness, deposition rate, and metal loading by tuning deposition parameters such as current density, deposition time, and electrolyte concentration (Osman et al., 2022). Although not the central focus of

this study, preliminary exploration of electrodeposition was conducted to evaluate its feasibility for bimetallic catalyst fabrication. Electrodeposition presents several advantages, including room temperature synthesis, selective deposition of metal combinations, and minimal precursor waste. However, its applicability in high-temperature catalytic reactions remains dependent on the thermal and chemical stability of the substrate and deposited phase (Salehabadi et al., 2024).

Electrodeposition is an electrochemical technique widely explored in catalyst design due to its exceptional precision in controlling metal loading, composition, and nanostructure formation. Unlike solution-based precipitation or impregnation routes, electrodeposition utilizes redox reactions at an electrode surface to directly deposit metal species from ionic precursors in an electrolyte. By manipulating potential, current density, pH, and electrolyte composition, this method allows atomic-level control over nucleation and growth, leading to films or nanoparticles with tailored morphologies and uniform thickness (Salehabadi et al., 2024).

In catalysis research, electrodeposition has been particularly valuable for synthesizing monometallic and bimetallic catalysts with gradient or layered structures. The technique enables deposition of multiple metals either sequentially or simultaneously, producing alloys or core-shell configurations that often exhibit synergistic catalytic behaviour. Such architectures enhance charge transfer and modify electronic structures of active metals, which are critical factors in reactions involving bond activation such as NH_3 decomposition, CO_2 reduction, or hydrogen evolution (Navik, et al., 2024). Furthermore, electrodeposition often occurs at ambient temperature and atmospheric pressure, making it an energy-efficient and environmentally benign alternative to high-temperature calcination methods. The process also generates minimal chemical waste, since metal precursors are almost entirely consumed during deposition. The electrochemical environment during electrodeposition provides additional versatility in tailoring catalyst surface characteristics. Parameters such as applied potential, bath composition, and deposition time can be adjusted to influence the size, orientation, and crystallinity of deposited nanoparticles (Zuo et al., 2024).

For instance, pulsed electrodeposition where current or potential is applied intermittently produces catalysts with enhanced surface roughness, high defect densities, and open porous morphologies. These structural features are highly desirable for gas-phase reactions because they increase active-site accessibility and improve

reactant adsorption dynamics. Studies have shown that such nanostructured electrodes can deliver superior catalytic performance compared with their conventionally synthesized counterparts (Sekhar et al., 2024). Recent investigations have extended electrodeposition into the fabrication of bimetallic catalysts for hydrogen-related reactions. Co-Ni, Fe-Ni, and Co-Fe systems deposited on conductive supports (e.g., Ni foam, carbon cloth, and stainless-steel mesh) have demonstrated remarkable efficiency in ammonia decomposition and water electrolysis (Zhou et al., 2021).

The bimetallic configuration often enhances the redox flexibility and modifies the electronic density around the active centres, facilitating easier N-H bond dissociation. Furthermore, electrodeposited catalysts frequently exhibit strong metal–substrate adhesion, which prevents particle detachment during repeated redox cycles. The technique therefore bridges the advantages of thin-film stability and nanostructured surface activity, making it an attractive candidate for developing next-generation catalytic systems (Koo et al., 2024).

However, the applicability of electrodeposition in high-temperature catalytic environments remains constrained by the nature of the substrate. Since electrodeposition requires an electrically conductive base, most deposits are made on metals, foams, or carbonaceous materials. These substrates may undergo oxidation or structural degradation under thermal conditions exceeding 600 °C temperatures typically encountered during NH_3 decomposition. Consequently, while electrodeposition excels in low- and moderate-temperature applications, its direct integration into high-temperature heterogeneous catalysis demands substrate innovation or post-deposition stabilization strategies (AlAmoudi et al., 2024). Approaches such as hybrid electrodeposition calcination or co-deposition of oxide-forming metals are being explored to enhance thermal endurance.

In a broader research context, electrodeposition continues to play an important role as a complementary synthesis pathway. Its ability to fabricate uniform metallic layers and bimetallic interfaces offers insight into fundamental catalytic mechanisms and structure activity relationships. For instance, electrodeposited catalysts have been employed as model systems to study surface diffusion, alloy segregation, and oxidation reduction dynamics. These studies inform the rational design of catalysts produced by other methods, such as hydrothermal or sol-gel synthesis, where achieving similar nanoscale precision is more challenging (Meng et al., 2024).

Although the present work employs the hydrothermal carbonization (HTC) method as the principal synthesis route, the concept of electrodeposition is included in this review to emphasize its significance within the spectrum of modern catalyst-fabrication techniques (Yu et al., 2023). The precise metal dispersion and tunable interface chemistry attainable by electrodeposition illustrate the broader trend toward controllable nanostructuring in catalytic materials. Insights gained from electrodeposited systems particularly those highlighting the influence of metal synergy, support conductivity, and electronic coupling provide a valuable foundation for understanding structure function relationships in other catalyst architectures. Thus, while not directly utilized in this study, electrodeposition remains a pivotal reference point for advancing the rational design of active, stable, and economically feasible catalysts for hydrogen-related energy conversion processes (Zou et al., 2024).

2.7.3 Comparison with Other Synthesis Techniques

Although numerous catalyst synthesis strategies have been reported across catalytic science, the selection of an appropriate method is extremely crucial for ammonia decomposition due to the harsh reaction environment and the sensitivity of metal dispersion to thermal restructuring (Zhong et al., 2023). Among conventional liquid-phase methods, the sol-gel technique is widely used for nanostructured metal oxides; however, sol-gel systems often suffer from uncontrolled hydrolysis/condensation kinetics and formation of gel networks that trap metal precursors unevenly, causing significant spatial heterogeneity in metal distribution after calcination. Co-precipitation, on the other hand, can yield satisfactory metal loading levels, but coprecipitated materials frequently exhibit broad particle size distributions and require extensive filtration/washing steps that can remove or rearrange surface species, reducing catalytic reproducibility. Impregnation is one of the most industrially common methods, but impregnation strongly depends on pore volume, pore shape, capillary wetting, and metal salt diffusivity; this inherently leads to surface metal agglomeration during drying/calcination, especially when the support contains both acidic and basic sites such as MgO-Al_2O_3. Such inhomogeneity directly deteriorates reducibility and lowers the ratio of accessible metal sites two of the most controlling parameters for NH_3 decomposition (Zhong et al., 2023). Combustion synthesis has also been explored for mixed metal oxide catalysts, particularly where high crystallinity is

desired; however, combustion routes induce extremely fast exothermic temperature jumps (> 1500 °C in microseconds), which promote sintering, collapse transient porosity, and severely diminish surface area. Furthermore, combustion-derived ash often contains residual carbon/nitrates that require multiple calcination cycles to eliminate fully (Lodewyckx et al., 2023). These limitations collectively reveal why many reported catalysts with apparently promising compositions perform poorly once tested above 500 °C. The reaction environment of ammonia decomposition demands not only metal dispersion, but controlled oxide–support coupling, manageable grain boundary stresses, and gradual crystallite evolution. Hydrothermal methods by virtue of slow nucleation, controlled growth, and reaction confinement within a liquid-filled autoclave uniquely satisfy this demand. Under hydrothermal conditions, primary crystallite size and lattice strain can be directed by tuning solvent polarity, pH, chelation strength, and precursor dissolution kinetics (Gupta et al., 2023). This allows mixed MgO-Al_2O_3 frameworks to form spinel sub-lattices capable of anchoring transition metal oxides without phase segregation. Therefore, hydrothermal synthesis is not simply “one more” synthesis method it is a synthesis philosophy that matches the mechanistic requirements of NH_3 decomposition.

In fact, literature shows that the most successful non-noble catalysts reported in the past five years for NH_3 decomposition share one common trait: the synthesis method allowed controlled nanoscale integration and moderated metal oxygen bond disruption during calcination. Hydrothermal synthesis excels specifically in these domains and therefore represents not only a feasible choice, but a technically rational and strategically superior route for preparing catalysts intended to operate in the high-temperature, redox-coupled regime required for carbon-free hydrogen generation from NH_3 (Duan et al., 2012).

2.8 Response Surface Methodology (RSM)

Response Surface Methodology (RSM) is a robust statistical and mathematical technique used for modelling and optimizing processes in which several variables influence the desired outcome. In catalyst development, RSM is particularly valuable as it enables systematic investigation of the effects of multiple synthesis or reaction parameters and their interactions, while minimizing the number of experimental runs required (Ahmad & Yadav, 2024). In the context of ammonia (NH_3) decomposition, the

catalytic activity is influenced by various operational and preparation parameters, such as reaction temperature, gas hourly space velocity (GHSV), metal loading, and synthesis variables (e.g., deposition time, precursor concentration, and applied voltage). RSM provides a structured framework to evaluate the combined influence of these variables on key performance metrics such as NH_3 conversion and H_2 yield. One of the widely used RSM designs is the Box-Behnken Design (BBD), which is well-suited for response optimization with three or more independent variables (Gönen et al., 2016). BBD avoids extreme combinations of variable levels, making it a safer and more efficient design for experimental catalytic studies, especially those involving high-temperature reactions or reactive gases like ammonia. In recent years, experimental design has become essential in the field of research because it reduces the number of experiments required to determine the optimal operating conditions for maximizing the desired output (Gönen et al., 2016). As a result of the numerous features associated with experimental design, scholars are progressively depending on these statistical techniques, including Response Surface Methodology (RSM), to facilitate the research process.

In this study, RSM is employed to optimize the synthesis and operational parameters of the bimetallic catalysts supported on $MgO\text{-}Al_2O_3$. The use of RSM facilitates the identification of optimal conditions for maximizing NH_3 conversion while minimizing energy input and material waste. Additionally, RSM enables the generation of empirical models that describe the behaviour of the system, which can be used to predict performance under untested conditions and guide future experimental work. The integration of RSM into the catalyst development workflow not only enhances the statistical reliability of the findings but also provides deeper insight into the interdependencies of key variables. This approach is critical in developing high-performance, economically viable catalysts for sustainable hydrogen production. The fundamental stages for using RSM in any research are depicted.

2.9 Reactor for The Ammonia Decomposition

The catalytic decomposition of ammonia to hydrogen is highly endothermic, achieving high conversion under high-temperature and low-pressure conditions. An efficient heat source is essential, but advances in both materials and reactor design remain challenging. To address these issues, researchers have explored various reactor

configurations (Nailwal et al., 2024). Reactors serve as the primary platform for evaluating catalyst performance, and their design significantly influences hydrogen yield and purity. Commonly studied reactor types for ammonia decomposition include fixed-bed, catalytic membrane, microreactor, micro-post, microwave plasma, solar, and fluidized-bed membrane reactors. Reactor design is especially critical in catalytic ammonia decomposition systems. An optimal design must enable rapid heating and precise temperature control during startup, shutdown, and load variations, while maximizing catalytic surface area and minimizing heat losses (Yu et al., 2023). The choice of reactor type and its operational parameters such as ammonia flow rate, partial pressure, reactor dimensions, pressure drop, temperature gradients, and sweep gas use strongly govern overall catalyst performance.

2.9.1 Fixed-Bed Reactors

Fixed-bed reactors are widely used but have limitations for fast catalytic reactions. Large temperature gradients due to their size and weight can reduce ammonia conversion efficiency, and they often suffer from high pressure drops and difficulties in maintaining consistent flow rates (He et al., 2023). Although decomposition typically occurs at 700–900 °C, with higher feed temperatures improving conversion, the inherent design constraints of fixed beds make them less suitable for processes requiring rapid heat transfer.

2.9.2 Catalytic Membrane Reactors

Catalytic membrane reactors, typically employing Ru or Ni catalysts on alumina supports, offer integrated reaction and separation. While some systems have shown promising performance at temperatures as low as 450 °C, they have not yet been fully optimized with the most effective catalysts (González et al., 2023)

2.9.3 Microreactors

Microreactors emerged in the early 1990s as a promising technology for on-demand hydrogen production, particularly for fuel-cell applications. Their small diffusion paths enable high heat-transfer coefficients, effectively eliminating temperature gradients. Compact design, high mixing efficiency, and large surface-area-to-volume ratios lead to superior mass and heat transfer rates (Cechetto et al., 2022) (Badakhsh & Bhagavathy, 2024). However, challenges include high pressure

drops, potential toxic emissions, complex combustion dynamics, and the need for additional oxidation catalysts. Scaling microreactors for industrial applications also remains difficult due to mass-transfer limitations in some configurations (Asif et al., 2023).

2.9.4 Micro-Post Reactors

Micro-post reactors consist of static pillar-like structures arranged in a flow channel and coated with catalyst. Their high mixing capacity enhances mass transfer to the catalyst surface, especially under high-flow conditions. For example, (Li et al., 2024) developed a micro-post reactor with 250 anodized aluminum posts coated with a Ru catalyst. The reactor achieved 85 % NH_3 conversion at 650 °C with an ammonia flow rate of 15 sccm, producing hydrogen equivalent to 13 W. Conversion is strongly influenced by pore structure and size. A typical micro-post reactor system comprises four sections: feed, reaction, post-treatment, and analysis Figure 2.14. In such setups, ammonia is pre-heated (~30 °C) to maintain gas pressure, mass-flow controllers regulate gas feeds, and a multi-zone electric furnace provides uniform heating for the membrane module. A vacuum pump (e.g., ULVAC DTC-22B) is often used to remove hydrogen from the permeate side, enhancing driving force for separation (Arsad et al., 2023; Dincer & Acar, 2014).

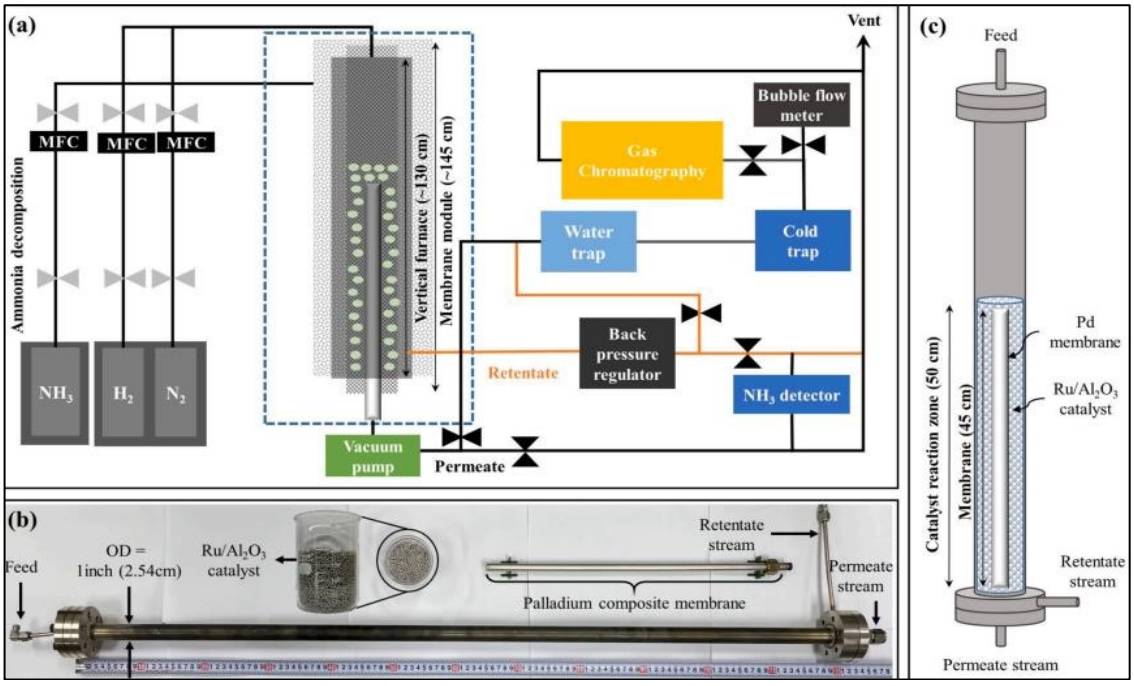


Figure 2.9 Schematic of Hydrogen Permeation and Ammonia Decomposition Test: (a) Flow Diagram of the Testing Rig, (b) Membrane Reactor Module, and (c) Schematic of the Membrane Reactor (Ghannadi & Dincer, 2024)

2.10 Catalytic Membrane Reactor for Ammonia Decomposition

The integration of catalytic and separation functions into a single unit through catalytic membrane reactors (CMRs) represents a significant advancement in the field of ammonia decomposition for hydrogen production (Lalman et al., 2023). Traditional reactor systems require separate units for hydrogen recovery and ammonia conversion, leading to increased costs and spatial requirements. In contrast, CMRs streamline the process by combining these functions, thus enhancing efficiency and reducing the footprint of hydrogen production facilities (Marcoberardino et al., 2017). CMRs utilize a selective membrane that allows for the simultaneous removal of hydrogen during the ammonia decomposition reaction over a catalyst, typically a Ni-based catalyst within a palladium (Pd) membrane reactor. This configuration not only improves ammonia conversion rates but also ensures the direct production of high-purity hydrogen. By shifting the reaction equilibrium via hydrogen removal, CMRs facilitate complete ammonia conversion at lower temperatures, thereby enhancing the overall thermodynamic efficiency of the process. The effectiveness of this setup is depicted in Figure 2.10, which shows a schematic diagram of a catalytic membrane reactor for NH_3 decomposition. This visual representation helps illustrate how CMRs function, integrating both the reaction and separation processes within a single unit, thereby improving the operational efficiency of hydrogen production from ammonia (Wan et al., 2021).

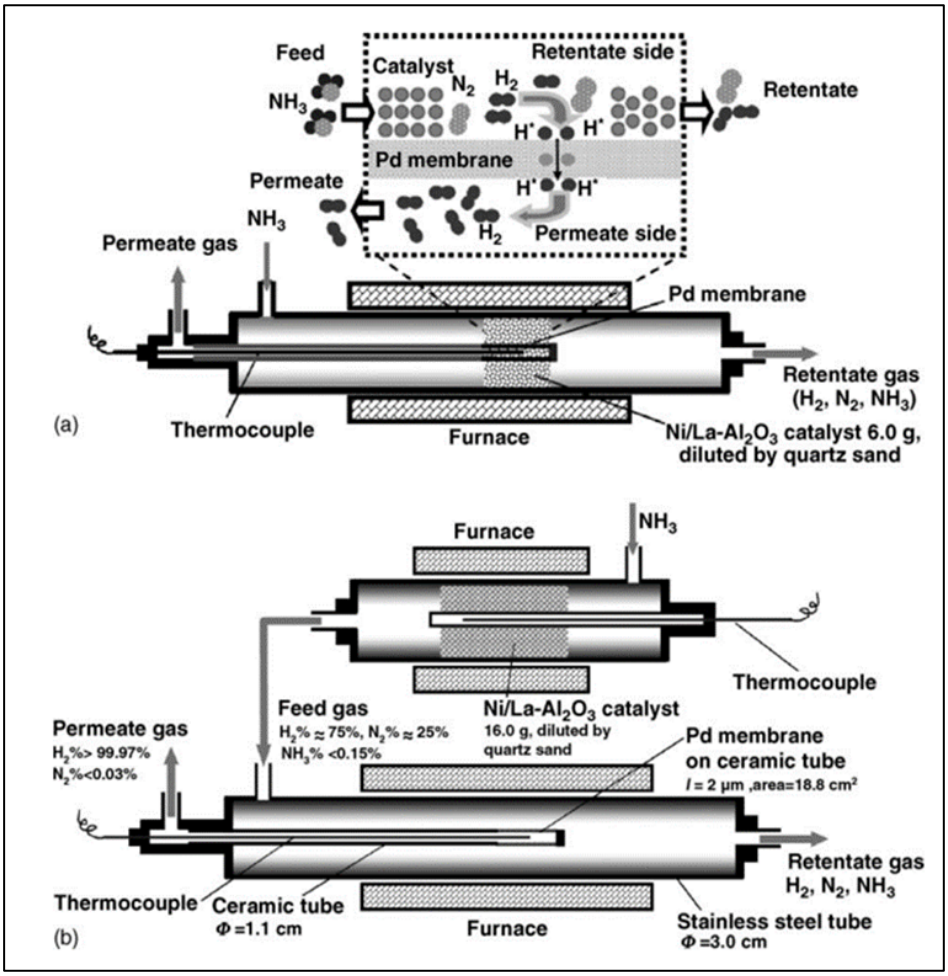


Figure 2.10 Schematic Diagram of (a) Membrane Reactor for NH_3 Decomposition and (b) NH_3 Cracker Integrated with Membrane Separator (Alharthi et al., 2023) (Adapted with Permission from Elsevier)

In a study by (Itoh et al., 2021) the effectiveness of Pd-coated membranes in boosting ammonia decomposition was demonstrated. Experiments showed that integrating these membranes into the reactor setup could increase ammonia conversion to nearly complete levels at optimized conditions of temperature and pressure, highlighting the potential of CMRs in enhancing the efficiency of hydrogen production. The utilization of CMRs also aligns with environmental sustainability goals by reducing the energy required for hydrogen production and minimizing the carbon footprint associated with traditional hydrogen production methods. These reactors are particularly promising for their ability to produce hydrogen at high purity levels, which is critical for applications such as fuel cells where impurities can significantly impact performance (Li et al., 2022). Membrane technology in CMRs typically involves either dense metallic membranes, like those made from Pd or its alloys, or proton-conducting ceramic membranes. These materials are chosen for their high hydrogen selectivity and

ability to operate across a broad temperature range. However, the high cost and challenges associated with scaling up these technologies remain significant hurdles (Chatterjee & Thynell, 2019).

The architectural design of CMRs often includes an inert sweep gas on the permeate side of the membrane to assist in the removal of hydrogen. This setup can, however, dilute the hydrogen stream, which is a disadvantage if high-purity hydrogen is required. Alternatively, vacuum conditions can be used to enhance hydrogen permeation without the need for a sweep gas, thereby maintaining the purity of the hydrogen produced. Innovations in CMR design continue to evolve, with studies exploring the use of advanced materials and configurations to further optimize ammonia conversion rates and hydrogen purity (Mensah et al., 2022).

These advancements are critical for the development of a more sustainable and economically viable hydrogen production industry. Optimizing the performance of CMRs involves a delicate balance between maximizing hydrogen recovery and maintaining operational efficiency and catalyst effectiveness (Nadiri et al., 2023). The strategic placement of catalysts within the reactor, the choice of membrane materials, and the control of operational parameters such as temperature and flow rates are all crucial factors that need to be finely tuned to achieve the best results.

2.11 Fixed Bed Reactor for NH_3 Decomposition

Fixed bed reactors (FBRs) have many large-scale applications in the industry, with one advantage being that the catalyst is immobilized, and the reaction is technically forced to be in contact with it. The FBRs did not include an H_2 separation unit, hence normally the H_2 yield, and purity are not included. The presence of NH_3 in the H_2-rich stream that feeds to the GC must be avoided to prevent corrosion. An FBR was used for the decomposition of NH_3 by using a commercial 5 Wt.% Ru/C catalyst on different promoter Cs loadings. The optimum Cs/Ru molar ratio was 4.5 and a further increase than that resulted in a decrease in the conversion of ammonia. At 400 °C ammonia conversion was nearly 100%. The use of Ru catalyst makes the high conversion of NH_3 possible at low temperatures, which supports the statement that Ru is the best catalyst for NH_3 decomposition. Several other studies also reported that the high conversion of NH_3 is obtained when using Ru as a catalyst for the FBR reactor. Among them, the study by (Koo et al., 2023) managed to have a 96.8% NH_3 conversion at 450 °C and 4

bar operating conditions when using a Ru-based catalyst without a membrane being used to observe the H_2 preproduction (Akarçay et al., 2020).

Even though the noble metal Ru is known as the best catalyst for NH_3 decomposition, the high price and unavailability make it difficult for practical production applications. Hence, the noble metal Ni is among the alternative metals that have been widely used to discover the potential to replace the noble Ru. Ni-based catalysts are important for NH_3 decomposition where they can perform effectively and even have the same performance as Ru-based catalysts but only happen at high temperature ranges. The study from (Gu et al., 2021) used a Ni-based catalyst and heated up to 650 °C in the FBR to convert 99.1% of NH_3. Another study that used a Ni-based catalyst is from (Xue et al., 2023) which managed to have 100% NH_3 conversion at 600 °C. The promising performance of Ni-based catalysts in converting NH_3 using FBR has motivated researchers to combine Ni with Ru as an effort to reduce the concentration of Ru for producing catalyst in NH_3 conversion. Hence the study from and managed to lower the temperature to around 500 °C and to convert the NH_3 up to 99.6% when combining the Ni with Ru as a catalyst (Sordakis et al., 2018).

Developed Co_3Mo_3N and γ-Mo_3N catalysts with the use of citric acid as a chelating agent. The catalyst was tested in a fixed bed quartz tube reactor at atmospheric pressure, temperature ranges of 300-600 °C, and constant GHSV of 6000 h^{-1}. At 550 °C, γ-Mo_3N performed a 71.9% NH_3 conversion while Co_3Mo_3N gave 97.3% conversion resulting in a better catalytic performance indicating that Co particles promote ammonia decomposition. Additionally, at a higher temperature of 600 °C, both catalysts gave 100% conversion. Besides that, the stability test was conducted and both catalysts showed no deactivation after 35 h of a continuous test. This was validated by measuring the crystallite size of the fresh (6.20 nm) and the used catalysts (6.19 nm) which observed no significant decrease (Li et al., 2023; Wijayanta et al., 2019).

CHAPTER 3
RESEARCH METHODOLOGY

3.1 Introduction

This chapter presents the comprehensive research methodology adopted for the design, synthesis, characterization, and catalytic evaluation of single and bimetallic oxide catalysts supported on $MgO\text{-}Al_2O_3$ for the decomposition of ammonia (NH_3) into hydrogen (H_2). The experimental framework was strategically structured into two consecutive and interdependent phases to ensure a systematic understanding of both material development and performance optimization. In Step 1 (Screening Stage), a series of monometallic catalysts $CoO/MgO\text{-}Al_2O_3$, $FeO/MgO\text{-}Al_2O_3$, and $ZnO/MgO\text{-}Al_2O_3$ were synthesized via a controlled hydrothermal process followed by thermal calcination. Each catalyst was thoroughly characterized to establish structure property correlations and to determine its intrinsic catalytic activity for NH_3 decomposition. The objective of this stage was to identify the most catalytically active and thermally stable base metal that could serve as a foundation for advanced multimodally systems.

Building upon these findings, Step 2 (Optimization Stage) focused on developing bimetallic catalysts $CoFeO/MgO\text{-}Al_2O_3$ and $CoZnO/MgO\text{-}Al_2O_3$ derived from the most promising monometallic precursor identified in Step I. These bimetallic systems were expected to exhibit enhanced hydrogen production efficiency through synergistic effects such as improved metal dispersion, stronger metal support interactions, and increased resistance to sintering and deactivation. Both single and bimetallic catalysts were synthesized using a two-step hydrothermal route, followed by calcination, detailed physicochemical characterization, and catalytic testing in a fixed-bed quartz reactor. Comprehensive characterization techniques including X-ray diffraction (XRD), field-emission scanning electron microscopy with energy-dispersive X-ray spectroscopy (FESEM-EDX), Brunauer-Emmett-Teller (BET) surface area analysis, thermogravimetric analysis (TGA), and temperature-programmed reduction (TPR) and X-ray photoelectron spectroscopy (XPS) were employed to evaluate the crystallinity, morphology, surface area, thermal stability, and reducibility of the prepared catalysts.

These analyses provided critical insights into how compositional and structural factors influence catalytic activity and durability. Catalytic activity tests were performed under precisely controlled conditions in thermocatalytic reactor. The hydrogen yield and NH_3 conversion efficiency was systematically evaluated as functions of temperature and gas hourly space velocity (GHSV). Furthermore, Response Surface Methodology (RSM), utilizing the Box-Behnken Design (BBD), was implemented to statistically optimize reaction parameters and to model the complex interactions between synthesis and operational variables. Finally, kinetic were conducted to elucidate the reaction mechanism and to determine the energy requirements and feasibility of NH_3 decomposition on the optimized catalysts. The combined experimental and analytical framework described in this chapter provides a coherent methodological pathway to achieving high-efficiency, cost-effective, and durable catalytic systems for sustainable hydrogen generation. overall research methodology for the development and evaluation of Co-Fe-Zn bimetallic catalysts is illustrated in Figure 3.1.

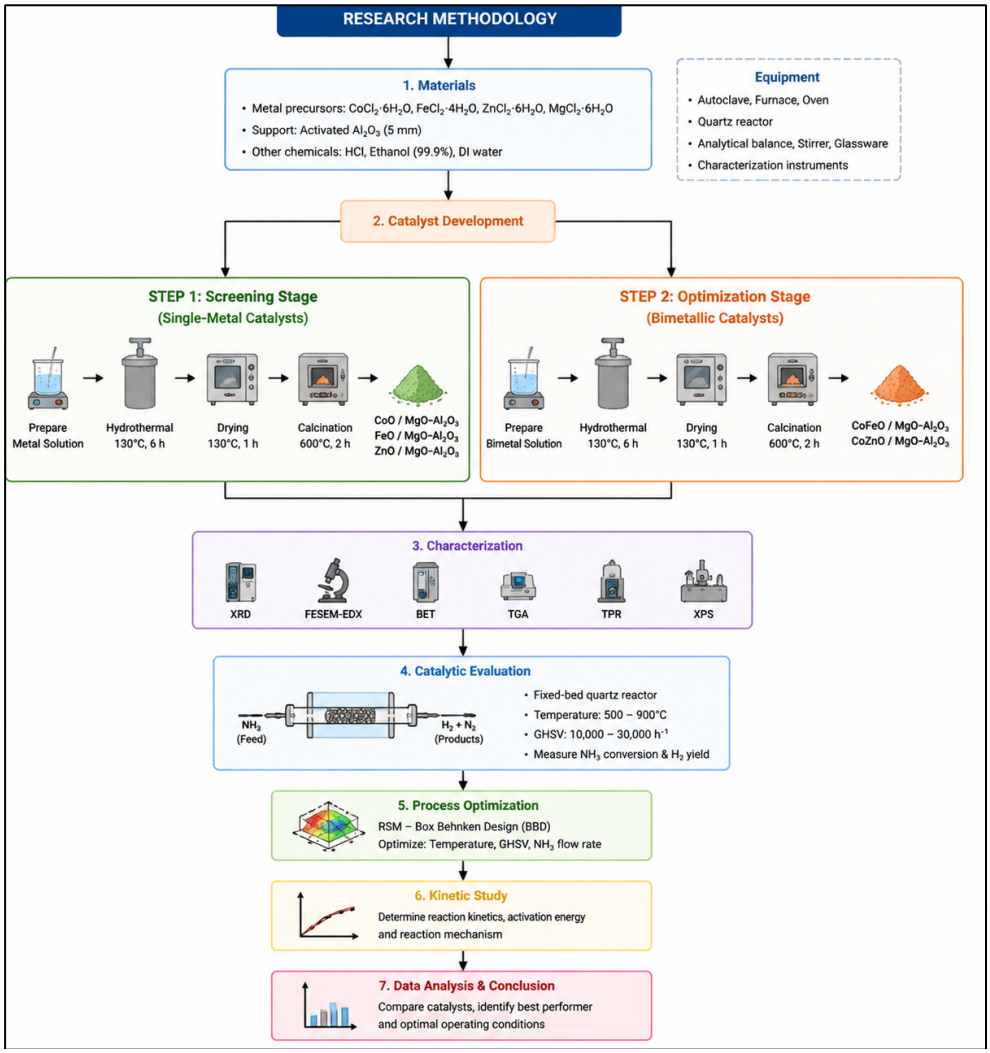


Figure 3.1 Flowchart of the Research Methodology Showing Catalyst Screening, Bimetallic Synthesis and Optimization, Characterization, Performance Testing, RSM Optimization, and Kinetic/Recyclability Analysis

3.2 Materials and Methods

3.2.1 Chemicals

All chemicals used were of analytical grade and utilized without further purification. The reagents included Cobalt chloride hexahydrate ($CoCl_2·6H_2O$ 99.9% purity), Iron chloride hexahydrate ($FeCl_2·6H_2O$ 99.8% purity), Zinc chloride hexahydrate ($ZnCl_2·6H_2O$ 99.9% purity), and Magnesium chloride hexahydrate ($MgCl_2·6H_2O$ 99.9% purity) as metal precursors. Activated alumina beads (Al_2O_3, 5 mm 99.9% purity) were used as the support substrate. Additional reagents such as hydrochloric acid (HCl) and absolute ethanol (C_2H_5OH, 99.9% purity) were purchased from Chemiz, Malaysia. Deionized water was used for all solution preparations and washing procedures.

3.2.2 Equipment and Apparatus

The experimental work was performed using standard laboratory glassware including 250 mL and 1000 mL beakers, measuring cylinders, glass rods, conical flasks, pipettes, analytical balance (±0.0001 g), and a magnetic stirrer. Hydrothermal synthesis was conducted in a TOMY Autoclave SS-325 (Japan), and the solid products were calcined in a Carbolite high-temperature furnace. Catalyst drying was carried out in a Memmert oven, and sieving was performed using an ASTM E-11 Standard Test Sieve (250 μm) to ensure uniform particle size distribution.

3.3 Development of Catalyst

3.3.1 Preparation of MgO-Al_2O_3 Support (Step 1)

A 1.0 M aqueous magnesium chloride solution ($MgCl_2 \cdot 6H_2O$) was prepared was prepared using deionized water under continuous stirring. Activated Al_2O_3 beads were introduced into the solution, and the suspension was transferred into a 100 ml of Teflon-lined stainless-steel autoclave. Hydrothermal treatment was performed at 130 °C for 6 hours to promote ion exchange and the formation of Mg-Al composite oxide precursors. The obtained solid was filtered, thoroughly washed with deionized water, and dried at 130 °C for 1 hour. Finally, the dried composite was calcined at 600 °C for 2 hours, yielding MgO-Al_2O_3 as a thermally stable mixed-oxide support with enhanced surface basicity (Cho et al., 2017).

3.3.2 Preparation of Single-Metal Catalysts of CoO, FeO, ZnO Supported on MgO-Al_2O_3 (Step 2)

Single-metal catalysts were synthesized via a hydrothermal method. A 1.0 M aqueous solution of each metal precursor ($CoCl_2 \cdot 6H_2O$, $FeCl_2 \cdot 4H_2O$, and $ZnCl_2$) was prepared using deionized water under continuous stirring to ensure homogeneous metal dispersion. A measured amount of MgO-Al_2O_3 support (2 g) was introduced into the solution, and the resulting suspension was transferred into a 100 ml Teflon-lined stainless-steel autoclave. Hydrothermal treatment was carried out at 130 °C for 6 h, followed by filtration, washing, and drying at 130 °C for 1 h. The dried samples were subsequently calcined at 600 °C for 2 h to obtain the metal-oxide-loaded MgO-Al_2O_3 composites (Cho et al., 2017).

This procedure yielded three catalysts: CoO/MgO-Al_2O_3, FeO/MgO-Al_2O_3, and ZnO/MgO-Al_2O_3.

3.3.3 Preparation of Bimetallic Catalysts (CoFeO and CoZnO Supported on MgO-Al_2O_3) (Step 3)

Based on the screening of single-metal catalysts, cobalt was identified as the most catalytically active component and selected for bimetallic formulation. Bimetallic catalysts were synthesized using a hydrothermal method, combining $CoCl_2 \cdot 6H_2O$ (99.9% purity) with either $FeCl_3 \cdot 6H_2O$ (99.5% purity) or $ZnCl_2$ (99.8% purity) in a 1:1 molar ratio. The mixed precursor solution was prepared in deionized water under continuous stirring. Subsequently, 2 g of MgO-Al_2O_3 support (99.9% purity) was added, and the suspension was transferred into a 100 mL Teflon-lined stainless-steel autoclave. Hydrothermal treatment was conducted at 130 °C for 6 h, followed by filtration, washing with deionized water, drying at 130 °C for 1 h, and calcination at 600 °C for 2 h. The resulting bimetallic oxide catalysts, CoFeO/MgO-Al_2O_3 and CoZnO/MgO-Al_2O_3, were expected to exhibit enhanced hydrogen production efficiency through synergistic effects, improved metal dispersion, and increased resistance to deactivation, addressing Objectives 1 and 2 of this study. The overall synthesis workflow is summarized in Figure 3.2.

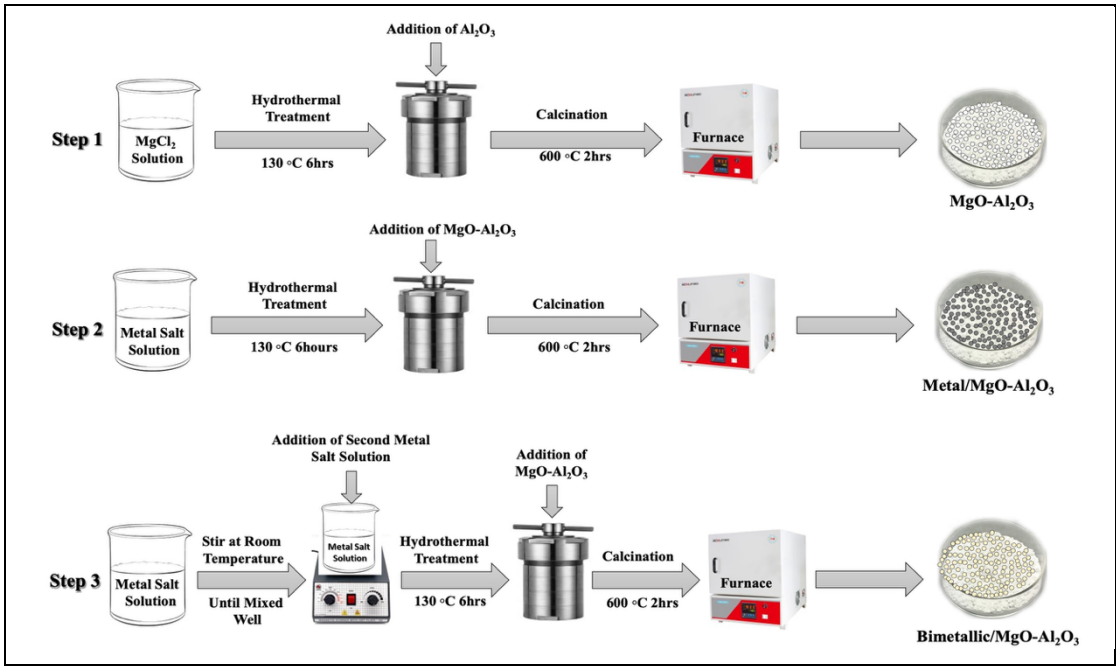


Figure 3.2 Schematic Illustration of the Three-Step Hydrothermal and Calcination Process Used for Synthesizing MgO-Al_2O_3 Support (Step 1), Single Metal/MgO-Al_2O_3 Catalyst (Step 2), and Bimetallic/MgO-Al_2O_3 Catalyst (Step 3)

3.4 Catalyst Characterization

Comprehensive physicochemical characterization was conducted to establish the relationship between structure and catalytic activity.

3.4.1 Catalyst Phase and Crystallinity

The crystalline structure and phase composition were determined using X-ray Diffraction (XRD) (Panalytical X'Pert Pro PW 3040/60) with Cu Kα radiation (λ = 0.154 nm) at 40 kV and 40 mA. Scans were recorded over 30°-90° (2θ) with a step size of 0.02°. Phase identification was carried out using the JCPDS database, and average crystallite sizes were calculated using the Debye-Scherrer equation. This analysis confirmed the formation of desired metal oxide phases and provided insight into metal dispersion and structural uniformity on the $MgO\text{-}Al_2O_3$ support.

3.4.2 Catalyst Morphological and Elemental Analyses

Field emission scanning electron microscopy (FESEM, JEOL JSM-7600F) was used to examine surface morphology, particle size, and dispersion of active species. Prior to imaging, samples were sputter-coated with a thin gold layer to prevent charging. Images were captured at multiple magnifications to assess surface roughness, porosity, and metal distribution. energy-dispersive x-ray spectroscopy (EDX) was employed to determine elemental composition and confirm the presence of Co, Fe, Zn, Mg, Al, and O, verifying homogeneous metal dispersion across the support.

3.4.3 Surface Characteristics by Brunauer-Emmett-Teller Surface Area and Porosity Analyser

Textural properties were analyzed by brunauer-emmett-teller (BET) surface area measurement using a BEL Japan BELSORP-mini analyser. Samples were degassed at 150 °C for 24 hours before measurement. Nitrogen adsorption desorption isotherms were recorded at 196 °C, and surface area was calculated using the BET method, while the Barrett-Joyner-Halenda (BJH) model provided pore size distribution and pore volume. These results confirmed that the catalysts possessed mesoporous structures with suitable surface area and pore geometry for enhanced NH_3 decomposition.

3.4.4 Catalyst Thermal Stability

Thermogravimetric Analysis (TGA) was conducted using a TA Instruments TGA 5500 under an inert atmosphere. Approximately 15 mg of sample was heated from room temperature to 900 °C at a rate of 10 °C/min. The resulting thermogram revealed distinct weight-loss stages corresponding to moisture removal, decomposition of hydroxides, and stabilization of metal oxides. The high thermal stability confirmed the structural robustness of the catalyst during high-temperature NH_3 decomposition.

3.4.5 Catalyst Reduction Potential

Temperature-Programmed Reduction (TPR) measurements were performed using a BELCAT-B analyser equipped with a thermal conductivity detector (TCD). About 0.05 g of catalyst was pretreated in nitrogen at 120 °C for 2 hours, then cooled to 40 °C before exposure to a 5 % H_2/Ar mixture. The temperature was raised to 1000 °C at 10 °C/min. The reduction peaks obtained indicated the presence of multiple reducible species and revealed the strength of metal support interactions. Lower reduction temperatures reflected enhanced metal dispersion and catalytic activity.

3.4.6 X-Ray Photoelectron Spectroscopy

X-ray photoelectron spectroscopy (XPS) measurements were performed using an Omicron DAR 400 XPS system equipped with a Mg/Al X-ray source and a CN10 charge neutralizer to compensate for surface charging effects. The analysis was conducted at an anode voltage of 10 kV and an emission current of 10.0 mA. Survey spectra were collected with a pass energy corresponding to a resolution of 1.0 eV, while high-resolution spectra were acquired at 0.1 eV resolution to accurately determine the chemical states of surface elements.

3.5 Catalytic Performance Evaluations

The thermocatalytic reactor configuration is illustrated in Figure 3.3, about 2g of catalyst supported on MgO-Al_2O_3 beads loaded were placed in a quartz reactor with an internal diameter of 22 mm. The system was purged with Ar gas at flow rate of 50 mL/min, while the temperature was ramped from room temperature to 650 °C. After that, the Ar gas flow was turned off and immediately switched to NH_3 feed to the

reactor. The NH_3 flow was regulated using a mass flow controller to maintain a GHSV of 5000 mL/gcat.h, with respect to the mass of deposited layer on the MgO-Al_2O_3 beads. The composition of H_2 in the outlet gas was measured online using a Siemens Calomat 6 Continuous Gas Analyzer. The data were recorded in real-time using a Continuous Emissions Monitoring System (CEMS) software to monitor the H_2 production yield over time (Cho et al., 2017; Nasir et al., 2026). Then the NH_3 conversion is calculated by using [Eq 3.1].

$$NH_3\% = [2y_{H2} / (3-2y_{H2})] \times 100\% \quad (3.1)$$

Where y_{H2} is the percentage fraction of H_2 production from the analyzer.

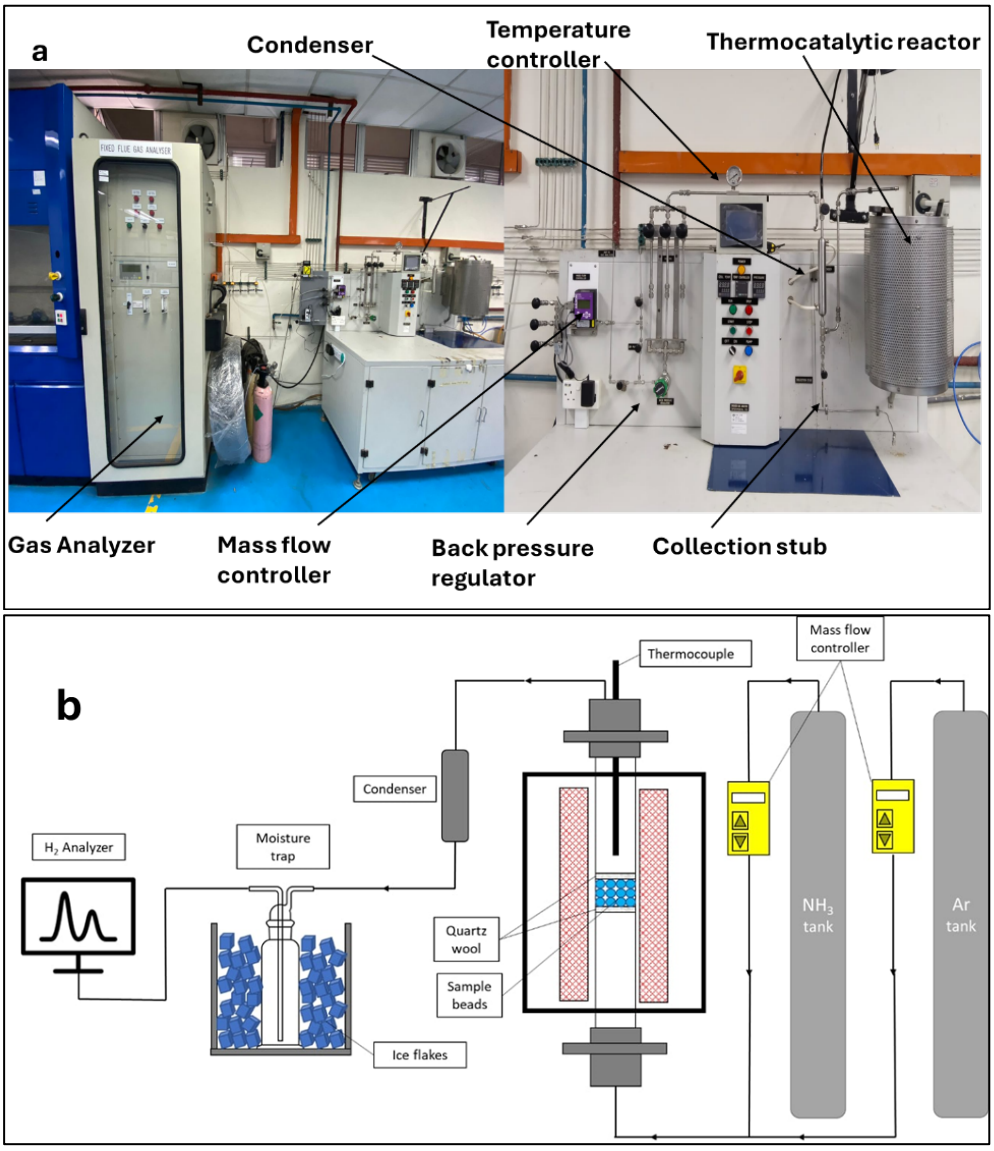


Figure 3.3 (a) Photographs of the Experimental Reactor System Used for Catalytic Performance Evaluation and (b) Schematic Diagram of the Thermocatalytic Reactor Setup for NH_3 Decomposition

3.6 Experimental Design Using Box-Behken Design (BBD)

Following the screening stage, the most active catalyst CoFeO/MgO-Al_2O_3 was selected for statistical optimization using Response Surface Methodology (RSM) to maximize the efficiency of ammonia (NH_3) decomposition and hydrogen (H_2) production. BBD is a response surface methodology that provides accurate equations for expressing the interplay between factors and responses. The Design-Expert program (version 13, Stat-Ease, Minneapolis, USA) was used for the purpose of designing experiments and analyzing the resulting data (Gönen et al., 2016).

Three independent variables, namely Concentration (A), Temperature(B), and Time (C) were optimized by using BBD for the CoFeO/MgO-Al_2O_3 catalyst via NH_3 conversion. The levels and ranges of independent variables and their codes are shown in Table 3.1.

Table 3.1
Codes and Actual Variables and Their Levels in BBD

codes	variables	Level 1(-1)	Level 2 (0)	Level 3 (+1)
A	Concentration (M)	0.2	0.6	1
B	Temperature (°C)	120	150	180
C	Time (hrs)	5	7	9

A second-order polynomial model was utilized to estimate the NH_3 conversion as presented in the following (Eq 3.2).

$$Y = \beta_0 + \mathbf{\Sigma}\, \beta_i X_i + \mathbf{\Sigma}\, \beta_{ii} X_i^2 + \mathbf{\Sigma\Sigma}\, \beta_{ij} X_i\, X_j \qquad (3.2)$$

Where Y is the expected response for NH_3 conversion percentage, β_0 is the constant, βi is the linear coefficient of the input parameter, βii is the quadratic coefficient of the input parameter, βij is the interaction coefficient between the input parameters, while Xi and Xj are the coded independent variables. BBD designs a total of 17 experiments (runs) to optimize and assess the effects of three independent factors on the NH_3 conversion which is shown in Table 3.2. These variables are A: Concentration (0.2 - 1.0 M), B: Temperature (120 - 180 °C), and C: Time (5- 9 hrs.).

The optimal ranges and levels for BBD-RSM were chosen based on the outcomes from

Run	Factor 1 A:Conc (M)	Factor 2 B:Temp C	Factor 2 C:Time hrs	Response 1 NH_3 conversion %
1	0.2	120	7	
2	1.0	120	7	
3	0.2	180	7	
4	1.0	180	7	
5	0.2	150	5	
6	1.0	150	5	
7	0.2	150	9	
8	1.0	150	9	
9	0.6	120	5	
10	0.6	180	5	
11	0.6	120	9	
12	0.6	180	9	
13	0.6	150	7	
14	0.6	150	7	
15	0.6	150	7	
16	0.6	150	7	
17	0.6	150	7	

preliminary experiments.

Table 3.2
The BBD Three-Variable Matrix for NH_3 Conversion Using $CoFeO/MgO\text{-}Al_2O_3$

3.7 Kinetic Study of Catalyst

To gain a deeper understanding of the reaction mechanism and rate behavior of ammonia (NH_3) decomposition, a detailed kinetic study was performed on the most active catalyst, identified as $CoFeO/MgO\text{-}Al_2O_3$ from the screening and optimization stages. This kinetic evaluation provides fundamental insight into the intrinsic reaction mechanism, surface processes, and diffusion characteristics governing the decomposition of NH_3 into hydrogen (H_2) and nitrogen (N_2). The kinetics of

CoFeO/MgO-Al_2O_3 catalyst for NH_3 conversion were studied using standard kinetic models: pseudo-first order (PFO), pseudo-second order (PSO) and intraparticle diffusion (IPD). The non-linear forms of PSO, PSO and IPD models are shown in (Eq 3.3 - 3.4) respectively.

$$qt = qe(1 - exp - k1t) \tag{3.3}$$

$$qt = qe2k2t \tag{3.4}$$

Where qe and qt represent adsorption capacity (mg/g) at equilibrium and time respectively and k is the rate constant (1/min).

3.8 The Recyclability of Catalyst

The recyclability and durability of the most active catalyst, CoFeO/MgO-Al_2O_3, were examined through a series of consecutive decomposition cycles to evaluate its long-term operational stability. After each catalytic run, the reactor was allowed to cool to ambient temperature, and the spent catalyst was regenerated in situ by mild thermal treatment under a 5 % H_2/Ar stream at 600 °C for 1 h to reactivate surface metal sites. The regenerated catalyst was then reused under identical reaction conditions feed composition, temperature window, and gas hourly space velocity to ensure accurate performance comparison.

The NH_3 conversion efficiency and H_2 yield were recorded for each cycle to detect any loss of activity or selectivity that could result from metal sintering, oxidation, or surface poisoning. Across several successive cycles, only minimal variation in conversion was observed, confirming the high structural integrity and redox resilience of the CoFeO/MgO-Al_2O_3 system. The strong metal support interaction and the thermal stability of the MgO-Al_2O_3 matrix effectively suppressed particle agglomeration, enabling consistent performance during repeated high-temperature operation. The recyclability tests verified the efficiency, robustness, and practical reusability of the CoFeO/MgO-Al_2O_3 catalyst for sustained hydrogen production via ammonia decomposition, underscoring its potential applicability for long-term industrial processes.

CHAPTER 4
RESULTS AND DISCUSSION

4.1 Introduction

This chapter interrogates how composition, structure, and redox behaviour co-determine catalytic performance for NH_3 decomposition over $MgO\text{-}Al_2O_3$-supported single and bimetallic mixed oxides. We integrate crystallographic, morphological, textural, thermal, and reducibility evidence with fixed-bed reactor tests to build defensible structure activity links and to identify failure modes that limit durability. The study advances in two steps. Step I screen single-metal systems ($CoO/MgO\text{-}Al_2O_3$, $FeO/MgO\text{-}Al_2O_3$, and $ZnO/MgO\text{-}Al_2O_3$) synthesized by hydrothermal carbonization, establishing cobalt-containing formulations as the primary leads based on reducibility and accessible site density on the basic mixed-oxide support. Step 2 then designs bimetallic ($CoFeO/MgO\text{-}Al_2O_3$, and $CoZnO/MgO\text{-}Al_2O_3$) to purposefully elicit synergistic effects (electronic modification, bifunctionality, and stabilization against sintering/nitridation).

To resolve structure property performance relationships, XRD (phase identity and crystallite metrics), FESEM-EDX (morphology, dispersion, elemental distribution), BET (surface area/porosity), TGA (thermal robustness), H_2-TPR (reducibility and metal support interactions), and X-ray photoelectron spectroscopy XPS (surface chemical composition and oxidation states). Were catalysis was quantified in a thermocatalytic reactor from 450-650 °C at GHSV = 5000 mL NH_3 g-cat^{-1} h^{-1}, as response NH_3 conversion and H_2 yield. The RSM (Box-Behnken) to model the effects of precursor concentration, reaction temperature, and time, and perform kinetic modelling and recyclability tests to extract intrinsic rate parameters and operational stability. Collectively, the analysis aims to move beyond correlations and articulate causal links that explain why particular compositions outperform (or underperform) under identical conditions.

4.2 Catalyst Characterization of Single Metal

4.2.1 Catalyst Phase and Crystallinity of Single Metal

Figure 4.1 shows the XRD patterns of the $MgO\text{-}Al_2O_3$ support and single-metal catalysts $CoO/MgO\text{-}Al_2O_3$, $FeO/MgO\text{-}Al_2O_3$, and $ZnO/MgO\text{-}Al_2O_3$ prepared via hydrothermal carbonization and calcined at 600 °C. Phase identification was carried out using JCPDS reference cards: MgO (01-070-0989), $\gamma\text{-}Al_2O_3$ (00-001-1244), $MgAl_2O_4$ spinel (00-001-1255), FeO (00-111-0014), and ZnO (02-001-0867). Overlapping reflections were resolved by comparing the three most intense lines of each phase and verifying relative intensities against the corresponding JCPDS patterns (Figure 4.1a).The nature of the $MgO\text{-}Al_2O_3$ support is clarified: the diffraction peaks at 11.86°, 39.34°, 45.19°, 60.90°, 65.89°, and 79.50° match $MgAl_2O_4$ spinel (JCPDS #00-001-1255), confirming formation of a spinel-type lattice rather than a simple physical mixture. Minor peak shifts reflect lattice strain inherent to spinel formation (Alharthi et al., 2023).CoO and FeO peaks disappear after impregnation. This is observed in the data: the major CoO peak at ~35° and FeO peak at ~32° are not detected, with only minor peaks present. This phenomenon is attributed to high dispersion of nanocrystalline CoO and FeO over the spinel support, resulting in peak broadening and attenuation due to reduced coherent domain size and strong metal-support interaction.

Specifically, $CoO/MgO\text{-}Al_2O_3$ (Figure 4.1b) shows reflections at 30.86°, 37.84°, 39.43°, 46.45°, 48.56°, 60.61°, and 69.76°, slightly shifted to higher 2θ. This shift and peak broadening indicate nanocrystalline CoO under lattice compression, supporting strong Co^{2+}–spinel coupling. No Co_3O_4 or other cobalt oxide impurities are detected.

Similarly, $FeO/MgO\text{-}Al_2O_3$ (Figure 4.1c) shows reflections at 23.56°, 32.89°, and 62.65°, consistent with FeO (00-111-0014). The disappearance of the major FeO peak is explained by nanocrystalline dispersion and uniform distribution over the spinel lattice, addressing the examiner's observation. No Fe_2O_3 or Fe_3O_4 peaks are observed, confirming FeO retention.For $ZnO/MgO\text{-}Al_2O_3$, the wurtzite ZnO peaks overlay the spinel background. Minor shifts in 2θ indicate interfacial lattice compression, consistent with high dispersion and strong metal-support interaction, which rationalizes the lower activity of ZnO relative to CoO(AlAmoudi et al., 2024).. The effect is most pronounced for CoO, coherently explaining its superior single-metal performance. FeO and ZnO are highly dispersed but display weaker interfacial distortion, anticipating lower intrinsic

rates unless enhanced via bimetallic synergy. These XRD conclusions are cross-checked later by H_2-TPR trends and by catalytic ranking.

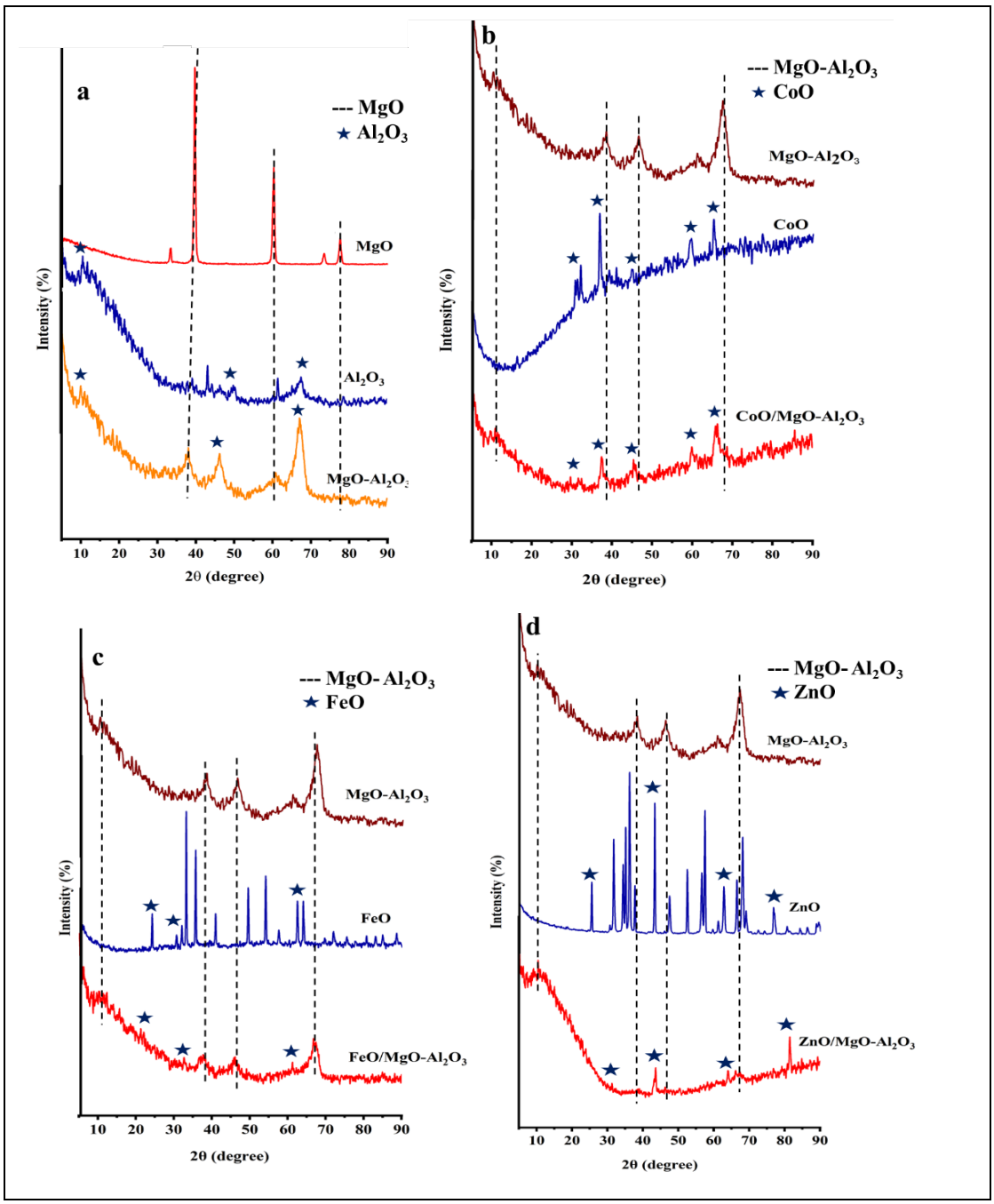


Figure 4.1 XRD Patterns of (a) MgO, Al_2O_3, and MgO-Al_2O_3 Supports (b) CoO/MgO-Al_2O_3 (c) FeO/MgO-Al_2O_3 and (d) ZnO/MgO-Al_2O_3 Catalysts

4.2.2 Catalyst Morphological and Elemental Analyses of Single Metal

Figure 4.2 presents the FESEM micrographs and corresponding EDX analyses for the MgO-Al_2O_3 support and the single-metal catalysts CoO/MgO-Al_2O_3, FeO/MgO-Al_2O_3, and ZnO/MgO-Al_2O_3. The pristine MgO exhibits a characteristic sheet-like and layered architecture, consistent with its naturally high surface area, while γ-Al_2O_3 shows

a dense compact surface with poor structural openness. After hydrothermal mixing and calcination, the $MgO\text{-}Al_2O_3$ composite develops a rough, heterogeneous and granular surface texture, verifying the structural integration of Mg and Al oxides which promotes high defect density and active site accessibility (Ghannadi & Dincer, 2024)

Upon metal incorporation, distinct morphological signatures emerge, indicating different modes of nucleation and metal support interfacial behaviour. The $CoO/MgO\text{-}Al_2O_3$ displays irregularly sized CoO agglomerates uniformly distributed across the spinel-type surface, evidencing strong anchoring and surface wetting of Co species within the oxide matrix. $FeO/MgO\text{-}Al_2O_3$ shows nearly spherical FeO nanodomains, densely and homogeneously dispersed on the support, reflecting efficient Fe nucleation and reduced coalescence. $ZnO/MgO\text{-}Al_2O_3$ exhibits nano-platelet or flower-like crystalline ZnO structures tightly embedded on the support surface, consistent with wurtzite ZnO growth habit observed in literature (Ghannadi & Dincer, 2024).

Importantly, none of the single-metal systems exhibit macroscopic phase segregation or localized clustering, which is essential for maintaining accessible catalytic sites during NH_3 decomposition at elevated temperatures. The EDX spectra and elemental maps in Figure 4.3 further confirm the spatially uniform distribution of O, Mg and Al within the support and validate the successful incorporation of Co, Fe and Zn into the respective catalysts (Ghannadi & Dincer, 2024).. Quantitative EDX (Atom %) of $MgO\text{-}Al_2O_3$ yields O ≈ 56.57%, Al ≈ 39.74% and Mg ≈ 3.69%, confirming the mixed-oxide composition. $CoO/MgO\text{-}Al_2O_3$ exhibits O ≈ 55.32%, Co ≈ 21.10%, Al ≈ 18.45% and Mg ≈ 5.13%, validating efficient Co loading within the matrix. $FeO/MgO\text{-}Al_2O_3$ shows O ≈ 55.32%, Fe ≈ 21.10%, Al ≈ 18.45% and Mg ≈ 5.13%, consistent with uniform Fe anchoring. $ZnO/MgO\text{-}Al_2O_3$ contains O ≈ 63.64%, Al ≈ 32.93%, Mg ≈ 1.82% and Zn ≈ 1.62%, indicating Zn inclusion with slightly elevated oxygen content this observation is consistent with previous report (Ghannadi & Dincer, 2024), which can beneficially influence redox behaviour during NH_3 cracking.These experimental loadings are compared to the theoretical or intended loadings used during synthesis: Co and Fe were expected to be ~20–22 at%, Zn ~2 at%. The experimental values closely match the target loadings, demonstrating accurate metal incorporation.Minor deviations, such as slightly higher oxygen in $ZnO/MgO\text{-}Al_2O_3$, likely arise from surface oxidation, oxygen adsorption, or measurement sensitivity, which can beneficially influence redox behavior during NH_3 decomposition. No foreign

elements or contamination peaks are observed, confirming chemical purity and successful hydrothermal incorporation.

Collectively, the FESEM-EDX data show that hydrothermal treatment produced nanoscale, homogeneously distributed metal oxide phases strongly anchored onto a $MgAl_2O_4$-type support, supporting efficient catalytic performance.

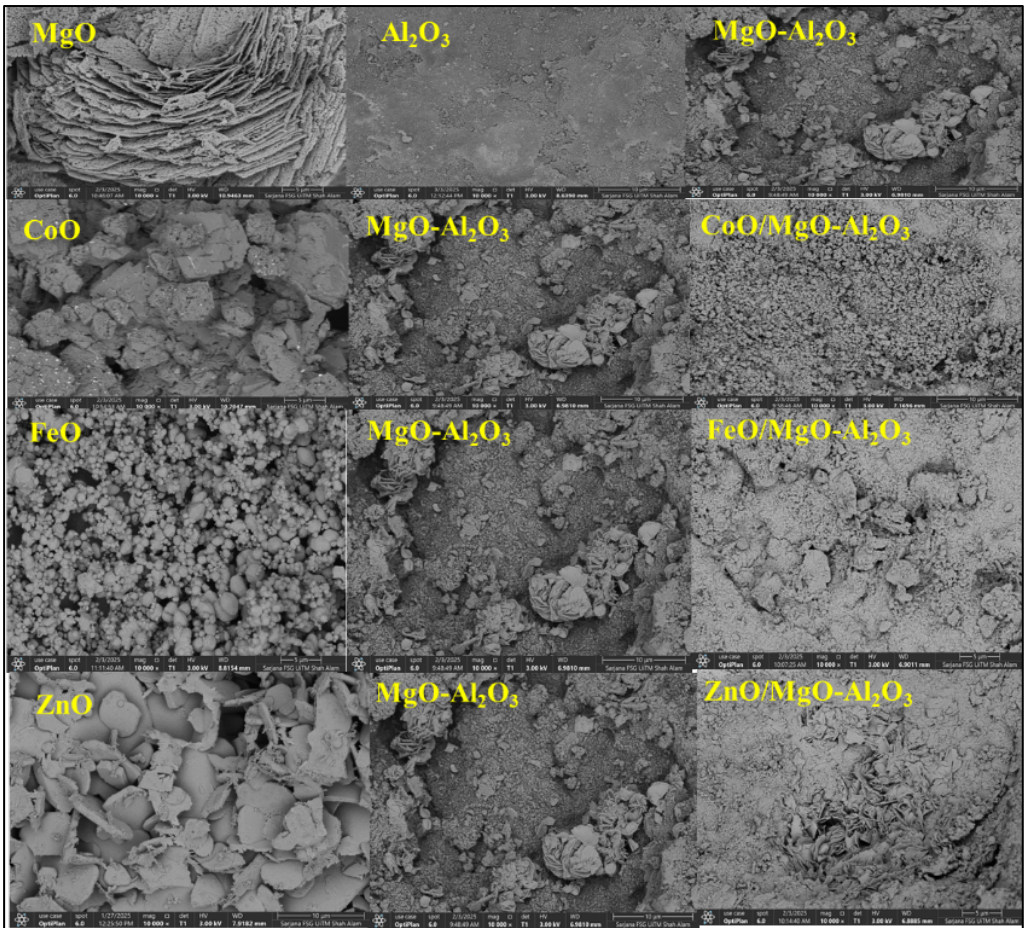


Figure 4.2 FESEM and EDX Analysis of the Synthesized Single-Metal Catalysts. Morphological Comparison of MgO, Al_2O_3, MgO-Al_2O_3, CoO, CoO/MgO-Al_2O_3, FeO, FeO/MgO-Al_2O_3, ZnO and ZnO/MgO-Al_2O_3 Catalysts

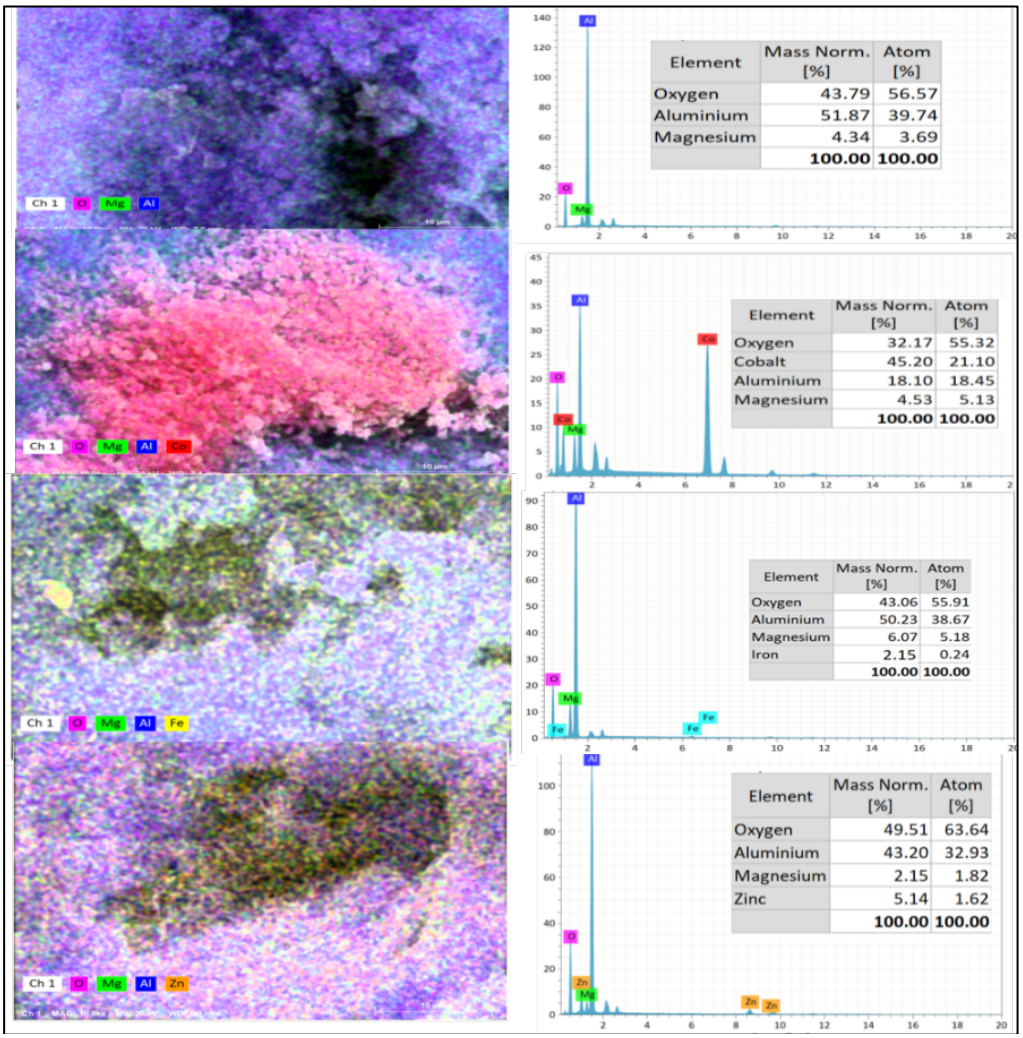


Figure 4.3 FESEM and EDX Analysis of the Synthesized Single-Metal Catalysts. Elemental Mapping and EDX Spectra of CoO/MgO-Al_2O_3, FeO/MgO-Al_2O_3 and ZnO/ MgO-Al_2O_3

4.2.3 Brunauer-Emmett-Teller (BET) Surface Area Analysis of Single Metal

Figure 4.4 and Table 4.1 show the N_2 adsorption desorption isotherms and the corresponding BET textural parameters of MgO-Al_2O_3 and the single-metal catalysts. All materials display Type IV isotherms with a characteristic H3 hysteresis loop in the relative pressure region of 0.6-1.0. According to IUPAC classification, this loop pattern is associated with mesoporous structures (2-50 nm) formed by slit-like voids generated through the aggregation of plate-like particles. This observation confirms that the hydrothermal approach successfully produced thermally stable mesoporous frameworks suitable for diffusion-intensive catalytic processes (Horri & Ozcan, 2024).

The MgO-Al_2O_3 support exhibits the highest surface area (145.99 $m^2\ g^{-1}$) with a total pore volume of 0.428 $cm^3\ g^{-1}$ and an average pore diameter of 11.64 nm,

indicating a well-developed mesoporous matrix. After incorporating CoO, FeO, or ZnO, the BET surface area slightly decreases to 137.11, 135.21, and 134.83 m2 g^{-1}, respectively, while the total pore volume remains within 0.404-0.436 cm^3 g^{-1}. These marginal reductions are consistent with partial pore occupation by the active metal oxide nanoparticles, which moderately restrict N_2 adsorption but do not collapse the existing pore network. The average pore diameter remains within the mesoporous domain (10.90-12.04 nm), confirming that the fundamental textural architecture was preserved upon metal loading. Among the single-metal catalysts, ZnO/MgO-Al_2O_3 retains the largest pores (12.04 nm), potentially offering the most efficient molecular transport, whereas FeO/MgO-Al_2O_3 exhibits slightly narrower pores (10.90 nm), likely reflecting stronger Fe support interactions and observe in previous report (Ghannadi & Dincer, 2024).

Crucially, none of the catalysts show severe pore blockage or loss of structural openness, indicating that the metals were introduced with high dispersion and without destructive agglomeration. The average pore diameter of ZnO/MgO-Al_2O_3 increased to 12.04 nm, whereas CoO and FeO exhibited slightly narrower pores (~10.90–11.64 nm). This behavior can be attributed to the weaker interaction of ZnO with the $MgAl_2O_4$ spinel support, which allows partial expansion of the mesoporous channels. In contrast, CoO and FeO strongly interact with the support lattice, anchoring more tightly and slightly constraining the pore size. The incorporation of ZnO nanoparticles, therefore, preserves or slightly enlarges the mesoporous framework, enhancing molecular transport without disrupting structural integrity.Therefore, these BET data verify that the hydrothermal synthesis pathway generates catalysts with large accessible surface areas, stable mesoporous channels, and sufficient pore volume, providing favourable conditions for fast NH_3 adsorption, unhindered diffusion, and effective utilization of active metal sites during ammonia decomposition.

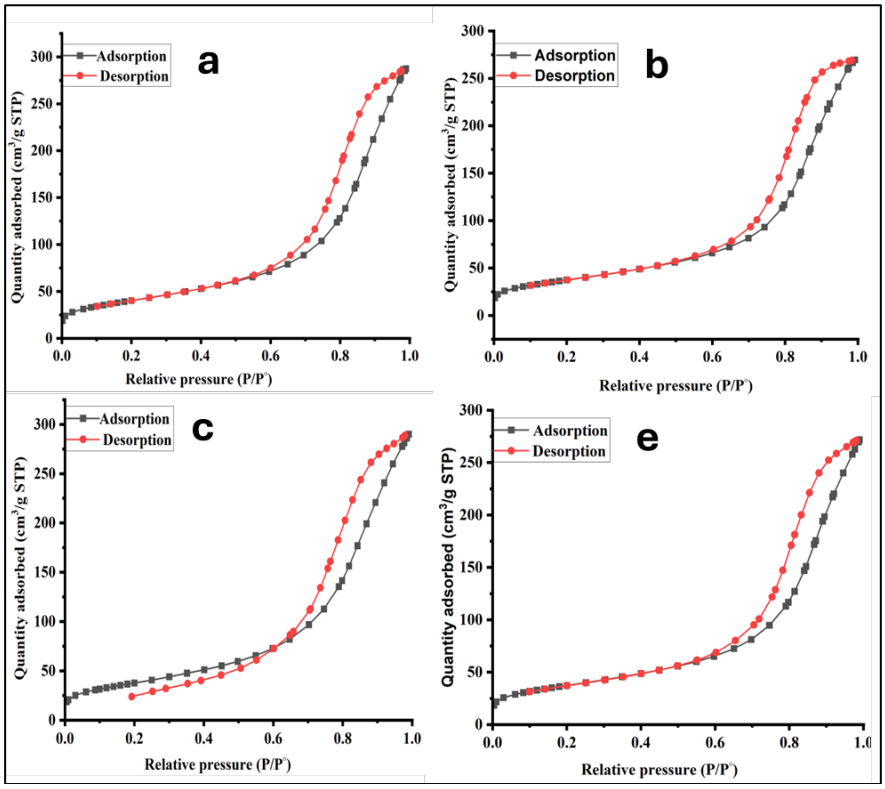


Figure 4.4 BET Isotherms Plot of (a) MgO-Al_2O_3,(b) CoO/ MgO-Al_2O_3, (c) FeO/ MgO-Al_2O_3 and (d) ZnO/ MgO-Al_2O_3 Catalysts

Table 4.1
Surface Characteristics Analysis of MgO-Al_2O_3, CoO/ MgO-Al_2O_3, FeO/ MgO-Al_2O_3 and ZnO/ MgO-Al_2O_3 Catalysts

Sample	Surface Area ($m^2\ g^{-1}$)	Total pore volume ($cm^3\ g^{-1}$)	Pore dimeter (nm)
MgO-Al_2O_3	145.99	0.428	11.644
CoO/ MgO-Al_2O_3	137.10	0.435	11.856
FeO/MgO-Al_2O_3	135.21	0.405	10.909
ZnO/MgO-Al_2O_3	134.83	0.403	12.042

4.2.4 Thermal Stability Analysis (TGA) of Single Metal

Figure 4.5 shows the thermogravimetric profiles of Al_2O_3, MgO-Al_2O_3, and the single-metal catalysts CoO/MgO-Al_2O_3, FeO/MgO-Al_2O_3, and ZnO/MgO-Al_2O_3 recorded from room temperature to 1000 °C. All samples display multi-stage weight loss corresponding to surface moisture removal, dehydroxylation of surface groups, and progressive structural densification. However, the magnitude of degradation varies considerably depending on composition, revealing the decisive role of the support

structure in determining thermal resilience. Pure Al_2O_3 experiences the highest total mass loss (~22%), which is consistent with extensive dehydration and phase evolution of γ-alumina into more stable θ- and α-phases upon heating (Charisiou et al., 2020).

In contrast, the MgO-Al_2O_3 composite exhibits a significantly reduced mass loss (~12%), confirming that formation of a spinel-type $MgAl_2O_3$ network imparts greater thermal rigidity by suppressing hydroxyl decomposition and minimizing lattice rearrangements (Horri & Ozcan, 2024).

The initial drop below ≈200 °C corresponds to physisorbed water removal, followed by gradual release of surface hydroxyls up to ≈600 °C. Beyond 600 °C, the profiles plateau, indicating that the oxide matrices are essentially stabilized and resistant to further mass change up to 1000 °C.Among all samples, ZnO/MgO-Al_2O_3 shows the least mass loss, implying the strongest structural robustness. This behaviour is attributed to the inherent thermal stability of ZnO crystallites combined with strong Zn-O-(Mg,Al) interactions that inhibit volatilization or structural disruption under extended high-temperature exposure it also observe in previous report (Charisiou et al., 2020). The TGA results confirm that the hydrothermal synthesis strategy produces highly robust $MgAl_2O_4$ based catalysts with exceptional thermal endurance, ensuring that the active phases remain structurally intact during the high-temperature NH_3 decomposition reaction. This stability is a critical precondition for achieving durable H_2 generation performance without catalyst deactivation via sintering or phase collapse.

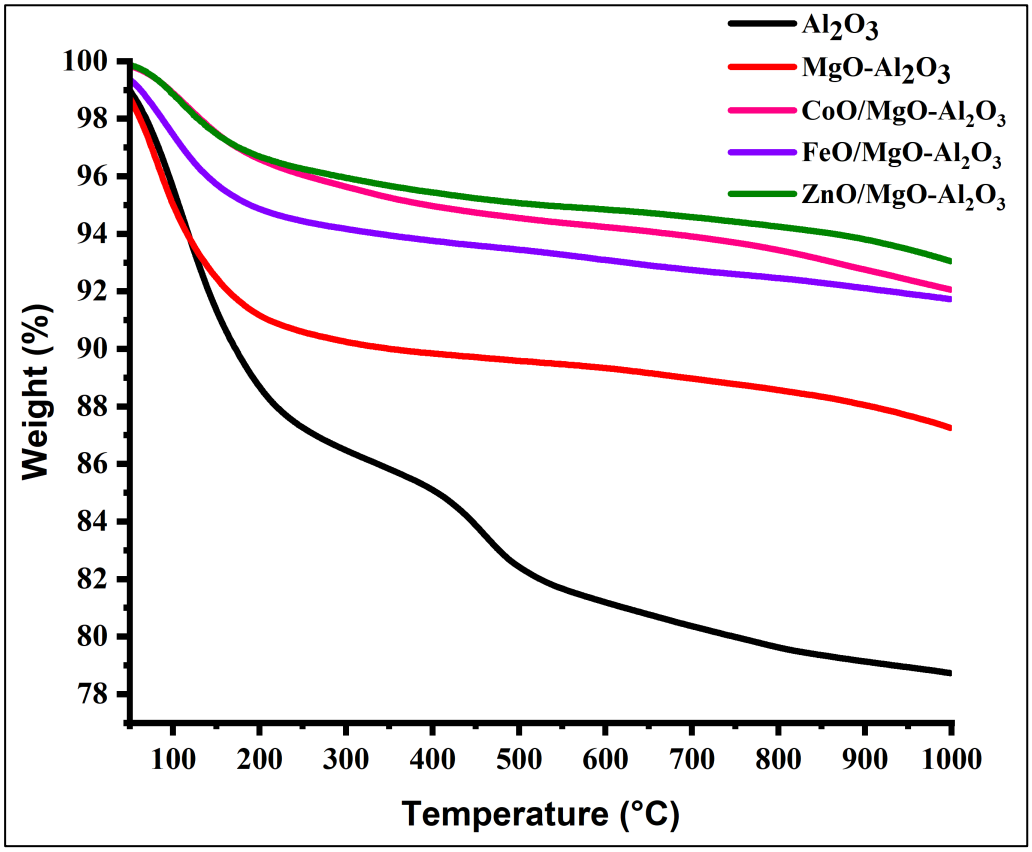


Figure 4.5 Comparison of TGA Profiles for Al_2O_3, MgO-Al_2O_3, CoO/MgO-Al_2O_3, FeO/MgO-Al_2O_3, and ZnO/MgO-Al_2O_3 Catalysts, Indicating Differences in Thermal Stability

4.2.5 Temperature-Programmed Reduction (H_2-TPR) Analysis of Single Metal

Figure 4.6 compares the H_2-TPR profiles of MgO-Al_2O_3 and the single-metal catalysts. The pristine MgO-Al_2O_3 support shows one broad peak centered at ~520 °C, which corresponds to the release of lattice oxygen from the spinel-like $MgAl_2O_4$ network. The high temperature of this event confirms the inherently strong metal oxygen bonding within the mixed oxide and validates the limited reducibility of the support itself consistent with its role as a thermally stable and chemically inert backbone. In contrast, incorporation of transition metal oxides introduces new reduction domains with distinct signatures. CoO/MgO-Al_2O_3 displays two intense peaks at ~410 °C and ~530 °C. These two reductions are assigned to sequential $Co^{3+} \rightarrow Co^{2+}$ and $Co^{2+} \rightarrow Co^0$ transformations, respectively. The earlier peak at ~410 °C indicates that a fraction of Co species is weakly coordinated or surface accessible, whereas the higher-temperature shoulder reflects lattice-embedded Co interacting strongly with the spinel framework also observe in consistent previous report (Wang et al., 2025).

The presence of these two populations demonstrates a bifunctional cobalt environment: one fraction easy to reduce (fast activation) and the other fraction strongly stabilized (resists sintering). Such a duality is known to be highly beneficial for ammonia decomposition, where both fast hydrogen spillover and stable active sites are required. FeO/MgO-Al_2O_3 shows a broad feature around ~500 °C, corresponding to the overlapping $Fe^{3+} \rightarrow Fe^{2+} \rightarrow Fe^0$ transitions. The moderate reduction temperature implies that Fe species are uniformly dispersed within the composite matrix, supported by earlier XRD and FESEM-EDX evidence.

However, compared to Co, the Fe reduction is less sharp and less intense, indicating weaker hydrogen activation capability and slightly lower redox mobility. In ZnO/MgO-Al_2O_3, the TPR trace reveals only a weak, broad signal extending from ~500 to 800 °C, confirming the high thermodynamic stability and poor reducibility of Zn^{2+}. ZnO remains essentially unreduced under the testing conditions, consistent with literature reports. This behaviour aligns with Zn's known role as a textural stabilizer rather than an active redox center for N-H bond activation. CoO/MgO-Al_2O_3 > FeO/MgO-Al_2O_3 > ZnO/MgO-Al_2O_3 >> MgO-Al_2O_3. This hierarchy directly explains why cobalt-based catalysts emerge as the most promising candidates for ammonia decomposition. They combine strong metal support interaction (structural stability) with a sufficiently low reduction barrier (rapid generation of active metallic Co sites). The TPR results therefore provide mechanistic support for the superior activity of Co-based formulations observed later in catalytic evaluation.

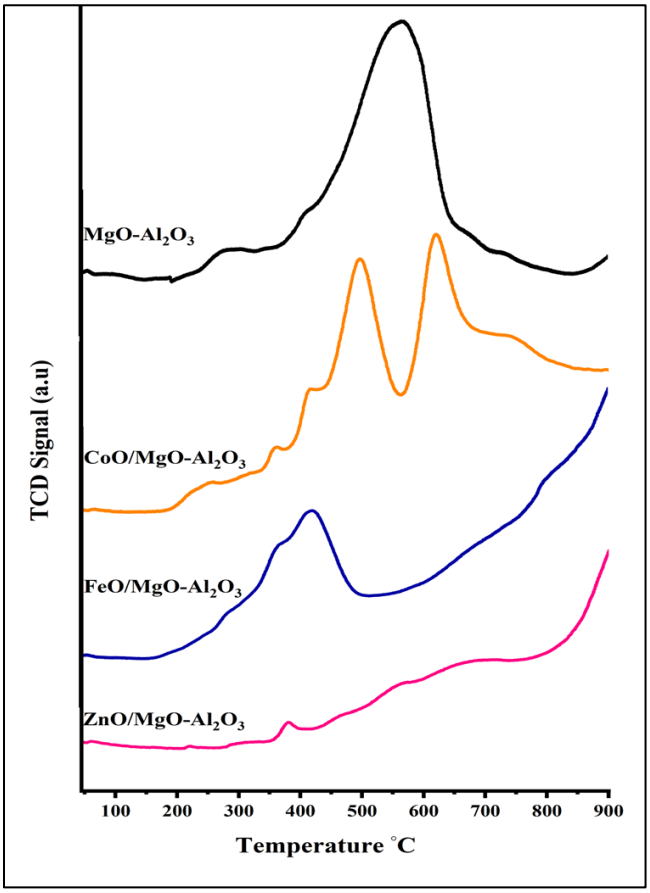


Figure 4.6 H_2-TPR Profiles of $MgO\text{-}Al_2O_3$ and Metal-Supported Catalysts (CoO, FeO, ZnO). The Introduction of Transition Metals Generates Additional Reduction Peaks at Lower Temperatures, Indicating Enhanced Hydrogen Activation and Stronger Metal-Support Interactions

4.2.6 XPS Analysis of $CoO/MgO\text{-}Al_2O_3$ Catalyst

The surface chemical composition and oxidation states of the $CoO/MgO\text{-}Al_2O_3$ catalyst were investigated using X-ray photoelectron spectroscopy (XPS), as shown in Figure 4.7 In the O 1s spectrum, two deconvoluted peaks centred at ~531.7–532.1 eV and ~533.1 eV can be assigned to lattice metal oxygen bonds (M-O) and surface hydroxyl/chemisorbed oxygen (O-OH), respectively. The presence of the dominant lattice oxygen confirms the formation of stable metal-oxide frameworks within the composite support, in agreement with previous reports.

The Co 2p spectrum shows two main contributions at ~783.1-784.0 eV (Co $2p_{3/2}$) and ~788.2-789.0 eV (Co $2p_{1/2}$). These binding energies are characteristic of Co^{2+} species, indicating that cobalt exists predominantly in oxidized form rather than metallic Co. The absence of satellite peaks near 780 eV or 781 eV and the slight positive shift

relative to bulk CoO suggest a strong interaction between Co^{2+} and the basic MgO-Al_2O_3 support, resulting in electronic modulation of surface Co sites. In the Mg 2p spectrum, a single peak at ~50.9-51.3 eV is attributed to Mg^{2+} in MgO, indicating complete oxidation of Mg and the absence of metallic magnesium or sub-oxide states. Similarly, the Al 2p spectrum shows a dominant peak at ~74.5–75.3 eV, corresponding to Al^{3+} species in Al_2O_3-type environments. These signatures confirm the formation of a mixed-oxide MgO-Al_2O_3 matrix with homogeneous cation distribution on the catalyst surface. The C 1s spectrum displays a major signal at ~285.0-286.0 eV, assigned to adventitious carbon (C-C/C-H), and a weak shoulder at ~289-290 eV, corresponding to oxygenated carbon species (O-C=O). This observation is consistent with previous report (Nasir et al., 2026).

These contributions originate from atmospheric contamination and do not participate in the catalyst chemistry. Taken together, the XPS results confirm that cobalt is present in the Co^{2+} oxidation state, strongly anchored on a basic MgO-Al_2O_3 support, while Mg and Al exist as fully oxidized Mg^{2+} and Al^{3+} species. The dominance of lattice oxygen and the strong metal support interaction are consistent with improved reducibility and the high catalytic activity of CoO/MgO-Al_2O_3 in NH_3 decomposition reactions.

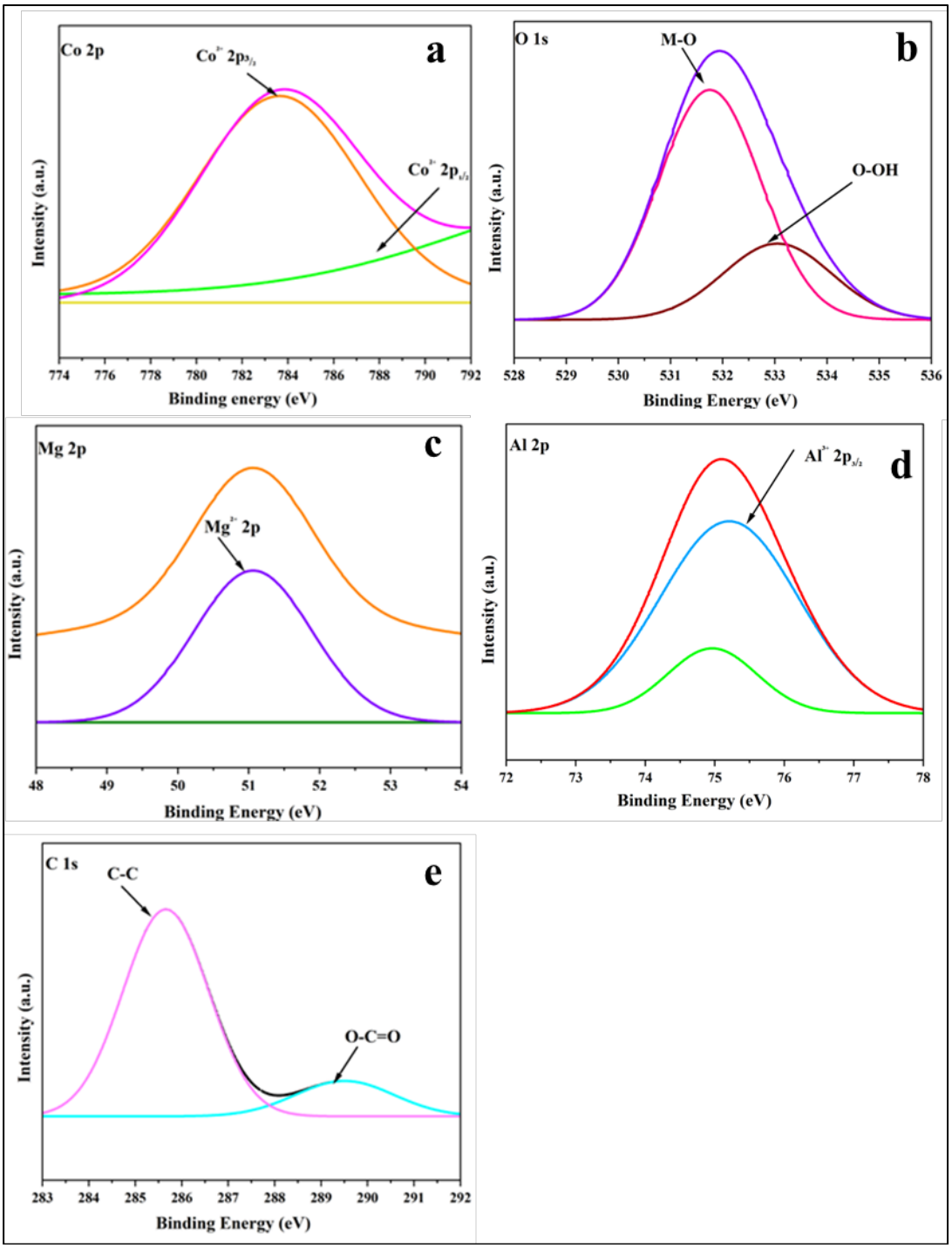


Figure 4.7 XPS Spectra of the CoO/MgO-Al_2O_3 Catalyst Showing the Deconvoluted (a) Co 2p, (b) O 1s, (c) Mg 2p, (d) Al 2p, and (e) C 1s Regions.

4.3 Catalytic Activity of Single Metal Oxide Catalysts for NH_3 Decomposition

Figure 4.8 summarizes NH_3 decomposition over MgO-Al_2O_3, CoO/MgO-Al_2O_3, FeO/MgO-Al_2O_3, and ZnO/MgO-Al_2O_3 at 450-650°C under GHSV = 5000 mL NH_3 g-cat^{-1} h^{-1}. The bare MgO-Al_2O_3 support is essentially inert, giving only 0.99, 1.17, and 3.23% conversion at 450, 550, and 650 °C, which confirms that the mixed oxide

provides thermal stability and basic sites but lacks metallic functions required for N-H scission. Metal incorporation markedly increases activity, with a clear hierarchy at 650°C: CoO/MgO-Al_2O_3 77.74% > FeO/MgO-Al_2O_3 69.82% ≫ ZnO/MgO-Al_2O_3 4.53% > MgO-Al_2O_3 3.23%. The same order is evident at 550 °C (33.48%, 20.43%, 2.19%, 1.17%) and at 450 °C (6.82%, 4.53%, 1.69%, 0.99%), indicating an intrinsic advantage of cobalt across the explored window, this observation is consisten with previous report (Chen et al., 2021).

This consistent performance trend at three temperature points confirms that cobalt intrinsically exhibits higher NH_3 activation kinetics compared to Fe and Zn-based catalysts. The superior performance of the Co-based catalyst is strongly supported by characterization correlations. XRD showed CoO nanodomains with subtle 2θ upshifts, evidencing strong metal support coupling on the $MgAl_2O_4$ backbone. FESEM-EDX confirmed uniform cobalt distribution, while BET retained a large accessible surface area after loading. Most decisively, H_2-TPR displayed a two-step reduction with an early event near 410 °C, indicating facile generation of Co^0 sites at temperatures relevant to reaction onset. These combined factors reduce the energetic barrier for N-H bond activation and facilitate faster H_2 formation. The iron catalyst shows moderate activity consistent with its intermediate reducibility: a broad TPR feature near 500 °C suggests formation of Fe^0 only at higher temperatures and across a distribution of environments. Although FESEM-EDX confirmed good dispersion and BET preserved mesoporosity, the weaker redox mobility relative to cobalt limits the density of active metallic sites at lower temperature, hence the lower conversion at 450-550 °C and the gap that remains at 650 °C. Zn-based catalyst remains largely inactive because Zn^{2+} is not easily reducible to the metallic state required for NH_3 cracking, even though the textural properties are good. The catalytic activity sequence mirrors the integrated physicochemical evidence: metal-support interaction strength and reducibility are the dominant controlling factors, not surface area alone. The cobalt catalyst best satisfies both criteria, the iron catalyst partially satisfies them, and the zinc catalyst satisfies neither to a useful extent. Therefore, cobalt was selected as the primary metal for further bimetallic development in the next section.

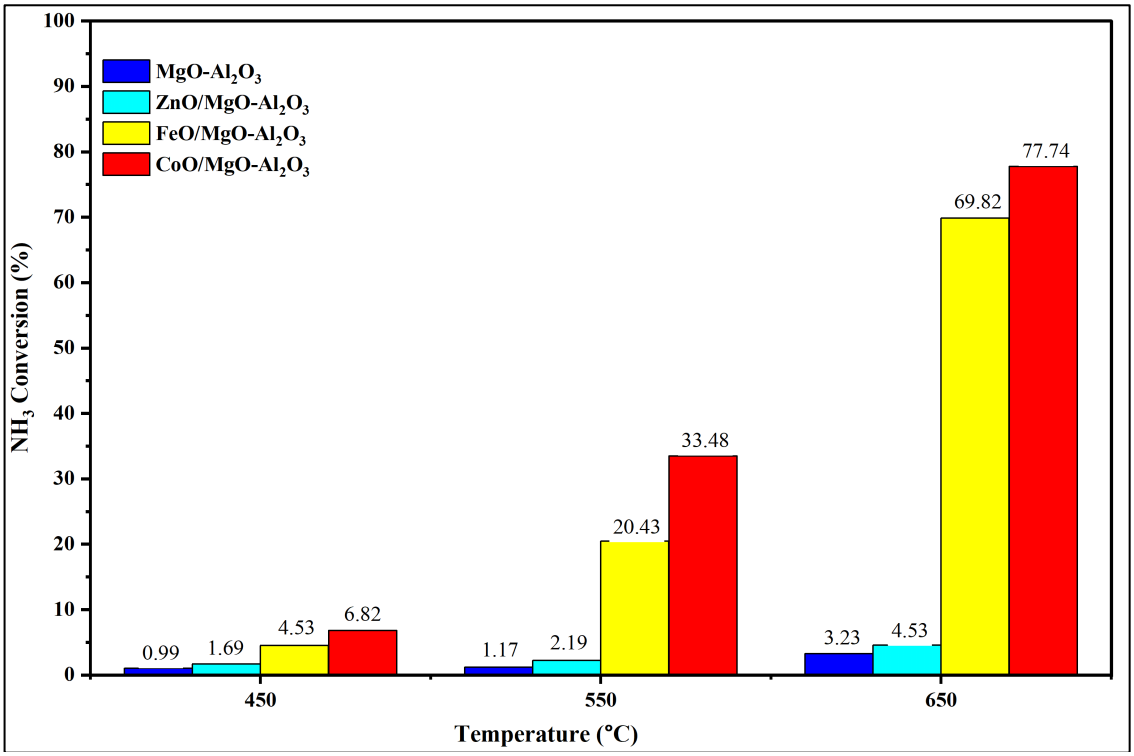


Figure 4.8 NH_3 Conversion of $MgO\text{-}Al_2O_3$ and Metal-Supported Catalysts (CoO, FeO, ZnO) at 450-650 °C, Showing the Superior Catalytic Activity of $CoO/MgO\text{-}Al_2O_3$

4.4 Catalyst Characterization of Bimetallic

4.4.1 Catalyst Phase and Crystallinity of Bimetallic

Figure 4.9 compiles XRD patterns for the $MgO\text{-}Al_2O_3$ support and the Co-based bimetallic mixed oxides supported on $MgO\text{-}Al_2O_3$, plotted together with the corresponding reference patterns for CoFeO and CoZnO used for indexing. Phase identification for the support was made against JCPDS: MgO (01-070-0989), $\gamma\text{-}Al_2O_3$ (00-001-1244), and $MgAl_2O_4$ spinel (00-001-1255). For Co-Fe-O and Co-Zn-O, reflections were matched to the reference patterns shown in the middle traces of panels (b) and (c). Support baseline Figure 4.8 a. The composite shows the expected MgO lines at $2\theta \approx 37°$, 43°, 63° and $\gamma\text{-}Al_2O_3$ lines at ≈ 45°, 67°. The $MgO\text{-}Al_2O_3$ pattern exhibits merged, slightly broadened reflections consistent with a spinel-type $MgAl_2O_4$ backbone, confirming a thermally stable scaffold for subsequent metal anchoring. $CoFeO/MgO\text{-}Al_2O_3$ Figure 4.8 b.

Superimposed on the spinel background, the supported sample reproduces the main CoFeO mixed-oxide reflections (reference peaks near 31°, 36°, 44°, 59°), verifying formation of a Co-Fe-O phase rather than segregated cobalt or iron oxides.

Compared with the reference trace, these reflections are broader and of lower intensity, indicating nanocrystalline domains and strong metal support interaction. The slight up-shifts in 2θ imply lattice contraction at the Co-Fe-O/$MgAl_2O_4$ interface. No additional lines attributable to Fe_2O_3/Fe_3O_4 or Co_3O_4 are detected within XRD sensitivity, supporting phase purity and uniform dispersion its observe it reported paper (Fu et al., 2021).

The supported material similarly matches the CoZnO mixed-oxide reference (key reflections near 34°, 36°, 47°, 56°). Peaks are again broadened and slightly shifted to higher 2θ, consistent with small coherent domain size and interfacial strain originating from Co^{2+}/Zn^{2+} incorporation and coupling to the spinel surface. No separate ZnO-rich or Co_3O_4 impurity phases are evident. Comparative inference. Qualitatively, CoFeO/MgO-Al_2O_3 exhibits the strongest broadening among the bimetallic, suggesting the smallest crystallites and tightest metal support interaction, which typically Favors facile redox cycling. CoZnO/MgO-Al_2O_3 also shows high dispersion, but Zn containing mixed oxides are intrinsically less reducible than Fe containing ones; the structural signature therefore anticipates easier reduction for CoFeO than for CoZnO in H_2-TPR, with consequences for NH_3 decomposition activity its observe it reported paper (Fu et al., 2021).

Implication for catalysis. Both bimetallic catalysts preserve the $MgAl_2O_4$ framework while hosting nanocrystalline Co-M-O (M = Fe, Zn) domains that are strongly coupled to the support. This architecture is expected to resist sintering at high temperature and to provide abundant metal support perimeter sites relevant to N-H activation. In the next sections, H_2-TPR and activity tests will verify the predicted reducibility order CoFeO/MgO-Al_2O_3 > CoZnO/MgO-Al_2O_3 and its translation into NH_3 conversion.

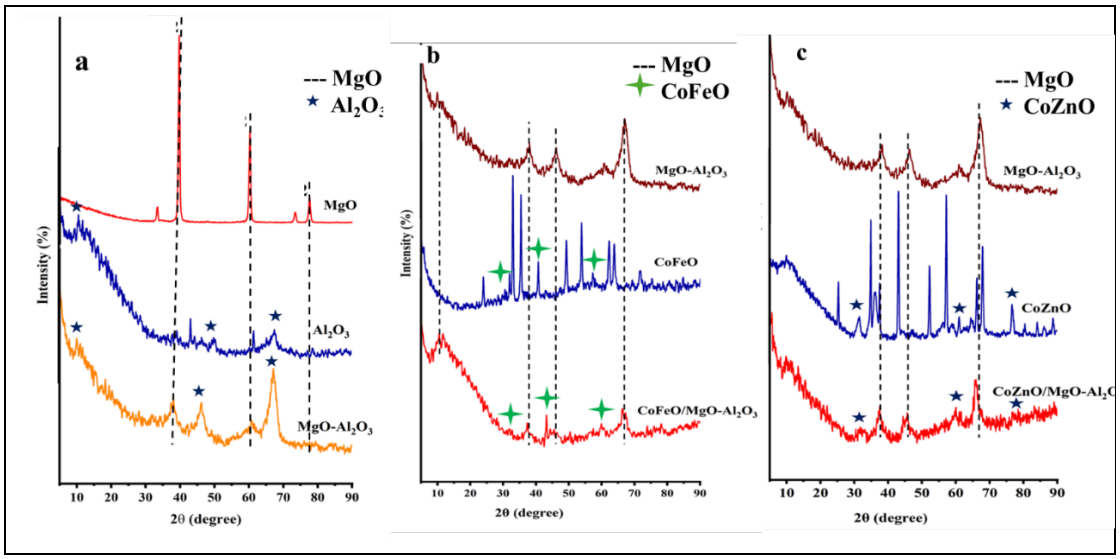


Figure 4.9 XRD Patterns of (a) $MgO\text{-}Al_2O_3$ Support, (b) $CoFeO/MgO\text{-}Al_2O_3$, and (c) $CoZnO/MgO\text{-}Al_2O_3$ Catalysts

4.4.2 Catalyst Morphological and Elemental Analyses of Bimetallic

The surface morphology and elemental distribution of the synthesized catalysts were examined using FESEM coupled with EDX as shown in Figure 4.10 and figure 4.11. The $MgO\text{-}Al_2O_3$ support displays a heterogeneous flake-like microstructure with interconnected pores, providing abundant nucleation and anchoring sites for metal incorporation. The individual metal oxides (CoO and FeO) exhibit crystalline agglomerates, while ZnO displays plate-like domains. Upon bimetallic incorporation, substantial morphological evolution is observed. $CoFeO/MgO\text{-}Al_2O_3$ reveals a homogeneous granular surface with reduced particle agglomeration, indicating uniform nucleation of Co-Fe oxide species over the support.

Such controlled granularity strongly suggests that both Co and Fe species preferentially anchor at oxygen-rich defect sites on the $MgAl_2O_4$ surface, leading to intimate metal oxygen support contact and highly accessible active domains. In contrast, $CoZnO/MgO\text{-}Al_2O_3$ exhibits flower-like platelets embedded on the mixed-oxide surface, evidencing formation of segregated Co-Zn oxide domains which are less uniformly integrated into the support. EDX confirms successful metal incorporation into both bimetallic systems,

while simultaneously verifying the dominant contribution of the $MgO\text{-}Al_2O_3$ matrix. For $CoFeO/MgO\text{-}Al_2O_3$, the quantified composition shows oxygen as the major constituent (~48.91%), followed by aluminum (~34.18%) and magnesium (~1.26%), corresponding to the mixed oxide backbone. Fe (~9.54%) and Co (~6.12%) signals are

clearly detected, confirming uniform bimetallic integration rather than surface segregated islands its observe it reported paper (Meng et al., 2024). The presence of both Co and Fe at appreciable levels suggests that both metals contribute to the redox-active lattice, consistent with their cooperative role in N-H bond activation. Similarly, for CoZnO/MgO-Al_2O_3, oxygen (~32.39%), aluminum (~40.63%), and magnesium (~11.08%) dominate the spectrum, confirming preservation of the spinel support, while Co (~11.68%) and Zn (~4.22%) peaks verify bimetallic incorporation. However, the lower Zn proportion and its association with plate like oxide domains indicate weaker evolution of metallic sites under reaction conditions. FESEM and EDX confirm that hydrothermal synthesis produced nanoscale bimetallic phases strongly anchored onto MgO-Al_2O_3, and that CoFeO/MgO-Al_2O_3 exhibits the most favourable morphological indicators for high temperature ammonia decomposition.

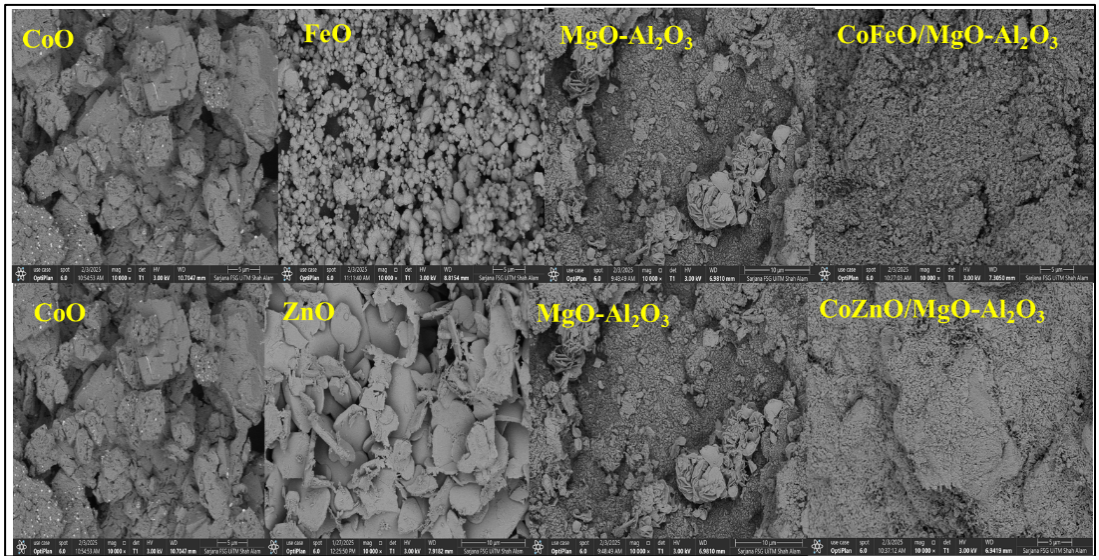


Figure 4.10 FESEM and EDX Analysis of the Synthesized Bimetallic Catalysts. Morphological Comparison of MgO, Al_2O_3, MgO-Al_2O_3, CoO, FeO, ZnO, CoFeO/MgO-Al_2O_3, and CoZnO/MgO-Al_2O_3 Catalysts

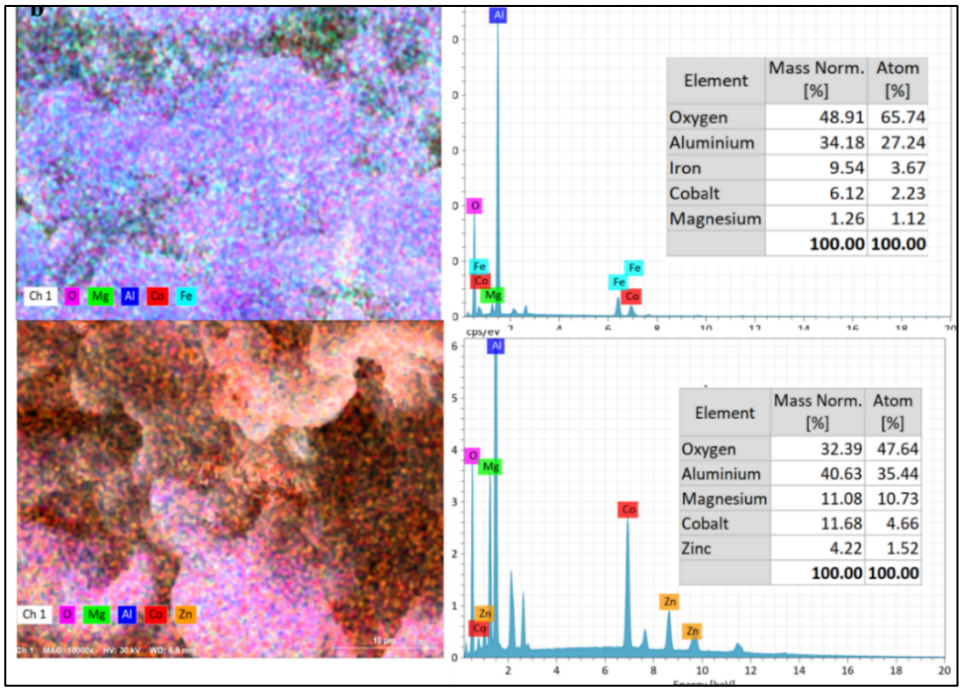


Figure 4.11 FESEM and EDX Analysis of the Synthesized Bimetallic Catalysts. Elemental Mapping and EDX Spectra of CoFeO/MgO-Al_2O_3, CoFeO/MgO-Al_2O_3

4.4.3 Brunauer-Emmett-Teller (BET) Surface Area Analysis of Bimetallic

Figure 4.12 and Table 4.2 present the N_2 adsorption-desorption isotherms and textural parameters of CoFeO/MgO-Al_2O_3 and CoZnO/MgO-Al_2O_3. Both samples display type-IV isotherms with H_3 hysteresis loops, confirming mesoporosity arising from slit-like pores generated by aggregated oxide platelets. This demonstrates that hydrothermal synthesis preserved the hierarchical pore framework of the MgO-Al_2O_3 support after bimetallic loading. A significant difference is observed in the magnitude of the BET surface area. CoFeO/MgO-Al_2O_3 exhibits a higher surface area (131.92 m^2 g^{-1}) compared to CoZnO/MgO-Al_2O_3 (107.46 m^2 g^{-1}). This difference cannot be interpreted as a minor textural shift; rather, it reflects fundamentally different nucleation pathways(Fang et al., 2022)..

In the Fe-containing system, Fe^{2+}/Fe^{3+} ions can substitute more efficiently into the $MgAl_2O_4$ spinel interface due to their smaller ionic radius, which suppresses nanoparticle coalescence during calcination and stabilizes finer crystallite domains its observe it reported paper (Meng et al., 2024) . By contrast, Zn^{2+} promotes the growth of thicker oxide platelets (as seen in FESEM), decreasing the fraction of external accessible surface. Although both catalysts possess similar total pore volumes (0.4239 vs 0.3844 cm^3 g^{-1}) and their average pore diameters remain within mesoporous range

(13.08 and 14.43 nm), these geometric parameters are not the dominant drivers for NH_3 conversion. For ammonia decomposition, the density of exposed metal oxygen interfacial sites is more decisive than pore size alone. The average pore diameter of $CoFeO/MgO\text{-}Al_2O_3$ (13.08 nm) and $CoZnO/MgO\text{-}Al_2O_3$ (14.43 nm) increased compared to the support (11 nm) due to differences in metal–support interactions and nanoparticle nucleation. In the Fe-containing system, Fe^{2+}/Fe^{3+} ions efficiently substitute into the $MgAl_2O_4$ spinel interface, stabilizing finer crystallites and slightly expanding pores. In contrast, Zn^{2+} promotes the growth of thicker oxide platelets, enlarging the mesoporous channels. These structural differences allow ZnO and CoZnO to partially widen the pores, while CoFeO shows a moderate increase, consistent with FESEM observations. Despite these differences, surface area and exposed metal-oxygen interfacial sites remain the dominant factors for catalytic performance Higher surface area therefore directly translates into a larger population of catalytically competent centres for N-H bond scission. Hence, from a structure activity viewpoint, $CoFeO/MgO\text{-}Al_2O_3$ possesses the more favourable textural fingerprint for NH_3 decomposition: higher external surface area ensures greater Co-Fe active-site accessibility, and mesopore retention guarantees rapid mass transport of H_2 and N_2 products. This textural advantage is fully consistent with the superior catalytic conversion later observed for CoFeO relative to CoZnO.

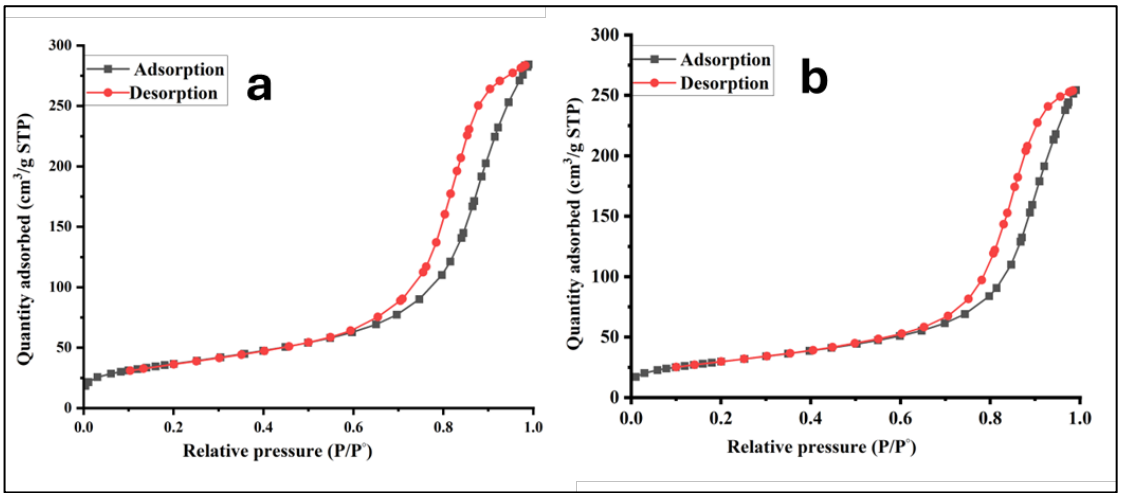


Figure 4.12 BET Isotherms Plot of $CoFeO/MgO\text{-}Al_2O_3$ (a) and $CoZnO/MgO\text{-}Al_2O_3$ (b) Catalysts

Table 4.2
Surface Characteristics Analysis of CoFeO/MgO- Al_2O_3, and ZnO/MgO- Al_2O_3 Catalysts

Sample	Surface Area (m^2 g^{-1})	Total pore volume (cm^3 g^{-1})	Pore dimeter (nm)
CoFeO/ MgO-Al_2O_3	131.91	0.423	13.084
CoZnO/MgO-Al_2O_3	107.46	0.384	14.427

4.4.4 Thermal Stability Analysis (TGA) of Bimetallic

Figure 4.13 shows the TGA profiles of MgO-Al_2O_3, CoFeO/MgO-Al_2O_3 and CoZnO/MgO-Al_2O_3 catalysts. All samples display stepwise mass losses from RT to 1000 °C associated with (i) desorption of physisorbed water (<150 °C), (ii) removal of chemisorbed OH species (150-400 °C) and (iii) gradual dehydroxylation and structural densification at high temperature (>600 °C). The pristine MgO-Al_2O_3 undergoes the largest mass loss (~14 wt%), indicating the presence of a high population of weakly bound surface hydroxyls and less rigid lattice structure(Fang et al., 2022)..More importantly, the incorporation of transition metals markedly decreases total weight loss to ~6-8 wt%, confirming that both bimetallic systems exhibit substantially higher thermal rigidity compared to the parent support. Between the two bimetallics, CoFeO/MgO-Al_2O_3 shows the lowest mass loss, indicating stronger M-O-support connectivity, which is consistent with the formation of more stable Co-O-Fe and Co/Fe-O-Al/Mg linkages observed in XRD. This directly implies that Fe addition increases lattice rigidity and suppresses dehydroxylation more effectively than Zn. CoZnO/MgO-Al_2O_3, while still more stable than the bare support, shows slightly higher weight loss than CoFeO, suggesting weaker Zn-O binding and less effective incorporation into the mixed oxide framework. This is aligned with the known thermodynamic behaviour of Zn^{2+}, which is less prone than Fe^{3+} to form thermally rigid spinel environments.The thermal stability trend is therefore: CoFeO/MgO-Al_2O_3 > CoZnO/MgO-Al_2O_3 > MgO-Al_2O_3 and it also observe it in reported paper (Zhong et al., 2023).

This trend is consistent with the expected catalytic behaviour: high temperature NH_3 decomposition favours catalysts with stable metal oxygen frameworks that resist collapse and sintering. Thus, the superior stability of CoFeO/MgO-Al_2O_3 reinforces why later catalytic tests showed higher NH_3 conversion for this bimetallic system.

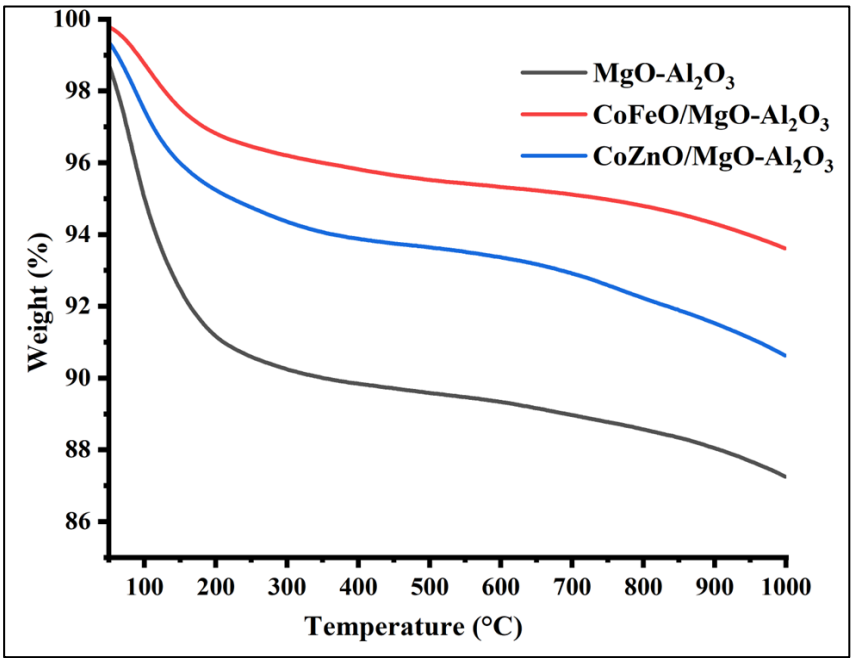


Figure 4.13 Comparison of TGA Profiles for MgO- Al_2O_3, CoFeO/MgO- Al_2O_3, and CoZnO/MgO- Al_2O_3 Catalysts, Indicating Differences in Thermal Stability

4.4.5 Temperature-Programmed Reduction (H_2-TPR) Analysis of Bimetallic

Figure 4.14 compares the reducibility of MgO-Al_2O_3, CoFeO/MgO-Al_2O_3 and CoZnO/MgO-Al_2O_3. The pristine MgO-Al_2O_3 shows only one broad high temperature event (~520 °C), which reflects the intrinsic resistance of the $MgAl_2O_4$-type framework to hydrogen transfer. This confirms that the support alone cannot generate metallic centres under typical NH_3 decomposition windows. Upon bimetallic incorporation, two fundamentally different redox regimes are observed. CoFeO/MgO-Al_2O_3 displays a dual-peak pattern, with the first reduction at ~400-450 °C, representing early H_2 uptake and partial collapse of Co^{3+}/Fe^{3+} to Co^{2+}/Fe^{2+}, and the second peak at ~530-560 °C corresponding to the formation of metallic Co^0/Fe^0 ensembles. The first peak falling inside the reaction window of NH_3 decomposition (450-650 °C) is an extremely important mechanistic indicator: CoFeO/MgO-Al_2O_3 is already generating metallic active centres in the exact temperature region where NH_3 cracking becomes thermodynamically feasible. This means that the catalyst does not need extreme pre-reduction to initiate turnover. It self-activates in situ inside the reaction zone. This is the textbook signature of a kinetically competent NH_3 decomposition catalyst.

CoZnO/MgO-Al_2O_3, by contrast, exhibits a broad, shifted reduction envelope (~480-650 °C). The delayed reduction indicates that Zn^{2+} rigidifies the oxide

environment, suppressing electron mobility and preventing early generation of Co^0. Mechanistically, Zn acts as a "redox diluent" rather than a "redox partner". Therefore, less Co^0 is available at the early stages of NH_3 cracking, which explains the lower activity and it also observe it in reported paper (Zhong et al., 2023). The reducibility order is thus: $CoFeO/MgO\text{-}Al_2O_3$ » $CoZnO/MgO\text{-}Al_2O_3$ » $MgO\text{-}Al_2O_3$ and this TPR hierarchy perfectly correlates with the catalytic activity hierarchy catalysts that can generate metallic sites earlier in the temperature trajectory give higher NH_3 conversion. CoFeO therefore does not only provide "more reducibility" it lowers the energetic barrier for metallic active centre formation. This is the fundamental origin of its superior activity.

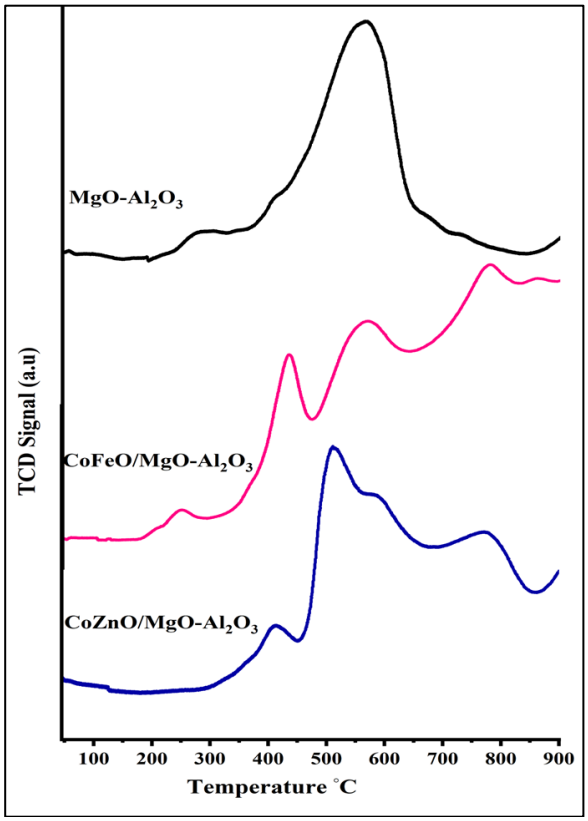


Figure 4.14 H2-TPR Profiles of $MgO\text{-}Al_2O_3$, $CoFeO/MgO\text{-}Al_2O_3$ and $CoZnO/MgO\text{-}Al_2O_3$ Catalysts. The Introduction of Transition Metals Generates Additional Reduction Peaks at Lower Temperatures, Indicating Enhanced Hydrogen Activation and Stronger Metal Support Interaction

4.4.6 XPS Analysis of $CoFeO/MgO\text{-}Al_2O_3$ Catalyst

The surface chemical composition and oxidation states of the $Co\text{-}FeO/MgO\text{-}Al_2O_3$ catalyst were examined using X-ray photoelectron spectroscopy (XPS), as

presented in Figure 4.15. In the O 1s spectrum, two deconvoluted peaks centred at approximately 531.2-531.8 eV and ~533.0-533.6 eV corresponds to lattice metal oxygen bonds (M-O) and surface hydroxyl/chemisorbed oxygen (O-OH), respectively. The dominant M-O component indicates the presence of well-anchored metal oxides within the MgO-Al_2O_3 matrix, which suggests strong coordination of transition metal cations with lattice oxygen. The secondary O-OH contribution is typically associated with adsorbed water, vacancy-stabilized oxygen, or surface-rich basic hydroxyl species, consistent with mixed oxide supports(Alekseev & Nilsson, 2024a).

The Co 2p region exhibits two principal peaks at ~782.6-783.8 eV (Co $2p_{3/2}$) and ~787.9-789.1 eV (Co $2p_{1/2}$), characteristic of Co^{2+} species in oxidized environments. The absence of metallic Co^0 signatures and shake-up features near 780-781 eV indicates that cobalt exists in a fully oxidized state and does not undergo surface reduction during catalyst preparation. The slight positive shift relative to pure CoO is attributed to strong metal–support electronic interactions, where the basic MgO domains donate electron density to surface oxygen, stabilizing Co^{2+} within mixed oxide clusters. This behavior is consistent with previously reported Co-based catalysts used for ammonia decomposition. The Fe 2p spectrum shows two well-resolved peaks at ~710.3-710.9 eV (Fe $2p_{3/2}$) and ~724.8-725.6 eV (Fe $2p_{1/2}$), indicative of Fe^{3+} oxidation states. The broad $2p_{3/2}$ envelope suggests the presence of Fe-O species such as Fe_2O_3 or FeOOH environments, rather than Fe^{2+} or metallic Fe^0. The absence of secondary satellite peaks confirms that iron is highly oxidized and strongly coordinated to lattice oxygen. Notably, the Fe $2p_{3/2}$ peak position is slightly shifted toward lower binding energies relative to bulk Fe_2O_3, reflecting electron redistribution between Fe and Co, and the formation of Co-Fe interfacial domains and it also observe it in reported paper (Wang, et al., 2023).

Such electronic synergy is reported to enhance catalytic performance by promoting N-H bond dissociation kinetics. The Mg 2p spectrum exhibits a single peak at ~50.7-51.4 eV, which is assigned to Mg^{2+} species in MgO frameworks. The absence of metallic magnesium or Mg^{1+} sub-oxide states indicate complete oxidation of Mg and strong structural stability of the support. The basic nature of Mg^{2+} provides electron-donating surface sites that assist in NH_3 adsorption and facilitate surface dissociation.

Similarly, the Al 2p peak positioned between ~74.4-75.3 eV is attributed to Al^{3+} species in Al_2O_3 lattice environments. The lack of metallic Al^0 signatures confirms that aluminium exists exclusively in oxidized form. The presence of Al_2O_3 enhances surface

area, promotes uniform metal dispersion, and prevents the formation of inactive spinel phases that typically reduce catalytic performance. The C 1s spectrum shows a major peak at ~284.8-285.6 eV, corresponding to adventitious carbon (C-C/C-H), and a weaker shoulder at ~288.7-290.2 eV, associated with oxygenated carbon groups (O-C=O) and it also observe it in reported paper (Wang, et al., 2023). These species originate from CO_2/C_x adsorption during air exposure and do not contribute to the catalyst's active chemistry. Taken together, the XPS results confirm that cobalt and iron exist as oxidized surface species (Co^{2+} and Fe^{3+}) uniformly distributed across the MgO-Al_2O_3 support. The presence of lattice oxygen suppressed metallic signatures, and strong metal support interactions indicate the formation of stable metal-oxide nanoclusters. These structural features are consistent with enhanced surface reducibility and the synergistic catalytic performance of Co-FeO/MgO-Al_2O_3 in NH_3 decomposition reactions(Alekseev & Nilsson, 2024a).

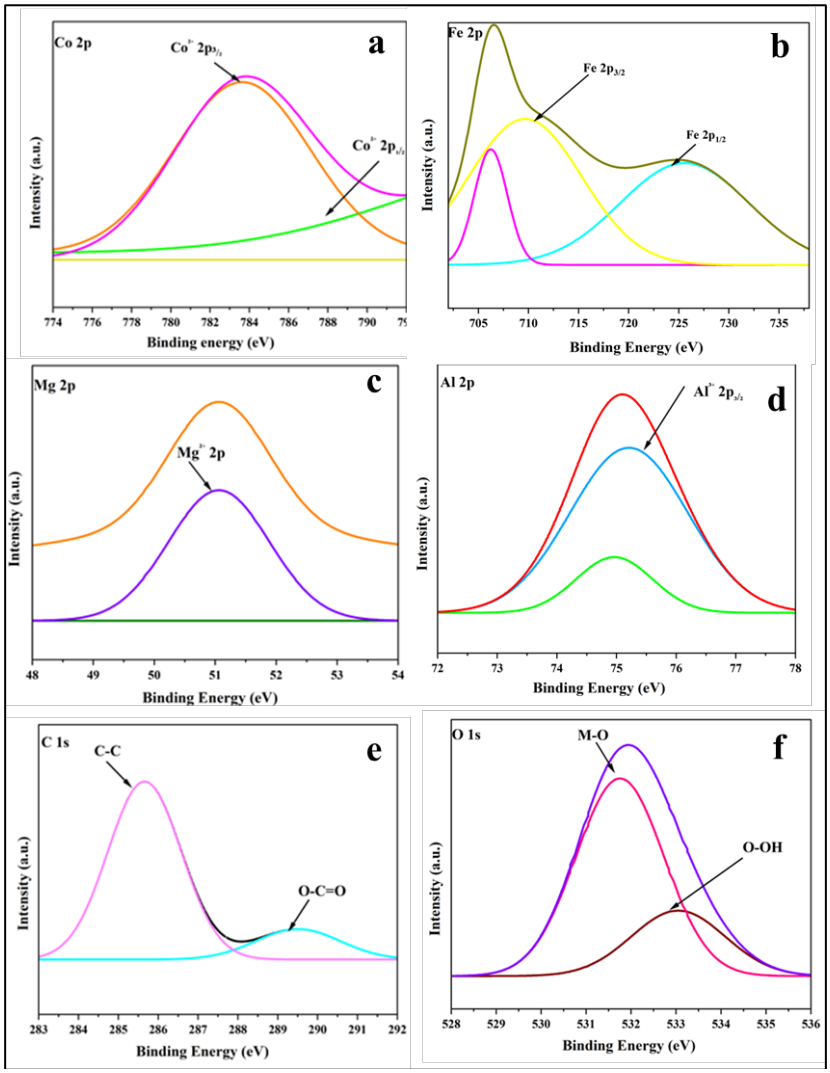


Figure 4.15 XPS Spectra of the $CoFeO/MgO\text{-}Al_2O_3$ Catalyst Showing the Deconvoluted (a) Co 2p, (b)Fe 2p, (c) Mg 2p, (d) Al 2p, (e) C 1s Regions and (f) O 1s

4.5 Catalytic Activity of Bimetallic Oxide Catalysts for NH_3 Decomposition

Figure 4.16 compares NH_3 decomposition over the bimetallic systems ($CoFeO/MgO\text{-}Al_2O_3$ and $CoZnO/MgO\text{-}Al_2O_3$) with the monometallic catalysts previously screened. A clear shift from the single-metal level is observed at 650 °C, $CoFeO/MgO\text{-}Al_2O_3$ reaches 87.23% conversion, followed by $CoZnO/MgO\text{-}Al_2O_3$ (81.74%), both markedly higher than the best monometallic $CoO/MgO\text{-}Al_2O_3$ (77.74%) and far above $FeO/MgO\text{-}Al_2O_3$ (69.82%), $ZnO/MgO\text{-}Al_2O_3$ (4.53%) and the inert $MgO\text{-}Al_2O_3$ support (3.23%) . The same ordering is already established at 550 °C and remains detectable even at 450 °C. This proves that introducing a second transition metal enhances NH_3 decomposition kinetics over cobalt (Peters et al., 2023).

The superior performance of CoFeO/MgO-Al_2O_3 originates from the electronic and structural complementarities between Co and Fe. XRD showed a well-defined CoFeO phase intimately coupled to the $MgAl_2O_4$ backbone, with subtle peak broadening indicating nanoscale domain formation rather than segregated crystals. FESEM confirmed fine granular morphology with minimal agglomeration, while EDX revealed a balanced Co:Fe ratio uniformly distributed across the support. BET showed preservation of high accessible area (131.9 $m^2\ g^{-1}$) and mesoporosity. Critically, H_2-TPR demonstrated that CoFeO/MgO-Al_2O_3 reduces in two steps at moderate temperatures, signifying efficient generation of Co^0 and Fe^0 sites within the temperature domain where NH_3 decomposition initiates. In other words, CoFeO/MgO-Al_2O_3 does not only provide more sites; it provides the right type of metallic environment exactly when the reaction requires them. CoZnO/MgO-Al_2O_3 also shows improved activity relative to its monometallic analogue. However, the CoZnO structure contains Zn^{2+}, which is highly resistant to reduction, evidenced by a delayed and broader high-T H_2-TPR response. FESEM reveals more compact platelets rather than fine granules, and BET confirms smaller accessible area (107.5 $m^2\ g^{-1}$). Thus, although Zn modifies cobalt electronic structure and strengthens thermal stability, it partially suppresses the population of readily reducible Co^0 sites. This explains why CoZnO/MgO-Al_2O_3 enhances activity relative to monometallic CoO, but not to the level of CoFeO.

Overall, the catalytic activity hierarchy is fully consistent with the physicochemical fingerprints established across XRD, FESEM/EDX, BET and H_2-TPR. CoFeO/MgO-Al_2O_3 integrates (i) high reducibility, (ii) nanoscale dispersion and (iii) optimal textural accessibility the three primary determinants for high N-H bond activation probability. This validates CoFeO/MgO-Al_2O_3 as the most rationally selected lead catalyst for further mechanistic analysis and optimization in the subsequent section.

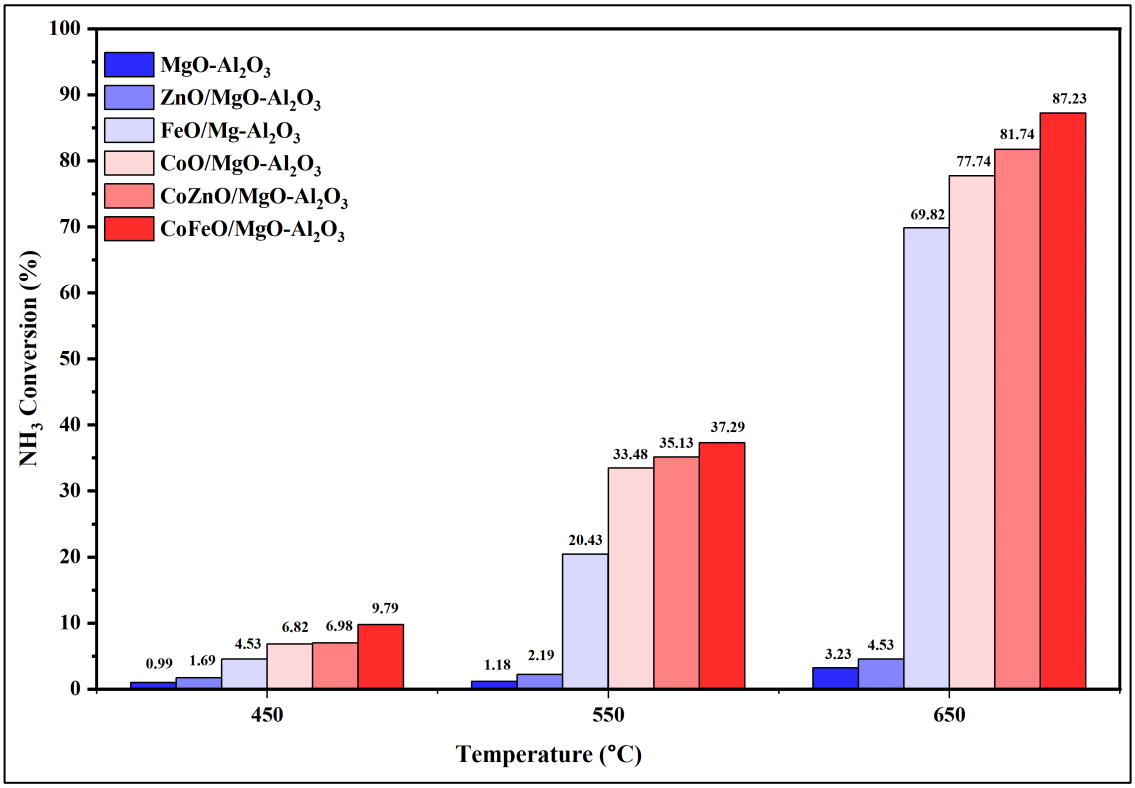


Figure 4.16 NH_3 Conversion of MgO- Al_2O_3 and Metal-Supported Catalysts (CoO, FeO, ZnO, CoFeO and CoZnO) at 450-650 °C, Showing the Superior Catalytic Activity of CoFeO/MgO- Al_2O_3

4.6 Response Surface Methodology of CoFeO/MgO-Al2O3

4.6.1 Box-Behnken Design

The BBD method was used to analyze the effects of three independent process parameters on CoFeO/MgO-Al_2O_3 catalyst performance for NH_3 conversion (response variable). The BBD approach generated a total of 17 experimental trials (runs) as shown in Table 4.3. The studied factors were the concentration of the synthesized CoFeO/MgO-Al_2O_3 catalyst (A), temperature (B), and time (C). A quadratic polynomial model was employed to describe the statistical relationship between the response and the process parameters(Agha et al., 2024). Eq.4.1 presents the empirical relationship between the tested variables and the response:

$$NH_3 \text{ conversion } (\%) = + 83.18 + 4.91A + 4.01B + 9.06C - 4.42AB + 1.22AC + 0.3952BC - 3.98A^2 - 6.74B^2 - 9.81C^2 \quad (4.1)$$

Equation indicates that the coefficients for concentration (A), temperature (B), and time (C) have a positive impact on NH_3 conversion using the CoFeO/MgO-Al_2O_3

catalyst. This implies that increasing concentration, temperature, and duration enhances NH_3 conversion efficiency (%).

Table 4.3
The BBD Three-Variable Matrixfor NH_3 Conversion Using CoFeO/MgO- Al_2O_3

Run	Factor 1 A:Conc (M)	Factor 2 B:Temp C	Factor 2 C:Time hrs	Response 1 NH_3 conversion %
1	0.2	120	7	57.19
2	1	120	7	77.28
3	0.2	180	7	76.47
4	1	180	7	78.87
5	0.2	150	5	58.04
6	1	150	5	63.98
7	0.2	150	9	72.35
8	1	150	9	83.18
9	0.6	120	5	54.47
10	0.6	180	5	59.29
11	0.6	120	9	73.18
12	0.6	180	9	79.57
13	0.6	150	7	84.46
14	0.6	150	7	85.11
15	0.6	150	7	80.43
16	0.6	150	7	83.41
17	0.6	150	7	82.48

4.6.2 Analysis of Variance

ANOVA is a fundamental statistical tool for evaluating the reliability and accuracy of the catalytic evaluation for the catalyst assisted NH_3 conversion. The corresponding ANOVA results are presented in Table 4.4. The F-values, sums of squares, and p-values were used to determine significant variables. The model demonstrates statistical significance, as evidenced by an F-value of 42.28 for NH_3 conversion (Aghaet al., 2024).

The coefficient of determination (R^2) for NH_3 conversion is 0.98, indicating an excellent agreement between the predicted and experimental data. Additionally, the high adjusted R^2 value (0.98) confirms a strong correlation between actual and predicted values. In general, based on (Table 4.3), variables with a p-value greater than 0.05 are considered statistically insignificant for NH_3 conversion, while those with a p-value less than 0.05 are significant. Accordingly, the catalyst model terms A, B, C, and AB were found to be significant. The graphical validation of the model provides insights into the residual distribution. The normal probability plot (Figure 4.17 (a) is used to evaluate the distribution of residuals. The residual values in this plot closely follow a straight line, indicating that the residuals are independent and uniformly distributed. The relationship between the actual and predicted NH_3 conversion values is illustrated in (Figure 4.17 (b). The alignment of data points along the diagonal line suggests that the model has been statistically validated. Need to support with reference.

Table 4.4
Analysis of Variance (ANOVA) for CoFeO/MgO- Al_2O_3 Catalytic Activity for NH_3 Conversion

Source	Sum of Squares	df	Mean Square	F-value	p-value	
Model	1792.45	9	199.16	42.28	< 0.0001	significant
A-Conc	192.67	1	192.67	40.90	0.0004	
B-Temp	128.64	1	128.64	27.31	0.0012	
C-Time	657.03	1	657.03	139.47	< 0.0001	
AB	78.23	1	78.23	16.61	0.0047	
AC	5.98	1	5.98	1.27	0.2971	
BC	0.6162	1	0.6162	0.1308	0.7283	
A^2	66.79	1	66.79	14.18	0.0070	
B^2	191.43	1	191.43	40.64	0.0004	
C^2	405.02	1	405.02	85.97	< 0.0001	
Residual	32.98	7	4.71			
Lack of Fit	19.51	3	6.50	1.93	0.2663	not significant
Pure Error	13.47	4	3.37			
Cor Total	1825.42	16				
R^2	0.9819		Adjusted R^2	0.9587	Predicted R^2	0.8175

4.6.3 Effect of Input Variables

As shown in Figure 4.17 (c), a perturbation plot was utilized to assess the combined effects of three input parameters on NH_3 conversion using the CoFeO/MgO-Al_2O_3 catalyst. These parameters are critical for optimizing NH_3 conversion efficiency(Agha et al., 2024).

- The steep curve for variable A (concentration of the catalyst solution) suggests that NH_3 conversion efficiency is highly sensitive to this parameter. Increasing concentration enhances NH_3 conversion due to the greater availability of active sites.
- Generally, NH_3 conversion efficiency decreases as temperature (variable B) increases.

- The curve for variable C (time) indicates the response's sensitivity to reaction duration.

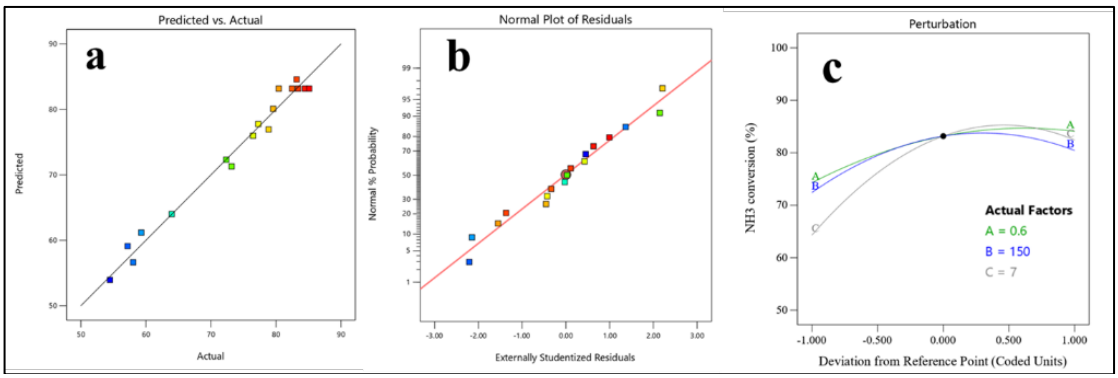


Figure 4.17 (a) Predicted vs. Cctual Values of NH_3 Conversion Using CoFeO/MgO-Al_2O_3 Catalyst, Demonstrating Model Accuracy (b) Normal Probability Plot of Residuals for CoFeO/MgO- Al_2O_3 Catalyst (c) Perturbation Plot for CoFeO/MgO- Al_2O_3 Catalyst

4.6.4 Three-Dimensional Response Surface

To understand the relationships between the independent parameters and NH_3 conversion efficiency (%), three-dimensional (3D) response surface plots and two-dimensional (2D) contour plots were generated using the quadratic model. Each combination of input factors, as presented in Table 4.3, was analyzed to evaluate their interactions. It was found that the concentration and temperature significantly influence NH_3 conversion efficiency, as indicated by a p-value of 0.0047 as shown in Table 4.4. 3D plot illustrates the key interactions among the studied variables affecting catalyst performance. Specifically, Figure 4.18 (a) presents the 3D plot depicting the correlation between concentration and temperature, while Figure 4.18 (b) shows the corresponding contour plot, respectively.

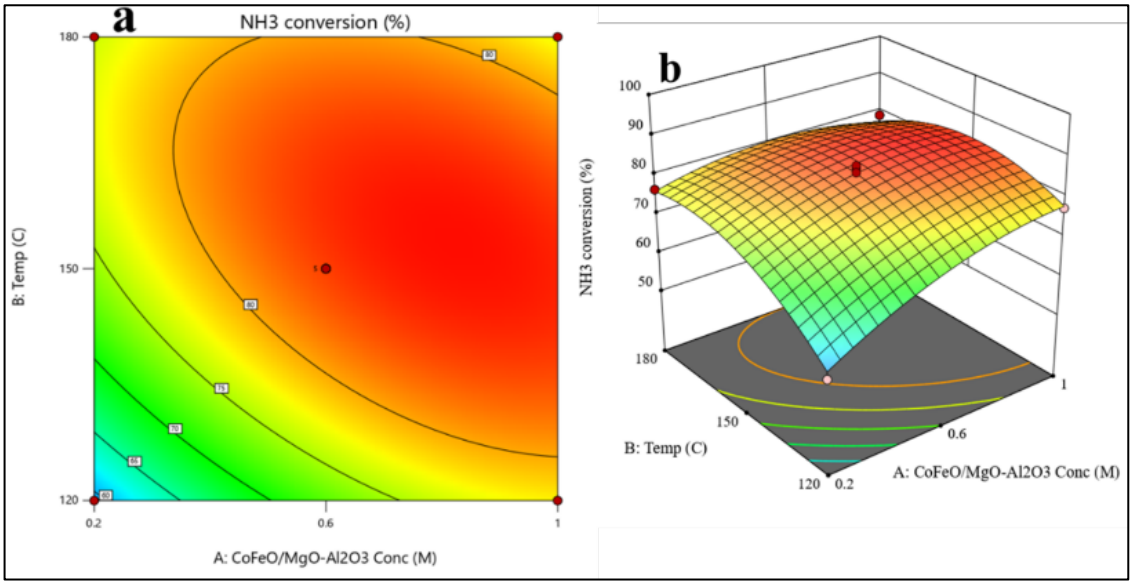


Figure 4.18 The Illustration of (a) Three-Dimensional (3D) Response Surface Plot Illustrates the Interaction Between CoFeO/MgO- Al_2O_3 Concentration and Temperature on NH_3 Conversion Efficiency (%) and (b) Two-Dimensional (2D) Contour Plot Representing the Same Data

4.6.5 Validation Study

The accuracy of the optimization model was assessed by evaluating different combinations of independent variables concentration, temperature, and time within their experimental ranges. (Figure 4.19) illustrates the model's robustness by comparing the predicted values from the Box-Behnken Design (BBD) model with the actual experimental results. The Figure 4.19 (a) graphs represent the RSM (Response Surface Methodology) optimization results, showing the predicted values for NH_3 conversion (%) based on input parameters. The Figure 4.19 (b) chart validates the model by comparing the experimental NH_3 conversion data with the predicted values. The highest NH_3 conversion obtained experimentally was 85.11%, which is in close agreement with the predicted value, demonstrating the reliability of the BBD model in optimizing NH_3 conversion efficiency.

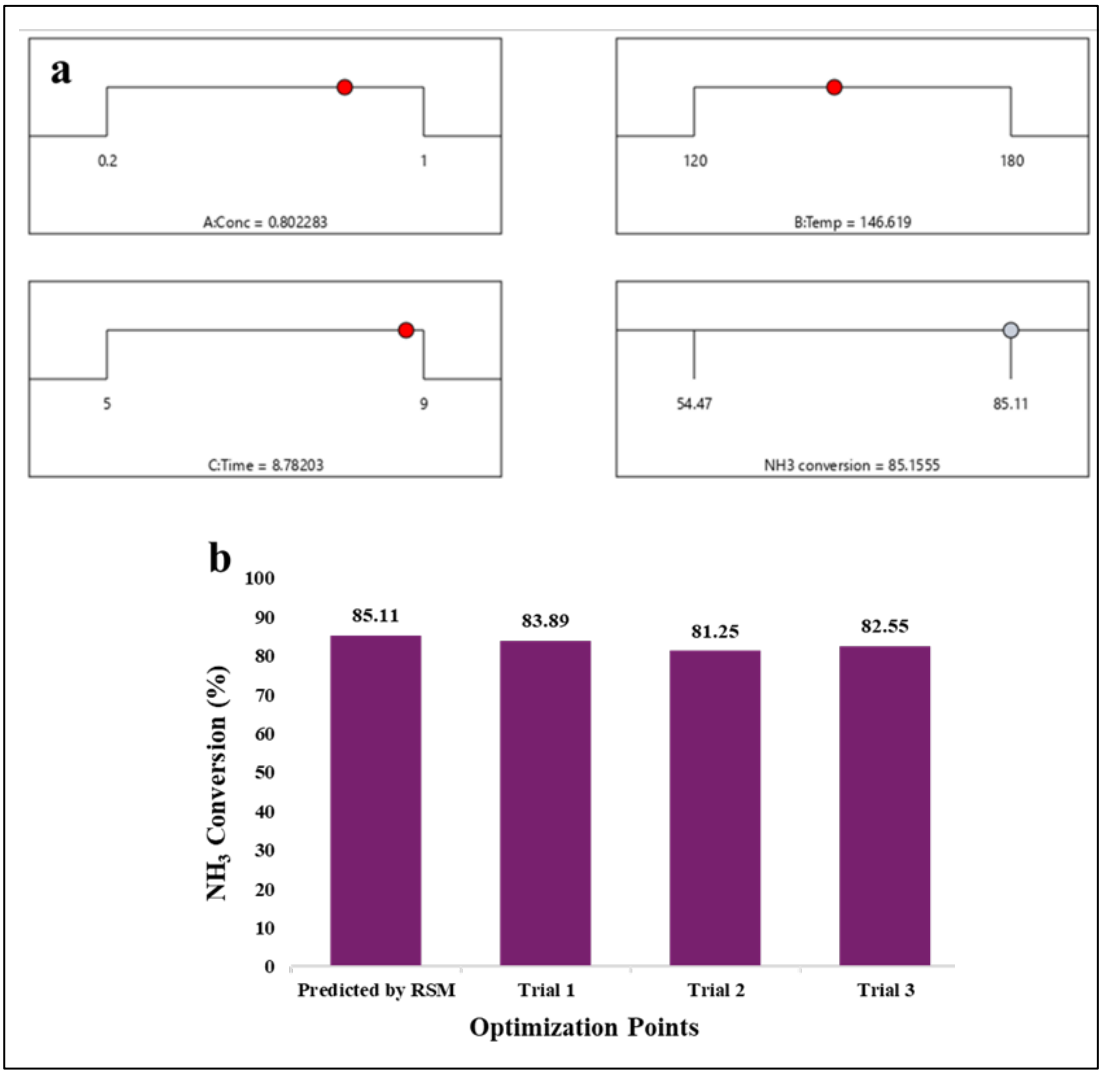


Figure 4.19 Optimization and Validation of NH_3 Conversion: (a) Predicted NH_3 Conversion from the BBD Model Based on Response Surface Methodology (RSM); (b) Experimental Results Validating the Predicted Conversion Rate

4.7 Kinetic Analysis of CoFeO/MgO-Al_2O_3 Catalyst

To elucidate the reaction kinetics of NH_3 decomposition, the experimental data were fitted using pseudo-first order (PFO) and pseudo-second order (PSO) kinetic models. The kinetic parameters, including the equilibrium conversion (q_e), rate constants (k_1 for PFO and k_2 for PSO), and the coefficient of determination (R^2), are summarized in Table 4.5 The corresponding kinetic curves at different temperatures (450-650 °C) are presented in Figure 4.20. The experimental NH_3 conversion (XNH_3) increases with temperature, highlighting the thermally activated nature of the process. At lower temperatures (450-550 °C), the reaction kinetics are relatively slow, with low equilibrium conversion values.

However, as the temperature rises to 600-650 °C, a significant enhancement in NH_3 decomposition is observed. The (PFO) rate constant (k_1) decreases with increasing

temperature, ranging from 0.2630 min^{-1} at 450 °C to 0.4696 min^{-1} at 650 °C. The corresponding R_2 values (0.96-0.99) indicate a reasonable fit but suggest deviations at higher temperatures. The calculated equilibrium conversions (q_e) are lower than the experimental values, particularly at elevated temperatures, implying that the reaction mechanism deviates from a simple first-order process. The PSO model exhibits slightly better agreement with experimental data, especially at higher temperatures.

The rate constant (k_2) decreases significantly with increasing temperature, from 0.0139 min^{-1} at 450 °C to 0.2637 min^{-1} at 650 °C. The R_2 values (0.84-0.89) indicate a moderate fit. Notably, the PSO model predicts a higher q_e at elevated temperatures, aligning better with experimental observations. The kinetic results suggest that the NH_3 decomposition reaction follows a mixed kinetic regime. At lower temperatures, the reaction kinetics are better described by the PFO model, while at higher temperatures, deviations occur, and the PSO model provides a more accurate fit observed in (Wang et al., 2022) . The declining rate constants (k_1 and k_2) with increasing temperature indicate a shift in reaction kinetics, potentially due to changes in surface reaction mechanisms and active site availability. While both models provide insight into the reaction kinetics, neither perfectly describes the entire temperature range. The observed discrepancies highlight the need for a more comprehensive kinetic approach, potentially incorporating reaction mechanisms beyond simple PFO or PSO models according to.

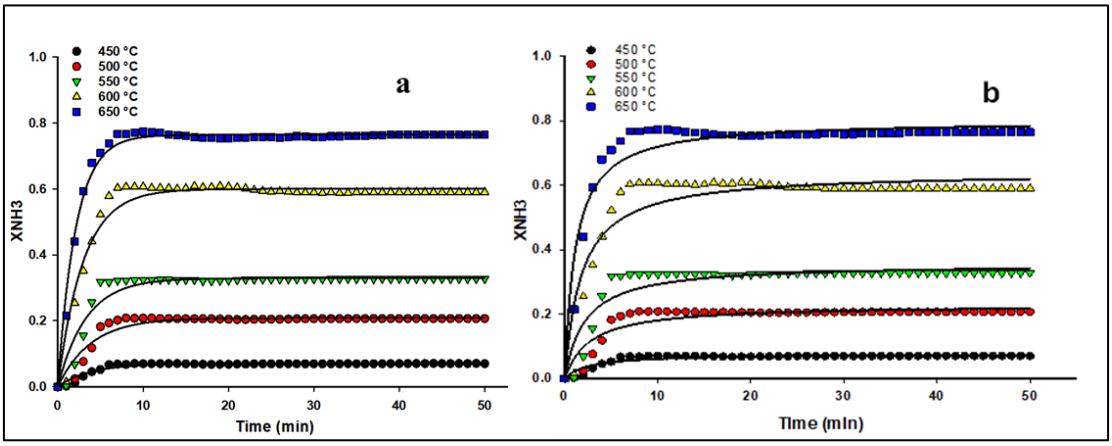


Figure 4.20 Kinetic Modelling of NH_3 Decomposition at Different Temperatures (450-650°C) Using (a) Pseudo-First Order (PFO) and (b) Pseudo-Second Order (PSO) Models

Table 4.5
PFO and PSO Kinetic Parameters for NH_3 Conversion by CoFeO/MgO- Al_2O_3

Temperature (°C)	XNH_3 exp. (%)	Pseudo-first order (PFO)			Pseudo-second order (PSO)		
		XNH_3 cal (%)	k_1 (min^{-1})	R^2	XNH_3 cal (%)	k_2 (min^{-1})	R^2
450	0.069824	0.0698	0.2630	0.96	0.0764	0.0139	0.84
500	0.20637	0.2085	0.2564	0.95	0.2287	0.0168	0.86
550	0.326729	0.3289	0.3018	0.95	0.3591	0.0219	0.86
600	0.590331	0.5999	0.3349	0.97	0.7001	0.0846	0.87
650	0.764083	0.7641	0.4696	0.99	1.0885	0.2637	0.89

4.8 The recyclability of CoFeO/MgO-Al_2O_3 Catalyst

The reusability of the optimized CoFeO/MgO-Al_2O_3 catalyst was examined over nine continuous reaction cycles under the optimum conditions obtained from RSM. The NH_3 conversion decreased gradually from 87.24% in cycle 1 to 73.45% in cycle 9, as shown in Figure 4.21. Although a slight decline was observed, the catalyst still maintained a high activity level, where the conversion remained above 80% for the first six cycles. The slow performance decay suggests that the catalyst structure is inherently stable, and the loss is mainly associated with surface site saturation during prolonged exposure to NH_3 reaction intermediates rather than any major structural damage.

This explanation is consistent with the previous characterization results: TGA confirmed high thermal stability, TPR verified moderate-temperature reducibility with strong metal support interaction, and BET demonstrated stable mesoporous structure with sufficient surface area. Based on these results, CoFeO/MgO-Al_2O_3 can be considered highly durable for NH_3 decomposition, retaining a significant fraction of its activity across multiple cycles. A simple mild H_2 treatment between cycles is expected to fully restore surface active sites if required, which confirms the potential of this catalyst for long-term use in practical hydrogen production applications. The observed

16% decrease in activity over nine cycles can be attributed to partial surface site saturation or coking, where adsorbed reaction intermediates temporarily occupy active sites. No significant structural degradation occurs, as confirmed by TGA, which demonstrates high thermal stability, and BET, which shows a stable mesoporous framework. H_2-TPR results indicate that the reducibility of the metal sites remains intact, confirming that the drop is surface-related rather than structural. Mild hydrogen treatment between cycles can fully restore active sites, ensuring long-term catalytic durability for NH_3 decomposition.

Collectively, these results indicate that CoFeO/MgO-Al_2O_3 is highly durable, retaining a significant fraction of its activity over multiple cycles while maintaining structural integrity, demonstrating its suitability for practical hydrogen production applications.

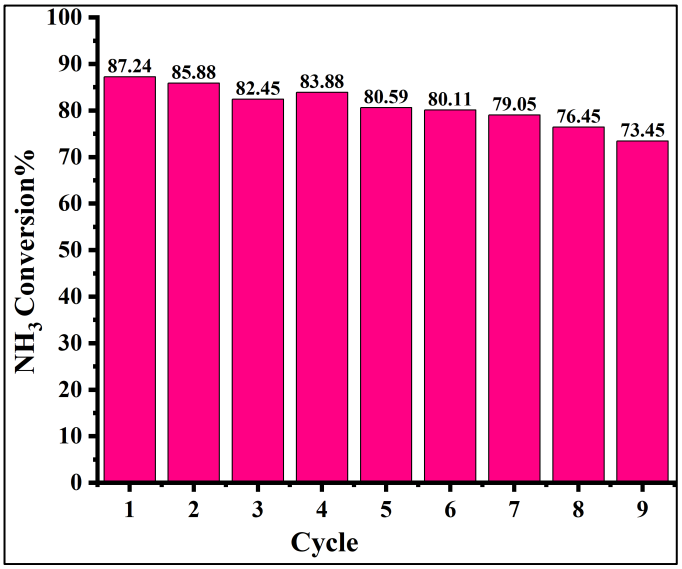


Figure 4.21 The Recyclability Performance of the Synthesized Catalyst Over Multiple Reaction Cycles

4.9 Summary

This chapter systematically established the structure activity relationships of MgO-Al_2O_3 supported catalysts for NH_3 decomposition, moving from initial single-metal screening to bimetallic optimization. All characterization results consistently revealed that cobalt generates the most favourable physicochemical attributes for catalytic activation: Co-containing systems exhibited stronger reducibility, higher density of accessible active sites, and more intimate metal support interaction, which in turn lowered the barrier for N-H bond scission. Based on this foundation, bimetallic design was then conducted using cobalt as the primary component. Between the two

bimetallic systems examined, CoFeO/MgO-Al_2O_3 demonstrated superior crystallinity, finer nanostructuring, enhanced metal dispersion, and more balanced redox characteristics compared to CoZnO/MgO-Al_2O_3. These features directly translated into significantly higher NH_3 conversion, confirming the presence of effective electronic synergy between Co and Fe species. Recyclability tests further confirmed that CoFeO/MgO-Al_2O_3 preserved high catalytic activity across repeated cycles, validating its structural stability under high-temperature operation. Collectively, the results in this chapter confirm that CoFeO/MgO-Al_2O_3 is the most promising catalyst developed in this work, and it was therefore selected for statistical optimization and subsequent process evaluation. The next chapter integrates these findings into the broader technological, scientific, and practical implications of using NH_3 as a carbon-free hydrogen carrier.

CHAPTER 5
CONCLUSION AND RECOMMENDATIONS

5.1 Conclusion

This study successfully developed and evaluated a new class of non-noble metal oxide catalysts supported on $MgO\text{-}Al_2O_3$ for carbon-free hydrogen production through ammonia (NH_3) decomposition. The research addressed the major industrial challenge of limited catalyst efficiency, cost, and long-term durability by investigating both monometallic (CoO, FeO, ZnO) and bimetallic (CoFeO, CoZnO) systems synthesized via hydrothermal carbonization. Among the monometallic catalysts, $CoO/MgO\text{-}Al_2O_3$ exhibited the highest catalytic activity, achieving 77.74% NH_3 conversion at 650 °C. This confirmed cobalt as the most active single component and informed the formulation of cobalt-based bimetallic systems designed to exploit synergistic metal-metal electronic effects capable of improving catalytic performance beyond monometallic limits.

The bimetallic $CoFeO/MgO\text{-}Al_2O_3$ catalyst demonstrated the highest activity, reaching 87.23% NH_3 conversion at 650 °C. Comprehensive characterization using XRD, FESEM-EDX, BET, TGA, H_2-TPR, and XPS revealed that its superior performance resulted from several interrelated structural and electronic advantages: (i) the formation of mixed-oxide nanodomains ensuring intimate Co-Fe interaction; (ii) uniform dispersion of metal species anchored to the oxygen-rich $MgAl_2O_4$ lattice; (iii) preservation of mesoporosity, which enhances NH_3 adsorption and diffusion; and (iv) multi-step reducibility that facilitates the in-situ generation of Co^0/Fe^0 active sites essential for N-H bond scission. These findings collectively indicate that the most impactful discovery of this research is the synergistic enhancement of catalytic performance through the Co-Fe bimetallic interaction on $MgO\text{-}Al_2O_3$, which significantly improves NH_3 conversion, stability, and reusability.The statistical optimization of process parameters using Response Surface Methodology (Box-Behnken design) yielded a predictive quadratic model capable of accurately forecasting catalytic conversion efficiency. Kinetic and recyclability assessments further confirmed that $CoFeO/MgO\text{-}Al_2O_3$ maintains catalytic stability and structural integrity after multiple reaction cycles, reinforcing its potential for continuous operation. The

structure-activity correlations established in this study therefore contribute not only to catalyst development but also to the broader understanding of reaction mechanisms in mixed-metal oxide systems for NH_3 decomposition.

In conclusion, this research identifies $CoFeO/MgO\text{-}Al_2O_3$ as an economically viable, thermally robust, and high-performance non-noble catalyst that advances ammonia-to-hydrogen conversion toward practical applications. The integrated experimental and statistical approach provides a rational framework for designing cost-effective catalytic systems and establishes a strong foundation for scaling hydrogen production technologies in alignment with the global transition toward carbon-neutral energy systems.

5.2 Recommendations

The $CoFeO/MgO\text{-}Al_2O_3$ catalyst developed in this study should be considered a viable alternative to noble-metal-based systems in mid-temperature NH_3 decomposition reactors. Its synthesis through hydrothermal carbonization is simple, reproducible, and environmentally benign, making it suitable for pilot-scale hydrogen production plants or on-site hydrogen generators for fuel cell applications. Future industrial-scale trials are recommended to evaluate its catalytic behaviour under continuous-flow conditions, where gas hourly space velocity (GHSV) and pressure fluctuations simulate realistic operating environments. Additionally, the mesoporous $MgAl_2O_4$ support may be adapted into monolithic substrates or coated onto ceramic honeycomb structures to enhance heat distribution, reduce pressure drop, and improve mechanical resilience during prolonged operation. Given that ammonia is already globally available, storable, and transportable, the integration of efficient catalysts such as $CoFeO/MgO\text{-}Al_2O_3$ with renewable energy systems could enable a practical pathway for carbon-free hydrogen supply chains. Policymakers and energy institutions should consider supporting pilot programs that deploy such catalysts in modular, decentralized NH_3 cracking units. This would promote clean hydrogen generation, contribute to decarbonizing industrial sectors, and advance progress toward net-zero emission targets.

5.3 Future Work

- Future investigations should extend beyond laboratory testing to assess long-term operational stability and deactivation behaviour under cyclic conditions.

Studies on catalyst poisoning resistance, thermal aging, and regeneration efficiency are essential to establish industrial reliability. In parallel, techno-economic analysis (TEA) and life-cycle assessment (LCA) should be conducted to quantify the cost-effectiveness and environmental impact of the CoFeO/MgO-Al_2O_3 system relative to conventional Ni- or Ru-based catalysts. Further research into ternary or doped mixed-oxide catalysts, as well as the integration of these catalytic frameworks with digital twin and AI-based process optimization tools, could pioneer next-generation intelligent reactors for hydrogen production.

- Upcoming research should move beyond bench-scale catalytic evaluation and deploy CoFeO/MgO-Al_2O_3 under realistic duty cycles, including repetitive thermal on/off, variable feed compositions, and impurity-rich NH_3 streams (H_2O, CO_2, NOx, trace lubrication vapors). Detailed deactivation mapping (sintering vs. nitriding vs. sulfate/chloride adsorption) must be quantified through in-situ/operando tracking tools (DRIFTS, in-situ XRD, near-ambient XPS), enabling mechanistic discrimination of surface restructuring pathways.
- Next generation catalyst design should investigate ternary metal oxides (Co-Fe-M) where M = Mo, Ce, or Ni, including doping/gradient architecture to tailor dual-site cooperativity, promote N-N recombination, and suppress nitrogen poisoning at high conversions. Tailored hierarchical porosity within MgO-Al_2O_3 (macro → meso → micro) should also be engineered to shorten diffusion pathlengths and reduce Knudsen transport bottlenecks.
- Strategic alignment with national and regional hydrogen roadmaps is recommended, particularly where ammonia cracking is foreseen as a maritime and offshore H_2 vector (Malaysia, Singapore, Japan, EU shipping corridors). CoFeO/MgO-Al_2O_3 should therefore be positioned as a plausible transition catalyst platform that can serve near-to-medium term ammonia/H_2 deployment while supply chains for noble-metal free systems mature.

REFERENCES

Abdullah, R. F., Rashid, U., Taufiq-Yap, Y. H., Ibrahim, M. L., Ngamcharussrivichai, C., & Azam, M. (2020). Synthesis of bifunctional nanocatalyst from waste palm kernel shell and its application for biodiesel production. *RSC Advances*, *10*(45), 27183–27193. https://doi.org/10.1039/d0ra04306k

Abouemara, K., Shahbaz, M., Mckay, G., & Al-Ansari, T. (2024a). The review of power generation from integrated biomass gasification and solid oxide fuel cells: current status and future directions. *Fuel*, *360*(PC), 130511. https://doi.org/10.1016/j.fuel.2023.130511

Abouemara, K., Shahbaz, M., Mckay, G., & Al-Ansari, T. (2024b). The review of power generation from integrated biomass gasification and solid oxide fuel cells: current status and future directions. *Fuel*, *360*(PC), 130511. https://doi.org/10.1016/j.fuel.2023.130511

Achomo, M. A., Kumar, A., Peela, N. R., & Muthukumar, P. (2024). Hydrogen production from steam reforming of methanol: A comprehensive review on thermodynamics, catalysts, reactors, and kinetic studies. *International Journal of Hydrogen Energy*, *58*(February), 1640–1672. https://doi.org/10.1016/j.ijhydene.2024.01.159

Adamou, P., Bellomi, S., Hafeez, S., Harkou, E., Al-Salem, S. M., Villa, A., Dimitratos, N., Manos, G., & Constantinou, A. (2023). Recent progress for hydrogen production from ammonia and hydrous hydrazine decomposition: A review on heterogeneous catalysts. *Catalysis Today*, *423*(January), 114022. https://doi.org/10.1016/j.cattod.2023.01.029

Afzali, N., & Keshavarzi, R. (2024). Metal-organic framework as light harvesting for photoelectrochemical water splitting: from fundamental to recent progress. *Photoelectrochemical Engineering for Solar Harvesting*, 67–107. https://doi.org/10.1016/B978-0-323-95494-5.00003-3

Agha, H. M., Abdulhameed, A. S., Jawad, A. H., Aazmi, S., Sidik, N. J., De Luna, Y., Wilson, L. D., ALOthman, Z. A., & Algburi, S. (2024). Enhancing cationic dye removal via biocomposite formation between chitosan and food grade algae: Optimization of algae loading and adsorption parameters. *International Journal of Biological Macromolecules*, *258*. https://doi.org/10.1016/j.ijbiomac.2023.128792

Agha, H. M., Abdulhameed, A. S., Jawad, A. H., Sidik, N. J., Aazmi, S., Wilson, L. D., & ALOthman, Z. A. (2024). Food-grade algae modified Schiff base-chitosan benzaldehyde composite for cationic methyl violet 2B dye removal: RSM statistical parametric optimization. *International Journal of Phytoremediation*, *26*(4), 459–471. https://doi.org/10.1080/15226514.2023.2246596

Ahmad, A., & Yadav, A. K. (2024). Parametric analysis of wastewater electrolysis for green hydrogen production: A combined RSM, genetic algorithm, and particle swarm optimization approach. *International Journal of Hydrogen Energy*, *59*, 51–62. https://doi.org/10.1016/J.IJHYDENE.2024.01.302

Ahmed, M. A., & Mohamed, A. A. (2024a). Advances in ultrasound-assisted synthesis of photocatalysts and sonophotocatalytic processes: A review. *IScience*, *27*(1), 108583. https://doi.org/10.1016/j.isci.2023.108583

Ahmed, M. A., & Mohamed, A. A. (2024b). Advances in ultrasound-assisted synthesis of photocatalysts and sonophotocatalytic processes: A review. *IScience*, *27*(1), 108583. https://doi.org/10.1016/j.isci.2023.108583

Akarçay, Ö., Kurtoğlu, S. F., & Uzun, A. (2020). Ammonia decomposition on a highly-dispersed carbon-embedded iron catalyst derived from Fe-BTC: Stable and high performance at relatively low temperatures. *International Journal of Hydrogen Energy*, *45*(53), 28664–28681. https://doi.org/10.1016/j.ijhydene.2020.07.188

Aker, V., & Ayas, N. (2023). Boosting hydrogen production by ethanol steam reforming on cobalt-modified Ni–Al2O3 catalyst. *International Journal of Hydrogen Energy*, *48*(60), 22875–22888. https://doi.org/10.1016/J.IJHYDENE.2022.12.310

AlAmoudi, O. M., Ullah Khan, W., Hantoko, D., Ali, S. A., & Hossain, M. M. (2024). Industrial waste-based Ni-catalysts for ammonia decomposition to produce clean hydrogen. *Fuel*, *367*(December 2023), 131489. https://doi.org/10.1016/j.fuel.2024.131489

AlAmoudi, O. M., Ullah Khan, W., Hantoko, D., Bakare, I. A., Ali, S. A., & Hossain, M. M. (2024a). Catalytic activity of Co/γ-Al2O3 catalysts for decomposition of ammonia to produce hydrogen. *Fuel*, *372*. https://doi.org/10.1016/j.fuel.2024.132230

AlAmoudi, O. M., Ullah Khan, W., Hantoko, D., Bakare, I. A., Ali, S. A., & Hossain, M. M. (2024b). Catalytic activity of Co/γ-Al2O3 catalysts for decomposition of

ammonia to produce hydrogen. *Fuel*, *372*. https://doi.org/10.1016/j.fuel.2024.132230

Alekseev, V. A., & Nilsson, E. J. K. (2024a). Reduced kinetics of NH3/n-heptane: Model analysis and a new small mechanism for engine applications. *Fuel*, *367*. https://doi.org/10.1016/j.fuel.2024.131464

Alekseev, V. A., & Nilsson, E. J. K. (2024b). Reduced kinetics of NH3/n-heptane: Model analysis and a new small mechanism for engine applications. *Fuel*, *367*(January), 131464. https://doi.org/10.1016/j.fuel.2024.131464

Alharthi, A. I., Abdel-Fattah, E., Hargreaves, J. S. J., Alotaibi, M. A., Din, I. U., & Al-Shalwi, M. N. (2023). Influence of Zn and Ni dopants on the physicochemical and activity patterns of CoFe2O4 derived catalysts for hydrogen production by catalytic cracking of methane. *Journal of Alloys and Compounds*, *938*, 168437. https://doi.org/10.1016/j.jallcom.2022.168437

Alharthi, A. I., Alotaibi, M. A., Abdel-Fattah, E., & Awadallah, A. E. (2024). Understanding the impact of support materials on CoFe2O4 catalyst performance for hydrogen fuel and nanocarbon production via methane decomposition. *Ceramics International*, *50*(20), 38029–38039. https://doi.org/10.1016/j.ceramint.2024.07.164

Ali Shah, Z., Marseglia, G., & De Giorgi, M. G. (2024a). Predictive models of laminar flame speed in NH3/H2/O3/air mixtures using multi-gene genetic programming under varied fuelling conditions. *Fuel*, *368*. https://doi.org/10.1016/j.fuel.2024.131652

Ali Shah, Z., Marseglia, G., & De Giorgi, M. G. (2024b). Predictive models of laminar flame speed in NH3/H2/O3/air mixtures using multi-gene genetic programming under varied fuelling conditions. *Fuel*, *368*(November 2023), 131652. https://doi.org/10.1016/j.fuel.2024.131652

Amin, A. (2024a). Review of autothermal reactors: Catalysis, reactor design, and processes. *International Journal of Hydrogen Energy*, *65*(March), 271–291. https://doi.org/10.1016/j.ijhydene.2024.03.372

Amin, A. (2024b). Review of autothermal reactors: Catalysis, reactor design, and processes. *International Journal of Hydrogen Energy*, *65*(March), 271–291. https://doi.org/10.1016/j.ijhydene.2024.03.372

Amini Horri, B., & Ozcan, H. (2024). Green hydrogen production by water electrolysis: Current status and challenges. *Current Opinion in Green and Sustainable Chemistry*, *47*, 100932. https://doi.org/10.1016/J.COGSC.2024.100932

Amiri, T. Y., Ghasemzageh, K., & Iulianelli, A. (2020). Membrane reactors for sustainable hydrogen production through steam reforming of hydrocarbons: A review. *Chemical Engineering and Processing - Process Intensification*, *157*, 108148. https://doi.org/10.1016/J.CEP.2020.108148

Andersen, J. A., Christensen, J. M., Østberg, M., Bogaerts, A., & Jensen, A. D. (2022). Plasma-catalytic ammonia decomposition using a packed-bed dielectric barrier discharge reactor. *International Journal of Hydrogen Energy*, *47*(75), 32081–32091. https://doi.org/10.1016/j.ijhydene.2022.07.102

Arsad, A. Z., Hannan, M. A., Al-Shetwi, A. Q., Begum, R. A., Hossain, M. J., Ker, P. J., & Mahlia, T. I. (2023). Hydrogen electrolyser technologies and their modelling for sustainable energy production: A comprehensive review and suggestions. *International Journal of Hydrogen Energy*, *48*(72), 27841–27871. https://doi.org/10.1016/j.ijhydene.2023.04.014

Arsad, S. R., Arsad, A. Z., Ker, P. J., Hannan, M. A., Tang, S. G. H., Goh, S. M., & Mahlia, T. M. I. (2024a). Recent advancement in water electrolysis for hydrogen production: A comprehensive bibliometric analysis and technology updates. *International Journal of Hydrogen Energy*, *60*(February), 780–801. https://doi.org/10.1016/j.ijhydene.2024.02.184

Arsad, S. R., Arsad, A. Z., Ker, P. J., Hannan, M. A., Tang, S. G. H., Goh, S. M., & Mahlia, T. M. I. (2024b). Recent advancement in water electrolysis for hydrogen production: A comprehensive bibliometric analysis and technology updates. *International Journal of Hydrogen Energy*, *60*, 780–801. https://doi.org/10.1016/J.IJHYDENE.2024.02.184

Arsad, S. R., Arsad, A. Z., Ker, P. J., Hannan, M. A., Tang, S. G. H., Goh, S. M., & Mahlia, T. M. I. (2024c). Recent advancement in water electrolysis for hydrogen production: A comprehensive bibliometric analysis and technology updates. *International Journal of Hydrogen Energy*, *60*(February), 780–801. https://doi.org/10.1016/j.ijhydene.2024.02.184

Asif, M., Sidra Bibi, S., Ahmed, S., Irshad, M., Shakir Hussain, M., Zeb, H., Kashif Khan, M., & Kim, J. (2023a). Recent advances in green hydrogen production, storage and commercial-scale use via catalytic ammonia cracking. *Chemical*

Engineering Journal, *473*(August), 145381. https://doi.org/10.1016/j.cej.2023.145381

Asif, M., Sidra Bibi, S., Ahmed, S., Irshad, M., Shakir Hussain, M., Zeb, H., Kashif Khan, M., & Kim, J. (2023b). Recent advances in green hydrogen production, storage and commercial-scale use via catalytic ammonia cracking. *Chemical Engineering Journal*, *473*(August), 145381. https://doi.org/10.1016/j.cej.2023.145381

Aslam, S., Rani, S., Lal, K., Fatima, M., Hardwick, T., Shirinfar, B., & Ahmed, N. (2023). Electrochemical hydrogen production: sustainable hydrogen economy. *Green Chemistry*, *25*(23), 9543–9573. https://doi.org/10.1039/d3gc02849f

Badakhsh, A., & Mothilal Bhagavathy, S. (2024). Caveats of green hydrogen for decarbonisation of heating in buildings. *Applied Energy*, *353*(PB), 122152. https://doi.org/10.1016/j.apenergy.2023.122152

Badreldin, A., Youssef, E., Djire, A., Abdala, A., & Abdel-Wahab, A. (2023). A critical look at alternative oxidation reactions for hydrogen production from water electrolysis. *Cell Reports Physical Science*, *4*(6), 101427. https://doi.org/10.1016/j.xcrp.2023.101427

Bai, J., Yin, D., Glarborg, P., Zhou, X., Lin, S., & Wu, H. (2023). Catalytic performance of sewage sludge char and ash in the decomposition of NH3. *Journal of the Energy Institute*, *107*(October 2022), 101197. https://doi.org/10.1016/j.joei.2023.101197

Balgehshiri, S. K. M., & Zohuri, B. (2023). The Impact of Energy Transition to Net-Zero Emissions on The World Economy and Global Strategies. *Journal of Economics & Management Research*, *4*(4), 1–7. https://doi.org/10.47363/jesmr/2023(4)185

Bo, S., Tang, F., Su, H., Zhang, X., Yu, F., Zhou, W., Liu, M., Cheng, W., Han, J., & Liu, Q. (2022). Valence-variable thiospinels for ampere-scale water electrolysis. *Catalysis Science & Technology*, *12*(22), 6875–6882. https://doi.org/10.1039/D2CY01371A

Brito, J., Pinto, F., Ferreira, A., Soria, M. A., & Madeira, L. M. (2023). Steam reforming of biomass gasification gas for hydrogen production: From thermodynamic analysis to experimental validation. *Fuel Processing Technology*, *250*(May). https://doi.org/10.1016/j.fuproc.2023.107859

Brzhezinskaya, M., Mishakov, I. V., Bauman, Y. I., Shubin, Y. V., Maksimova, T. A., Stoyanovskii, V. O., Yu. Gerasimov, E., & Vedyagin, A. A. (2022). One-pot functionalization of catalytically derived carbon nanostructures with heteroatoms for toxic-free environment. *Applied Surface Science*, *590*(March), 153055. https://doi.org/10.1016/j.apsusc.2022.153055

Cai, F., Guo, Y., Ibrahim, J. J., Zhang, J., & Sun, Y. (2021). A highly active and stable Pd/MoC catalyst for hydrogen production from methanol decomposition. *Applied Catalysis B: Environmental*, *299*(July), 120648. https://doi.org/10.1016/j.apcatb.2021.120648

Cechetto, V., Di Felice, L., & Gallucci, F. (2023). Advances and Perspectives of H2 Production from NH3 Decomposition in Membrane Reactors. In *Energy and Fuels* (Vol. 37, Issue 15, pp. 10775–10798). American Chemical Society. https://doi.org/10.1021/acs.energyfuels.3c00760

Cechetto, V., Di Felice, L., Gutierrez Martinez, R., Arratibel Plazaola, A., & Gallucci, F. (2022a). Ultra-pure hydrogen production via ammonia decomposition in a catalytic membrane reactor. *International Journal of Hydrogen Energy*, *47*(49), 21220–21230. https://doi.org/10.1016/j.ijhydene.2022.04.240

Cechetto, V., Di Felice, L., Gutierrez Martinez, R., Arratibel Plazaola, A., & Gallucci, F. (2022b). Ultra-pure hydrogen production via ammonia decomposition in a catalytic membrane reactor. *International Journal of Hydrogen Energy*, *47*(49), 21220–21230. https://doi.org/10.1016/j.ijhydene.2022.04.240

Cechetto, V., Di Felice, L., Medrano, J. A., Makhloufi, C., Zuniga, J., & Gallucci, F. (2021a). H2 production via ammonia decomposition in a catalytic membrane reactor. *Fuel Processing Technology*, *216*. https://doi.org/10.1016/j.fuproc.2021.106772

Cechetto, V., Di Felice, L., Medrano, J. A., Makhloufi, C., Zuniga, J., & Gallucci, F. (2021b). H2 production via ammonia decomposition in a catalytic membrane reactor. *Fuel Processing Technology*, *216*(January), 106772. https://doi.org/10.1016/j.fuproc.2021.106772

Cechetto, V., Struijk, C. L., Di Felice, L., de Leeuw den Bouter, A. W. N., & Gallucci, F. (2023). Adsorbents development for hydrogen cleanup from ammonia decomposition in a catalytic membrane reactor. *Chemical Engineering Journal*, *455*(September 2022), 140762. https://doi.org/10.1016/j.cej.2022.140762

Cerrillo, J. L., Morlanés, N., Kulkarni, S. R., Realpe, N., Ramírez, A., Katikaneni, S. P., Paglieri, S. N., Lee, K., Harale, A., Solami, B., Jamal, A., Mani Sarathy, S., Castaño, P., & Gascon, J. (2022a). High purity, self-sustained, pressurized hydrogen production from ammonia in a catalytic membrane reactor. *Chemical Engineering Journal*, *431*. https://doi.org/10.1016/j.cej.2021.134310

Cerrillo, J. L., Morlanés, N., Kulkarni, S. R., Realpe, N., Ramírez, A., Katikaneni, S. P., Paglieri, S. N., Lee, K., Harale, A., Solami, B., Jamal, A., Mani Sarathy, S., Castaño, P., & Gascon, J. (2022b). High purity, self-sustained, pressurized hydrogen production from ammonia in a catalytic membrane reactor. *Chemical Engineering Journal*, *431*. https://doi.org/10.1016/j.cej.2021.134310

Charisiou, N. D., Italiano, C., Pino, L., Sebastian, V., Vita, A., & Goula, M. A. (2020). Hydrogen production via steam reforming of glycerol over Rh/γ-Al2O3 catalysts modified with CeO2, MgO or La2O3. *Renewable Energy*, *162*, 908–925. https://doi.org/10.1016/j.renene.2020.08.037

Chatterjee, T., & Thynell, S. T. (2019). Development of a reaction mechanism for liquid-phase decomposition of ammonia borane. *Thermochimica Acta*, *682*(September), 178427. https://doi.org/10.1016/j.tca.2019.178427

Chen, C., Wang, Z., Yu, Z., Han, X., He, Y., Zhu, Y., & Konnov, A. A. (2023). Experimental and kinetic modeling study of laminar burning velocity enhancement by ozone additive in NH3+O2+N2 and NH3+CH4/C2H6/C3H8+air flames. *Proceedings of the Combustion Institute*, *39*(4), 4237–4246. https://doi.org/10.1016/j.proci.2022.07.025

Chen, H., & Kyprianidis, K. (2024). Dynamic Modelling and Surrogate-based Optimization of Auto-thermal Reforming for Enhanced Hydrogen Production. *Computer Aided Chemical Engineering*, *53*, 1027–1032. https://doi.org/10.1016/B978-0-443-28824-1.50172-1

Chen, H., Sun, W., Hu, X., Wang, Q., Wu, T., An, S., Ding, C., Chen, C., Huang, L., & Wang, N. (2023). Additive WO2 promotes Ni - based catalyst for hydrogen production from auto-thermal reforming of acetic acid. *Fuel*, *339*(September 2022), 126914. https://doi.org/10.1016/j.fuel.2022.126914

Chen, H., Wang, C., Zheng, M., Liu, C., Li, W., Yang, Q., Zhou, S., & Feng, X. (2023). Reactive ball-milling synthesis of Co-Fe bimetallic catalyst for efficient hydrogenation of carbon dioxide to value-added hydrocarbons. *Journal of Energy Chemistry*, *84*, 210–218. https://doi.org/10.1016/j.jechem.2023.05.025

Chen, W. H., Biswas, P. P., Ong, H. C., Hoang, A. T., Nguyen, T. B., & Dong, C. Di. (2023). A critical and systematic review of sustainable hydrogen production from ethanol/bioethanol: Steam reforming, partial oxidation, and autothermal reforming. *Fuel*, *333*, 126526. https://doi.org/10.1016/J.FUEL.2022.126526

Chen, W. H., Chou, W. S., Chein, R. Y., Hoang, A. T., & Juan, J. C. (2024). Multiple-objective optimization on ammonia decomposition using membrane reactor. *International Journal of Hydrogen Energy*, *52*, 1002–1017. https://doi.org/10.1016/j.ijhydene.2023.05.081

Chen, Y. L., Juang, C. F., & Chen, Y. C. (2021). The effects of promoter cs loading on the hydrogen production from ammonia decomposition using ru/c catalyst in a fixed-bed reactor. *Catalysts*, *11*(3), 1–15. https://doi.org/10.3390/catal11030321

Cheng, G., Luo, E., Zhao, Y., Yang, Y., Chen, B., Cai, Y., Wang, X., & Dong, C. (2023). Analysis and prediction of green hydrogen production potential by photovoltaic-powered water electrolysis using machine learning in China. *Energy*, *284*, 129302. https://doi.org/10.1016/J.ENERGY.2023.129302

Cho, E. H., Koo, K. Y., Lee, H. W., Park, Y. K., Yoon, W. L., & Ko, C. H. (2017). Preparation of egg-shell-type Ni/Ru bimetal alumina pellet catalysts: Steam methane reforming for hydrogen production. *International Journal of Hydrogen Energy*, *42*(29), 18350–18357. https://doi.org/10.1016/j.ijhydene.2017.04.170

Dang, H. Van, Wang, Y. H., & Wu, J. C. S. (2021). Z-scheme photocatalyst Pt/GaP-TiO2-SiO2:Rh for the separated H2 evolution from photocatalytic seawater splitting. *Applied Catalysis B: Environmental*, *296*(February). https://doi.org/10.1016/j.apcatb.2021.120339

Daturi, M., Avila, P., Serrano-lotina, A., Cruz, K., & Ba, M. A. (2023). *Applied Surface Science Bimetallic MnO 2 -supported catalysts for selective reduction of NO with NH 3 . Operando IR studies*. *610*(September 2022). https://doi.org/10.1016/j.apsusc.2022.155550

Di Carlo, A., Dell'Era, A., & Del Prete, Z. (2011). 3D simulation of hydrogen production by ammonia decomposition in a catalytic membrane reactor. *International Journal of Hydrogen Energy*, *36*(18), 11815–11824. https://doi.org/10.1016/j.ijhydene.2011.06.029

Di Marcoberardino, G., Binotti, M., Manzolini, G., Viviente, J. L., Arratibel, A., Roses, L., & Gallucci, F. (2017a). Achievements of European projects on membrane

reactor for hydrogen production. *Journal of Cleaner Production*, *161*, 1442–1450. https://doi.org/10.1016/j.jclepro.2017.05.122

Di Marcoberardino, G., Binotti, M., Manzolini, G., Viviente, J. L., Arratibel, A., Roses, L., & Gallucci, F. (2017b). Achievements of European projects on membrane reactor for hydrogen production. *Journal of Cleaner Production*, *161*(June 2017), 1442–1450. https://doi.org/10.1016/j.jclepro.2017.05.122

Do, T. N., Kwon, H., Park, M., Kim, C., Kim, Y. T., & Kim, J. (2023). Carbon-neutral hydrogen production from natural gas via electrified steam reforming: Techno-economic-environmental perspective. *Energy Conversion and Management*, *279*, 116758. https://doi.org/10.1016/J.ENCONMAN.2023.116758

Dolganov, A. V., Yudina, A. D., Boykova, T. V., Klimaeva, L. A., Okina, E. V., & Kostryukov, S. G. (2024). The electrocatalytic hydrogen evolution reaction in the presence of a metal-free organic catalyst based on 1,10-phenanthroline: the first example of a reaction proceeding by an intramolecular mechanism. *Catalysis Science & Technology*, *14*(10), 2951–2958. https://doi.org/10.1039/D4CY00182F

Duan, X., Ji, J., Qian, G., Fan, C., Zhu, Y., Zhou, X., Chen, D., & Yuan, W. (2012a). Ammonia decomposition on Fe(1 1 0), Co(1 1 1) and Ni(1 1 1) surfaces: A density functional theory study. *Journal of Molecular Catalysis A: Chemical*, *357*, 81–86. https://doi.org/10.1016/j.molcata.2012.01.023

Duan, X., Ji, J., Qian, G., Fan, C., Zhu, Y., Zhou, X., Chen, D., & Yuan, W. (2012b). Ammonia decomposition on Fe(1 1 0), Co(1 1 1) and Ni(1 1 1) surfaces: A density functional theory study. *Journal of Molecular Catalysis A: Chemical*, *357*, 81–86. https://doi.org/10.1016/j.molcata.2012.01.023

Dudek, R. B., Tian, X., Blivin, M., Neal, L. M., Zhao, H., & Li, F. (2019). Perovskite oxides for redox oxidative cracking of n-hexane under a cyclic redox scheme. *Applied Catalysis B: Environmental*, *246*(November 2018), 30–40. https://doi.org/10.1016/j.apcatb.2019.01.048

El ouardi, M., El Idrissi, A., Arab, M., Zbair, M., Haspel, H., Saadi, M., & Ait Ahsaine, H. (2024). Review of photoelectrochemical water splitting: From quantitative approaches to effect of sacrificial agents, oxygen vacancies, thermal and magnetic field on (photo)electrolysis. *International Journal of Hydrogen Energy*, *51*, 1044–1067. https://doi.org/10.1016/J.IJHYDENE.2023.09.111

El-Mekaoui, A., Cetina-Quiñones, A. J., Casillas-Reyes, A., San-Pedro, L., Tapia, J., Canto-Esquivel, J. C., & Bassam, A. (2024). Empowering indigenous groups: Unveiling a new approach to adaptive-participative sustainable energy in solar pumping projects via a Mayan community in Central America. *Energy Research & Social Science*, *114*, 103589. https://doi.org/10.1016/J.ERSS.2024.103589

El-Shafie, M. (2023). Hydrogen production by water electrolysis technologies: A review. *Results in Engineering*, *20*(August), 101426. https://doi.org/10.1016/j.rineng.2023.101426

El-Shafie, M., & Kambara, S. (2024). Comprehensive analysis of hydrogen production from various water types using plasma: Water vapour decomposition in the presence of ammonia and novel reaction kinetics analysis. *International Journal of Hydrogen Energy*, *52*, 14–30. https://doi.org/10.1016/j.ijhydene.2022.11.209

Emam, A. S., Hamdan, M. O., Abu-Nabah, B. A., & Elnajjar, E. (2024a). A review on recent trends, challenges, and innovations in alkaline water electrolysis. In *International Journal of Hydrogen Energy* (Vol. 64, pp. 599–625). Elsevier Ltd. https://doi.org/10.1016/j.ijhydene.2024.03.238

Emam, A. S., Hamdan, M. O., Abu-Nabah, B. A., & Elnajjar, E. (2024b). A review on recent trends, challenges, and innovations in alkaline water electrolysis. *International Journal of Hydrogen Energy*, *64*(March), 599–625. https://doi.org/10.1016/j.ijhydene.2024.03.238

Emam, A. S., Hamdan, M. O., Abu-Nabah, B. A., & Elnajjar, E. (2024c). A review on recent trends, challenges, and innovations in alkaline water electrolysis. *International Journal of Hydrogen Energy*, *64*(March), 599–625. https://doi.org/10.1016/j.ijhydene.2024.03.238

Emam, A. S., Hamdan, M. O., Abu-Nabah, B. A., & Elnajjar, E. (2024d). A review on recent trends, challenges, and innovations in alkaline water electrolysis. *International Journal of Hydrogen Energy*, *64*(February), 599–625. https://doi.org/10.1016/j.ijhydene.2024.03.238

Evro, S., Oni, B. A., & Tomomewo, O. S. (2024). Carbon neutrality and hydrogen energy systems. *International Journal of Hydrogen Energy*, *78*, 1449–1467. https://doi.org/10.1016/J.IJHYDENE.2024.06.407

Faheem, H. H., Tanveer, H. U., Abbas, S. Z., & Maqbool, F. (2021a). Comparative study of conventional steam-methane-reforming (SMR) and auto-thermal-reforming (ATR) with their hybrid sorption enhanced (SE-SMR & SE-ATR)

and environmentally benign process models for the hydrogen production. *Fuel*, *297*. https://doi.org/10.1016/j.fuel.2021.120769

Faheem, H. H., Tanveer, H. U., Abbas, S. Z., & Maqbool, F. (2021b). Comparative study of conventional steam-methane-reforming (SMR) and auto-thermal-reforming (ATR) with their hybrid sorption enhanced (SE-SMR & SE-ATR) and environmentally benign process models for the hydrogen production. *Fuel*, *297*, 120769. https://doi.org/10.1016/J.FUEL.2021.120769

Falascino, E., Joshi, R. K., Kumar, S., Jawdekar, T., Kudva, I. K., Shinde, S. G., Cheng, Z., Tong, A., & Fan, L. S. (2024a). Enabling plastic waste gasification by autothermal chemical looping with > 90 % syngas purity for versatile feedstock handling. *Applications in Energy and Combustion Science*, *19*, 100270. https://doi.org/10.1016/J.JAECS.2024.100270

Falascino, E., Joshi, R. K., Kumar, S., Jawdekar, T., Kudva, I. K., Shinde, S. G., Cheng, Z., Tong, A., & Fan, L. S. (2024b). Enabling plastic waste gasification by autothermal chemical looping with > 90 % syngas purity for versatile feedstock handling. *Applications in Energy and Combustion Science*, *19*, 100270. https://doi.org/10.1016/J.JAECS.2024.100270

Fang, H., Liu, D., Luo, Y., Zhou, Y., Liang, S., Wang, X., Lin, B., & Jiang, L. (2022). Challenges and Opportunities of Ru-Based Catalysts toward the Synthesis and Utilization of Ammonia. *ACS Catalysis*, *12*(7), 3938–3954. https://doi.org/10.1021/acscatal.2c00090

Feng, P., Lee, M., Wang, D., & Suzuki, Y. (2023). Ammonia thermal decomposition on quartz and stainless steel walls. *International Journal of Hydrogen Energy*, *48*(75), 29209–29219. https://doi.org/10.1016/j.ijhydene.2023.04.106

Florez, J., AlAbbad, M., Vazquez-Sanchez, H., Morales, M. G., & Sarathy, S. M. (2024). Optimizing islanded green ammonia and hydrogen production and export from Saudi Arabia. *International Journal of Hydrogen Energy*, *56*(November 2023), 959–972. https://doi.org/10.1016/j.ijhydene.2023.12.075

Fu, E., Qiu, Y., Lu, H., Wang, S., Liu, L., Feng, H., Yang, Y., Wu, Z., Xie, Y., Gong, F., & Xiao, R. (2021a). Enhanced NH3 decomposition for H2 production over bimetallic M(M=Co, Fe, Cu)Ni/Al2O3. *Fuel Processing Technology*, *221*. https://doi.org/10.1016/j.fuproc.2021.106945

Fu, E., Qiu, Y., Lu, H., Wang, S., Liu, L., Feng, H., Yang, Y., Wu, Z., Xie, Y., Gong, F., & Xiao, R. (2021b). Enhanced NH3 decomposition for H2 production over

bimetallic M(M=Co, Fe, Cu)Ni/Al2O3. *Fuel Processing Technology*, *221*. https://doi.org/10.1016/j.fuproc.2021.106945

Fu, E., Qiu, Y., Lu, H., Wang, S., Liu, L., Feng, H., Yang, Y., Wu, Z., Xie, Y., Gong, F., & Xiao, R. (2021c). Enhanced NH3 decomposition for H2 production over bimetallic M(M=Co, Fe, Cu)Ni/Al2O3. *Fuel Processing Technology*, *221*(March), 106945. https://doi.org/10.1016/j.fuproc.2021.106945

Fu, W., Guan, X., Huang, Z., Liu, M., & Guo, L. (2019a). Efficient photocatalytic overall water splitting over a core-shell GaInZnON@GaInON homojunction. *Applied Catalysis B: Environmental*, *255*(April), 117741. https://doi.org/10.1016/j.apcatb.2019.05.043

Fu, W., Guan, X., Huang, Z., Liu, M., & Guo, L. (2019b). Efficient photocatalytic overall water splitting over a core-shell GaInZnON@GaInON homojunction. *Applied Catalysis B: Environmental*, *255*(April), 117741. https://doi.org/10.1016/j.apcatb.2019.05.043

Gallenberger, J., Moreno Fernández, H., Alkemper, A., Li, M., Tian, C., Kaiser, B., & Hofmann, J. P. (2023). Stability and decomposition pathways of the NiOOH OER active phase of NiOx electrocatalysts at open circuit potential traced by ex situ and in situ spectroscopies. *Catalysis Science & Technology*, *13*(16), 4693–4700. https://doi.org/10.1039/D3CY00674C

Gan, M., Liao, F., Chen, Q., Pang, F., Xu, Y., Su, Y., & Huang, L. (2024). Y2Ti2O7 pyrochlore supported nickel-based catalysts for hydrogen production by auto-thermal reforming of acetic acid. *Materials Science and Engineering: B*, *302*(December 2023), 117264. https://doi.org/10.1016/j.mseb.2024.117264

Ganguli, A., & Bhatt, V. (2023). Hydrogen production using advanced reactors by steam methane reforming: A review. *Frontiers in Thermal Engineering*, *3*(April), 1–15. https://doi.org/10.3389/fther.2023.1143987

Gao, H., Huang, C., Han, Y., Wang, D., Tao, W., Li, B., Xia, H., Li, F., Xu, Z., & Wang, Y. (2025). MOFs-derived magnetic CoFe bimetallic alloys catalyst radical and non-radical peroxydisulfate activation for efficient rapid organic dye degradation. *Journal of Water Process Engineering*, *70*. https://doi.org/10.1016/j.jwpe.2025.107128

García-Hernández, A. E., Segovia-Hernández, J. G., Sánchez-Ramírez, E., Zarazúa, G. C., Araujo, I. F. H., & Quiroz-Ramírez, J. J. (2024). Sustainable aviation fuel from Butanol: A Study in optimizing Economic and Environmental impact

through process intensification. *Chemical Engineering and Processing - Process Intensification*, *200*, 109769. https://doi.org/10.1016/J.CEP.2024.109769

Ghannadi, M., & Dincer, I. (2024). A new system for hydrogen and methane production with post-combustion amine-based carbon capturing option for better sustainability. *Energy Conversion and Management*, *301*(September 2023), 118026. https://doi.org/10.1016/j.enconman.2023.118026

Godfrey, S., Hamzat, A. K., Whidborne, J., Kuang, B., & Jenkins, K. W. (2024). Integration of renewable energy sources in tandem with electrolysis: A technology review for green hydrogen production. *International Journal of Hydrogen Energy*, *xxxx*. https://doi.org/10.1016/J.IJHYDENE.2024.06.342

Gönen, S. Ö., Erol Taygun, M., & Küçükbayrak, S. (2016a). Evaluation of the factors influencing the resultant diameter of the electrospun gelatin/sodium alginate nanofibers via Box-Behnken design. *Materials Science and Engineering C*, *58*, 709–723. https://doi.org/10.1016/j.msec.2015.09.024

Gönen, S. Ö., Erol Taygun, M., & Küçükbayrak, S. (2016b). Evaluation of the factors influencing the resultant diameter of the electrospun gelatin/sodium alginate nanofibers via Box-Behnken design. *Materials Science and Engineering C*, *58*, 709–723. https://doi.org/10.1016/j.msec.2015.09.024

Gonzalez, S., Atia, H., Rockstroh, N., Lund, H., Bartling, S., Wohlrab, S., & Armbruster, U. (2024). Impact of chelating agents on precursor formation and efficiency of Ni/MgO-Al2O3 catalysts in dry reforming of methane. *Catalysis Today*, *429*. https://doi.org/10.1016/j.cattod.2023.114475

González-Tejero, M., Villachica-Llamosas, J. G., Ruiz-Aguirre, A., & Colón, G. (2023a). High-Performance Photocatalytic H2 Production Using a Binary Cu/TiO2/SrTiO3 Heterojunction. *ACS Applied Energy Materials*, *6*(7), 4007–4015. https://doi.org/10.1021/acsaem.3c00219

González-Tejero, M., Villachica-Llamosas, J. G., Ruiz-Aguirre, A., & Colón, G. (2023b). High-Performance Photocatalytic H2 Production Using a Binary Cu/TiO2/SrTiO3 Heterojunction. *ACS Applied Energy Materials*, *6*(7), 4007–4015. https://doi.org/10.1021/acsaem.3c00219

Grubert, E. (2023). Water consumption from electrolytic hydrogen in a carbon-neutral US energy system. *Cleaner Production Letters*, *4*(October 2022), 100037. https://doi.org/10.1016/j.clpl.2023.100037

Gu, Y., Ma, Y., Long, Z., Zhao, S., Wang, Y., & Zhang, W. (2021). One-pot synthesis of supported Ni@Al2O3 catalysts with uniform small-sized Ni for hydrogen generation via ammonia decomposition. *International Journal of Hydrogen Energy*, *46*(5), 4045–4054. https://doi.org/10.1016/j.ijhydene.2020.11.003

Gupta, S., Fernandes, R., Patel, R., Spreitzer, M., & Patel, N. (2023). A review of cobalt-based catalysts for sustainable energy and environmental applications. *Applied Catalysis A: General*, *661*(May). https://doi.org/10.1016/j.apcata.2023.119254

Hamid, A., Deris, R. R. R., Shaffee, S. N. A., Hin, T. Y. Y., Ametefe, D. S., & Ibrahim, M. L. (2025). A systematic review on environmentally friendly hydrogen production methods: comparative analysis of reactor technologies for optimal efficiency and sustainability. In *Sustainable Chemistry for Climate Action* (Vol. 6). Elsevier B.V. https://doi.org/10.1016/j.scca.2025.100088

Hassan, Q., Sameen, A. Z., Salman, H. M., & Jaszczur, M. (2023). Large-scale green hydrogen production via alkaline water electrolysis using solar and wind energy. *International Journal of Hydrogen Energy*, *48*(88), 34299–34315. https://doi.org/10.1016/j.ijhydene.2023.05.126

He, H., Jiang, H., Yang, F., Liu, J., Zhang, W., Jin, M., & Li, Z. (2023a). Bimetallic NixCo10-x/CeO2 as highly active catalysts to enhance mid-temperature ammonia decomposition: Kinetics and synergies. *International Journal of Hydrogen Energy*, *48*(13), 5030–5041. https://doi.org/10.1016/j.ijhydene.2022.10.255

He, H., Jiang, H., Yang, F., Liu, J., Zhang, W., Jin, M., & Li, Z. (2023b). Bimetallic NixCo10-x/CeO2 as highly active catalysts to enhance mid-temperature ammonia decomposition: Kinetics and synergies. *International Journal of Hydrogen Energy*, *48*(13), 5030–5041. https://doi.org/10.1016/j.ijhydene.2022.10.255

Hebish, A. A., Zulkifli, N. W. M., Julkapli, N. M., & Patah, M. F. A. (2024). The impact of operating conditions on H2-free catalytic deoxygenation of triglycerides for bio-jet fuel synthesis: A step towards sustainable aviation. *Applied Catalysis O: Open*, 206926. https://doi.org/10.1016/j.apcato.2024.206926

Hoseinpour, M., Karami, R., Rasul, M., Aghaei, J., Hassan, N., Khan, M. M. K., & Trabelsi, M. A. (2024a). Green Hydrogen as a Sustainable Future Energy:

Technologies and Challenges. *Reference Module in Earth Systems and Environmental Sciences*. https://doi.org/10.1016/B978-0-323-93940-9.00277-2

Hoseinpour, M., Karami, R., Rasul, M., Aghaei, J., Hassan, N., Khan, M. M. K., & Trabelsi, M. A. (2024b). Green Hydrogen as a Sustainable Future Energy: Technologies and Challenges. *Reference Module in Earth Systems and Environmental Sciences*. https://doi.org/10.1016/B978-0-323-93940-9.00277-2

Hossein Ali, Y. R., & Shin, D. (2022). Green Hydrogen Production Technologies from Ammonia Cracking. *Energies*, *15*(21). https://doi.org/10.3390/en15218246

Hu, X., Yang, J., Sun, W., Wang, N., An, S., Wang, Q., Zhang, Y., Xie, X., & Huang, L. (2020). Y-Zr-O solid solution supported Ni-based catalysts for hydrogen production via auto-thermal reforming of acetic acid. *Applied Catalysis B: Environmental*, *278*(June), 119264. https://doi.org/10.1016/j.apcatb.2020.119264

Hussain, M., Ali, O., Raza, N., Zabiri, H., Ahmed, A., & Ali, I. (2023). Recent advances in dynamic modeling and control studies of biomass gasification for production of hydrogen rich syngas. *RSC Advances*, *13*(34), 23796–23811. https://doi.org/10.1039/D3RA01219K

Ishaq, H., & Crawford, C. (2023). CO2-based alternative fuel production to support development of CO2 capture, utilization and storage. *Fuel*, *331*. https://doi.org/10.1016/j.fuel.2022.125684

Itoh, N., Kikuchi, Y., Furusawa, T., & Sato, T. (2021). Tube-wall catalytic membrane reactor for hydrogen production by low-temperature ammonia decomposition. *International Journal of Hydrogen Energy*, *46*(38), 20257–20265. https://doi.org/10.1016/j.ijhydene.2020.03.162

Jawad, A. H., Deris, R. R. R., Agha, H. M., Hapiz, A., Wu, R., & ALOthman, Z. A. (2025). Olive (Olea europaea) stone powder as a sustainable biosorbent for methyl violet 2B dye removal: multivariable optimization with desirability functions. *Biomass Conversion and Biorefinery*. https://doi.org/10.1007/s13399-024-06480-7

Jeje, S. O., Marazani, T., Obiko, J. O., & Shongwe, M. B. (2024a). Advancing the hydrogen production economy: A comprehensive review of technologies, sustainability, and future prospects. *International Journal of Hydrogen Energy*, *78*(June), 642–661. https://doi.org/10.1016/j.ijhydene.2024.06.344

Jeje, S. O., Marazani, T., Obiko, J. O., & Shongwe, M. B. (2024b). Advancing the hydrogen production economy: A comprehensive review of technologies, sustainability, and future prospects. *International Journal of Hydrogen Energy*, *78*(June), 642–661. https://doi.org/10.1016/j.ijhydene.2024.06.344

Jia, X., Hu, X., Wang, Q., Chen, B., Xie, X., & Huang, L. (2022). Auto-thermal reforming of acetic acid for hydrogen production by ZnxNiyCrOm±δ catalysts: Effect of Cr promoted Ni-Zn intermetallic compound. *Chinese Journal of Chemical Engineering*, *43*, 216–221. https://doi.org/10.1016/J.CJCHE.2021.04.017

Jiang, B., Ning, H., Xie, K., Wang, Z., & Zuo, S. (2024). Sulfur-tolerant mechanism in catalytic combustion of toluene over Co/5Mg-γ-Al2O3 catalyst: Dual functions of MgO. *Applied Catalysis A: General*, *670*. https://doi.org/10.1016/j.apcata.2023.119554

Jolaoso, L. A., Zaman, S. F., Podila, S., Driss, H., Al-Zahrani, A. A., Daous, M. A., & Petrov, L. (2018). Ammonia decomposition over citric acid induced γ-Mo2N and Co3Mo3N catalysts. *International Journal of Hydrogen Energy*, *43*(10), 4839–4844. https://doi.org/10.1016/j.ijhydene.2018.01.092

Joseph Sekhar, S., Samuel, M. S., Glivin, G., Le, T. G., & Mathimani, T. (2024). Production and utilization of green ammonia for decarbonizing the energy sector with a discrete focus on Sustainable Development Goals and environmental impact and technical hurdles. *Fuel*, *360*(October 2023). https://doi.org/10.1016/j.fuel.2023.130626

Joshi, N. C., Sinha, S., Bhatnagar, P., Nath, Y., Negi, B., Kumar, V., & Gururani, P. (2024). A concise review on waste biomass valorization through thermochemical conversion. *Current Research in Microbial Sciences*, *6*, 100237. https://doi.org/10.1016/J.CRMICR.2024.100237

Jung, S. C., & Chung, K. H. (2024). Enhanced hydrogen production through cracking of ammonia water using liquid plasma on titanate-based perovskite catalysts. *Energy Conversion and Management*, *311*. https://doi.org/10.1016/j.enconman.2024.118509

Jung, S., & Chung, K. (2024). Enhanced hydrogen production through cracking of ammonia water using liquid plasma on titanate-based perovskite catalysts. *Energy Conversion and Management*, *311*(April), 118509. https://doi.org/10.1016/j.enconman.2024.118509

Kabatas, M. A. B. (2023). A Comprehensive Review on Electrocatalytic Applications of 2D Metallenes. 1–26.

Kalinichenko, D., Wodrich, L., Lee, A. J. H., Kozlowski, T., & Brooks, C. S. (2024a). Analysis of nuclear microreactor efficacy with hydrogen production methods. *Progress in Nuclear Energy*, *168*(December 2023), 104994. https://doi.org/10.1016/j.pnucene.2023.104994

Kalinichenko, D., Wodrich, L., Lee, A. J. H., Kozlowski, T., & Brooks, C. S. (2024b). Analysis of nuclear microreactor efficacy with hydrogen production methods. *Progress in Nuclear Energy*, *168*(December 2023), 104994. https://doi.org/10.1016/j.pnucene.2023.104994

Kanaan, R., Affonso Nóbrega, P. H., Achard, P., & Beauger, C. (2023). Economical assessment comparison for hydrogen reconversion from ammonia using thermal decomposition and electrolysis. *Renewable and Sustainable Energy Reviews*, *188*(August). https://doi.org/10.1016/j.rser.2023.113784

Karka, S., & Kamesh, R. (2024). Data analysis and machine learning aided integrated catalyst activity and process modelling for selective H2 production from biomass gasification. *Biomass and Bioenergy*, *187*, 107291. https://doi.org/10.1016/J.BIOMBIOE.2024.107291

Karthik, P. E., Sangaletti, L., Ferroni, M., & Alessandri, I. (2024a). Investigation of electrocatalytic oxygen evolution reaction (OER) selectivity against methanol oxidation on stainless steel. *Catalysis Science & Technology*, *14*(8), 2268–2274. https://doi.org/10.1039/D4CY00030G

Karthik, P. E., Sangaletti, L., Ferroni, M., & Alessandri, I. (2024b). Investigation of electrocatalytic oxygen evolution reaction (OER) selectivity against methanol oxidation on stainless steel. *Catalysis Science & Technology*, *14*(8), 2268–2274. https://doi.org/10.1039/D4CY00030G

Kassi, A. H., & Al-Hattab, T. A. (2024a). A CFD model of natural gas steam reforming in a catalytic membrane reactor: Effect of various operating parameters on the performance of CMR. *International Journal of Hydrogen Energy*, *56*(December 2023), 780–796. https://doi.org/10.1016/j.ijhydene.2023.12.156

Kassi, A. H., & Al-Hattab, T. A. (2024b). A CFD model of natural gas steam reforming in a catalytic membrane reactor: Effect of various operating parameters on the performance of CMR. *International Journal of Hydrogen Energy*, *56*(December 2023), 780–796. https://doi.org/10.1016/j.ijhydene.2023.12.156

Kerschbaumer, A., Wielend, D., Leeb, E., Schimanofsky, C., Kleinbruckner, N., Neugebauer, H., Irimia-Vladu, M., & Sariciftci, N. S. (2023). How to use a rotating ring-disc electrode (RRDE) subtraction method to investigate the electrocatalytic oxygen reduction reaction? *Catalysis Science & Technology*, *13*(3), 834–843. https://doi.org/10.1039/D2CY01744J

Khan, W. U., Al Shoaibi, A., Chandrasekar, S., & Hossain, M. M. (2023). Synthesis of COx-free hydrogen via natural gas decomposition over titanium dioxide-supported bimetallic catalysts. *International Journal of Hydrogen Energy*, *48*(80), 31224–31233. https://doi.org/10.1016/j.ijhydene.2023.04.225

Khosroshahi, N., Ardakan, N. G., Azaddehghan, P., & Safarifard, V. (2024). Synergy in action: MOF-derived CoFeO3/Ce-MOF nanocomposites as piezo-photocatalysts for sustainable chromium reduction and nitrogen fixation. *Journal of Environmental Chemical Engineering*, *12*(6). https://doi.org/10.1016/j.jece.2024.114277

Kim, D., Choi, S., Jeong, S., Bae, M., Katikaneni, S. P., Bae, J., Heo, S., & Lee, J. H. (2021a). Kinetic modeling of diesel autothermal reforming for fuel cell auxiliary power units. *Chemical Engineering Journal*, *424*(May), 130564. https://doi.org/10.1016/j.cej.2021.130564

Kim, D., Choi, S., Jeong, S., Bae, M., Katikaneni, S. P., Bae, J., Heo, S., & Lee, J. H. (2021b). Kinetic modeling of diesel autothermal reforming for fuel cell auxiliary power units. *Chemical Engineering Journal*, *424*(May), 130564. https://doi.org/10.1016/j.cej.2021.130564

Kim, T. W., Lee, E. H., Byun, S., Seo, D. W., Hwang, H. J., Yoon, H. C., Kim, H., & Ryi, S. K. (2022). Highly selective Pd composite membrane on porous metal support for high-purity hydrogen production through effective ammonia decomposition. *Energy*, *260*. https://doi.org/10.1016/j.energy.2022.125209

Koo, K. Y., Im, H. B., Song, D., & Jung, U. (2023). Ammonia decomposition over Ru-coated metal-structured catalysts for COx-free hydrogen production. *International Journal of Hydrogen Energy*, *xxxx*. https://doi.org/10.1016/j.ijhydene.2023.08.004

Koo, K. Y., Im, H. B., Song, D., & Jung, U. (2024a). Ammonia decomposition over Ru-coated metal-structured catalysts for COx-free hydrogen production. *International Journal of Hydrogen Energy*, *52*, 534–545. https://doi.org/10.1016/j.ijhydene.2023.08.004

Koo, K. Y., Im, H. B., Song, D., & Jung, U. (2024b). Ammonia decomposition over Ru-coated metal-structured catalysts for COx-free hydrogen production. *International Journal of Hydrogen Energy*, *52*, 534–545. https://doi.org/10.1016/j.ijhydene.2023.08.004

Krishnan, A., Nighojkar, A., & Kandasubramanian, B. (2023a). Emerging towards zero carbon footprint via carbon dioxide capturing and sequestration. *Carbon Capture Science and Technology*, *9*(July), 100137. https://doi.org/10.1016/j.ccst.2023.100137

Krishnan, A., Nighojkar, A., & Kandasubramanian, B. (2023b). Emerging towards zero carbon footprint via carbon dioxide capturing and sequestration. *Carbon Capture Science and Technology*, *9*(July), 100137. https://doi.org/10.1016/j.ccst.2023.100137

Kuttin, K. W., Leghari, A., Yu, H., Xia, Z., Ding, L., & Yu, G. (2024a). Carbon dioxide-steam reforming gasification of carbonized biomass pellet for high syngas yield and TAR reduction through CFD modeling. *Chemical Engineering Science*, *287*(December 2023), 119716. https://doi.org/10.1016/j.ces.2024.119716

Kuttin, K. W., Leghari, A., Yu, H., Xia, Z., Ding, L., & Yu, G. (2024b). Carbon dioxide-steam reforming gasification of carbonized biomass pellet for high syngas yield and TAR reduction through CFD modeling. *Chemical Engineering Science*, *287*(December 2023), 119716. https://doi.org/10.1016/j.ces.2024.119716

Lalman, C., Karunathilake, H., & Ruparathna, R. (2023). To Dispose or to Reuse? Analyzing the Life Cycle Impacts and Costs of Disposal, Sterilization, and Reuse of Electrophysiological Catheters. *Sustainability (Switzerland)*, *15*(6). https://doi.org/10.3390/su15065363

Le, P. A., Trung, V. D., Nguyen, P. L., Bac Phung, T. V., Natsuki, J., & Natsuki, T. (2023). The current status of hydrogen energy: an overview. *RSC Advances*, *13*(40), 28262–28287. https://doi.org/10.1039/d3ra05158g

Lee, J. E., Lee, J., Jeong, H., Park, Y. K., & Kim, B. S. (2023). Catalytic ammonia decomposition to produce hydrogen: A mini-review. *Chemical Engineering Journal*, *475*(September), 146108. https://doi.org/10.1016/j.cej.2023.146108

Lee, S., Kim, H. S., Park, J., Kang, B. M., Cho, C. H., Lim, H., & Won, W. (2021). Scenario-based techno-economic analysis of steam methane reforming process for hydrogen production. *Applied Sciences (Switzerland)*, *11*(13). https://doi.org/10.3390/app11136021

Lee, S. U., Le, T. A., Kim, Y., Lee, Y. J., Kim, J. R., Kim, T. W., Jeong, K. E., & Chae, H. J. (2024a). CeO2-conjugated CoFe layered double oxides as efficient non-noble metal catalysts for NH3-decomposition enabling carbon-free hydrogen production. *Chemical Engineering Journal*, *500*. https://doi.org/10.1016/j.cej.2024.156986

Lee, S. U., Le, T. A., Kim, Y., Lee, Y. J., Kim, J. R., Kim, T. W., Jeong, K. E., & Chae, H. J. (2024b). CeO2-conjugated CoFe layered double oxides as efficient non-noble metal catalysts for NH3-decomposition enabling carbon-free hydrogen production. *Chemical Engineering Journal*, *500*. https://doi.org/10.1016/j.cej.2024.156986

Lee, S. U., Le, T. A., Kim, Y., Lee, Y. J., Kim, J. R., Kim, T. W., Jeong, K. E., & Chae, H. J. (2024c). CeO2-conjugated CoFe layered double oxides as efficient non-noble metal catalysts for NH3-decomposition enabling carbon-free hydrogen production. *Chemical Engineering Journal*, *500*. https://doi.org/10.1016/j.cej.2024.156986

Li, B., Hou, Y., Gao, J., Li, Y., Wang, B., Huang, Z., Wang, J., Chang, L., & Xie, K. (2024a). Rational amelioration of redox equilibrium by constructing hollow nanotube Co-Mn/TiO2 catalyst to boost simultaneous removal of NO and Hg0. *Applied Catalysis B: Environmental*, *341*(September 2023), 123353. https://doi.org/10.1016/j.apcatb.2023.123353

Li, C. C., Hsieh, C. H., & Lin, Y. C. (2022). Ni/SiO2 catalysts derived from carbothermal reduction of nickel phyllosilicate in the hydrogenation of levulinic acid to γ-valerolactone: The efficacy of nitrogen decoration. *Molecular Catalysis*, *523*(May 2021). https://doi.org/10.1016/j.mcat.2021.111720

Li, C., Guo, L., Chen, G., Fu, Y., Zhang, X., Zou, Y., Duan, J., & Wang, W. (2023). CoNi alloy catalyst supported on Zr-modified Y2O3 for ammonia decomposition to COx-free hydrogen. *Colloids and Surfaces A: Physicochemical and Engineering Aspects*, *671*(May), 131671. https://doi.org/10.1016/j.colsurfa.2023.131671

Li, G., Yu, X., Yin, F., Lei, Z., Zhang, H., & He, X. (2022). Production of hydrogen by ammonia decomposition over supported Co3O4 catalysts. *Catalysis Today*, *402*(February), 45–51. https://doi.org/10.1016/j.cattod.2022.02.020

Li, J. C., Xu, H., Zhou, K., & Li, J. Q. (2024a). A review on the research progress and application of compressed hydrogen in the marine hydrogen fuel cell power system. *Heliyon*, *10*(3), e25304. https://doi.org/10.1016/j.heliyon.2024.e25304

Li, J. C., Xu, H., Zhou, K., & Li, J. Q. (2024b). A review on the research progress and application of compressed hydrogen in the marine hydrogen fuel cell power system. *Heliyon*, *10*(3), e25304. https://doi.org/10.1016/j.heliyon.2024.e25304

Li, M., Saedy, S., Fu, S., Stellema, T., Kortlever, R., & van Ommen, J. R. (2024b). Enhancing the durability of Pt nanoparticles for water electrolysis using ultrathin SiO2 layers. *Catalysis Science and Technology*, *14*(5), 1328–1335. https://doi.org/10.1039/d3cy00996c

Li, Q., Zhao, Y., Liu, T., Luo, Z., Luo, K., & Wang, T. (2024c). Kinetic and optimization study of ultrasound-assisted biodiesel production from waste coconut scum oil using porous CoFe2O4@sulfonated graphene oxide magnetic nanocatalysts: CI engine approach. *Renewable Energy*, *236*. https://doi.org/10.1016/j.renene.2024.121457

Li, T., Zuo, J., Zhao, Z., Li, W., Zhang, K., Wang, Q., Du, H., Liu, H., Aili, E., & Ye, Y. (2025). Hydrogen production by ammonia decomposition: A strategy to enhance the activity and stability of metal catalysts. In *International Journal of Hydrogen Energy* (Vol. 97, pp. 1153–1167). Elsevier Ltd. https://doi.org/10.1016/j.ijhydene.2024.11.455

Li, X., Wang, Q., Wu, S., Hu, Z., & Bai, J. (2024d). Critical upstream technologies for hydrogen energy industry: Research progress on ammonia decomposition catalysts. *Sustainable Chemistry and Pharmacy*, *38*(February), 101492. https://doi.org/10.1016/j.scp.2024.101492

Li, X., Wang, Q., Wu, S., Hu, Z., & Bai, J. (2024e). Critical upstream technologies for hydrogen energy industry: Research progress on ammonia decomposition catalysts. *Sustainable Chemistry and Pharmacy*, *38*(February), 101492. https://doi.org/10.1016/j.scp.2024.101492

Li, Y., Wang, W., Cheng, M., Qian, Q., Zhu, Y., & Zhang, G. (2022). Environmentally benign general synthesis of nonconsecutive carbon-coated RuP2 porous microsheets as efficient bifunctional electrocatalysts under neutral conditions for energy-saving H2 production in hybrid water electrolysis. *Catalysis Science and Technology*, *12*(13), 4339–4349. https://doi.org/10.1039/d2cy00055e

Liu, F., Wang, F., Hao, X., Fan, Z., & Tan, J. (2024). Effects of foam cathode electrode structure on alkaline water electrolysis for hydrogen production. *Chemical Engineering Science*, *298*, 120307. https://doi.org/10.1016/J.CES.2024.120307

Liu, J., Ju, X., Tang, C., Liu, L., Li, H., & Chen, P. (2020). High performance stainless-steel supported Pd membranes with a finger-like and gap structure and its application in NH3 decomposition membrane reactor. *Chemical Engineering Journal*, *388*. https://doi.org/10.1016/j.cej.2020.124245

Liu, Y., Xu, M., Yang, Z., Ding, X., Zhu, M., & Han, Y. F. (2022). Syngas to olefins with low CO2 formation by tuning the structure of FeCx-MgO-Al2O3 catalysts. *Chemical Engineering Journal*, *450*. https://doi.org/10.1016/j.cej.2022.137167

Liu, Z. Y., Lai, J. W., Yang, G., Ren, B. P., Lv, Z. Y., Si, L. P., Zhang, H., & Liu, H. Y. (2022a). Electrocatalytic hydrogen production by CN– substituted cobalt triaryl corroles. *Catalysis Science & Technology*, *12*(16), 5125–5135. https://doi.org/10.1039/D2CY00606E

Liu, Z. Y., Lai, J. W., Yang, G., Ren, B. P., Lv, Z. Y., Si, L. P., Zhang, H., & Liu, H. Y. (2022b). Electrocatalytic hydrogen production by CN– substituted cobalt triaryl corroles. *Catalysis Science & Technology*, *12*(16), 5125–5135. https://doi.org/10.1039/D2CY00606E

Lodewyckx, S., Beasy, K., & Mattila, P. (2023). Pieces of a jigsaw: Opportunities and challenges in the nascent Australian hydrogen mobility market. *International Journal of Hydrogen Energy*, *48*(52), 19821–19833. https://doi.org/10.1016/j.ijhydene.2023.01.362

Lucentini, I., García Colli, G., Luzi, C. D., Serrano, I., Martínez, O. M., & Llorca, J. (2021). Catalytic ammonia decomposition over Ni-Ru supported on CeO2 for hydrogen production: Effect of metal loading and kinetic analysis. *Applied Catalysis B: Environmental*, *286*(January). https://doi.org/10.1016/j.apcatb.2021.119896

Lucentini, I., Garcia, X., Vendrell, X., & Llorca, J. (2021a). Review of the Decomposition of Ammonia to Generate Hydrogen. *Industrial and Engineering Chemistry Research*, *60*(51), 18560–18611. https://doi.org/10.1021/acs.iecr.1c00843

Lucentini, I., Garcia, X., Vendrell, X., & Llorca, J. (2021b). Review of the Decomposition of Ammonia to Generate Hydrogen. *Industrial and Engineering*

Chemistry Research, *60*(51), 18560–18611. https://doi.org/10.1021/acs.iecr.1c00843

Łuczak, J., & Lieder, M. (2023). Nickel-based catalysts for electrolytic decomposition of ammonia towards hydrogen production. *Advances in Colloid and Interface Science*, *319*(July). https://doi.org/10.1016/j.cis.2023.102963

Lundin, S., Fuerst, T., Ganley, J., Wolden, C., Way, D., Sean-Thomas B. Lundin, T. F. F., & Jason C. Ganley, Colin A. Wolden, J. D. W. (2016). Applications of hydrogen permeable membranes in ammonia synthesis and decomposition. *NH3 Fuel Conference*. https://nh3fuelassociation.org/wp-content/uploads/2016/09/sean-lundin-applications-of-hydrogen-permeable-membranes-in-ammonia-synthesis-nh3fa2016.pdf%0Ahttps://nh3fuelassociation.org/2016/08/22/hydrogen-permeable-membranes-in-ammonia-synthesis-and-decompo

Luo, Y., Shi, Y., Liao, S., Chen, C., Zhan, Y., Au, C. T., & Jiang, L. (2019). Coupling ammonia catalytic decomposition and electrochemical oxidation for solid oxide fuel cells: A model based on elementary reaction kinetics. *Journal of Power Sources*, *423*(March), 125–136. https://doi.org/10.1016/j.jpowsour.2019.03.064

Ma, Y., Wang, S., & Duan, X. (2023a). Recent advances in direct gas–solid-phase photocatalytic conversion of CO2 for porous photocatalysts under different CO2 atmospheres. *Chemical Engineering Journal*, *455*(October 2022), 140654. https://doi.org/10.1016/j.cej.2022.140654

Ma, Y., Wang, S., & Duan, X. (2023b). Recent advances in direct gas–solid-phase photocatalytic conversion of CO2 for porous photocatalysts under different CO2 atmospheres. *Chemical Engineering Journal*, *455*(October 2022), 140654. https://doi.org/10.1016/j.cej.2022.140654

Makwana, J., Dhass, A. D., Ramana, P. V., Sapariya, D., & Patel, D. (2023a). An analysis of waste/biomass gasification producing hydrogen-rich syngas: A review. *International Journal of Thermofluids*, *20*(October), 100492. https://doi.org/10.1016/j.ijft.2023.100492

Makwana, J., Dhass, A. D., Ramana, P. V., Sapariya, D., & Patel, D. (2023b). An analysis of waste/biomass gasification producing hydrogen-rich syngas: A review. *International Journal of Thermofluids*, *20*(October), 100492. https://doi.org/10.1016/j.ijft.2023.100492

Maleki, F., Bararzadeh Ledari, M., Fani, M., & kamelizadeh, D. (2024). Sustainable hydrogen supply chain development for low-carbon transportation in a fossil-based port region: A case study in a tourism hub. *International Journal of Hydrogen Energy*, *65*, 95–111. https://doi.org/10.1016/J.IJHYDENE.2024.03.362

Meng, C., Su, K., Li, Z., & Zhang, M. (2021). Dimethyl 2,5-furandicarboxylate synthesis from 2,5-furanodicarboxylic acid and dimethyl carbonate in presence of MgO-Al2O3 and tetrabutylammonium bromide. *Molecular Catalysis*, *510*. https://doi.org/10.1016/j.mcat.2021.111707

Meng, S., Li, S., Sun, S., Bogaerts, A., Liu, Y., & Yi, Y. (2024a). NH3 decomposition for H2 production by thermal and plasma catalysis using bimetallic catalysts. *Chemical Engineering Science*, *283*. https://doi.org/10.1016/j.ces.2023.119449

Meng, S., Li, S., Sun, S., Bogaerts, A., Liu, Y., & Yi, Y. (2024b). NH3 decomposition for H2 production by thermal and plasma catalysis using bimetallic catalysts. *Chemical Engineering Science*, *283*(October 2023), 119449. https://doi.org/10.1016/j.ces.2023.119449

Meng, S., Li, S., Sun, S., Bogaerts, A., Liu, Y., & Yi, Y. (2024c). NH3 decomposition for H2 production by thermal and plasma catalysis using bimetallic catalysts. *Chemical Engineering Science*, *283*(May 2023), 119449. https://doi.org/10.1016/j.ces.2023.119449

Mensah, A. T., Berne, F., Allard, S., Soreau, S., & Gallard, H. (2022). Kinetic modelling of the bromine-ammonia system: Formation and decomposition of bromamines. *Water Research*, *224*(September). https://doi.org/10.1016/j.watres.2022.119058

Miao, M., Sha, M., Cao, C., Lei, S., & Meng, Q. (2022). Theoretical study on Fe-M (M = Mo, Ni, Pt) bimetallic catalysts to promote ammonia decomposition. *Chemical Physics Letters*, *808*(September), 140134. https://doi.org/10.1016/j.cplett.2022.140134

Mohamad Nasir, A. A. S., Mohamad, N. A., Abd Malek, N. N., Raja Deris, R. R., Yaakob, M. K., & Ibrahim, M. L. (2026). Bimetallic M–Ni/AlNi3 (M= Co, Fe, Mo) on Al2O3 beads catalysts for ammonia cracking. *Journal of Physics and Chemistry of Solids*, *210*. https://doi.org/10.1016/j.jpcs.2025.113319

Molinari, R., Marino, T., & Argurio, P. (2014). Photocatalytic membrane reactors for hydrogen production from water. *International Journal of Hydrogen Energy*, *39*(14), 7247–7261. https://doi.org/10.1016/J.IJHYDENE.2014.02.174

Muhammed, N. S., Gbadamosi, A. O., Epelle, E. I., Abdulrasheed, A. A., Haq, B., Patil, S., Al-Shehri, D., & Kamal, M. S. (2023a). Hydrogen production, transportation, utilization, and storage: Recent advances towards sustainable energy. *Journal of Energy Storage*, *73*(PD), 109207. https://doi.org/10.1016/j.est.2023.109207

Muhammed, N. S., Gbadamosi, A. O., Epelle, E. I., Abdulrasheed, A. A., Haq, B., Patil, S., Al-Shehri, D., & Kamal, M. S. (2023b). Hydrogen production, transportation, utilization, and storage: Recent advances towards sustainable energy. *Journal of Energy Storage*, *73*(PD), 109207. https://doi.org/10.1016/j.est.2023.109207

Nadiri, S., Shu, B., Goldsmith, C. F., & Fernandes, R. (2023). Development of comprehensive kinetic models of ammonia/methanol ignition using Reaction Mechanism Generator (RMG). *Combustion and Flame*, *251*, 112710. https://doi.org/10.1016/j.combustflame.2023.112710

Nailwal, B. C., Chotalia, P., Salvi, J., Goswami, N., Muhmood, L., Adak, A. K., & Kar, S. (2024a). Ammonia decomposition for hydrogen production using packed bed catalytic membrane reactor. *International Journal of Hydrogen Energy*, *49*, 1272–1287. https://doi.org/10.1016/j.ijhydene.2023.09.229

Nailwal, B. C., Chotalia, P., Salvi, J., Goswami, N., Muhmood, L., Adak, A. K., & Kar, S. (2024b). Ammonia decomposition for hydrogen production using packed bed catalytic membrane reactor. *International Journal of Hydrogen Energy*, *49*, 1272–1287. https://doi.org/10.1016/j.ijhydene.2023.09.229

Nailwal, B. C., Chotalia, P., Salvi, J., Goswami, N., Muhmood, L., Adak, A. K., & Kar, S. (2024c). Ammonia decomposition for hydrogen production using packed bed catalytic membrane reactor. *International Journal of Hydrogen Energy*, *49*, 1272–1287. https://doi.org/10.1016/j.ijhydene.2023.09.229

Nailwal, B. C., Chotalia, P., Salvi, J., Goswami, N., Muhmood, L., Adak, A. K., & Kar, S. (2024d). Ammonia decomposition for hydrogen production using packed bed catalytic membrane reactor. *International Journal of Hydrogen Energy*, *49*, 1272–1287. https://doi.org/10.1016/j.ijhydene.2023.09.229

Nailwal, B. C., Chotalia, P., Salvi, J., Goswami, N., Muhmood, L., Adak, A. K., & Kar, S. (2024e). Ammonia decomposition for hydrogen production using packed bed catalytic membrane reactor. *International Journal of Hydrogen Energy*, *49*, 1272–1287. https://doi.org/10.1016/j.ijhydene.2023.09.229

Nemitallah, M. A., Alnazha, A. A., Ahmed, U., El-Adawy, M., & Habib, M. A. (2024a). Review on techno-economics of hydrogen production using current and emerging processes: Status and perspectives. *Results in Engineering*, *21*, 101890. https://doi.org/10.1016/J.RINENG.2024.101890

Nemitallah, M. A., Alnazha, A. A., Ahmed, U., El-Adawy, M., & Habib, M. A. (2024b). Review on techno-economics of hydrogen production using current and emerging processes: Status and perspectives. *Results in Engineering*, *21*, 101890. https://doi.org/10.1016/J.RINENG.2024.101890

Nemitallah, M. A., Alnazha, A. A., Ahmed, U., El-Adawy, M., & Habib, M. A. (2024c). Review on techno-economics of hydrogen production using current and emerging processes: Status and perspectives. *Results in Engineering*, *21*(November 2023), 101890. https://doi.org/10.1016/j.rineng.2024.101890

Ochoa, A., Arregi, A., Amutio, M., Gayubo, A. G., Olazar, M., Bilbao, J., & Castaño, P. (2018). Coking and sintering progress of a Ni supported catalyst in the steam reforming of biomass pyrolysis volatiles. *Applied Catalysis B: Environmental*, *233*(March), 289–300. https://doi.org/10.1016/j.apcatb.2018.04.002

Ogbonnaya, C., Abeykoon, C., Damo, U. M., & Turan, A. (2019). The current and emerging renewable energy technologies for power generation in Nigeria: A review. *Thermal Science and Engineering Progress*, *13*(April), 100390. https://doi.org/10.1016/j.tsep.2019.100390

Okolie, J. A., Epelle, E. I., Nanda, S., Castello, D., Dalai, A. K., & Kozinski, J. A. (2021). Modeling and process optimization of hydrothermal gasification for hydrogen production: A comprehensive review. *The Journal of Supercritical Fluids*, *173*, 105199. https://doi.org/10.1016/J.SUPFLU.2021.105199

Oliveira, M. L. M., Alves, C. M. A. C., Andrade, C. F., de Azevedo, D. C. S., Lobo, F. L., Fuerte, A., Ferreira-Aparicio, P., Caravaca, C., & Valenzuela, R. X. (2025). Recent Progress and Perspectives on Functional Materials and Technologies for Renewable Hydrogen Production. In *ACS Omega*. American Chemical Society. https://doi.org/10.1021/acsomega.4c10407

Oni, A. O., Giwa, T., Font-Palma, C., & Fadare, D. A. (2023). Comparative techno-economic and life cycle greenhouse gas assessment of ammonia production from thermal decomposition of methane and steam methane reforming technologies. *International Journal of Greenhouse Gas Control*, *123*(September 2022), 103819. https://doi.org/10.1016/j.ijggc.2022.103819

Osman, A. I., Mehta, N., Elgarahy, A. M., Hefny, M., Al-Hinai, A., Al-Muhtaseb, A. H., & Rooney, D. W. (2022). Hydrogen production, storage, utilisation and environmental impacts: a review. In *Environmental Chemistry Letters* (Vol. 20, Issue 1). Springer International Publishing. https://doi.org/10.1007/s10311-021-01322-8

Ouabi, H., Lajouad, R., Kissaoui, M., & El Magri, A. (2024a). Hydrogen production by water electrolysis driven by a photovoltaic source: A review. *E-Prime - Advances in Electrical Engineering, Electronics and Energy*, *8*, 100608. https://doi.org/10.1016/J.PRIME.2024.100608

Ouabi, H., Lajouad, R., Kissaoui, M., & El Magri, A. (2024b). Hydrogen production by water electrolysis driven by a photovoltaic source: A review. *E-Prime - Advances in Electrical Engineering, Electronics and Energy*, *8*, 100608. https://doi.org/10.1016/J.PRIME.2024.100608

Pattanayak, P., Singh, P., Bansal, N. K., Paul, M., Dixit, H., Porwal, S., Mishra, S., & Singh, T. (2022a). Recent progress in perovskite transition metal oxide-based photocatalyst and photoelectrode materials for solar-driven water splitting. *Journal of Environmental Chemical Engineering*, *10*(5), 108429. https://doi.org/10.1016/j.jece.2022.108429

Pattanayak, P., Singh, P., Bansal, N. K., Paul, M., Dixit, H., Porwal, S., Mishra, S., & Singh, T. (2022b). Recent progress in perovskite transition metal oxide-based photocatalyst and photoelectrode materials for solar-driven water splitting. *Journal of Environmental Chemical Engineering*, *10*(5), 108429. https://doi.org/10.1016/j.jece.2022.108429

Peters, S., Abdel-Mageed, A. M., & Wohlrab, S. (2023). Thermocatalytic Ammonia Decomposition – Status and Current Research Demands for a Carbon-Free Hydrogen Fuel Technology. *ChemCatChem*, *15*(2). https://doi.org/10.1002/cctc.202201185

pidjoe. (n.d.). The Future of Hydrogen.

Pourali, M., Esfahani, J. A., Jahangir, H., Farzaneh, A., & Kim, K. C. (2022). Ammonia decomposition in a porous catalytic reactor to enable hydrogen storage: Numerical simulation, machine learning, and response surface methodology. *Journal of Energy Storage*, *55*(PD), 105804. https://doi.org/10.1016/j.est.2022.105804

Qi, H., Xu, H., Zhang, J., Xu, Z., Zhong, L., Cui, P., Zhu, Z., & Wang, Y. (2023). Thermodynamic and techno-economic analyses of hydrogen production from different algae biomass by plasma gasification. *International Journal of Hydrogen Energy*, *48*(92), 35895–35906. https://doi.org/10.1016/j.ijhydene.2023.06.038

Qin, C., Ruan, S., He, C., & Zhang, L. (2024). Nickel perovskite catalysts for ammonia decomposition: DFT calculations and microreaction kinetics. *Colloids and Surfaces A: Physicochemical and Engineering Aspects*, *691*(April), 133898. https://doi.org/10.1016/j.colsurfa.2024.133898

Rolo, I., Costa, V. A. F., & Brito, F. P. (2024). Hydrogen-Based Energy Systems: Current Technology Development Status, Opportunities and Challenges. *Energies*, *17*(1), 1–74. https://doi.org/10.3390/en17010180

Ronduda, H., Młotek, M., Góral, W., Zybert, M., Ostrowski, A., Sobczak, K., Krawczyk, K., & Raróg-Pilecka, W. (2024). Cobalt catalysts for COx-free hydrogen production: Effect of catalyst type on ammonia decomposition in gliding discharge plasma reactor. *Journal of CO2 Utilization*, *82*. https://doi.org/10.1016/j.jcou.2024.102755

Saeidi, S., Sápi, A., Khoja, A. H., Najari, S., Ayesha, M., Kónya, Z., Asare-Bediako, B. B., Tatarczuk, A., Hessel, V., Keil, F. J., & Rodrigues, A. E. (2023a). Evolution paths from gray to turquoise hydrogen via catalytic steam methane reforming: Current challenges and future developments. In *Renewable and Sustainable Energy Reviews* (Vol. 183). Elsevier Ltd. https://doi.org/10.1016/j.rser.2023.113392

Saeidi, S., Sápi, A., Khoja, A. H., Najari, S., Ayesha, M., Kónya, Z., Asare-Bediako, B. B., Tatarczuk, A., Hessel, V., Keil, F. J., & Rodrigues, A. E. (2023b). Evolution paths from gray to turquoise hydrogen via catalytic steam methane reforming: Current challenges and future developments. *Renewable and Sustainable Energy Reviews*, *183*(June). https://doi.org/10.1016/j.rser.2023.113392

Sahu, S., Kunj, P., Kaur, A., Khatri, M., Singh, G., & Arya, S. K. (2024a). Catalytic strategies for algal-based carbon capture and renewable energy: A review on a sustainable approach. *Energy Conversion and Management*, *310*, 118467. https://doi.org/10.1016/J.ENCONMAN.2024.118467

Sahu, S., Kunj, P., Kaur, A., Khatri, M., Singh, G., & Arya, S. K. (2024b). Catalytic strategies for algal-based carbon capture and renewable energy: A review on a sustainable approach. *Energy Conversion and Management*, *310*, 118467. https://doi.org/10.1016/J.ENCONMAN.2024.118467

Salehabadi, A., Zanganeh, J., & Moghtaderi, B. (2024a). Mixed metal oxides in catalytic ammonia cracking process for green hydrogen production: A review. *International Journal of Hydrogen Energy*, *63*(January), 828–843. https://doi.org/10.1016/j.ijhydene.2024.03.189

Salehabadi, A., Zanganeh, J., & Moghtaderi, B. (2024b). Mixed metal oxides in catalytic ammonia cracking process for green hydrogen production: A review. *International Journal of Hydrogen Energy*, *63*(January), 828–843. https://doi.org/10.1016/j.ijhydene.2024.03.189

Samia, saeed, F., Jia, L., Arain, M., Ahmed, A., Yikai, F., Zhenda, C., Hussain, I., Abbas Ashraf, G., Ben Ahmed, S., & Dai, H. (2024a). Emerging trends in metal-organic framework (MOFs) photocatalysts for hydrogen energy using water splitting: A state-of-the-art review. *Journal of Industrial and Engineering Chemistry*, *131*(July 2023), 54–135. https://doi.org/10.1016/j.jiec.2023.10.055

Samia, saeed, F., Jia, L., Arain, M., Ahmed, A., Yikai, F., Zhenda, C., Hussain, I., Abbas Ashraf, G., Ben Ahmed, S., & Dai, H. (2024b). Emerging trends in metal-organic framework (MOFs) photocatalysts for hydrogen energy using water splitting: A state-of-the-art review. *Journal of Industrial and Engineering Chemistry*, *131*(July 2023), 54–135. https://doi.org/10.1016/j.jiec.2023.10.055

Shamjitha, C., & Vargeese, A. A. (2023). Development of bimetallic spinel catalysts for low-temperature decomposition of ammonium dinitramide monopropellants. *Defence Technology*, *30*, 47–54. https://doi.org/10.1016/j.dt.2023.05.007

Sharifishourabi, M., Dincer, I., & Mohany, A. (2024). Advancing energy transition with novel biomass-solar based multigeneration energy system using hydrogen and storage options for sustainable cities. *Sustainable Cities and Society*, *108*, 105457. https://doi.org/10.1016/J.SCS.2024.105457

Shi, F., Wang, H., Chen, Y., Lu, Y., Hou, D., Liu, C., Lu, Y., Lin, X., Yang, X., Zheng, Z., & Zheng, Y. (2023). Green diesel-like hydrocarbon production by H2-free catalytic deoxygenation of oleic acid via Ni/MgO-Al2O3 catalysts: Effect of the metal loading amount. *Journal of Environmental Chemical Engineering*, *11*(5). https://doi.org/10.1016/j.jece.2023.110520

Shi, T., Sridhar, D., Zeng, L., & Chen, A. (2022). Recent advances in catalyst design for the electrochemical and photoelectrochemical conversion of methane to value-added products. *Electrochemistry Communications*, *135*, 107220. https://doi.org/10.1016/j.elecom.2022.107220

Shokry, S. A., El Morsi, A. K., Sabaa, M. S., Mohamed, R. R., & El Sorogy, H. E. (2014). Study of the productivity of MWCNT over Fe and Fe–Co catalysts supported on SiO2, Al2O3 and MgO. *Egyptian Journal of Petroleum*, *23*(2), 183–189. https://doi.org/10.1016/j.ejpe.2014.05.005

Sikiru, S., Oladosu, T. L., Amosa, T. I., Olutoki, J. O., Ansari, M. N. M., Abioye, K. J., Rehman, Z. U., & Soleimani, H. (2024). Hydrogen-powered horizons: Transformative technologies in clean energy generation, distribution, and storage for sustainable innovation. *International Journal of Hydrogen Energy*, *56*, 1152–1182. https://doi.org/10.1016/J.IJHYDENE.2023.12.186

Sitar, R., Shah, J., Zhang, Z., Wikoff, H., Way, J. D., & Wolden, C. A. (2022). Compact ammonia reforming at low temperature using catalytic membrane reactors. *Journal of Membrane Science*, *644*(October 2021), 120147. https://doi.org/10.1016/j.memsci.2021.120147

Solanki, B. S., Lim, H., Yoon, S. J., Ham, H. C., Park, H. S., Lee, H. E., & Lee, S. H. (2025). Recent advancement of non-noble metal catalysts for hydrogen production by NH3 decomposition. In *Renewable and Sustainable Energy Reviews* (Vol. 207). Elsevier Ltd. https://doi.org/10.1016/j.rser.2024.114974

Sordakis, K., Tang, C., Vogt, L. K., Junge, H., Dyson, P. J., Beller, M., & Laurenczy, G. (2018). Homogeneous Catalysis for Sustainable Hydrogen Storage in Formic Acid and Alcohols. *Chemical Reviews*, *118*(2), 372–433. https://doi.org/10.1021/acs.chemrev.7b00182

Spatolisano, E., Pellegrini, L. A., de Angelis, A. R., Cattaneo, S., & Roccaro, E. (2023). Ammonia as a Carbon-Free Energy Carrier: NH3 Cracking to H2. *Industrial and Engineering Chemistry Research*, *62*(28), 10813–10827. https://doi.org/10.1021/acs.iecr.3c01419

Sun, H., Li, L., Chen, Y., Kim, H., Xu, X., Guan, D., Hu, Z., Zhang, L., Shao, Z., & Jung, W. C. (2023). Boosting ethanol oxidation by NiOOH-CuO nano-heterostructure for energy-saving hydrogen production and biomass upgrading. *Applied Catalysis B: Environmental*, *325*(January), 122388. https://doi.org/10.1016/j.apcatb.2023.122388

Sun, S., Jiang, Q., Zhao, D., Cao, T., Sha, H., Zhang, C., Song, H., & Da, Z. (2022). Ammonia as hydrogen carrier: Advances in ammonia decomposition catalysts for promising hydrogen production. *Renewable and Sustainable Energy Reviews*, *169*, 112918. https://doi.org/10.1016/j.rser.2022.112918

Sun, Z., Zhang, X., Li, H., Liu, T., Sang, S., Chen, S., Duan, L., Zeng, L., Xiang, W., & Gong, J. (2020). Chemical looping oxidative steam reforming of methanol: A new pathway for auto-thermal conversion. *Applied Catalysis B: Environmental*, *269*(February), 118758. https://doi.org/10.1016/j.apcatb.2020.118758

Tao, X., Yu, F., Yu, P., Yu, H., Zhao, T., Li, M., & Wang, H. (2025). Local coordination configuration of Ni and Co in MgAl2O4 spinel structure and the performance of NiCo/MgO-Al2O3 catalyst for dry reforming of methane. *Chemical Engineering Journal*, *507*. https://doi.org/10.1016/j.cej.2025.160708

Tawalbeh, M., Muhammad Nauman Javed, R., Al-Othman, A., & Almomani, F. (2023). The novel contribution of non-noble metal catalysts for intensified carbon dioxide hydrogenation: Recent challenges and opportunities. *Energy Conversion and Management*, *279*(February), 116755. https://doi.org/10.1016/j.enconman.2023.116755

Theofanidis, S. A., Galvita, V. V., Poelman, H., Batchu, R., Buelens, L. C., Detavernier, C., & Marin, G. B. (2018). Mechanism of carbon deposits removal from supported Ni catalysts. *Applied Catalysis B: Environmental*, *239*(August), 502–512. https://doi.org/10.1016/j.apcatb.2018.08.042

Tonelli, D., Rosa, L., Gabrielli, P., Caldeira, K., Parente, A., & Contino, F. (2023). Global land and water limits to electrolytic hydrogen production using wind and solar resources. *Nature Communications*, *14*(1), 1–14. https://doi.org/10.1038/s41467-023-41107-x

Triviño, M. L. T., Doi, S., Kang, Y. S., Lee, C. U., Sekine, Y., & Seo, J. G. (2023). Achieving equilibrium conversions for low-temperature NH3 decomposition: Synergy between catalyst and electric field effects. *Chemical Engineering Journal*, *476*(October). https://doi.org/10.1016/j.cej.2023.146715

Wan, Z., Tao, Y., Shao, J., Zhang, Y., & You, H. (2021). Ammonia as an effective hydrogen carrier and a clean fuel for solid oxide fuel cells. *Energy Conversion and Management*, *228*(December 2020), 113729. https://doi.org/10.1016/j.enconman.2020.113729

Wang, C., Jiang, W., Si, N., Wang, Z., & Zhang, H. (2025a). CoFe and NiFe LDH-derived MMO catalysts for enhanced hydrogen storage kinetics performance of MgH2. *International Journal of Hydrogen Energy*, *98*, 1–13. https://doi.org/10.1016/j.ijhydene.2024.12.043

Wang, C., Jiang, W., Si, N., Wang, Z., & Zhang, H. (2025b). CoFe and NiFe LDH-derived MMO catalysts for enhanced hydrogen storage kinetics performance of MgH2. *International Journal of Hydrogen Energy*, *98*, 1–13. https://doi.org/10.1016/j.ijhydene.2024.12.043

Wang, E., Navik, R., Miao, Y., Gao, Q., Izikowitz, D., Chen, L., & Li, J. (2024). Reviewing direct air capture startups and emerging technologies. In *Cell Reports Physical Science* (Vol. 5, Issue 2). The Author(s). https://doi.org/10.1016/j.xcrp.2024.101791

Wang, F. M., & Tang, S. F. (2024). Electronic structure modification of ultrathin MnFeOOH and integration with Ni3S2 as bifunctional electrocatalysts for improved alkaline water splitting. *Catalysis Science & Technology*, *14*(3), 581–589. https://doi.org/10.1039/D3CY01556D

Wang, J., & Azam, W. (2024). Natural resource scarcity, fossil fuel energy consumption, and total greenhouse gas emissions in top emitting countries. *Geoscience Frontiers*, *15*(2), 101757. https://doi.org/10.1016/j.gsf.2023.101757

Wang, W., Wang, R., Jiang, X., He, Z. H., Wang, K., Yang, Y., & Liu, Z. T. (2022). Solvent-free aerobic selective oxidation of benzyl alcohol over La-Co bimetallic catalyst: A kinetic study. *Applied Catalysis A: General*, *634*(December 2021), 118537. https://doi.org/10.1016/j.apcata.2022.118537

Wang, Y., Su, B., Yang, X., Chen, Z., & Wang, S. (2024). A green hydrogen production system based on solar-assisted biogas steam reforming. *Applied Thermal Engineering*, *248*, 123067. https://doi.org/10.1016/J.APPLTHERMALENG.2024.123067

Wang, Y., Zhou, H., Yao, D., Olguin, G., Ding, H., Qu, B., Xie, W., Fu, Z., Guo, Y., Wang, X., Li, A., & Ji, G. (2024). Ni-CaO-CaZrO3 bi-functional materials for

high purity hydrogen production via sorption enhanced steam reforming of ethanol. *Journal of Cleaner Production*, *446*, 141397. https://doi.org/10.1016/J.JCLEPRO.2024.141397

Wei, S., Li, C., Ren, H., Yan, Y., & Li, J. (2024). Design and optimization of hydrogen production system model for dimethyl ether self-heating steam reforming. *International Journal of Hydrogen Energy*, *49*, 1450–1467. https://doi.org/10.1016/j.ijhydene.2023.08.369

Weinand, J. M., McKenna, R., Kleinebrahm, M., Scheller, F., & Fichtner, W. (2021). The impact of public acceptance on cost efficiency and environmental sustainability in decentralized energy systems. *Patterns*, *2*(7). https://doi.org/10.1016/j.patter.2021.100301

Wijayanta, A. T., Oda, T., Purnomo, C. W., Kashiwagi, T., & Aziz, M. (2019). Liquid hydrogen, methylcyclohexane, and ammonia as potential hydrogen storage: Comparison review. *International Journal of Hydrogen Energy*, *44*(29), 15026–15044. https://doi.org/10.1016/j.ijhydene.2019.04.112

Woo, Y., Park, J. M., Bae, J. W., & Park, M. J. (2023). Kinetic modeling of the steam reforming of light hydrocarbon mixture from waste resources: Effects of gas composition on hydrogen production. *International Journal of Hydrogen Energy*, *48*(41), 15383–15391. https://doi.org/10.1016/j.ijhydene.2023.01.050

Wu, K., Zhou, C., Pi, G., Yang, J., Wu, D., & Liu, S. (2024). High-efficient N 2 O decomposition over dual-phase hydrogen / oxygen-transporting membrane reactors. *Ceramics International*, *February*. https://doi.org/10.1016/j.ceramint.2024.05.061

Wu, Z. W., Li, X., Qin, Y. H., Deng, L., Wang, C. W., & Jiang, X. (2020). Ammonia decomposition over SiO2-supported Ni–Co bimetallic catalyst for COx-free hydrogen generation. *International Journal of Hydrogen Energy*, *45*(30), 15263–15269. https://doi.org/10.1016/j.ijhydene.2020.04.007

Xie, Y., Sun, L., Pan, X., Zhou, Z., & Zhao, G. (2023). Selective two-electron electrocatalytic conversion of 5-Hydroxymethylfurfural boosting hydrogen production under neutral condition over Co(OH)2-CeO2 catalyst. *Applied Catalysis B: Environmental*, *338*(February), 123068. https://doi.org/10.1016/j.apcatb.2023.123068

Xu, J., Holthaus, P., Yang, N., Jiang, S., Heupel, A., Schönherr, H., Yang, B., Krumm, W., & Jiang, X. (2019). Catalytic tar removal using TiO2/NiWO4-Ni5TiO7

films. *Applied Catalysis B: Environmental*, *249*(March), 155–162. https://doi.org/10.1016/j.apcatb.2019.03.006

Xu, Y., Zhu, Y., Shen, P., Chen, G., & Li, X. (2022). Production of hydrogen by steam reforming of phenol over Ni/Al2O3-ash catalysts. *International Journal of Hydrogen Energy*, *47*(28), 13592–13603. https://doi.org/10.1016/j.ijhydene.2022.02.097

Xue, S., Lan, T., Zhao, G., Nie, Q., Meng, C., Xu, X., & Lu, Y. (2023). NiCx/Ni-foam discovered as a promising high-temperature WGSR catalyst. *Fuel*, *353*(March), 129270. https://doi.org/10.1016/j.fuel.2023.129270

Yadav, D., Lu, X., Ma, B. C., & Jing, D. (2024a). Advancements in microreactor technology for hydrogen production via steam reforming: A comprehensive review of numerical studies. *Journal of Power Sources*, *596*(January), 234090. https://doi.org/10.1016/j.jpowsour.2024.234090

Yadav, D., Lu, X., Ma, B. C., & Jing, D. (2024b). Advancements in microreactor technology for hydrogen production via steam reforming: A comprehensive review of numerical studies. *Journal of Power Sources*, *596*, 234090. https://doi.org/10.1016/J.JPOWSOUR.2024.234090

Yadav, D., Lu, X., Ma, B. C., & Jing, D. (2024c). Advancements in microreactor technology for hydrogen production via steam reforming: A comprehensive review of numerical studies. *Journal of Power Sources*, *596*(January), 234090. https://doi.org/10.1016/j.jpowsour.2024.234090

Yadav, D., Lu, X., Vishwakarma, C. B., & Jing, D. (2023). Advancements in microreactor technology for hydrogen production via steam reforming: A comprehensive review of experimental studies. *Journal of Power Sources*, *585*, 233621. https://doi.org/10.1016/J.JPOWSOUR.2023.233621

Yao, L., Wang, W., Zhu, T., Wang, Y., Liang, Y., Fu, J., Wang, J., Cheng, Y., & Liu, S. (2020). A rational design of CdS/ZnFe2O4/Cu2O core-shell nanorod array photoanode with stair-like type-II band alignment for highly efficient bias-free visible-light-driven H2 generation. *Applied Catalysis B: Environmental*, *268*(August 2019), 118460. https://doi.org/10.1016/j.apcatb.2019.118460

Yu, S., Xiang, T., Alharbi, N. S., Al-aidaroos, B. A., & Chen, C. (2023a). Recent development of catalytic strategies for sustainable ammonia production. *Chinese Journal of Chemical Engineering*, *62*, 65–113. https://doi.org/10.1016/j.cjche.2023.03.028

Yu, S., Xiang, T., Alharbi, N. S., Al-aidaroos, B. A., & Chen, C. (2023b). Recent development of catalytic strategies for sustainable ammonia production. *Chinese Journal of Chemical Engineering*, *62*, 65–113. https://doi.org/10.1016/j.cjche.2023.03.028

Yu, X., Yin, F., Li, G., Zhang, J., & Chen, B. (2024a). Preparation of nickel aluminate supported Ni nanocatalyst and its catalytic activity for ammonia decomposition to produce hydrogen. *International Journal of Hydrogen Energy*, *437*(April), 114774. https://doi.org/10.1016/j.ijhydene.2024.04.019

Yu, X., Yin, F., Li, G., Zhang, J., & Chen, B. (2024b). Preparation of nickel aluminate supported Ni nanocatalyst and its catalytic activity for ammonia decomposition to produce hydrogen. *International Journal of Hydrogen Energy*, *April*, 1–9. https://doi.org/10.1016/j.ijhydene.2024.04.019

Yuan, Y., Wang, W., Li, D., Hu, R., Yan, A., & Wang, Z. (2025). Highly efficient and stable non-noble metal CoM@NC (M = Ni, Mo) catalysts for NH3 decomposition. *Molecular Catalysis*, *572*. https://doi.org/10.1016/j.mcat.2024.114800

Zainal, B. S., Ker, P. J., Mohamed, H., Ong, H. C., Fattah, I. M. R., Rahman, S. M. A., Nghiem, L. D., & Mahlia, T. M. I. (2024a). Recent advancement and assessment of green hydrogen production technologies. *Renewable and Sustainable Energy Reviews*, *189*(PA), 113941. https://doi.org/10.1016/j.rser.2023.113941

Zainal, B. S., Ker, P. J., Mohamed, H., Ong, H. C., Fattah, I. M. R., Rahman, S. M. A., Nghiem, L. D., & Mahlia, T. M. I. (2024b). Recent advancement and assessment of green hydrogen production technologies. *Renewable and Sustainable Energy Reviews*, *189*(PA), 113941. https://doi.org/10.1016/j.rser.2023.113941

Zainal, B. S., Ker, P. J., Mohamed, H., Ong, H. C., Fattah, I. M. R., Rahman, S. M. A., Nghiem, L. D., & Mahlia, T. M. I. (2024c). Recent advancement and assessment of green hydrogen production technologies. *Renewable and Sustainable Energy Reviews*, *189*(PA), 113941. https://doi.org/10.1016/j.rser.2023.113941

Zhang, J., Xu, H., & Li, W. (2006). High-purity COx-free H2 generation from NH3 via the ultra permeable and highly selective Pd membranes. *Journal of Membrane Science*, *277*(1–2), 85–93. https://doi.org/10.1016/j.memsci.2005.10.014

Zhang, T., Tang, X. Y., Yang, W. W., & Ma, X. (2023). Comprehensive performance study on reflux solar methanol steam reforming reactor for hydrogen

production. *International Journal of Hydrogen Energy*, *48*(3), 879–893. https://doi.org/10.1016/j.ijhydene.2022.10.002

Zhang, W., Zhou, W., Li, Y., Ren, J., & Wang, Z. (2023a). Enhanced ammonia decomposition activity over unsupported Co3O4: Unravelling the promotion effect of alkali metal. *Applied Catalysis B: Environmental*, *330*. https://doi.org/10.1016/j.apcatb.2023.122644

Zhang, W., Zhou, W., Li, Y., Ren, J., & Wang, Z. (2023b). Enhanced ammonia decomposition activity over unsupported Co3O4: Unravelling the promotion effect of alkali metal. *Applied Catalysis B: Environmental*, *330*(March), 122644. https://doi.org/10.1016/j.apcatb.2023.122644

Zhang, W., Zhou, W., Li, Y., Ren, J., & Wang, Z. (2023c). Enhanced ammonia decomposition activity over unsupported Co3O4: Unravelling the promotion effect of alkali metal. *Applied Catalysis B: Environmental*, *330*(March), 122644. https://doi.org/10.1016/j.apcatb.2023.122644

Zhang, X., Wei, J., Wang, C., Wang, L., Guo, Z., & Song, Y. (2024). Recent advance of Fe-based bimetallic persulfate activation catalysts for antibiotics removal: Performance, mechanism, contribution of the key ROSs and degradation pathways. *Chemical Engineering Journal*, *487*(January), 150514. https://doi.org/10.1016/j.cej.2024.150514

Zhao, Z., Zhang, M., Wu, Y., Song, W., Yan, J., Qi, X., Yang, J., Wen, J., & Zhang, H. (2024a). Ammonia Energy: Synthesis and Utilization. In *Industrial and Engineering Chemistry Research* (Vol. 63, Issue 18, pp. 8003–8024). American Chemical Society. https://doi.org/10.1021/acs.iecr.4c00384

Zhao, Z., Zhang, M., Wu, Y., Song, W., Yan, J., Qi, X., Yang, J., Wen, J., & Zhang, H. (2024b). Ammonia Energy: Synthesis and Utilization. *Industrial and Engineering Chemistry Research*. https://doi.org/10.1021/acs.iecr.4c00384

Zheng, T., Zhou, D., Zhan, Y., & Xu, Y. (2023a). Integration design optimization of self-thermal methanol steam reforming microreactor for hydrogen production. *International Journal of Hydrogen Energy*, *48*(84), 32642–32653. https://doi.org/10.1016/j.ijhydene.2023.05.013

Zheng, T., Zhou, D., Zhan, Y., & Xu, Y. (2023b). Integration design optimization of self-thermal methanol steam reforming microreactor for hydrogen production. *International Journal of Hydrogen Energy*, *48*(84), 32642–32653. https://doi.org/10.1016/j.ijhydene.2023.05.013

Zheng, T., Zhou, W., Chu, X., & Lian, Y. (2022a). Trapezoidal cavity for high reforming temperature performance of auto-thermal methanol steam reforming micro-reactor for hydrogen production. *International Journal of Hydrogen Energy*, *47*(8), 5053–5063. https://doi.org/10.1016/j.ijhydene.2021.11.164

Zheng, T., Zhou, W., Chu, X., & Lian, Y. (2022b). Trapezoidal cavity for high reforming temperature performance of auto-thermal methanol steam reforming micro-reactor for hydrogen production. *International Journal of Hydrogen Energy*, *47*(8), 5053–5063. https://doi.org/10.1016/j.ijhydene.2021.11.164

Zhong, J. J., Huang, S. P., Gu, J. F., Li, Y., Ding, K. N., Zhang, Y. F., Lin, W., & Chen, W. K. (2023a). Theoretical study of transition metal atom pairs anchored in g-CN monolayers for ammonia decomposition. *Applied Surface Science*, *609*(May 2022). https://doi.org/10.1016/j.apsusc.2022.155280

Zhong, J. J., Huang, S. P., Gu, J. F., Li, Y., Ding, K. N., Zhang, Y. F., Lin, W., & Chen, W. K. (2023b). Theoretical study of transition metal atom pairs anchored in g-CN monolayers for ammonia decomposition. *Applied Surface Science*, *609*(May 2022). https://doi.org/10.1016/j.apsusc.2022.155280

Zhong, X., Qin, Y., Ding, X., Wang, F., & Liu, J. (2023). Zn-Co bimetallic catalysts before and after calcination: Research on their different properties for cycloaddition and Friedel-Crafts acylation reactions. *Applied Catalysis A: General*, *668*(August), 119483. https://doi.org/10.1016/j.apcata.2023.119483

Zhou, C., Wu, K., Huang, H., Cao, C. F., Luo, Y., Chen, C. Q., Lin, L., Au, C., & Jiang, L. (2021). Spatial Confinement of Electron-Rich Ni Nanoparticles for Efficient Ammonia Decomposition to Hydrogen Production. *ACS Catalysis*, *11*(16), 10345–10350. https://doi.org/10.1021/acscatal.1c02420

Zhou, Q., Zhong, X., Xie, X., Jia, X., Chen, B., Wang, N., & Huang, L. (2020). Auto-thermal reforming of acetic acid for hydrogen production by ordered mesoporous Ni-xSm-Al-O catalysts: Effect of samarium promotion. *Renewable Energy*, *145*, 2316–2326. https://doi.org/10.1016/J.RENENE.2019.07.078

Zhou, X., Jin, H., Ma, Z., Li, N., Li, G., Zhang, T., Lu, P., & Gong, X. (2022). Biochar sacrificial anode assisted water electrolysis for hydrogen production. *International Journal of Hydrogen Energy*, *47*(86), 36482–36492. https://doi.org/10.1016/j.ijhydene.2022.08.190

Zhu, N., Hong, Y., Qian, F., & Liang, J. (2024). Research progress on plasma-catalytic hydrogen production from ammonia: Influencing factors and reaction

mechanism. *International Journal of Hydrogen Energy*, *59*(September 2023), 791–807. https://doi.org/10.1016/j.ijhydene.2024.02.016

Zou, X., Su, H. Y., Sun, X., Pang, W., Hao, X., Xu, Y., & Sun, K. (2024a). Interplay between surface structure, reaction condition and mechanism for ammonia decomposition on Ru catalyst. *Applied Surface Science*, *649*(December 2023), 159175. https://doi.org/10.1016/j.apsusc.2023.159175

Zou, X., Su, H. Y., Sun, X., Pang, W., Hao, X., Xu, Y., & Sun, K. (2024b). Interplay between surface structure, reaction condition and mechanism for ammonia decomposition on Ru catalyst. *Applied Surface Science*, *649*(December 2023), 159175. https://doi.org/10.1016/j.apsusc.2023.159175

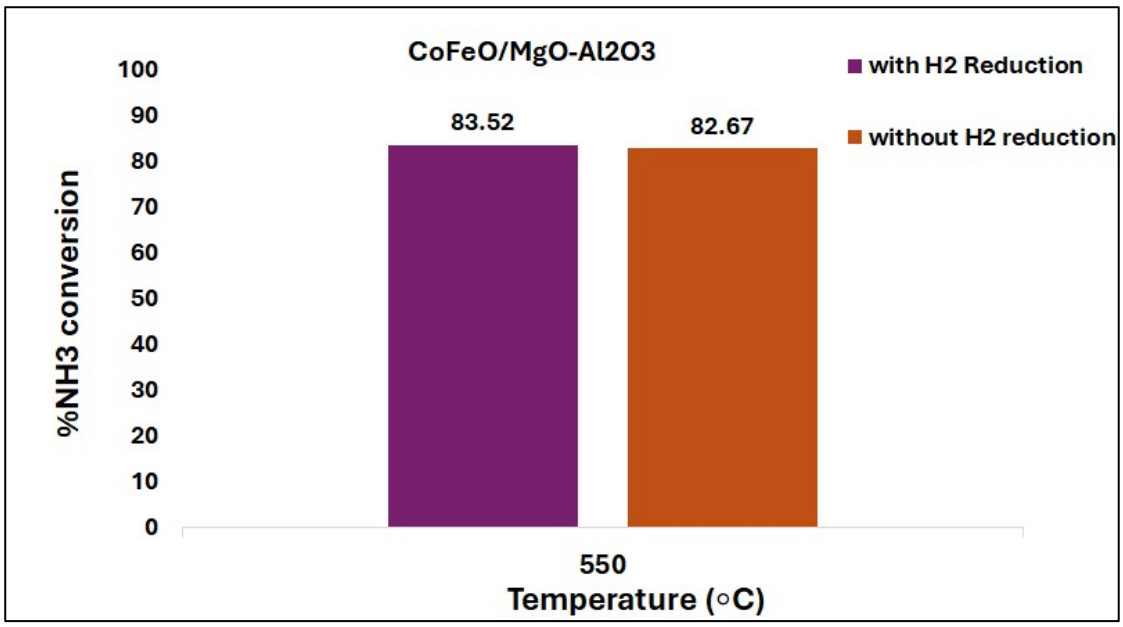
Zou, X., Su, H. Y., Sun, X., Pang, W., Hao, X., Xu, Y., & Sun, K. (2024c). Interplay between surface structure, reaction condition and mechanism for ammonia decomposition on Ru catalyst. *Applied Surface Science*, *649*(October 2023), 159175. https://doi.org/10.1016/j.apsusc.2023.159175

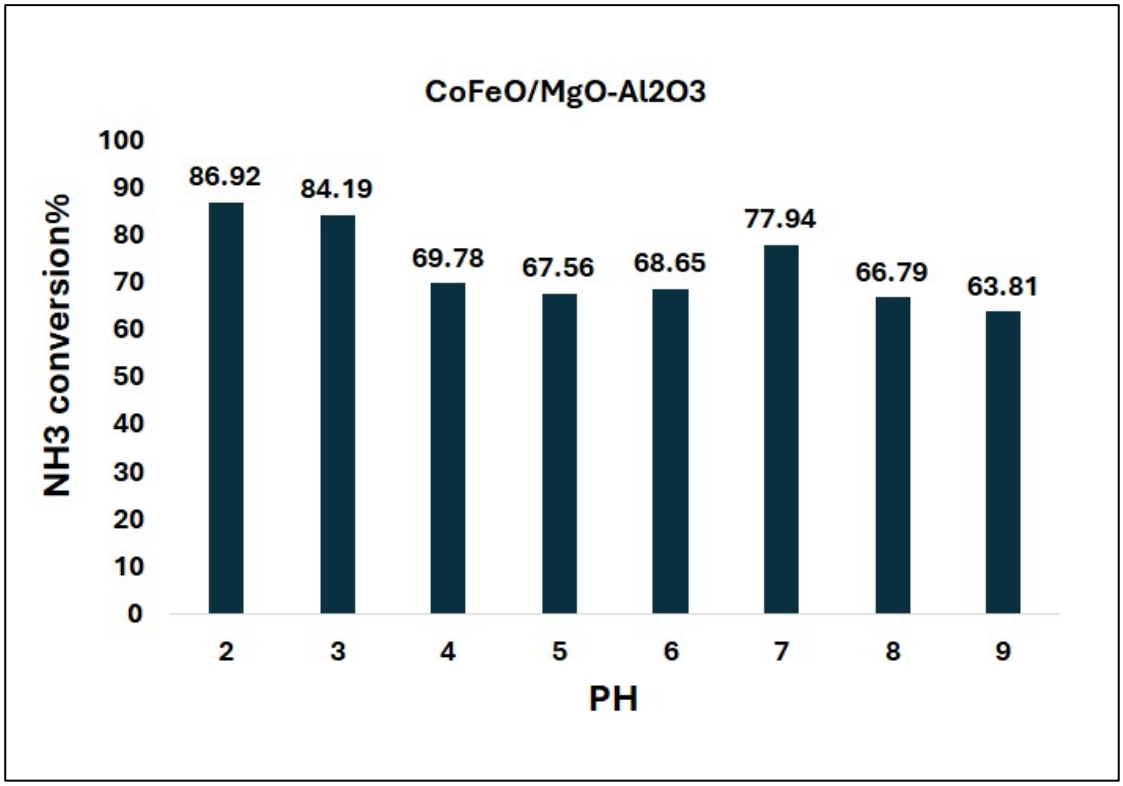
Zuo, Y., Wu, H., Hua, J., Zheng, J., Xu, L., Ye, M., & Wan, C. (2024). Preparation of layered porous carbon supported ruthenium catalyst and its performance for ammonia borane hydrolyzing to hydrogen. *Ranliao Huaxue Xuebao/Journal of Fuel Chemistry and Technology* , *52*(3), 429–437. https://doi.org/10.1016/S1872-5813(23)60385-8

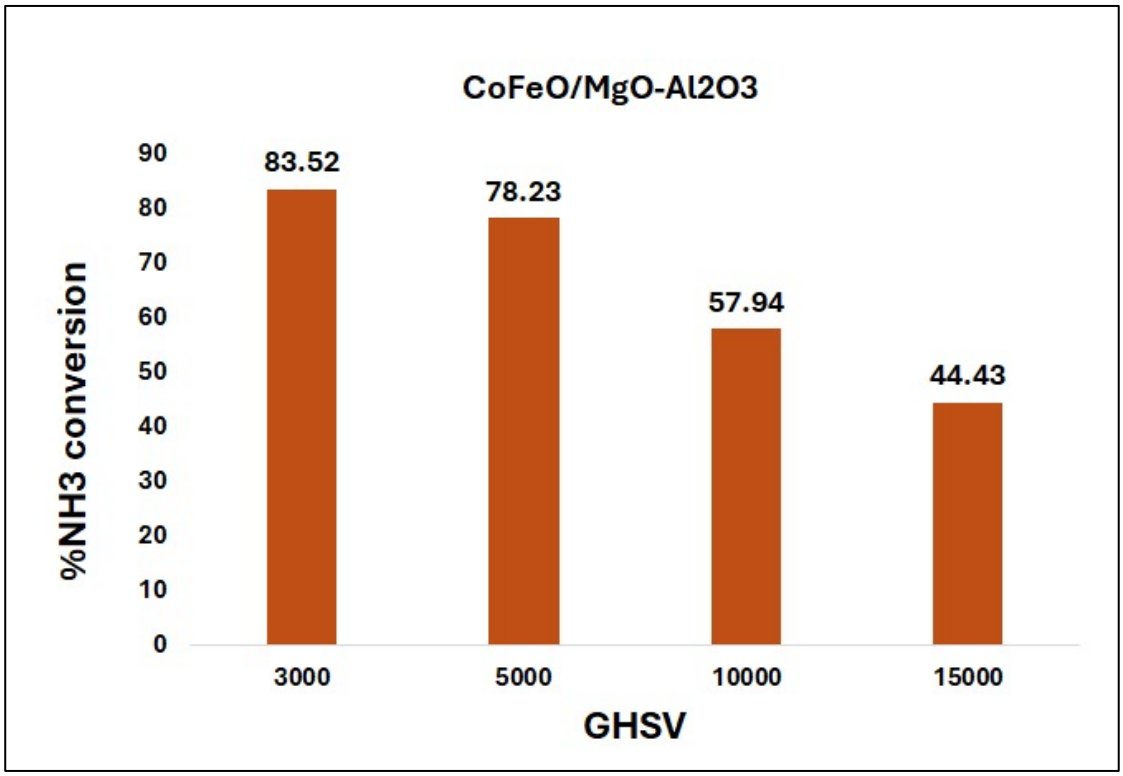
APPENDICES

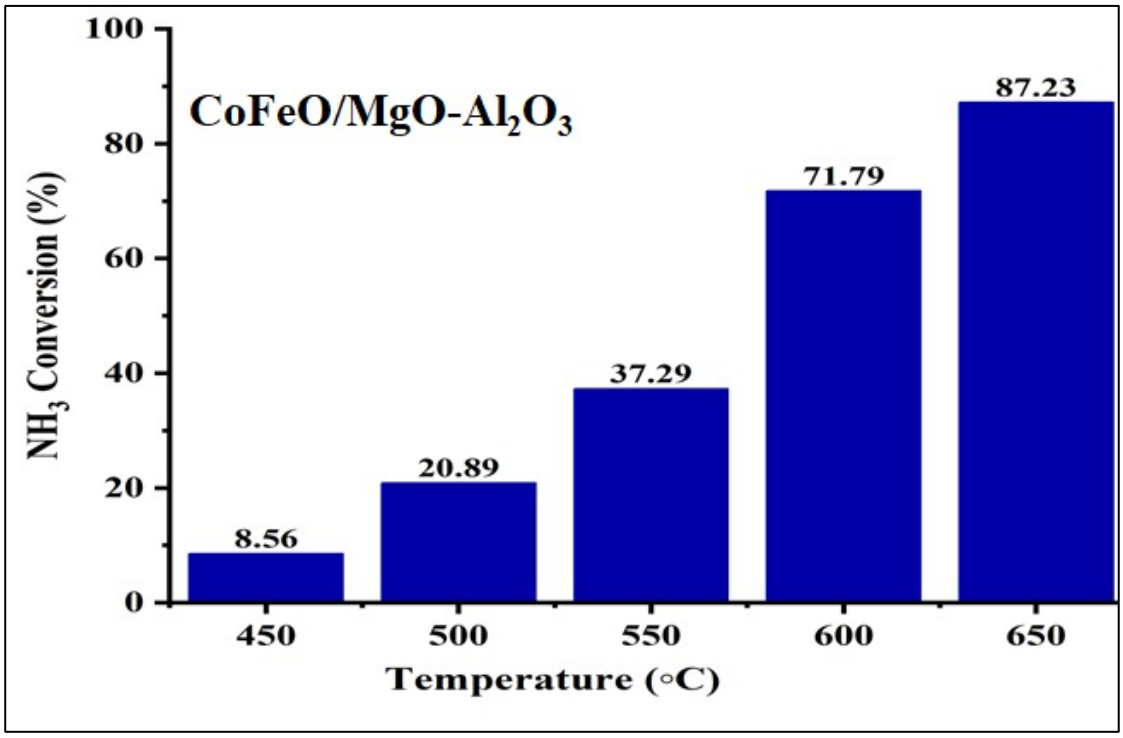
APPENDIX 1

NH_3 Conversion Performance of $CoFeO/MgO–Al_2O_3$ Catalyst Under Various Reaction Conditions



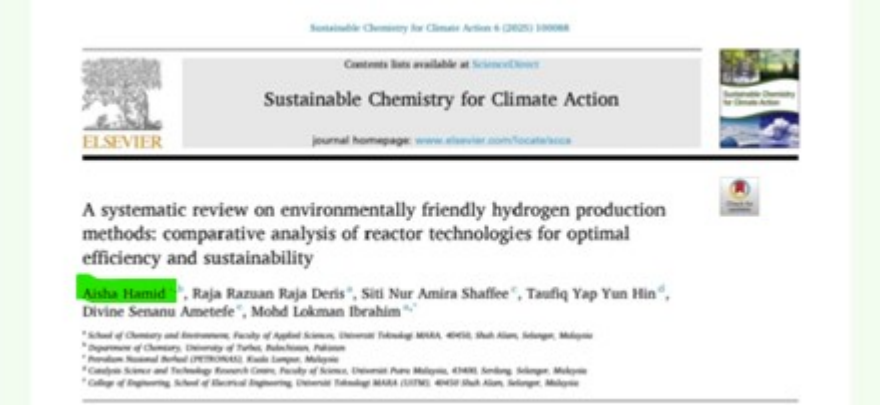



CoFeO/MgO-Al2O3
%NH3 conversion
90
80
70
60
50
40
30
20
10
0
83.52
78.23
57.94
44.43
3000
5000
10000
15000
GHSV


CoFeO/MgO-Al2O3
NH3 Conversion (%)
100
80
60
40
20
0
8.56
20.89
37.29
71.79
87.23
450
500
550
600
650
Temperature (◦C)

APPENDIX 2

Author's Publication Screenshots



Sustainable Chemistry for Climate Action 6 (2025) 100088

Contents lists available at ScienceDirect

Sustainable Chemistry for Climate Action

journal homepage: www.elsevier.com/locate/scca

A systematic review on environmentally friendly hydrogen production methods: comparative analysis of reactor technologies for optimal efficiency and sustainability

Aisha Hamid [a,b], Raja Razuan Raja Deris [a], Siti Nur Amira Shaffee [c], Taufiq Yap Yun Hin [d], Divine Senanu Ametefe [e], Mohd Lokman Ibrahim [a,*]

[a] School of Chemistry and Environment, Faculty of Applied Sciences, Universiti Teknologi MARA, 40450, Shah Alam, Selangor, Malaysia
[b] Department of Chemistry, University of Turbat, Balochistan, Pakistan
[c] Petroleum Nasional Berhad (PETRONAS), Kuala Lumpur, Malaysia
[d] Catalysis Science and Technology Research Centre, Faculty of Science, Universiti Putra Malaysia, 43400, Serdang, Selangor, Malaysia
[e] College of Engineering, School of Electrical Engineering, Universiti Teknologi MARA (UiTM), 40450 Shah Alam, Selangor, Malaysia



Moroccan Journal of Chemistry
ISSN : 2351-812X

Mor. J. Chem., 2025, Volume 13, Issue 1, Page 1-33
https://revues.imist.ma/index.php/morjchem
https://doi.org/ 10.48317/IMIST.PRSM/morjchem-v13i1.51688

Eco-Friendly Approaches to Hydrogen Production: Efficiency and Innovations in Ammonia Decomposition

A. Hamid[1,2], S. N.A. Shaffee[3], R. R. R. Deris[1], T. Y. Y. Hin[4], T. Y. Hua [5], J. Dah[6], M. L. Ibrahim[1*]

[1]School of Chemistry and Environment, Faculty of Applied Sciences, Universiti Teknologi MARA, 40450, Shah Alam, Selangor, Malaysia.
[2]Department of Chemistry, University of Turbat, Balochistan, Pakistan
[3]Petroliam Nasional Berhad (PETRONAS), Kuala Lumpur, Malaysia
[4]Catalysis Science and Technology Research Centre, Faculty of Science, Universiti Putra Malaysia, 43400, Serdang, Selangor, Malaysia
[5]Petroleum and Chemical Engineering, Faculty of Engineering, Universiti Teknologi Brunei, Gadong, BE1410, Brunei Darussalam,
[6]College of Computing, Informatics and Mathematics, Universiti Teknologi MARA (UiTM), 40150 Puncak Perdana, Selangor, Malaysia

*For Corresponding author: Email address: mohd_lokman@uitm.edu.my

Received 03 Oct 2024,
Revised 04 Nov 2024,
Accepted 07 Nov 2024

Abstract: This study delves into the transformative potential of ammonia decomposition as a sustainable hydrogen production method, responding to critical deficiencies in current energy systems heavily reliant on fossil fuels. Amid escalating environmental challenges and the pressing need for clean energy alternatives, hydrogen



International Journal of Hydrogen Energy 169 (2025) 150825

Contents lists available at ScienceDirect

International Journal of Hydrogen Energy

journal homepage: www.elsevier.com/locate/he

Sustainable ammonia decomposition: Economical catalyst and eco-friendly reactor technologies for hydrogen production

Mohd Lokman Ibrahim [a,b,*], Sai Ravindra Panuganti [c,**], Zamzila Kassim [c], Siti Nur Amira Shaffee [c], Fatin Nordiana Che M Idza [c], Noor Ashikin Mohamad [a], Salma Izati Sinar Mashuri [a], Nurul Najwa Abd Malek [a], Aisha Hamid [a], Ahmad Alif Syamsuddin Mohamad Nasir [a], Muhamad Kamil Yaakob [a], Mohd Muzamir Mahat [a], Muhd Firdaus Kasim [a,b], Raja Razuan Raja Deris [a], Salman Raza Naqvi [d]

[a] School of Chemistry and Environment, Faculty of Applied Sciences, Universiti Teknologi MARA, 40450, Shah Alam, Selangor, Malaysia
[b] Centre for Functional Materials and Nanotechnology, Institute of Science, Universiti Teknologi MARA, 40450, Shah Alam, Selangor, Malaysia
[c] PETRONAS Research Sdn Bhd, Kawasan Institusi Bangi, Lot 3288 3289 Off Jalan Ayer Itam, Kajang, Selangor 43000, Malaysia
[d] Department of Engineering and Chemical Sciences, Karlstad University, Sweden

APPENDIX 3

List of Conferences and Appreciation Certificates of Author



CERTIFICATE OF APPRECIATION

This certificate is proudly presented to:

Aisha Hamid Baloch

for your participation in the
ORAL PRESENTATION
at
9TH INTERNATIONAL CONFERENCE FOR YOUNG CHEMISTS
organized by
SCHOOL OF CHEMICAL SCIENCES
UNIVERSITI SAINS MALAYSIA
on
9–11TH OCTOBER 2024

Prof. Dr. Rohana Adnan
Dean
School of Chemical Sciences
Universiti Sains Malaysia

Dr. Oh Wen Da
Advisor, ICYC2024
School of Chemical Science
Universiti Sains Malaysia



UNIVERSITI TEKNOLOGI MARA

Certificate of

APPRECIATION

to

Aisha Hamid Baloch

in recognition for contribution of knowledge

Development of bimetallic supported on 3D-structured metals catalysts for ammonia decomposition

IOS COLLOQUIUM SERIES 4/2024

26 April 2024

onlae (Webex.com)

DIRECTED BY

INSTITUTE OF SCIENCE (IOS)
UNIVERSITI TEKNOLOGI MARA

DEVELOPMENT OF BIMETALLIC SUPPORTED ON 3D-STRUCTURED METALS CATALYSTS FOR AMMONIA DECOMPOSITION

AISHA HAMID
PhD Student (AS950)
Faculty of Applied Sciences
UiTM Shah Alam

26 April 2024 (Friday)
3.00 pm - 4.30 pm
https://uitm.my.webex.com/uitm.my/j.php?MTID=mf0fd86b96b494e2eec3854887ad6dc21

Facebook

ios@uitm.edu.my https://ios.uitm.edu.my https://www.facebook.com/ios.uitm

University of Nottingham
UK | CHINA | MALAYSIA

POCER 2026

CERTIFICATE
OF APPRECIATION

This is presented to

Ms Aisha Hamid

Universiti Teknologi MARA, Malaysia

For attending as a **PRESENTER** at the 8th International Conference and Postgraduate Colloquium of Environmental Research (POCER 2026), held on 8-9 July 2026 at University of Nottingham Malaysia.

Assoc Prof Dr Ianatul Khoiroh
Chair, POCER 2026

In Collaboration with

Supporting Airline Partners

Sponsors

Supported by

AUTHOR'S PROFILE



Aisha Hamid obtained Bachelor of Science in chemistery (Hons.) in 2020 from University of Turbat Balochistan, Pakistan, M.Sc. in Applied sciences (2022) from University of Turbat Balochistan, Pakistan. Visiting lecturer at Faculty of Applied Sciences, University of Turbat Balochistan, Pakistan.

LIST OF PUBLICATION

Hamid, A., Deris, R. R. R., Shaffee, S. N. A., Hin, T. Y. Y., Ametefe, D. S., & Ibrahim, M. L. (2025). A systematic review on environmentally friendly hydrogen production methods: comparative analysis of reactor technologies for optimal efficiency and sustainability. In *Sustainable Chemistry for Climate Action* (Vol. 6). Elsevier B.V. https://doi.org/10.1016/j.scca.2025.100088

Baloch, A. H., Shaffee, S. N. A., Deris, R. R. R., Hin, T. Y. Y., Hua, T. Y., Dah, J., & Ibrahim, M. L. (2025). Eco-Friendly Approaches to Hydrogen Production: Efficiency and Innovations in Ammonia Decomposition. *Moroccan Journal of Chemistry*, *13*(1), 1-33.

Ibrahim, M. L., Panuganti, S. R., Kassim, Z., Shaffee, S. N. A., Idza, F. N. C. M., et al. (2025). Sustainable ammonia decomposition: Economical catalyst and eco-friendly reactor technologies for hydrogen production. *International Journal of Hydrogen Energy, 169*, Article 150825. https://doi.org/10.1016/j.ijhydene.2025.150825

Ammonia Decomposition over CoFeO/MgO-Al_2O_3 Bimetallic Catalyst for COx-Free Hydrogen Production (Under reviwe to *International Journal of Hydrogen Energy)*